Production of polyketide-based pharmaceuticals and nutraceuticals using metabolically engineered *Actinobacteria*

Dissertation

zur Erlangung des Grades
der Doktorin der Ingenieurwissenschaften
der Naturwissenschaftlich-Technischen Fakultät
der Universität des Saarlandes

von

Selma Beganovic

Saarbrücken
2023

Tag des Kolloquiums:	11. Januar 2024
Dekan:	Prof. Dr. Ludger Santen
Berichterstatter:	Prof. Dr. Christoph Wittmann
	Prof. Dr. Andriy Luzhetskyy
Akademischer Mitarbeiter:	Dr. Jannik Zimmermann
Vorsitz:	Prof. Dr. Uli Kazmaier

Publications

Partial results of this work have been published in advance authorized by the Institute of Systems Biotechnology (Universität des Saarlandes) represented by Prof. Dr. Christoph Wittmann.

Peer-reviewed articles

Kuhl, M., Rückert, C., Gläser, L., **Beganovic, S.**, Luzhetskyy, A., Kalinowski, J. 2021. Microparticles enhance the formation of seven major classes of natural products in native and metabolically engineered actinobacteria through accelerated morphological development. Biotechnol. Bioeng. 118, 3076-3093.

Beganovic, S., Rückert-Reed, C., Sucipto, H., Shu, W., Gläser, L., Patschkowski, T., Struck, B., Kalinowski, J., Luzhetskyy, A., Wittmann, C. Multiomics analysis of mutagenized *Streptomyces rimosus* reveals synergistic changes in primary and secondary metabolism and morphology that drive oxytetracycline production towards high efficiency. Submitted to Microb Cell Fact.

Beganovic, S., Weiland, F., Kohlstedt, M., Wittmann, C. Metabolic engineering of *Corynebacterium glutamicum* for high-level production of the plant polyphenol curcumin. In preparation.

Conference contributions

Becker, J., Kuhl, M., **Beganovic, S.**, Gläser, L., Wittmann, C. Mission to morphology – bioprocess engineering for natural product formation in *Streptomyces*. 13th Meeting of the Slovenian Biochemical Society with International Participation. September 2019. Dobrna, Slovenia.

Beganovic, S., Slemc, L., Petkovic, H., Sucipto, H., Luzhetskyy, A., Wittmann, C. Oxytetracycline biosynthesis by *Streptomyces rimosus* in synthetic medium. HIPS Symposium. June 2019. Saarbrücken, Germany.

Beganovic, S., Slemc, L., Petkovic, H., Sucipto, H., Luzhetskyy, A., Wittmann, C. Systems biology of oxytetracycline production in *Streptomyces rimosus*. 13th

Meeting of the Slovenian Biochemical Society with International Participation. September 2019. Dobrna, Slovenia.

Acknowledgment

Even though this is the last chapter of my thesis I am writing, people that I want to express my gratitude to, are at the heartbeat of experience that pursing doctoral studies has brought upon me. First and foremost, this endeavor would not have been possible without my mentor, Prof. Dr. Christoph Wittmann, who took me under his wing and guided through the complexities of my scientific journey. I am deeply indebted for your support, patience, and trust in my work. I am immensely thankful for every piece of knowledge and expertise you shared with me during our invaluable discussions. I am thankful for giving me the opportunity to make my own contribution to the scientific community.

Special thanks to Prof. Dr. Andriy Luzhetskyy for making vital contributions to our collaborative projects. Thank you for accepting the position of my second examiner and reviewing my thesis promptly. I would like to extend my gratitude to our collaboration partner Dr. Christian Rückert-Reed for diligent assessment of complex bioinformatic data sets. Hereby, I express my deep gratitude to the funding bodies, which financially supported my doctoral research: the German Ministry of Education and Research (BMBF) through grants ERA CoBioTech MISSION (031B0611) and MyBio (031B0822), and the German Research Foundation through grant INST 256/418-1.

Many thanks to each comrade at the Institute for Systems Biotechnology for making an inspiring and supporting environment to work. Special thanks to Susanne Haßdenteufel for handling each administrative issue quickly and efficiently, for listening to my presentations, and accepting my spontaneous visits to your office. I am deeply grateful to Michel Fritz for kind technical support, and Michael Kohlstedt for introducing me into the complex world of bioreactors and supporting me during long fermentations. Huge thanks to Lars and Martin for always having the time to answer “just one question” and teaching me valuable lessons that I will take with me wherever I go next. Very special thanks to the beloved colleagues from my office: Iza, Muzi, and Julian. Thank you for sharing the office with me, continuous, selfless support, laughter, and hugs.

There are no enough words to express my gratitude to my beloved friend Sofija. We stepped our foot to the iSBio on the same day. Thank you for each meal we cooked

together, each walk, long philosophical discussions, and unconditional support. Big thanks to my dear Uči, Berina, for bringing uplifting, relaxing spirit to my life.

Želim da se zahvalim mojim najmilijima. Mama, babo, i seko Amila, hvala vam za vašu bezuslovnu podršku i ljubav. Hvala sam što uvijek vjerujete u mene, što ste me naučili da uvijek težim ka najboljem. Hvala i mojoj novoj produženoj porodici Ristićima za svu podršku i zajedničke odmore, kao i nebeskim silama koje su spojile moje i Pekijeve puteve u malom Saarbruckenu. Hvala ti Peki što si upotpunio moj život, za tvoje beskrajno strpljenje i podsticanje onda je mi je to najviše trebalo. Na kraju, duboko se zahvaljujem mojoj nani Sabihi za prve lekcije iz hemije i što je usadila u meni ljubav prema nauci.

Table of content

Summary

In this work, *Streptomyces rimosus* and *Corynebacterium glutamicum* have been employed for the production of polyketide compounds, oxytetracycline and curcumin, as representatives of pharmaceuticals and nutraceuticals, respectively.

Multi-omics systems biology tools enabled elucidation of the mechanisms underpinning superior oxytetracycline formation in the classical industrial producer *S. rimosus* HP126. Randomly introduced mutations modulated metabolism of *S. rimosus* towards elevated CoA-thioester formation and downstream oxytetracycline. Enhanced activity of acetyl-CoA supporting, and reduced activity of malonyl-CoA consuming pathways, as well as boosted activity of the oxytetracycline biosynthetic gene cluster supported 12-fold boosted production of oxytetracycline.

Genetic engineering of the native phenylpropanoid catabolic pathway enabled high-level production of multipotent plant polyphenol curcumin in *C. glutamicum*. Adjusting the ratio of growth and biotransformation substrates allowed additional boost in titre. Toning down consumption of acetyl-CoA by the TCA cycle enabled increased formation of curcumin. Moreover, production of curcumin induced global changes on gene expression level and in fatty acid composition. Finally, fed-batch fermentation of CUR-8 strain resulted with 806 mg L^{-1}, surpassing insofar achieved titres.

Zusammenfassung

In dieser Arbeit wurden *Streptomyces rimosus* und *Corynebacterium glutamicum* zur Produktion von Polyketide, Oxytetracyclin und Curcumin, als Vertreter für Arzneimittel und Nutrazeutika eingesetzt.

Multi-Omics-Systembiologie-Tools ermöglichten die Aufklärung des Mechanismus, der der überlegenen Bildung von Oxytetracyclin im klassischen industriellen Produzenten *S. rimosus* HP126 zugrunde liegt. Zufällig eingeführte Mutationen modulierten den Stoffwechsel von *S. rimosus* hin zur erhöhten Bildung von CoA-Thioestern und nachfolgendem Oxytetracyclin. Die gesteigerte Aktivität des acetyl-CoA-unterstützenden und die reduzierte Aktivität des malonyl-CoA-verbrauchenden Stoffwechselwegs, sowie die gesteigerte Aktivität des Oxytetracyclin-Biosynthese-Gengruppe, unterstützten eine zwölffache Steigerung der Oxytetracyclin-Produktion.

Die genetische Modifikation des nativen Phenylpropanoid-Katabolismus Wegs ermöglichte die hochgradige Produktion des vielseitigen Pflanzenpolyphenols Kurkumin. Die Anpassung des Verhältnisses von Wachstums- und Biotransformationssubstraten ermöglichte eine zusätzliche Steigerung des Titers. Die Reduzierung des Verbrauchs von Acetyl-CoA durch den TCA-Zyklus ermöglichte eine erhöhte Bildung von Kurkumin. Darüber hinaus führte die Produktion von Kurkumin zu globalen Veränderungen auf der Ebene der Genexpression und der Fettsäurezusammensetzung. Schließlich führte die Chargenfermentation des CUR-8-Stamms zu einer Ausbeute von 806 mg L^{-1}, was bisher erreichte Titel übertraf.

1. Introduction

1.1. General introduction

For thousands of years humans have been relying on the power of nature to heal diverse diseases (Dias et al., 2012). The earliest fossil records of human use of plants for medicinal purposes are at least 60,000 years old (Yuan et al., 2016). Traditional medicinal practices around the world, such as Chinese traditional medicine, Ayurveda, Kampo, and Unani, rely on the usage of natural based remedies (Alves and Rosa, 2007; Watanabe et al., 2011). Today, it is known that potent healing properties of traditional medicines stem from an immense array of natural products (NPs), i.e. biologically active compounds produced by numerous plant, fungal, algal, and bacterial species. Functionally, NPs are secondary metabolites, and as such, they have evolved as a part of endogenous defence mechanism against biotic and abiotic stress in their host. Enzymes that catalyse their biosynthesis are often collocated within biosynthetic gene clusters (BGCs) (van der Heul et al., 2018), whose activation usually requires specific environmental conditions (Craney et al., 2013).

A prominent feature of NPs is their great chemical diversity and complexity, which enables them to carry out different biological and drug-like activities. Their function in native producers is often selected for the defence against pathogens, which makes them suitable for the treatment of infectious diseases and cancer, as they are able to trigger cell death (Laraia and Waldmann, 2017). Indeed, through history, NPs have played a pivotal role in drug discovery for the treatment of infectious diseases. Moreover, NPs have also had a significant impact on the development of anticancer, hypocholesterolemic, and immunomodulatory drugs (Lautie et al., 2020; Ramírez-Rendon et al., 2022). Today, nearly 50% of clinically used drugs have directly, or indirectly natural origins. From the vast choice of natural products, polyketides, as a class of secondary metabolites, stand out in their abundance and biological activities (Yuzawa and Kuzuyama, 2020). They are of utmost importance for disease treatment and nurturing of human health, but also have valuable place in veterinary and agricultural practices (Yuzawa et al., 2018).

Despite their pronounced biological activity, and practically untapped sources, polyketides, and other classes of NPs, exhibit significant challenges for drug discovery. These include tedious screening of large libraries, isolation, characterization, and

optimization of production process. In their native hosts, NPs are typically formed in finite quantities, far below an industrially applicable range (Atanasov et al., 2021). However, this barrier towards large-scale, sustainable production of NPs can be overcome, for example by applying methods that fall under the umbrella of systems metabolic engineering. Thereby, multi-omics technologies enable the understanding of the underlying mechanisms and bottlenecks behind the biosynthesis of polyketides (and other secondary metabolites) (Lee et al., 2011). Genetic engineering plays an indispensable role in rewiring of the primary metabolism to the upgrade production of native and heterologous metabolites (Yuan and Alper, 2019). The production of NPs in non-native, heterologous hosts is a common. This is especially apparent in the field of plant NPs, where microbial cell factories provide the opportunity for a resource-conscious and environmentally friendly production (Liu et al., 2017).

Evidently, efforts towards upgrading native producers and engineering traditional and non-conventional heterologous hosts are at the cornerstone for establishing sustainable, high-level production of polyketides, and NPs in general.

1.2. Objectives

In light of the previously highlighted benefits of polyketides in human welfare, this work aims to explore the applicability of actinobacterial microbial cell factories for the production of polyketide antibiotic oxytetracycline, and the plant polyketide nutraceutical curcumin. In that regard, this work consists of two major parts.

The first part tackles the unexplored mechanisms behind the remarkable capacity of the industrial producer of oxytetracycline. The *Streptomyces rimosus* ATCC 10970 wild type, *S. rimosus* HP126 the oxytetracycline industrial producer, and its derivative lacking the oxytetracycline biosynthetic gene cluster, should be evaluated on systems level. The strains ought to be examined in terms of growth, substrate utilization, product formation, and pH. Metabolomics and transcriptome studies attempted to investigate the metabolic rewiring, which upgraded *S. rimosus* wild type for industrial scale production of oxytetracycline.

The second part deals with establishing, to this date, the first *Corynebacterium glutamicum* cell factory for production of the plant polyphenol curcumin. The endogenous metabolism of *C. glutamicum* need to be tailored towards efficient

curcumin production, by elimination of competing pathways. In order to select the best performing cluster, a screening of candidates for curcumin BGC was supposed to be carried out. Optimization of the nutrients and engineering of acetyl-CoA and malonyl-CoA were meant to enrich the supply of precursors for curcumin biosynthesis. Additionally, transcriptome and metabolome analysis aimed to investigate the effects of curcumin production on multiple cellular levels. Finally, the screening of optimal bioprocess conditions, is intended to scale up the production to the level of stirred-tank bioreactors.

2. Theoretical background

2.1. Polyketides

Polyketides are structurally and functionally diverse family of natural products (Till and Race, 2014). The name “polyketide” stems from the common occurrence of keto groups at multiple alternate carbon atoms (Hopwood and Sherman, 1990). They show broad range of biological activities, including antibacterial (tetracycline, erythromycin A, rifamycin) (Jia et al., 2010b), antiviral (balticolid) (Duarte et al., 2012), antifungal (amphotericin B) (Caffrey et al., 2001), anticancer (doxorubicin, epothilone) (Weissman and Leadlay, 2005), cholesterol-lowering (lovastatin) (Campbell and Vederas, 2010), antiparasitic (avermectine) (Dlugónska, 2015), antifungals (soraphen A) (Ligon et al., 2002), insecticidal (spinosyn A) (Li et al., 2021b), immunosuppressing (rapamycin) (Yoo et al., 2017), and anti-inflammatory (flavonoids) (Tauchen et al., 2020) (**Fig. 1**). As such, polyketides have become of prominent importance for human healthcare, and are widely used for the treatment of acute and chronic diseases. To illustrate their significance, the market for polyketide-derived drugs is estimated to US$20 billion.

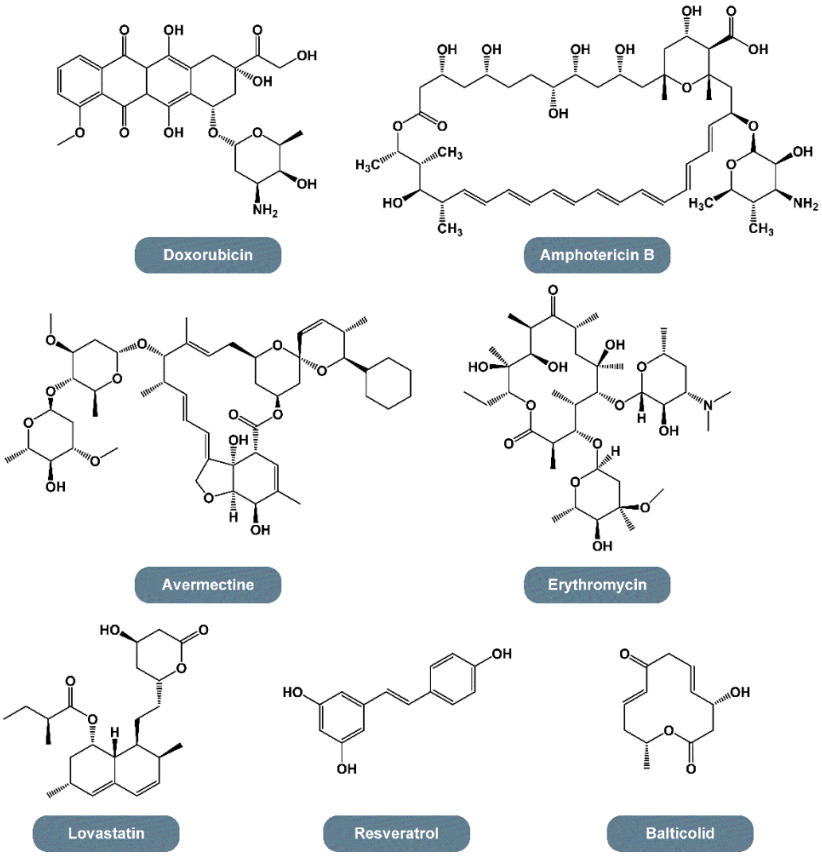

Figure 1. Examples of polyketides and their respective molecular structure.

2.2. Polyketides as pharmaceuticals

Attributable to their pronounced biological activities and functionalities, polyketides have immense clinical importance (Gokulan et al., 2014). Overall, they constitute 20% of the most sold pharmaceuticals (Baerson and Rimando, 2007). Extensive medical application of polyketides is tightly associated with their endogenous roles in natural producers. Namely, polyketides are evolutionary optimized for various functions, among which competition with other organisms is one of the most common ones (Dias et al., 2012; Atanasov et al., 2021). Essentially, this means that polyketides are often specialized to induce cell death, which makes them an inexhaustible source for the development of antibiotic and anticancer drugs (Monfil and Casas-Flores, 2014).

Among polyketide chemotherapeutics, anthracyclines have taken a centre stage in the cancer treatment (Sarker et al., 2020). Naturally produced by *Streptomyces paucetius*, doxorubicin and daunorubicin anthracyclines are potent antineoplastic drugs in clinical practice since the 1980s (Aubel-Sadron and Londos-Gagliardi, 1984; Khosla and Keasling, 2003). They are commonly prescribed to treat multiple types of cancers, predominantly, breast and bladder cancer, Kaposi's sarcoma, lymphoma, and acute and lymphocytic leukaemia (Sarker et al., 2020). Doxorubicin and daunorubicin inhibit topoisomerase 2, the enzyme essential for cell division, and thereby stop or reduce the growth of cancer cells (Bodley et al., 1989; Hande, 2008). Epothilones are another example of polyketide chemotherapeutics (Tang et al., 2005). Isolated from *Sorangium cellulosum* in the early 1990s (Julien et al., 2000; Sarker et al., 2020), they exert antitumor activity by interfering with tubulin formation during cell proliferation (Fumoleau et al., 2007).

Furthermore, polyketides are a valuable source of cholesterol lowering drugs, lovastatin, being a prime illustration (Baerson and Rimando, 2007; Cacho et al., 2015). In nature, lovastatin is produced by the fungus *Aspergillus terreus* (Mulder et al., 2015).The hypocholesterolemic effect is achieved via inhibition of 3-hydroxy-3-methyl glutaryl coenzyme A (HMG-CoA) reductase, an enzyme involved in biosynthesis of cholesterol (Goswami et al., 2013).

Notably, microorganisms have had a pivotal role in the antibiotic drug development from the early years of the so-called "golden age of antibiotics" (Ribeiro da Cunha et al., 2019). Indeed, the majority of the clinically applied antibiotics are of microbial origin (Cragg and Newman, 2001). Among them, *Streptomyces* genus has an extraordinary

value for antibiotic drug development. Nearly 50% clinically applied antibiotics stem from streptomycetes, and a significant portion of these antibiotics are polyketides (Zhang et al., 2020). Tetracycline, erythromycin, nystatin, avermectin, and spiramycin, naturally produced by, *S. auerofaciens* (Pogue et al., 2017), *S. erythreus* (Weber et al., 1985), *S. noursei* (Zotchev et al., 2000), *S. avermitilis* (Chen et al., 2016), and *S. spiramyceticus* (Wang et al., 2021), respectively, include some of the most well-known representatives of clinically approved polyketide antibiotics (Baerson and Rimando, 2007).

Historically, polyketide-derived antibiotics have played a significant role in antibiotic drug development, and today, they are still major source of novel antibiotics (Robertsen and Musiol-Kroll, 2019). Advances in methods for cultivation made it possible to cultivate previously "unculturable" strains from complex bacterial communities, such as those of soil-dwelling and marine actinomycetes (Chaudhary et al., 2019; Mu et al., 2021). Furthermore, next generation sequencing technologies and genome mining enabled rapid, accurate and affordable genome sequencing and identification of enzymes carrying out polyketide synthesis (Nett et al., 2009). These advances are crucial in combating ever-growing antimicrobial resistance (AMR) and bacterial persistence. At least 700,000 death cases each year are associated with AMR. Without proper response, estimates say that the number might increase to staggering 10 million during the next three decades (Miethke et al., 2021).

Oxytetracycline as a prominent example of polyketide antibiotics. One of the earliest findings during the "golden era of antibiotics" was oxytetracycline, a tetracycline class antibiotic, discovered in 1950 (Finlay et al., 1950). It is a broad-spectrum antibiotic that is commonly prescribed to treat variety of bacterial infections in humans (Pelosato et al., 2022) and animal feeds (Injac et al., 2008). It is naturally produced by soil actinomycete *Streptomyces rimosus*, which led to it initially be named as terramycin (Finlay et al., 1950). It was first commercialized by Pfizer under the trade name Terramicina® (Sversut et al., 2017). Even during ever-growing threat of antibiotic resistance, tetracyclines remains one of the most often prescribed antibiotics (Van Boeckel et al., 2014), with yearly production of oxytetracycline being estimated to >10,000 tons (Pethick et al., 2013). Nowadays, there are more than 20 industrial suppliers of oxytetracycline, and according to recent estimates, prices have stabilized at approximately 20 US-$ kg^{-1} (Beganovic et al., 2023, submitted to Microb. Cell Fact.).

Physiochemical properties and mode of action. From the structural point of view, oxytetracycline is an aromatic polyketide, comprised of four fused six-carbon rings (A, B, C, and D), which are decorated with multiple functional groups (**Fig. 2**) (Chopra and Roberts, 2001). Basic oxytetracycline scaffold is synthesized by type II polyketide synthase, utilizing overall nine molecules of malonyl-CoA (Pickens and Tang, 2010). Distinct feature of oxytetracycline, and of other tetracycline antibiotics, is a presence of C2-amide group and one aromatic ring (D ring) (Chopra et al., 1992).

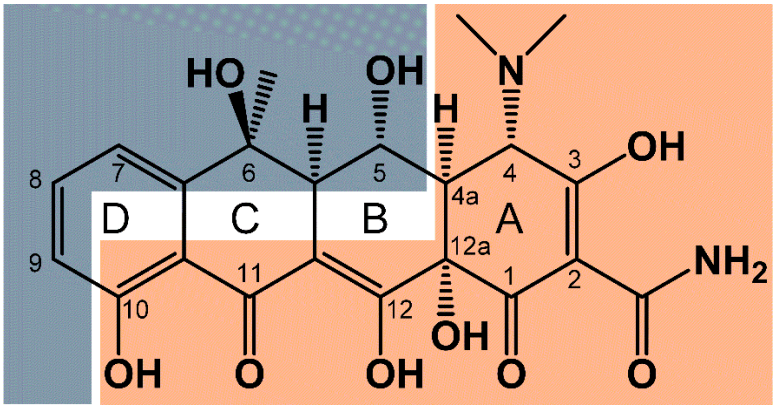

Figure 2. Molecular structure of oxytetracycline. Represented are the four rings (A through D, from left to right) with the associated functional groups. The lower periphery, involved in inhibition of protein biosynthesis, is depicted in orange, while the upper periphery associated with derivatives of increased biological activity is shown in grey (Petković et al., 2017).

The peripheral segments of the oxytetracycline molecule can further be distinguished into the upper and lower periphery (**Fig. 2**) (Petković et al., 2017). The lower periphery spreads from C10 to C4a carbon atoms (Petković et al., 2017), and carries out interaction with the 30S ribosomal subunit, whereby blocking the docking of the incoming tRNAs and arresting the protein biosynthesis (Chopra and Roberts, 2001; Nelson and Levy, 2011). Specifically, the C2-amide group and the oxygen functional groups at C10-C1 carbon atoms are involved in interaction with 16S ribosomal RNA (rRNA) (Robertsen and Musiol-Kroll, 2019). As a consequence, modifications at this part of the molecule are detrimental for the function of the antibiotic (Petković et al., 2017). In contrast, derivatives made by modifications of the functional groups within the upper periphery can even have increased activity (Pickens and Tang, 2010; Nelson and Levy, 2011).

Importantly, oxytetracycline acts as a strong chelating agent, which influences its antibacterial and pharmacokinetic properties (Sversut et al., 2017). Precisely, chelation

of Mg^{2+}+ ions, coordinated by the A ring, further increases binding of oxytetracycline to the ribosome and its antibacterial effect (Jenner et al., 2013). Chelating properties enable oxytetracycline to be effective against Gram-negative bacteria, which are characterized by the additional layer of outer membrane. In order to pass this barrier, oxytetracycline forms complexes with Mg^{2+} ions, enabling it to pass though porins in the outer membrane. However, in order to diffuse through the cell membrane, it dissociates from Mg^{2+} ions. Finally, the Mg^{2+} complex forms again in the cytoplasm, and strengthens the interaction with ribosome (Zakeri and Wright, 2008; Robertsen and Musiol-Kroll, 2019).

Spectrum of action and applications. Oxytetracycline inhibits a wide range of Gram-positive and Gram-negative bacteria (Nelson and Levy, 2011), but also of the spirochaetae, chlamydiae, mycoplasma, rickettsiae, and protozoan parasites (Sversut et al., 2017). In clinical practice, oxytetracycline is used to treat infectious of the respiratory and urinary tract, soft tissues, and skin (Papich, 2016). In agriculture, oxytetracycline is administrated to promote growth (Soler et al. 2016), and to prevent outbreaks of bacterial diseases in cattle and poultry (Szekely and Didaskalou 2016; Sudha et al. 2022), and foulbrood disease of honey bees (Waite et al. 2003). Furthermore, it finds extensive application in aquaculture to prevent diseases in salmonids, catfish, and lobsters (Leal et al. 2019).

Second generation derivatives of oxytetracycline. Emergence of the AMR initiated the development of modified tetracyclines with the improved performance. These derivatives constitute the group of the second generation tetracycline (Petković et al. 2017). First oxytetracycline derivative was made by alterations of the C6 hydroxyl group, and brought about formulation of methacycline (6-methylene-5-hydroxytetracycline). Another round of modifications of methycycline gave rise to doxycycline (6-deoxy-5-hydroxytetracycline) (Robertsen and Musiol-Kroll, 2019). These derivatisations principally increased the spectrum of antibacterial activity against *Escherichia coli*, *Pseudomonas aeruginosa*, *Staphylococcus aureus* and *Enterococcus faecalis* (Nguyen et al., 2014). Doxycycline has increased activity, stability, and pharmacological properties compared to its parental molecule. Although doxycycline was approved by the USA Food and Drug Administration (FDA) in 1967, it is still broadly prescribed today, not only for the treatment of bacterial caused

infections, but also for the treatment of malaria and for chemoprophylaxis (Nelson and Levy, 2011; Petković et al., 2017).

2.3. Polyketides in the food industry

Beside their key role in drug development, polyketide compounds have important applications in food industry (Rugbjerg et al., 2018). In order to meet the growing demand for clean label ingredients, natural polyketide pigments are becoming an attractive “organic” alternative to synthetic food colorants (Lebeau et al., 2017). Many fungi, algae, and plants naturally produce polyketides that give them vibrant colours. - known examples are red and yellow *Monascus* pigments, produced by filamentous fungi (Dufossé et al., 2014). *Talaromyces* species produce azaphilone (Mapari et al., 2010), while orevactaene is obtained from *Epicoccum nigrum*. However, from the use of filamentous fungi in the food industry raises safety concerns, linked to the formation hazardous mycotoxins (Mapari et al., 2009). Still, this shortcoming has been addressed by selecting naturally and engineered mycotoxin- free and non-pathogenic fungal strains (Jia et al., 2010a).

Industrially, most of the natural food colorants that are food-approved in the United States and the European Union are of plant origin (Mortensen, 2006). For instance, turmeric is a source of the orange-yellow polyketide pigment curcumin that is marketed under names such as Natural Yellow 3, diferuloylmethane, CI 75300 or E100 (Panzarini et al., 2021). Curcumin is commonly used to colour baked goods, dairy products, cereals, mustard, beverages, meat, eggs, fish, sausages, ice cream, food concentrates, and confectionery. Depending of the food category, the amount of added curcumin varies between 5 and 500 mg kg^{-1} (Solymosi et al., 2015; Sharifi-Rad et al., 2020). Due to its antimicrobial and antioxidant properties, curcumin provides additional benefits than beautiful colour. The compound reduced the abundance of bacteria, molds, and yeasts in meat samples, and suppressed undesired lipid peroxidation of soybean oil. Thus, curcumin can increase stability of food, and is a highly relevant natural food preservative (Abdeldaiem, 2014).

Polyketides as functional food ingredients. An emerging field in the food area relates to the conceptual design of functional foods (Henry, 2010). There are several definitions for functional foods, and they all share the aspect to be food and/or dietary

components that support human health beyond basic nutrition (Bagchi, 2014). Functional foods can be classified into three major groups: (i) conventional food containing naturally occurring bioactive substances , (ii) food that artificially is enriched in bioactive compounds, and (iii) and specific food ingredients that have probiotic and/or prebiotic effects (Henry, 2010; Temple, 2022). Among these latter ingredients, plant flavonoids receive special attention. Structurally, these compounds are derived from a polyketide scaffold that is synthesized by type III PKS complexes. With more than 5,000 described compounds, flavonoids can be sub-grouped into structurally diverse chalcones, flavanones, flavones, flavonols, aurones, isoflavonoids, flavanediols, anthocynins, and tannins (Hurst, 2008). The existing extraordinary diversity is a result of numerous modifications of the basic polyketide scaffold by various tailoring enzymes (Winkel-Shirley, 2001; Katsuyama et al., 2007; Hurst, 2008). The main dietary source of flavonoids are fruits, vegetables, red wine, and green tea (Yao et al., 2004). Health-promoting benefits of flavonoids are versatile and include: anti-inflammatory, antioxidant, anti-cancer, anti-hypertensive, anti-proliferative, and anti-virus activity (Xiao et al., 2011).

Unfortunately, due to the nutrient-poor soils and processing conditions using in agriculture, most of the food that we eat today is depleted in these functional components. Therefore, dietary supplements with concentrated and increased bioavailability of functional ingredients are becoming an often chosen solution to deal with this problem (Ghosh et al., 2019). In this regard, the dietary supplement market is expected to reach 220.8 billion US$ by 2027 (https://www.marketsandmarkets.com/). A considerable fraction of the market is constituted by the historically and medically relevant plant polyketide curcumin (Farooqui and Farooqui, 2019). Therefore, the next parts of this subchapter aim to explore this valuable compound more into detail.

Curcumin as a prominent example of a functional food ingredient. Curcumin, is a bioactive polyphenolic compound that occurs in the rhizome of turmeric (*Curcuma longa*, L.), a perennial plant from the ginger family (*Zingiberaceae*). The plant is native to India, but has been meanwhile introduced to other tropical and subtropical regions of Southeast Asia and China (Srivastava et al., 2011). What is commercially known as curcumin, is actually a mixture of curcumin, and its related derivatives demethoxycurcumin and bisdemethoxycurcumin. The three compounds together are generally named as curcuminoids (Goel et al., 2008). In the mixture, curcumin is the

most active and abundant derivative (77%), followed by demethoxycurcumin (17%) and bisdemethoxycurcumin (3%) (**Fig. 3**) (Hm Leung et al., 2013). Together, curcuminoids are found enriched up to 5% in the turmeric root (Goel et al., 2008). Dried turmeric powder, also known as Indian saffron or golden spice, has a distinct aromatic flavour and vibrant yellow colour. As such, it has been used more than 2000 years in Asian cuisine, medicine, cosmetics and fabric dying (Lee et al., 2013c).

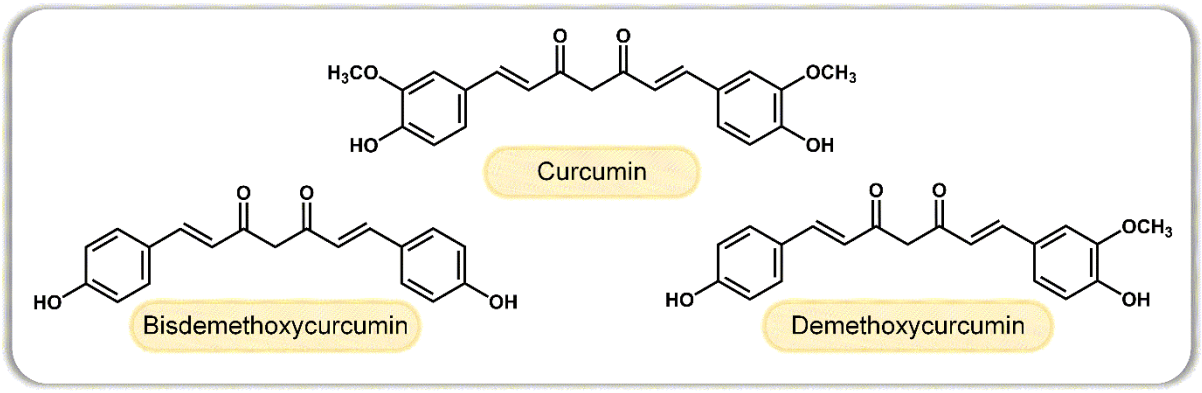

Figure 3. Molecular structure of the three major curcuminoids. Curcumin, demethoxycurcumin, and bisdemethoxycurcumin differ in the number of *O*-methoxy groups, containing either two, one, or none, respectively (Goel et al., 2008).

Physicochemical properties of curcumin. Chemically, curcuminoids are diarylheptanoids. They are synthesized by PKSIII using precursors that stem from the phenylpropanoid pathway (see below for more details). Vogel and Palletier were first to isolate curcumin (Vogel and Pelletier, 1815), followed by purification in crystalline form (Daube, 1870). Curcumin was later identified as diferuloylmethane or 1,6-heptadiene-3,5-dione-1,7-bis(4-hydroxy-3-methoxyphenyl)-(1E,6E), enabling its first chemical synthesis (Miłobędzka et al., 1910).

A prominent feature of curcumin is its keto-enol tautomerism (**Fig. 4A**), resulting from the carbonyl groups at carbon atoms three and five in the heptadiene chain. In polar, acidic, and neutral environments, the keto-form prevails, while non-polar and basic conditions lead to formation of the enol form (Rege et al., 2019). The pH-influenced tautomerism of curcumin is important, as it influences its bioactivity. For example, curcumin acts as an antioxidant only in its keto form by exchanging a proton from the methylene group at the carbon position four between the electron-withdrawing

carbonyl groups. Subsequent stabilization of the resulting carbon radical is achieved by resonance of the carbonyl groups (Jovanovic et al., 1999; Rege et al., 2019).

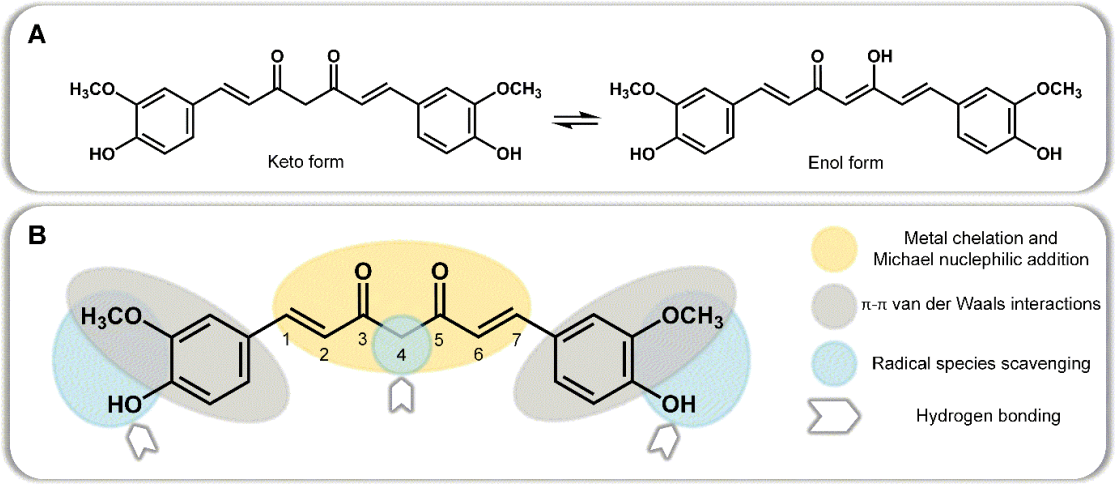

Figure 4. Structural background of curcumin bioactivity. Keto-enol tautomerism of curcumin **(A)**. Keto form predominates in polar, acidic medium. It is characterized by presence of methylene group at carbon atom four that can act as a hydrogen donor for scavenging of free radicals, including hydroxyl radicals, hydrogen peroxide, singlet oxygen and superoxide anion. Enol form predominates in basic, nonpolar medium and is characterized by absence of active methylene group. It is prone to breaking of the hepta-diene linker and cannot function as radical scavenger and thereby does not exhibit antioxidant activity (Sitabja and Santosh, 2021). Pharmacophore structure and biological function relation **(B)**.

Furthermore, curcumin is hydrophobic and exhibits exceptionally low solubility in water (3×10^{-8} M) (Kharat et al., 2017). However, the compound dissolves readily in polar organic solvents such as methanol, ethanol, dimethylsulfoxide, acetone, and acetonitrile. Additionally, it is soluble in hydrocarbon solvents like hexane and cyclohexane (Yixuan et al., 2021).

Bioavailability of curcumin. This pronounced hydrophobicity significantly reduces the bioavailability of curcumin and hinders its application in water-based products (Kharat et al., 2017). The bioavailability of curcumin is also limited by chemical instability under physiological conditions. Namely, at physiological pH, curcumin ratherrapidly degrades, resulting in cleavage products such as bicyclopentadione, vanillin, and ferulic acid (Schneider et al., 2015). Upon digestion, curcumin undergoes hepatic and intestinal biotransformation in the form of reduction, glucuronidation, and sulfation. Consequently, the amount of ingested curcumin that reaches the bloodstream is very low (Garcea et al., 2004; Lao et al., 2006).

Nevertheless, several strategies can be applied to address these issues and increase the bioavailability of curcumin. For instance, co-administration of adjuvants like piperine (alkaloid from black pepper, *Piper nigrum*, L.), silibinin (flavonoid from milk thistle, *Sylbum marianum*, L.) and quercetin (plant flavonol) inhibit the liver enzyme UDP-glucuronyltransferase that plays a key role in hepatic metabolic biotransformation of curcumin (Liu et al., 2020). Next, the incorporation of curcumin into carrier systems such as liposomes, micelles, hydrogels, emulsions, nanoparticles, hallossite particles, and capsules protects it from metabolic clearance and improves absorption into the gastrointestinal tract (Anand et al., 2007; Cheng et al., 2017).

Medicinal properties of curcumin. Curcumin, exhibits remarkable pharmacological effects, including: antimicrobial, anticancer, chemopreventive, anti-inflammatory, antioxidant, antidiabetic, antilipidemic, and neuroprotective activities (**Fig. 4C**). These activities have been confirmed *in vitro* and *in vivo* and opened the way for nearly 500 human clinical trials (Fu et al., 2021).

The multiple bioactive properties of curcumin can be ascribed to its structural complexity and the presence of three main functional groups: an aromatic *o*-methoxy phenolic group, an α, β-unsaturated β-diketone moiety, and a seven-carbon linker (Priyadarsini, 2013). These pharmacophores mediate interactions with indeed a long list of targets, such as transcription factors (Minassi et al., 2013), enzymes (Singh and Misra, 2009), free radicals and metals (Jagetia, 2021), enabling it to interfere with multiple cellular pathways (Tomeh et al., 2019). For example, the *o*-methoxyphenolic group and the methylenic hydrogen have been found essential for antioxidant activity, as they are involved in free radical scavenging by donating electron or hydrogen atom (El-Magboub et al., 2014). Moreover, curcumin interacts with many targets via covalent and non-covalent binding (Hatamipour et al., 2018). Furthermore, non-covalent binding is mediated by hydrogen-bonding *via* the β-diketone moiety and hydroxyl substituents at the aromatic rings, and hydrophobic interactions. Additionally, the β-diketone moiety carries out covalent interaction with protein thiols through Michael interactions (Michael nucleophilic addition) and acts as chelator of transient metals, thereby reducing metal-induced toxicity (Patiño-Morales et al., 2020). Certain protein interactions are mediated by π-π van der Waals interactions by the aromatic rings (**Fig. 4B**) (Hu et al.; Priyadarsini, 2013; El-Magboub et al., 2014).

Most of the health-promoting benefits of curcumin are supported by its antioxidant and anti-inflammatory activity. As already described, curcumin is a potent radical scavenger, but also increases the serum levels of native antioxidants like the enzymes superoxide dismutase (SOD), glutathione peroxidase (GSH) and lipid peroxidases (Bala et al., 2006).

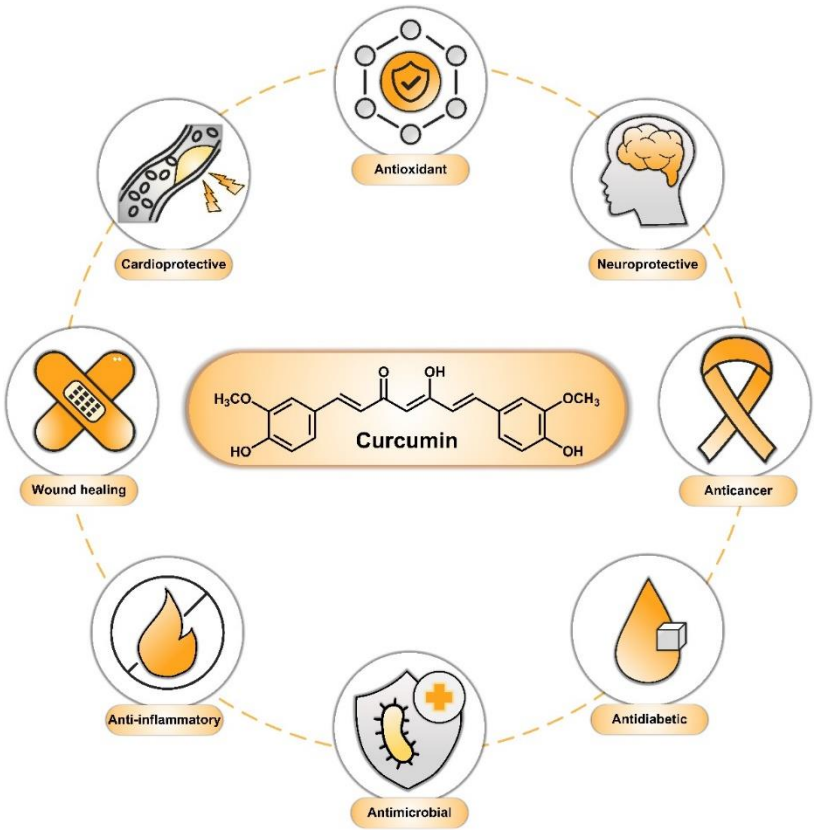

Figure 4C. Health-promoting bioactivities of curcumin. Curcumin is a multipotent polyphenolic compound that is demonstrated to exert multiple bioactivities, such as antioxidant, anti-inflammatory, and antimicrobial. These properties have been associated with neuroprotection, cardioprotection, lowering of blood sugar, wound healing, and reduction of tumor progression (Xu et al., 2018; Fu et al., 2021).

Notably, oxidative stress and inflammation are tightly connected (Reuter et al., 2010). On one hand, inflammatory cells can produce high amount of reactive species, which results in oxidative stress at the site of the inflammation. On the other hand, reactive species can trigger intracellular signalling pathways that increase the expression of pro-inflammatory genes (Reuter et al., 2010). Both, oxidative stress and inflammation, are involved in number of chronic diseases: arthritis, metabolic syndrome, cancer,

allergy, colitis, multiple sclerosis, diabetes, obesity, depression, Alzheimer's disease, Parkinson's disease, fatigue, psoriasis, cerebral injury, epilepsy, renal ischemia, and acquired deficiency syndrome AIDS (Hewlings and Kalman, 2017). Among other modes of action, curcumin has been shown to inhibit the nuclear factor (NF)-κ, a transcription factor whose dysregulation has been widely associated to inflammation, tumour development, anti-apoptosis, and metastasis (Thangapazham et al., 2006; Kunnumakkara et al., 2020).

2.4. Biosynthesis of polyketides

Infinite structural diversity of polyketides is result of heterogeneity of their respective biosynthetic machineries, called polyketide synthases (PKS) (Ray and Moore, 2016). PKS are a family of large, multifunctional enzymes that show resemblance with fatty acid synthesis (FAS) enzymes (Hopwood and Sherman, 1990). Until this point, three classes of PKS, distinguished by their structure and mode of action, have been identified: type I, II, and III (Shen, 2003). Despite compositional and mechanistic differences, enzymes from all three classes share one common feature. That is, the basic polyketide scaffold is synthesized by sequential decarboxylative condensation of coenzyme A (CoA)-activated acyl precursors, simple building blocks, derived from primary metabolism (Shen, 2003; Fischbach and Walsh, 2006). Because of this, the most often recruited polyketide precursors, acetyl-CoA and malonyl-CoA, represent key nodes connecting the primary and secondary metabolism (Shi and Tu, 2015; Yang et al., 2021a). Following parts of this subchapter will elaborate principles behind all three groups of PKSs.

Polyketide synthase type I. From all three classes of PKSs, type I has been shown to be the most intricate and the most versatile one. These catalysts are mega-enzymes, organized into modules that are further comprised of multiple, non-iteratively performing, function-specific domains (Donadio et al., 1991; Chen and Du, 2016). This kind of structural composition has led to type I PKSs also being named as modular PKSs (Kwan and Schulz, 2011). The essential domains that are contained within each module, include: acyltransferase (AT), keto synthase (KS), and acyl carrier protein (ACP). These domains select, activate and catalyse decarboxylative condensation between the nascent polyketide chain and the extender unit, creating a β-ketoacyl-*S*-ACP intermediate (Cheng et al., 2009). In some cases, additional modifications of the

intermediate can be carried out by optional domains such as: β-ketoreductase (KR), dehydratase (DH), and enoyl reductase (ER) (Sabatini et al., 2018). In principle, growing polyketide chain is passed from one module to another until the fully elongated polyketide is liberated by final domain, in linear or cyclized shape (Rath et al., 2010; Risdian et al., 2019). Although there are some isolated examples of type I polyketides that remain in linear form, such as tautomycetin (Choi et al., 2007), the fully grown polyketide chain generally undergoes process of cyclization, catalysed by the terminal domain, typically thioesterase (TE) (Fischbach and Walsh, 2006; Little and Hertweck, 2022). For this reason, type I polyketides are often regarded as macrocyclic polyketides or macrolides. Variation in catalytic domains, as well as in type of selected CoA-activated acyl precursors and extender units, affords the structural variety of polyketide molecules (Cheng et al., 2003).

Polyketide synthase type II. The principle hallmark of type II PKSs is that they are represented by several individual, mono-functional polypeptides that produce aromatic polyketides in iterative fashion (Weissman, 2009). A minimal set of enzymes that are required for assembly of type II polyketide scaffold are KS units (KS_α and KS_β) and ACP, which together make “minimal PKS”. This minimal PKS catalyses decarboxilative Claisen condensation of malonyl-CoA extender units with an acyl starter unit (Hertweck et al., 2007). During the elongation of the polyketide chain, ACP functions as an anchor for the growing chain, while KS_α catalyses condensation of the extender units (Miyanaga, 2017). The length of the polyketide-β-keto linear intermediate is defined by the number of added extender units, which is essentially controlled by KS_β unit (Szu et al., 2011). Subsequent folding pattern of the linear intermediate is determined by additional enzymes such as KR, cyclases and aromatases. Lastly, maturation of final products often involves functionalization by tailoring enzymes like oxygenases, glycosyltransferases and methyltransferases (Hertweck et al., 2007).

Type II polyketides are widespread among bacteria (Wang et al., 2020a), and streptomycetes as an outstanding producers certainly allure special attention. Oxytetracycline, doxorubicin, jadomycin B, actinorhodin, benastatin A, mithramycin and tetracenomycin C are only few examples from the wide palette of the type II polyketides naturally produced by streptomycetes (Risdian et al., 2019).

Biosynthesis of oxytetracycline as a representative of type II polyketides. Biosynthesis of the basic poly-β-ketone OTC backbone is catalysed by the minimal

PKS through successive decarboxylative Claisen condensations of eight malonyl-CoA extender units to malonate, the amidated starter unit (Pickens and Tang, 2010; Petković et al., 2017). The minimal PKS is comprised of the ketosynthase KS_{α}, KS_{β}, often regarded as chain length factor (CFL), and ACP (Zhang et al., 2007b). These enzymes are encoded by *oxyA*, *oxyB*, and *oxyC* genes from the OTC BGC, respectively (Yu et al., 2012). As in other canonical type II PKS; KS and CFL (KS_{α} and KS_{β}) associate to form a heterodimer that participates in the elongation of the poly-β-ketone by accepting acetate from malonyl-CoA extender unit, brought by malonyl-ACP (Wang et al., 2011). Transfer of the malonyl moiety to holo-ACP that results in synthesis of the malonyl-ACP intermediate is catalysed by malonyl-CoA:ACP acyltransferase (MAT) (Zhang et al., 2007a), which can be shared with fatty acid biosynthesis (Revill et al., 1995). Importantly, the amidated starter unit sets OTC, and tetracycline family of antibiotics, apart from other aromatic polyketides, which typically utilize acetate as a common starter unit (Pickens and Tang, 2010).

Amidation of the starter unit is catalysed by *oxyD* amidotransferase in ATP-dependent reaction, using glutamine as donor of the amino group. However, the exact substrate of *oxyD* is unknown, and it can be either malonyl-CoA, or malonyl-ACP (Thomas and Williams, 1983; Zhang et al., 2006; Zhang et al., 2007b). The *oxyABCD* together make the so-called the "*oxy* extended minimal PKS" (Pickens and Tang, 2010). In the subsequent enzymatic reactions, the basic skeleton of the oxytetracycline molecule is firstly reduced, and afterwards modified by cyclases and aromatases yielding in an entirely aromatised intermediate, called pretetramide. Region-specific reduction of the C9 keto group by *oxyJ* oxidoreductase directs initial folding of the linear poly-β-ketone (Zhang et al., 2006).

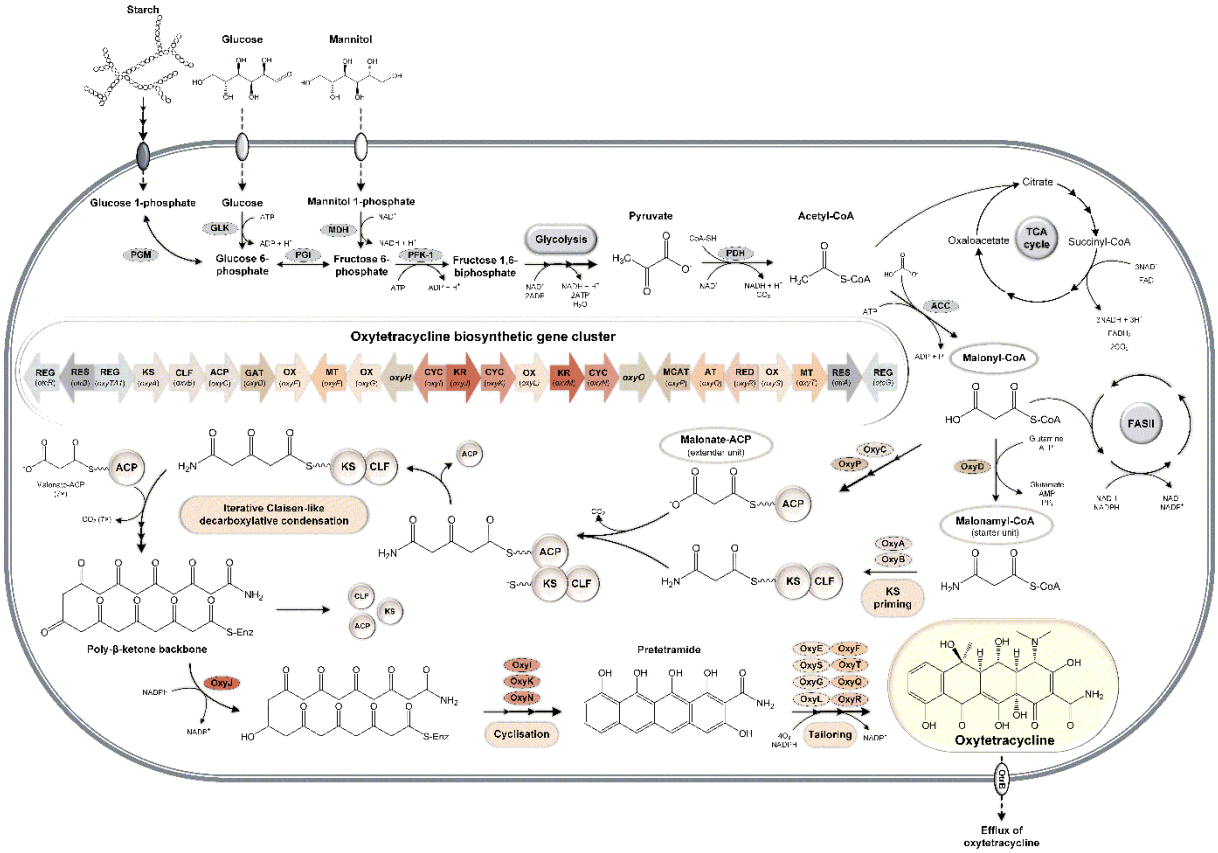

Figure 5. Biosynthesis of oxytetracycline. As illustrated, biosynthesis of the poly-β-ketone oxytetracycline backbone is catalysed by the minimal PKS. Amidated starter unit is elongated by eight acetate units from malonyl-CoA. The linear poly-β-intermediate is subsequently reduced and four distinct rings are formed, either spontaneously, or by specific cyclases/aromatases, giving the first stable intermediate designated as pretetramide. Furthermore, this intermediate is tailored and functionalized by multiple enzymes, such as methyltransferases, oxygenases, aminotransferases, and reductases, yielding in the final, fully decorated and functional OTC (Pickens and Tang, 2010; Petković et al., 2017). Abbreviations: TCA: tricarboxylic acid; FAS: fatty acid synthesis; PGM: phosphoglucomutase; GLK; glucokinase; PGI: phosphoglucoisomerase; MDH: mannitol dehydrogenase; PFK1: phosphofructokinase 1; PDH: pyruvate dehydrogenase; ACC: acetyl-CoA carboxylase; KS: ketosynthase; CLF: chain length factor; ACP: acyl carrier protein; GAT: glutamine amidotransferase; OX: oxygenase; MT: methyltransferase; KR: ketoreductase; CYC: cyclase; ARO: aromatase; MCAT: malonyl-CoA:ACP acyltransferase; AT: aminotransferase; REG: regulation; RES: resistance.

Sequentially, there are four cyclization/aromatisation steps that lead to formation of the pretetramide intermediate (Thamchaipenet, 1994). Specifically, these include first C7-C12 aldol (D) ring, second C5-C14 aldol (C) ring, third C3-C16 aldol (B) ring, and fourth C1-C18 Claisen (A) ring cyclization (Xu et al., 2016; Petković et al., 2017). The first and second ring formation is governed by *oxyK* and *oxyN* cyclases/aromatases, respectively (Petkovic et al., 1999; Zhang et al., 2007b; Zhang et al., 2008b). The following third ring cyclization occurs spontaneously (Xu et al., 2016). Due to the presence of the C2-amide moiety, the final fourth ring could also be formed spontaneously, but there are indications that this process is facilitated by *oxyI* and *oxyH*

cyclises (Lukežič et al., 2020). In the following reactions, pretetramide goes through multiple tailoring reactions catalysed by methyltransferases (*oxyF* and *oxyT*), oxygenases (*oxyL*, *oxyE*, and *oxyS*), aminotransferases (*oxyQ*) and reductases (*oxyR*) (Zhang et al., 2007b; Zhang et al., 2008b; Wang et al., 2009; Wang et al., 2013). The final product is fully functional oxytetracycline molecule, characterised by four aromatic rings and C2-amide group (**Fig. 5**) (Zhang et al., 2006; Pickens and Tang, 2010).

Polyketide synthase type III. Predominantly present in plants (Austin and Noel, 2003), type III PKSs are comprised of only a KS domain, and as such represent structurally the simplest PKSs (Palmer and Alper, 2019). Unlike the type I and type II PKSs, they do not rely on ACP to anchor the polyketide chain (Shen, 2003; Chan et al., 2009), but rather use acyl-CoAs directly as substrates (Risdian et al., 2019). Type III PKSs act in iterative manner to produce aromatic polyketides by condensation of malonyl-CoA with CoA-activated derivatives of phenylpropanoid pathway (Bisht et al., 2021). For instance, chalcone synthase (CH), a representative of plant type III PKSs, catalyse condensation of *p*-coumaroyl-CoA with three acetate units from malonyl-CoA extender molecules and intramolecular cyclization, yielding in naringenin chalcone (Álvarez-Álvarez et al., 2015), versatile bioactive compound that is shown to promote cardiovascular health (Salehi et al., 2019). Alternatively, another example of type III PKSs, named stilbene synthase (STS), uses same precursors as CH, but with different cyclization patterns to produce chemopreventive and cardioprotective agent resveratrol (Beekwilder et al., 2006; King et al., 2006). These elemental polyketides can further be modified and functionalized by rainbow of tailoring enzymes generating immense structural diversity of plant type III polyketides that include flavonoids, stilbenes and curcuminoids (Katsuyama et al., 2007; Bisht et al., 2021).

Biosynthesis of curcuminoids as an example of type III polyketides. In the natural producer, *C. longa*, curcumin and related curcuminoids are synthesized by collaborative activities of the type III PKS and the phenylpropanoid pathway. Principally, two aryl groups are derived from two molecules of L-phenylalanine through the central phenylpropanoid metabolic route (Kita et al., 2008). First, L-phenylalanine is deaminated by L-phenylalanine ammonia lyase (PAL) to cinnamic acid (Chouhan et al., 2017). Subsequently, cinnamate is step-wise activated by hydroxylation and methylation reactions into hydroxycinnamic acids: *p*-coumaric acid, caffeic acid and

ferulic acid by cinnamate 4-hydroxylase (C4H), 4-coumarate 3-hydroxylase (C3H) and caffeic acid O-methyltransferase (COMT), respectively (Rodrigues et al., 2020).

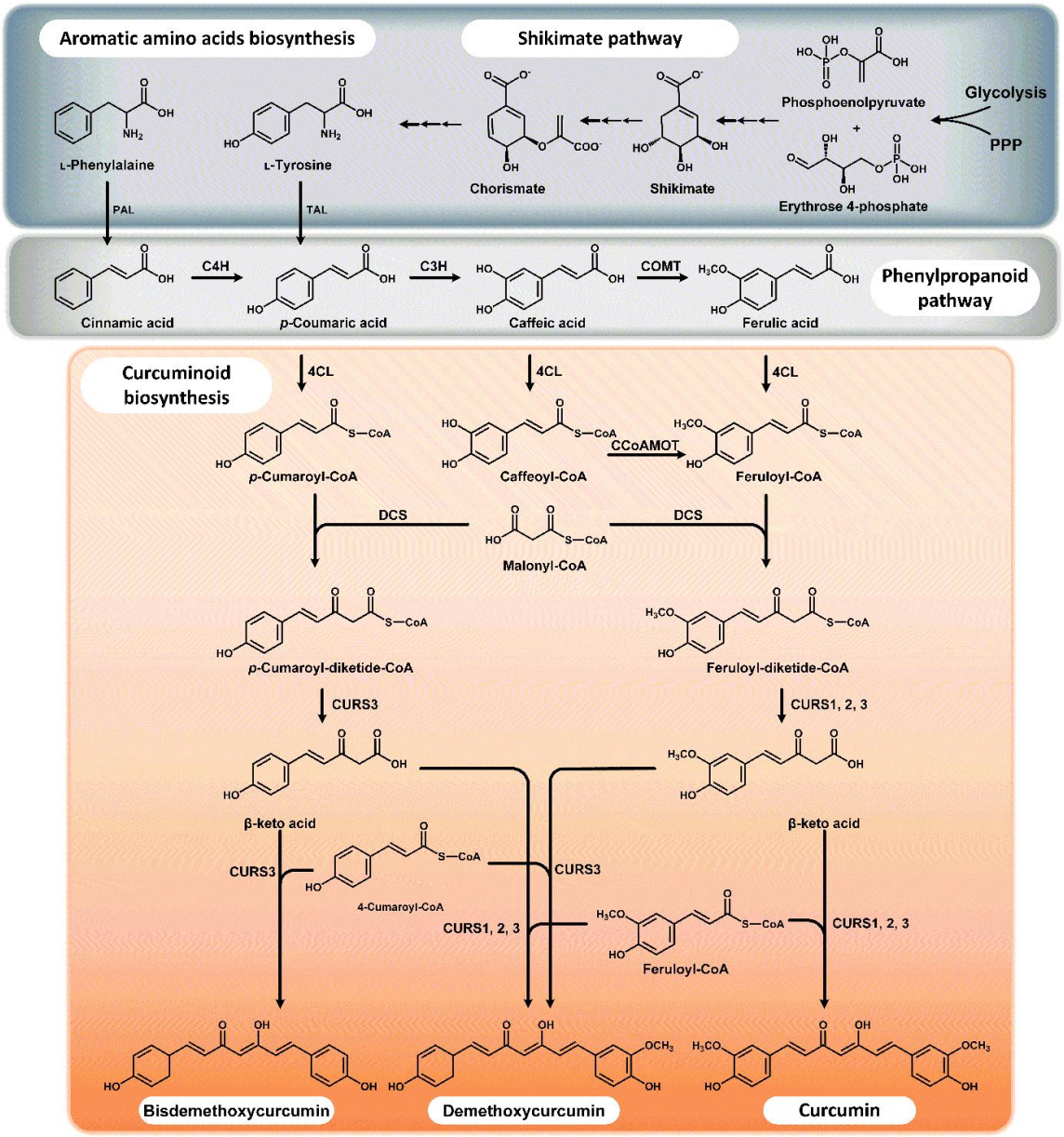

Figure 6. Biosynthesis of curcumin and related curcuminoids. The phenylpropanoid pathway is initiated by deamination of the aromatic amino acids L-phenylalanine and L-tyrosine by enzymes PAL and TAL, yielding in cinnamic and *p*-coumaric acid, respectively. Additionaly, *p*-coumaric acid can be synthetized by stepwise reaction from cinnamic acid by C4H. The final product of the phenylpropanoid pathway is ferulic acid, which is synthetized from *p*-coumaric acid via caffeic acid by C3H and COMT. The first committed reaction of the curcuminoid biosynthetic pathway is catalyzed by 4CL producing CoA-activated forms of the phenylpropanoids. Subsequently, DCS elongates feruloyl-CoA or *p*-coumaroyl-CoA for one acetate unit from malonyl-CoA, resulting in formation of β-keto acids. Finally, CURS catalyzes condensation of β-keto acids with one more unit of either feruloyl-CoA or *p*-coumaroyl-CoA. Depending on the combination of starter and elongation units, curcumin, demethoxycurcumin, or bisdemethoxycurcumin are produced. Abbreviations: PPP: pentose phosphate pathway; PAL: L-phenylalanine ammonia lyase; TAL: L-tyrosine ammonia lyase; C4H: cinnamate 4-hydroxylase; C3H: 4-coumarate 3-hydroxylase; COMT: caffeic acid *O*-methyltransferase; 4CL: 4-coumarate-CoA ligase; CCoAOMT: caffeoyl-CoA *O*-methyltransferase; DCS: diketide-CoA synthase; CURS: curcumin synthase (Rodrigues et al., 2015b).

Alternatively, *p*-coumaric acid can directly be made via deamination of L-tyrosine by L-tyrosine ammonia lyase (TAL) (Rodrigues et al., 2015a). Adjacent aryl groups are connected by central carbon unit derived from malonyl-CoA. Two type III PKS are collaboratively involved in biosynthesis of curcuminoids. Namely, diketide-CoA synthase (DCS) and curcumin synthase (CURS) (Katsuyama et al., 2009a). Further insights into native biosynthetic pathway of curcuminoids have revealed three different CURS (CURS1, 2 and 3) (Katsuyama et al., 2009b).

In order to be recruited by DCS, *p*-coumarate and ferulate first need to be activated into corresponding CoA-thioesters by 4-coumarate-CoA ligase (4CL) (Rainha et al., 2022a). DCS catalyses carboxylation of feruloyl-CoA and *p*-coumaroyl-CoA into feruloyldiketide-CoA and *p*-coumaroyldiketide-CoA (Peng et al., 2021). The curcumin synthases have dual function. Firstly, they catalyze formation of corresponding β-keto acids, and finally decarboxylative condensation of β-keto acids with another molecule of either feruloyl-CoA or p-coumaroyl-CoA (Katsuyama et al., 2011). Three CURS show different affinity for feruloyl-CoA, *p*-coumaroyl-CoA and their β-keto acids (Peng et al., 2021). *In vitro* analysis of CURS1 revealed strong preference for feruloyl-CoA, although it can accept *p*-coumaroyl-CoA as well (Katsuyama et al., 2009a). Additionally, characterization of CURS2 and CURS3 demonstrated that CURS2 prefers feruloyl-CoA, while CURS3 showed similar affinity for both feruloyl-CoA and *p*-coumaroyl-CoA (Katsuyama et al., 2009b). Practically, differential expression of three CURSs, availability of the substrate and combination of the starter and extender units, define the formation of curcumin, demethoxycurcumin, and bisdemethoxycurcumin in different ratios (**Fig. 6**) (Katsuyama et al., 2009b; Rodrigues et al., 2015b; Fadus et al., 2017).

2.5. Microbial cell factories for production of polyketides

The term microbial cell factories refers to microorganisms that have been designed and optimized for production of target molecules, preferably from renewable resources (Cho et al., 2022). The spectrum of products made by microbial fermentation includes not only bulk chemicals, but also enzymes, pigments, medicines, cosmetics, prebiotics, and nutraceuticals (Dufossé et al., 2014; Dhakal et al., 2019; Lee et al., 2019; Rangel et al., 2020). Fermentative production is often carried out under relatively low temperature and pressure conditions and it does not call for use of toxic catalysts and

solvents. As such, they serve as a valuable alternative to the traditional chemical synthesis or extraction methods (Yixuan et al., 2021; Cho et al., 2022). In their natural environment, microbes are typically not optimized for efficient production of desired molecules from wanted feedstocks. Metabolic engineering technologies enable evading these bottlenecks and designing a robust host for overproduction of molecules of interest, both native and non-native to its metabolism (Rangel et al., 2020).

Design-Build-Test-Learn cycle. Metabolic engineering of the microbial cell factories encompasses four fundamental modules: design, build, test, and learn (Liu and Nielsen, 2019). First, design (D) of biological system involves careful selection of a host and *in silico* construction of the biosynthetic pathway for the production of the compound of interest. Host selection is influenced by available feeds, toxicity of the product and processing conditions for midstream production and downstream purification (Nielsen and Keasling, 2016). *E. coli* and *S. cerevisiae* are two of the most commonly used hosts for microbial-based production of target compounds (Ferrer-Miralles and Villaverde, 2013; Kavšček et al., 2015). However, in certain instances they might not be the most suitable choice. Therefore, other microbes with more superior physiological background, such as actinomycetes for production of antibiotics and other polyketides, and *C. glutamicum* for lignin valorisation, are emerging as more attractive hosts (Becker and Wittmann, 2019; Choi et al., 2019; Cho et al., 2022). Next, build (B) the biological system using inputs from D and available tools of synthetic biology. Third, test (T) the biological system under specified physiological conditions using “omics” methods, and lastly learn (L) from the integrated data and apply this knowledge for improvements of the DBT modules of the cycle and host optimization (Nielsen and Keasling, 2016).

Systems biology tools in systems metabolic engineering. Systems metabolic engineering is an emerging field that combines classical metabolic engineering with advances in systems biology, synthetic biology, and evolutionary engineering (Alper and Wittmann, 2013) It aims to understand microorganisms as complex systems in which observed phenotypes are result of intertwining of networks of genes, proteins, and metabolites (Rangel et al., 2020). Systems biology is an approach to examine perplex biological systems through high-throughput measurements of various levels of cellular organisations, including genome (genomics), transcriptome (transcriptomics), proteome (proteomics), metabolome (metabolomics), and metabolic fluxes (fluxomics)

(Choi et al., 2019; Dhillon et al., 2020). These methodologies, collectively named as “omics” technologies, allow for rapid strain characterization under defined physiological conditions (Rangel et al., 2020). As the flow of biochemical information in the cell is not straightforward, but rather multidirectional and comprises interactions between different levels of “omes”, it is highly recommended to evaluate the biological systems on multiple levels, in what is called “multi-omics” profiling (Amer and Baidoo, 2021).

The advent of computational biology tools enables integration of “big data” obtained by “omics” technologies into actionable knowledge (Tavassoly et al., 2018) that can aid in understanding of the metabolism and physiology of the organisms (Nielsen et al., 2022). Additionally, genome-scale metabolic reconstructions combine systems biology and mathematical modelling to predict biological capabilities of the organisms, eliminating the need to test all experimental conditions which significantly reduces duration of the DBTL cycle (O’Brien et al., 2015).

Homologous recombination for targeted genome based engineering. Homologous recombination is a natural process that occurs across all domains of life and viruses (Porteus, 2007). This universal biological mechanism involves exchange between two identical or similar fragments of double-stranded or single-stranded nucleic acids. Functionally, homologous recombination facilitates genetic rearrangements introducing genetic variability, repairs double-stranded DNA (dsDNA) breaks, or mediates interspecial horizontal gene transfer (Thompson and Schild, 2001; Bailly et al., 2007; Krejci et al., 2012). Scientifically, homologous recombination can be used as a powerful tool for precise targeted genome based modifications, including deletions, replacements and insertions (Porteus, 2007).

In *C. glutamicum*, homologous recombination is widely used site-directed genome engineering (Lobanova et al., 2022). This methodology relies on the application of integrative plasmids, which cannot replicate within the bacterial host (Nešvera and Pátek, 2011). These plasmids can be maintained only in case of single-crossover by homologous recombination between homology regions flanking the integration construct and the desired genome region. For marker-less modifications, second single-crossover homologous recombination must take place (Lobanova et al., 2022). This second recombination event is often initiated with counter-selectable markers, such as *Bacillus subtilis* levansucrase *sacB* (Tan et al., 2012). Expression of *sacB* in *C. glutamicum* leads to lethal sucrose sensitivity (Jäger et al., 1992). Therefore, second

recombination event and loss of the vector backbone carrying the sacB marker is necessary for survival (Reyrat et al., 1998).

Lambda Red-mediated recombineering. The phage λ-derived homologous recombination systems is a powerful strategy for targeted genome based engineering (Poteete, 2013). The system relies primarily on three Red (recombination-defective) proteins from the phage λ: Exo, Beta, and Gam, which are normally involved in the integration of the λ prophage into the *E. coli* genome *via* site-specific homologous recombination (Poteete, 2001; Groth and Calos, 2004; Poteete, 2013; Murphy Kenan, 2016). Therefore, genetic engineering based on this approach coined the procedure called recombineering (recombinational engineering). Essentially, λ-Red system has been developed based on the findings that genomic modifications in *E. coli* can readily be accomplished by recombination with a PCR-generated selectable marker in a presence of the λ-Red proteins. Notably, the PCR-generated templates need to be flanked with short sequences homologous to the target region on bacterial chromosome (Gust et al., 2003). In practice, the λ-Red system facilitates simple, fast and efficient generation of insertions, deletions, and point mutations on bacterial or artificial plasmids and linear targets introduced into *E. coli* by transformation (Mosberg et al., 2010; Poteete, 2013).

The genes encoding the Red proteins, *exo*, *beta*, and *gam*, are clustered within the P_L operon of the phage λ (Poteete, 2001). Exo is a exonuclease that degrades (dsDNA) in a 5' to 3' direction, creating long, intact 3' single-stranded DNA (ssDNA) overhangs (Katashkina et al., 2009). The ssDNA overhangs are further stabilized by Beta that facilitates recombination with the homologous genomic targets (Sawitzke et al., 2007). Gam binds and inhibits the RecBCD and SbcCD *E.coli* nucleases, thereby preventing the degradation of the introduced linear dsDNA fragments (Court et al., 2002). For the recombineering with a dsDNA template, all three components are required, while in case when an ssDNA substrate is used, Beta is sufficient to carry out the recombination.

The λ-Red system is routinely applied for targeted genome based engineering of *Streptomyces* species (Li et al., 2021c). It has been proven to be an efficient method for the deletion of the entire secondary metabolite BGCs (Gust et al., 2003). In order to apply the λ-Red system in *Streptomyces*, the strategy requires few modifications. First, the disruption cassette must include *oriT* (origin of transfer) sequence, which is

needed for its conjugal transfer from *E. coli* mating host to *Streptomyces*. Moreover, *Streptomyces* are typically equipped with a strong methyl-specific restriction of the introduced DNA. In order to evade this restriction, *E. coli* host for conjugation should be methylation-deficient (Gust et al., 2004).

Remarks associated with microbial production of polyketides. When the desired compounds are of polyketide origin, hosts that are equipped with the ability to synthetize a comprehensive extent of CoA-activated precursors are a more favourable option (Pfeifer and Khosla, 2001). Indeed, PKS can employ diverse substrates such as acetyl-CoA (Cardenas and Da Silva, 2016), propionyl-CoA (Wiesmann et al., 1995), isobutyryl-CoA (Cropp et al., 2001), isovaleryl-CoA (Samappito et al., 2003), malonyl-CoA (Pickens and Tang, 2010), methylmalonyl-CoA (Marsden et al., 1994), ethylmalonyl-CoA (Liu and Reynolds, 2001), *p*-coumaroyl-CoA (Palmer et al., 2020), and feruloyl-CoA (Katsuyama et al., 2009a). Notably, supply of these precursors needs to be well coordinated with the biosynthesis of polyketides, as their metabolic pools are tightly regulated. On top of that, host needs to provide adequate phosphopantetheinyl transferase (PPTase) that is involved in posttranslational activation of the ACP. Namely, in the functional ACP, a thiol group of a 4'-phosphopantetheine group is covalently attached to the conserved serine residue within the active site of the ACP (Weissman et al., 2004). Although PPTases exist in all prokaryotes and eukaryotes, they can be selective in terms of substrate choice. Therefore, it is necessary to ensure an expression and activity of the proper PPTase (Pfeifer and Khosla, 2001). Finally, as polyketides are biologically active molecules, it is needed to provide resistance mechanism to the inhibitory effects of the polyketide (Watanabe and Oikawa, 2007). Self-resistance genes are often cognate part of the polyketide BGCs. As an example, *S. rimosus* oxytetracycline BGC includes three resistance genes: ribosomal protection protein (*otrA*) and two efflux proteins (*otrBC*). Coordinate upregulation of these genes improved the production of oxytetracycline by 179% compared to the wild-type strain (Yin et al., 2017).

Actinobacteria as superior microbial cell factories. As a result of their pronounced potential for production of biologically active compounds, *Actinobacteria* represent attractive microbial cell factories for production of polyketide and other compounds that find application in pharmaceutical, agricultural, environmental, and industrial sphere (Nakashima et al., 2005). Generally speaking, they are Gram-positive bacteria with

genomes of moderate to high GC content (Ul-Hassan and Wellington, 2009) that can thrive in diverse ecosystems, including terrestrial and aquatic environments with temperate, or even extreme conditions (Qin et al., 2016). Some species even form symbiotic relationships with other organisms such as invertebrates (Himaya and Kim, 2013). Two striking features stand out *Actinobacteria* as a suitable host for microbial-based production. Foremost, they exhibit peculiar metabolic capabilities (Nakashima et al., 2005). It is not uncommon for actinobacterial genomes to encode dozens of secondary metabolites, or enzymes that enable them to catabolize complex polymers, like lignocellulose (Větrovský et al., 2014). Secondly, *Actinobacteria*, unlike *E. coli*, are not covered with the lipopolysaccharide envelope, thereby exhibiting reduced toxicity and more convenient system for production (Sutcliffe, 2010).

Actinomycetes is a class within the phylum of *Actinobacteria*. They are an omnipresent group of Gram-positive bacteria, are a source of nearly 50% of all NPs of microbial origin (Selim et al., 2021). Within this group, spore-forming *Streptomyces* genus attracts peculiar interest, since close to 80% of known antibiotics stem from from this genus alone (Dharmaraj, 2010). *Streptomyces* appear to have fungal-like filamentous morphology. They are characterized by remerable metabolic diversity and production of wide array of secondary metabolites (Holtmann et al., 2017; Manteca and Yagüe, 2018). This prominent metabolic versatility equipped them with an ability to colonize and thrive in diverse environmental conditions, including soil (Schlatter et al., 2009), saltwater (Mohamed and Chaudrhy, 2005), freshwater (Shaikh et al., 2015), desert (Rateb et al., 2011), frozen soil (Zhang et al., 2016), and volcanic environments (Sivalingam et al., 2019).

Notably, nearly 10,000 medically and industrially relevant NPs (Anandan et al., 2016), including myriad of antibiotics (Manteca and Yagüe, 2018), antifungals (Prapagdee et al., 2008), anticancers (Sivalingam et al., 2019), antiparasitics (Sun et al., 2002), immunosupressants (Sun et al., 2002), enzymes (El-Naggar, 2021), and pigments (Zhang et al., 2023) are derived from this taxa, solely. Given their strong in-built ability to produce valuable NPs, *Streptomyces* are often utilized as microbial cell factories for industrial scale production of polyketides and other NPs. Some selected examples of typically employed species as cultivation platform include: *Streptomyces coelicolor* (Sohoni et al., 2012), *Streptomyces lividans* (Rückert et al., 2015), *Streptomyces albus* (Lopatniuk et al., 2017), *Streptomyces avermitilis* (Ding and Ye, 2023), and *S. rimosus*

(Wang et al., 2019), for production of polyketide antibiotics actinorhodin (Scaffaro et al., 2016), soraphen A (Zirkle et al., 2004), salinomycin (Wei et al., 2022), avermectin (Ikeda et al., 2001), and oxytetracycline (Wang et al., 2019), respectively.

C. glutamicum is a Gram-positive, facultative anaerobic, soil bacterium with moderate to high GC content that belongs to the phylum of actinobacteria (Ikeda and Nakagawa, 2003; Wolf et al., 2021). Number of characteristics make *C. glutamicum* a suitable host for fermentative production of compounds. (a) It is non-pathogenic organism with a generally regarded as safe (GRAS) status that does not form spores and grows rather fast to high cell densities on a large scale (≥750 cubic meters) (Wolf et al., 2021; Cankar et al., 2023). (b) It is endotoxin free microbe that is not prone to phage-induced lysis (Song et al., 2012; Schwardmann et al., 2022). (c) *C. glutamicum* is able to utilize diverse carbon substrates (such as sugars, sugar alcohols, organic acids, and aromatic compounds), as well as substrate mixtures such as hydrolysed lignocellulosic biomass and waste streams, thereby supporting the circular economy (Becker and Wittmann, 2017; Wolf et al., 2021). (d) The microbe exhibits high tolerance to toxic compounds and other form of stress, making it a robust cell factory for production of bulk and variety of high-value molecules (Liu et al., 2021).

C. glutamicum has been used for decades as a principal industrial producer of amino acids in white biotechnology (Wendisch et al., 2016; Becker et al., 2018b). Nearly 6 million tons of L-glutamate and L-lysine produced by fermentation of *C: glutamicum* each year, demonstrate the scope of its relevance (Becker et al., 2018b). The insights into the gene expression and regulation, protein secretion, and cellular metabolism of the microorganism enabled its streamlining into a comprehensive producer of various added-value compounds including pharmaceuticals and nutraceuticals (Joo-Young et al., 2016; Liu et al., 2021). Many of these compounds are of polyketide origin, such as 6-methylsalicylate (Kallscheuer et al., 2019), kaempferol (Kallscheuer et al., 2017), resveratrol (Kallscheuer et al., 2016b), piceatannol (Kallscheuer et al., 2016b), naringenin (Kallscheuer et al., 2016b), quercetin (Kallscheuer et al., 2017), and noreugenin (Milke et al. 2019).

3. Systems biology of oxytetracycline production in *S. rimosus*

3.1. Materials and methods

3.1.1. Microorganisms

Streptomyces rimosus ATCC 10970 (American Type Culture Collection, Manassas, VA, USA), its oxytetracycline producing derivative *S. rimosus* HP126, as well as derivative of the industrial producer with deleted oxytetracycline BGC (*S. rimosus* HP126 Δv3) (Beganovic, et al. 2023; submitted to Microb. Cell Fact.) were used in this work. The industrial producer was kindly donated by Prof. Hrvoje Petkovic (Biotechnical Faculty, University of Ljubljana, Slovenia). For strain maintenance, spores were stored in 20% ($^{v}/_{v}$) glycerol at -80°C.

3.1.2. Media and cultivation

Strains were propagated on mannitol soy (MS) agar (20.0 g L^{-1} mannitol, 20.0 g L^{-1} soy flour (Schoenenberger Hensel, Magstadt, Germany) and 20.0 g L^{-1} agar (Becton & Dickinson, Heidelberg, Germany) plates at 30°C for (Kieser et al., 2000) 7 days, upon which the sporulating mycelium was amended with 5 mL sterile deionized water. Afterwards, spores from 4 agar plates were collected using a glass cell spreader, centrifuged (5,500 × *g*, 4°C, 6 min), and the obtained pellet was resuspended in 4 mL 20% ($^{v}/_{v}$) ice-cold glycerol. The content of viable spores was determined using serial dilutions that were prepared in triplicate from the obtained stock and plated on Tryptone Soy Broth (TSB) (30.0 g L^{-1}) agar (Sigma Aldrich, Steinheim, Germany).

For production of oxytetracycline in complex medium, vegetative and production medium were used. The vegetative medium contained per litre: 30.0 g corn starch (Sigma Aldrich), 5.0 g NaCl, 4.0 g $CaCO_3$, 4.0 g corn steep liquor (Sigma Aldrich), 4.0 g $(NH_4)_2SO_4$, 3.0 g soy flour, 150.0 mg KH_2PO_4. The oxytetracycline production medium contained per litre: 75.0 g corn starch, 10.0 g soy flour, 7.0 g $CaCO_3$, 7.0 g $(NH_4)_2SO_4$, 2.50 g corn steep liquor, 2.0 g NaCl, 75.0 mg amylase (Sigma Aldrich), 75.0 mg KH_2PO_4, 5.0 mg $CoCl_2$. The pH of the medium was adjusted to 7.0 with 6M NaOH.

In order to choose an appropriate simple sugar, which is favourable for production of oxytetracycline in a minimal medium, a sugar screening experiment was carried out. *S. rimosus* ATCC10970 was first grown in 50 mL of a complex mannitol LB medium (20.0 g L^{-1} LB and10.0 g L^{-1} mannitol) in 500 mL baffled shake flask for 24 h. Next, a second pre-culture (0.30 g L^{-1} KH_2PO_4) was inoculated in mannitol-based minimal medium, and finally a main culture (0.15 g L^{-1} KH_2PO_4) with a varying, single carbon source. The main culture was inoculated in 5 mL medium in test tubes and cultivated at 30°C, 230 rpm and 80% humidity. All experiments were carried out in triplicates, together with Wei Shu (Institute for Systems Biotechnology, University of Saarland, Saarbrücken, Germany).

For production of oxytetracycline in minimal medium, previously established mineral salt medium, which was shown to promote growth of related *Streptomyces* species was adapted (Gläser et al., 2020). The medium contained per litre: 20.0 g MOPS, 10 g mannitol (Sigma Aldrich), 15.0 g $(NH_4)_2SO_4$, 1.0 g NaCl, 0.15 g KH_2PO_4, 0.20 g $MgSO_4 \cdot H_2O$, 55.0 mg $CaCl_2$, 20.0 mg $FeSO_4 \cdot 7H_2O$, 7.20 mg $CoCl_2 \cdot 2H_2O$, 2.0 mg $FeCl_3 \cdot 6H_2O$, 2.0 mg $MnSO_4 \cdot H_2O$, 1.0 mg nicotinamide, 1.0 mg riboflavin, 0.50 mg pyridoxine·HCl, 0.50 mg thiamine·HCl, 0.50 mg $ZnSO_4 \cdot H_2O$, 0.20 mg biotin, 0.20 mg $CoCl_2 \cdot 2H_2O$, 0.20 mg $Na_2B_4O_7 \cdot 10H_2O$, 0.10 mg 4-aminobenzoic acid, and 0.10 mg $(NH_4)_6Mo_7O_{24} \cdot 4H_2O$. The concentration of KH_2PO_4 in the minimal medium amounted to 0.15 g L^{-1} in order to trigger production of oxytetracycline (McDowall et al., 1999).

3.1.3. Production of oxytetracycline in complex medium

Batch cultivation in complex medium was conducted in 500 mL non-baffled shake flasks filled with 50 mL medium on a rotary shaker at 30°C, 230 rpm and 80% humidity (Multitron, Infors AG, Bottmingen, Switzerland) in a two-step manner. The first pre-culture in the vegetative medium was inoculated to an initial spore concentration of 1 × 10^7 spores mL^{-1} and grown for 24 h. Subsequently, 5 mL of the first pre-culture was used to inoculate the main culture in the production medium and the main cultures were grown for 120 h. All experiments were conducted in triplicate.

3.1.4. Production of oxytetracycline in minimal mediumn

Batch cultivation was carried out in 500 mL baffled shake flasks with 50 mL medium on a rotary shaker at 30°C, 230 rpm and 80% relative humidity. Hereby, cultivation, involved a first pre-culture in complex mannitol LB medium (20.0 g L^{-1} LB and10.0 g L^{-1} mannitol), a second pre-culture in mannitol-based minimal medium (0.30 g L^{-1} KH_2PO_4) and a main culture in mannitol-based minimal medium at reduced phosphate level (0.15 g L^{-1} KH_2PO_4). The first pre-culture was inoculated to an initial spore concentration of 1 × 10^7 spores mL^{-1} and grown for 24 h. Subsequently, cells, were harvested (8,500 × *g*, room temperature, 5 min), washed once and used to inoculate the second pre-culture to an initial cell concentration of 0.50 g cell dry weight (CDW) L^{-1}. The second pre-culture was grown for 15 h, followed by cell harvesting and washing (8,500 × *g*, room temperature, 7 min), and inoculation of the main culture to an initial cell concentration of 0.50 g L^{-1}. All experiments were done in triplicate.

3.1.5. Quantification of cell concentration

Cell broth was collected by vacuum filtration using a nitrocellulose filter (Ø 0.20 µm, Sartorius, Göttingen, Germany). Cells were washed twice with an equivalent volume of 0.90% NaCl, and their dry weight was quantified using a moisture analyser (HB43-S, Mettler-Toledo, Columbus, OH, USA) as described before (Kuhl et al., 2020). In addition, the cell concentration was analysed as optical density (OD) at a wavelength of 600 nm (UV-1600PC spectrophotometer, VWR, Hannover, Germany). For early phases of the cultures, this yielded a linear correlation between cell dry mass and optical density, as previously observed for other strains of *Streptomyces* (Kuhl et al., 2020). The correlation factor differed between the strains: CDW [g L^{-1}] = 0.917 × OD_{600} (*S. rimosus* ATCC 10970), CDW [g L^{-1}] = 0.412 × OD_{600} (*S. rimosus* HP126 and *S. rimosus* HP126 Δv3). The correlation allowed to infer cell dry weights from OD readings during the first 8 h in which samples did not provide enough cells for precise gravimetric analysis (Kuhl et al., 2020). All measurements were conducted in triplicate.

3.1.6. Quantification of mannitol and phosphate

Mannitol was analysed in culture supernatant by HPLC (Agilent 1260 Infinity Series, Agilent Technologies, Waldbronn, Germany) using ion-moderated partition

chromatography on a reversed phase column as stationary phase (Aminex HPX-87H, Bio-Rad, Hercules, CA, USA) and 7 mM H_2SO_4 (0.50 mL min^{-1}, 65°C) as mobile phase. Mannitol was quantified by refractive index detection and external standards.

The phosphate level in culture supernatant was analysed by anion exchange chromatography (Thermo Scientific, Karlsruhe, Germany) using a Dionex IonPac AS9-HC column as stationary phase (2 mm × 250 mm, Thermo Scientific) and 12 mM Na_2CO_3 (0.25 mL min^{-1}, 30°C) as mobile phase. The phosphate ions were quantified using suppressed conductivity detection and external standards.

3.1.7. Quantification of oxytetracycline

First, oxytetracycline was extracted from culture broth. For this purpose, a 250 µL broth sample was acidified to pH 1.5 using 37% HCl, incubated on ice for 15 minutes, and centrifuged (16,000 × *g*, 4°C, 10 min). The obtained supernatant was analysed by HPLC (Agilent 1260 Infinity Series, Agilent Technologies, Waldbronn, Germany) on a reversed phase column (Nucleodur C18 Isis, 3 µm, 100 mm × 3 mm, Macherey-Nagel, Düren, Germany) using a gradient of 0.10% formic acid (eluent A) and methanol (eluent B) at 0.80 mL min^{-1} and 40°C. The fraction of eluent B in the gradient was as follows: 0-7 min, 0%; 7-8 min, 0-32%; 9-11 min, 32-100%; 12-15 min, 100-0%. Oxytetracycline was detected at 275 nm using a diode-array detector and quantified using external standards.

3.1.8. Analysis of morphology

Ten microliters of culture sample, collected at 8, 24, 48 and 72 h, were transferred on object glass, covered by a plastic cover glass, and observed under bright-field microscope (Olympus IX microscope, Hamburg, Germany). The software ImageJ 1.53 (Schneider et al., 2012) was used to automatically determine the Feret diameter of the pellets, formed by *S. rimosus*, representing the smallest circle into which a pellet fit, (Kuhl et al., 2020). At least 100 aggregates were analysed per sample.

3.1.9. Transcriptome analysis

Transcription profiling was performed as described previously (Kuhl et al., 2020). In short, cells were collected by centrifugation (20,000 x *g*, 4 °C, 1 min), and the obtained pellet was immediately frozen in liquid nitrogen. Total RNA was isolated (Quick-RNA Miniprep Plus kit, Zymo Research, Freiburg, Germany), purified (RNA Clean & Concentrator-5 kit, Zymo Research, Freiburg, Germany), and quantified (DropSense 16, Trine an NV, Gentbrugge, Belgium). The quality of the obtained RNA was validated (RNA 6000 Nano kit, Agilent 2100 Bioanalyzer, Agilent Technologies). Then, 2.5 µg of total RNA (RIN > 9) was depleted from rRNA (Ribo-Zero rRNA Removal Kit Bacteria, Illumina, San Diego, CA, USA). The completeness of the depletion was checked (Agilent RNA Pico 6000 kit, Agilent 2100 Bioanalyzer, Agilent Technologies). The obtained mRNA was converted to a cDNA library (TruSeq Stranded mRNA Sample Preparation Guide, Illumina, San Diego, CA, USA). After quality control and quantification (Agilent High Sensitivity DNA kit, Agilent 2100 Bioanalyzer, Agilent Technologies), all created cDNA libraries were sequenced using a 75-base read length (NextSeq 500, Illumina). The obtained reads were mapped to the genome of strain R7 (chromosome and plasmid) with Bowtie2 using standard settings (Langmead and Salzberg, 2012) except for increasing the maximal allowed distance for paired reads to 600 bases. ReadXplorer 2.2.3 was used to visualize read alignments (Hilker et al., 2016). For counting reads mapping to gene features, FeatureCounts v.2.0.0 (Liao et al., 2014) was applied using the parameters -M -O and -s 1. With the resulting data, DESeq2 (Love et al., 2014) was used to QC the datasets via several methods, including calculation of the sample-to-sample distances. In addition, DESeq2 was used to calculate DGE datasets. Raw datasets (sequenced reads) as well as processed datasets (input matrix and normalized read counts from DESeq2) are available from GEO (GSE168592). For statistical analysis, Student's t test was carried out, and the data were filtered for genes with a log2-fold change ≥ 1 ($p \leq 0.05$).

Transcriptome profiling was kindly carried out by Christian Rückert-Reed Thomas Patschkowski, Ben Struck, and Jörn Kalinowski as part of collaboration with the Center for Biotechnology (Bielefeld University, Bielefeld, Germany).

3.1.10. Quantification of intracellular CoA-thioesters

The analysis of CoA-thioesters was adapted from recent work (Gläser et al., 2020). In short, culture samples (5 mg CDW) were quenched with an appropriate amount of quenching and extraction buffer (25 mM formic acid, 95% acetonitrile, -20°C). Extraction of the intracellular CoA-thioesters was then accomplished through mixing and cooling steps on ice for 10 minutes, followed by centrifugation (15,000 × *g*, 4°C, 10 min) and collection of the obtained supernatant into 10 mL ice-cold deionized water. The cell pellet was washed two times with 8 mL ice-cold water, and all supernatants were put together afterwards. The extracts were frozen in liquid nitrogen, freeze-dried, and subsequently resuspended in 500 µL pre-cooled buffer (25 mM ammonium formate, 2% MeOH, pH 3.0, 4°C). The buffered extracts were clarified from debris (15,000 × *g*, 4°C, 10 minutes).

Analysis of the extracts was carried out using a triple quadrupole MS (QTRAP 6500, AB Sciex, Darmstadt, Germany), coupled to an LC system (Agilent 1290 Infinity System, Waldbronn, Germany). The analytes of interest were separated on a reversed phase column (Gemini, C18, 100 mm × 2.1 mm, 1.5 µm, 110 Å, Phenomenex, Aschaffenburg, Germany) at 40°C and a flow rate of 0.60 mL min^{-1}, using a gradient of eluent A (50 mM formic acid, pH 8.1) and eluent B (methanol). The fraction of eluent B was as follows: 0-12 min, 0-15%; 12-16 min, 15-100%; 16-18 min, 100%; 18-20 min, 100-0%; 20-25 min, 0%.

For absolute quantification, ^{13}C-labelled cell extracts were used as internal standard (Gläser et al., 2020). For this purpose, *S. rimosus* was grown on 99% [$^{13}C_6$] mannitol (Omicron, Biochemicals, South Bend, United States). To obtain fully ^{13}C-enriched cell extracts, the inoculum size for both the second pre-culture, as well as for the main culture, was kept below 1% of the finally harvested cell concentration (Wittmann, 2007). Extraction of the ^{13}C CoA-thioesters was conducted as described above. The concentration of individual ^{13}C CoA-thioesters was determined using synthetic standards. For later absolute quantification, an appropriate amount of ^{13}C extract was added to the samples during the initial quenching step (Gläser et al., 2020).

3.2. Results and discussion

3.2.1. Production of oxytetracycline in complex and minimal medium

S. rimosus ATCC10970 and its derivative *S. rimosus* HP126 were cultivated in a complex, industrial medium for production of oxytetracycline for 120 h. During this time, the mutagenized *S. rimosus* HP126 accumulated 4.49 ± 0.04 g L^{-1} oxytetracycline (**Fig. S1A**), demonstrating gram-scale production capacity of this strain.

Mannitol can be used as a sole carbon source for efficient oxytetracycline production. In order to deduce the cellular responses, contributing to the extraordinary production potential of *S. rimosus* HP126, simplified medium that would enable conducting multi-omics analysis had to be used. For this purpose, the wild type strain was cultivated in the phosphate limiting medium supplemented with different simple sugars. From tested carbon sources, cultivation in mannitol-based medium resulted with highest oxytetracycline titre (17 ± 4 mg L-1) (**Fig. S1B**). Therefore, mannitol was selected as a carbon source for further studies in minimal medium.

S. rimosus ATCC 10970 was studied in a batch process, using a phosphate limiting, mineral salt medium with mannitol as a sole carbon source (**Fig. 7A, C**). Within 96 h, the strain completely utilised the provided substrate and achieved a final oxytetracycline titre of 27 ± 2 mg L^{-1}. Along the process, the strain went through three culture phases. Initially, the microbe exhibited an exponential growth and reached its maximum growth rate (μ = 0.16 ± 0.0 h^{-1}), which ended after 4 h with exhaustion of the supplied phosphate. The subsequent transition phase was marked by reduced growth, and finally, cells entered into a stationary phase. The initial growth phase was characterised by acidification of the culture medium to a pH of 5.5. Regarding oxytetracycline production, the specific productivity was the highest during the stationary phase (**Fig. 7A, C**).

Next, the classical mutant *S. rimosus* HP126, previously derived from *S. rimosus* ATCC 10970, was studied under the same cultivation conditions. Over a culture period of 120 h, the mutant accumulated 340 ± 17 mg (oxytetracycline) L^{-1}, 12-fold more than the parent wild type, demonstrating remarkable production capacity of the classically mutagenized *S. rimosus* HP12. In comparison, it grew slightly faster during the initial growth phase (μ = 0.19 ± 0.0 h^{-1}). Hereby, the producer exhibited an almost two-fold higher specific phosphate uptake rate (q_{PO4^-} = 12.9 ± 3.8 mg g^{-1} h^{-1}), which led to an

earlier onset of phosphate limitation, and triggered production of oxytetracycline already after 4 h. The exponential growth phase of the mutant strain was followed by a phase of reduced growth, after which the strain entered the stationary phase that lasted until complete depletion of mannitol. Overall, the productivity of oxytetracycline increased linearly until 30 h, and maintained at this level until the end. The average productivity during this time was 1.1 ± 0.0 mg g^{-1} h^{-1}. The pH of the culture broth initially decreased, and stabilised at pH 5.5 during the stationary phase (**Fig. 7B, D**).

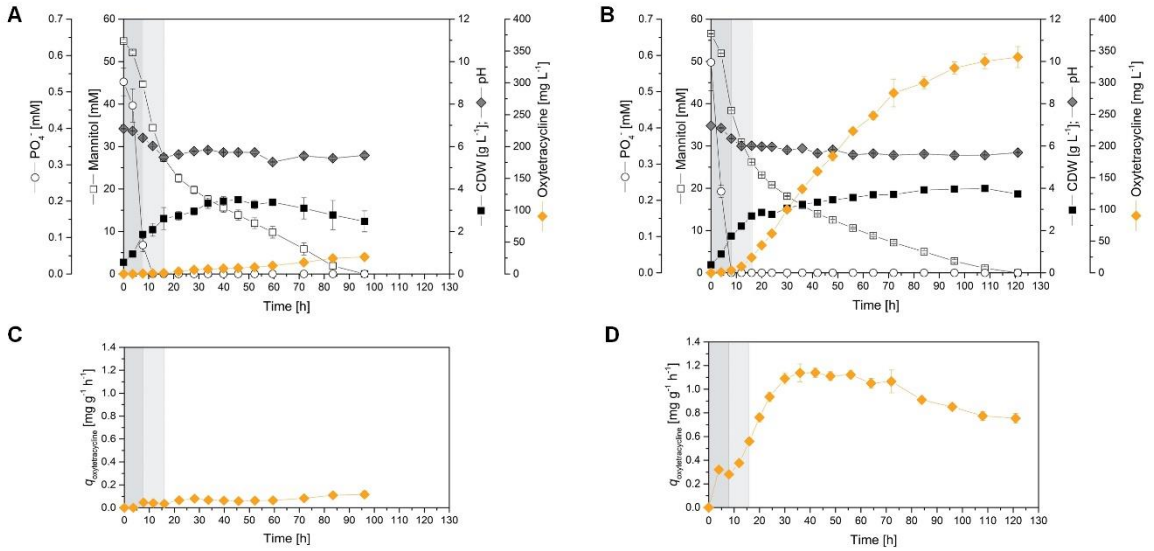

Figure 7. Production of oxytetracycline in the wild type *S. rimosus* ATCC 10970 and its classically derived derivative *S. rimosus* HP126. *S. rimosus* ATCC 10970 (**A**, **C**) and *S. rimosus* HP126 (**B**, **D**) were grown in mannitol-based mineral salt medium, which initiated oxytetracycline production through phosphate limitation (Petkovic et al., 2006). The time profiles show the consumption of mannitol and phosphate, the formation of cell dry weight (CDW), the production of oxytetracycline and the pH. The different exponential growth, transition, and stationary phases are highlighted by different shades of grey. The data were used to calculate the specific oxytetracycline productivity over time in *S. rimosus* ATCC 10970 (**C**) and *S. rimosus* HP126 (**D**), respectively. n = 3

3.2.2. Morphology of the *S. rimosus* ATCC10970 and HP126

Microscopic analysis of *S. rimosus* ATCC 10970 revealed that the strain formed dense pellets of pronounced size heterogeneity (**Fig. 8**). Namely, the Feret diameter differed up to tenfold between different pellets (36 µm to 327 µm). Additionally, protruding filaments were noticeable at the pellet surface (**Fig. 8A**). These were present already during exponential growth and became more pronounced during later stages. In addition, pellet aging was characterised by fragmentation and disintegration processes inside the aggregates (**Fig. 8C, E, G**). The morphology of *S. rimosus* HP126 strain was very different. Unlike the wild type, the mutant did not form pellets, but rather loose

mycelial networks of hyphae, corresponding more to a mat-type morphology (**Fig. 8B, D, F, H**). During the process, the morphology of the mutant was not severely impacted by aging of the culture and imposed mechanical stressed.

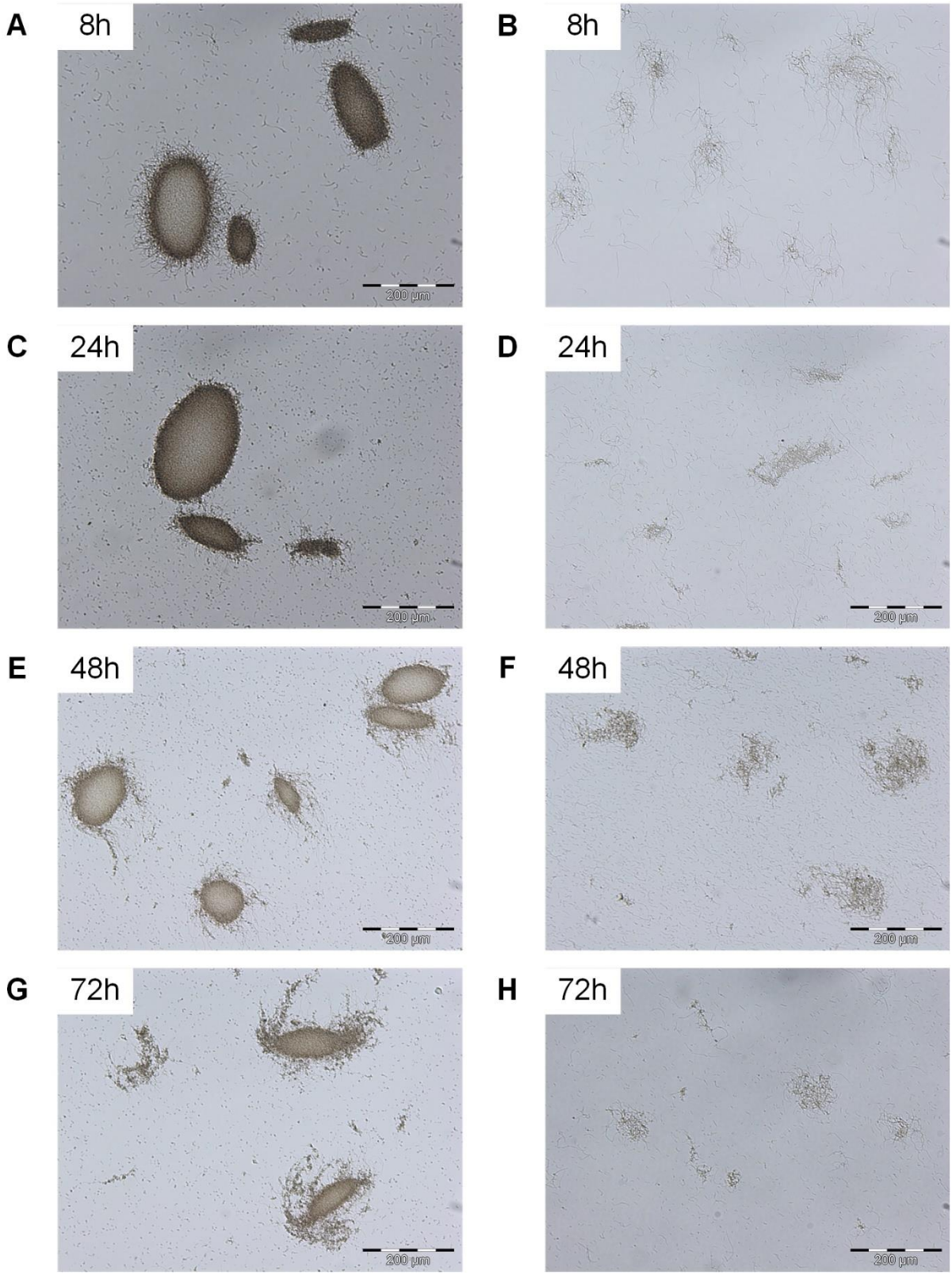

Figure 8. Microscopic analysis of oxytetracycline-producing *S. rimosus*. During growth on a mannitol-based medium, *S. rimosus* ATCC 10970 formed pellets of variable size with protruding filaments (**A**, **C**, **E**, **G**). *S. rimosus* HP126 formed mycelial mats of a loose structure instead (**B**, **D**, **F**, **H**).

3.2.3. Global transcriptome changes in the classical oxytetracycline producer

In order to investigate the foundations underlying the enhanced production of oxytetracycline in the classically mutagenized *S. rimosus* HP126 strain, global gene expression levels were determined after 24 h, which corresponds to early stationary and production phase. Overall, 15.7% from 8534 genes were downregulated and 12.5% were upregulated in *S. rimosus* HP126, as compared to the wild type strain.

3.2.4. Expression of oxytetracycline biosynthetic genes

All genes comprising the oxytetracycline BGC were upregulated in the classical producer strain (average $\log_2$-fold change = 2.3), where oxygenase *oxyQ* (*SRIMR7_02475*) exhibited the strongest activation ($\log_2$-fold change = 3.0) (**Fig. 9**). Among the genes determining components of acyl-CoA carboxylase complex, which is responsible for conversion of acetyl-CoA to the oxytetracycline precursor malonyl-CoA, only the biotin carboxylase subunit (*SRIMR7_14740*) exhibited altered expression ($\log_2$-fold change = -1.5) (**Fig. 9, Table S1**). Overall, the most prominent upregulation in genes of CoA-thioester metabolism was observed in genes encoding the subunits of branched-chain alpha-keto acid dehydrogenase (BCKADH) complex (*SRIMR7_19995*, *SRIMR7_20000*, *SRIMR7_20005*; $\log_2$-fold change up to 5.0), which is involved in conversion of branched-chain alpha-keto acids to corresponding acyl-CoAs, as a part of degradation pathways of branched-chain amino acids (BCAAs). Furthermore, genes determining the enzymes governing initial steps in oxidative degradation of phenylacetate, which yields in acetyl-CoA and succinyl-CoA, namely phenylacetate-CoA ligase (*SRIMR7_35410*), E, C and D subunits of 1,2-phenylacetyl-CoA epoxidase (*SRIMR7_19935*, *SRIMR7_19940*, *SRIMR7_19945*), were strongly upregulated in the mutagenized *S. rimosus* strain ($\log_2$-fold change up to 4.6). On the other hand, downregulation in crotonyl-CoA carboxylase/reductase (*SRIMR7_01685*, *SRIMR7_07225*), methylmalonyl-CoA mutase (*SRIMR7_07230*, *SRIMR7_12355*), 3-hydroxybutyryl-CoA dehydrogenase (*SRIMR7_02335*, *SRIMR7_336600*) and valine dehydrogenase (*SRIMR7_21110*) was noticed (**Fig. 9, Table S1**).

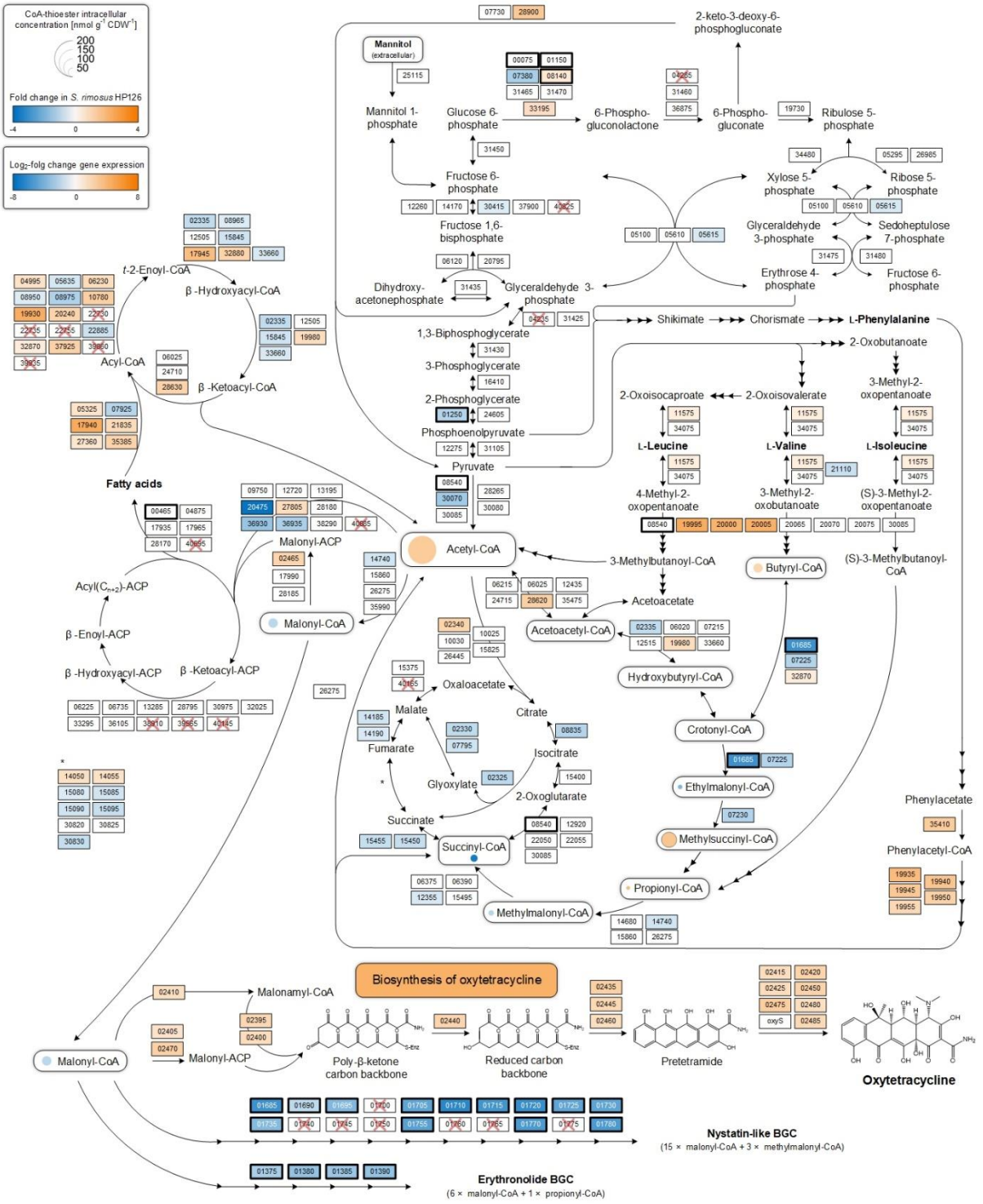

Figure 9. Multiomics profiling of the classical oxytetracycline producing *S. rimosus* HP126. Log_2-fold changes in expression of genes encoding enzymes that catalyze reactions of major catabolic and anabolic pathways, as well as biosynthesis of oxytetracycline and other malonyl-CoA-derived secondary metabolites during early production phase (24 h), are depicted in rectangulars. The wild type *S. rimosus* ATCC10970 was used as a reference. Genome sequencing of the strain revealed deletion, as well as duplication or even multiplication of some genes. Missing genes were depicted by red cross over the rectangular, while thicker frame around the rectangular represents duplication or multiplication of the given gene. Bubble charts represent concentrations of CoA-thioesters, and their changes compared to *S. rimosus* ATCC10970. Enzymes were assigned to certain reaction based on search of the Kyoto Encyclopedia of Genes and Genomes (KEGG) pathway maps and gene annotations obtained during RNAseq.

3.2.5. Expression of central carbon metabolism genes

Insight into expression levels of genes involved into degradation of the supplied carbon source revealed upregulation of 2-keto-3-deoxygluconate 6-phosphate (KDPG)/ 2-keto-4-hydroxyglutarate (KHG) aldolase (*SRIMR7_28900*), which catalyses conversion of KDPG to glyceraldehyde 3-phosphate and pyruvate, and KHG to glyoxylate and pyruvate (log_2-fold change = 3.2). Likewise, glucose 6-phosphate dehydrogenase (*SRIMR7_08140*, *SRIMR7_33195*), rate-limiting enzyme of pentose phosphate pathway, showed increased expression. Majority of the genes that determine the enzymes of the tricarboxylic acid (TCA) cycle showed decreased expression (**Fig. 9**). As an example, aconitate hydratase (*SRIMR7_08835*) was the gene with the most strongly decreased activity (log_2-fold change = -2.4). Next, assessment of the genes associated with β-oxidation of fatty acids demonstrated elevated expression of several long chain fatty acid CoA ligases (**Fig. 9**), a group of rate-limiting enzymes that initiate degradation of fatty acids by catalysing their conversion into active form of acyl-CoAs (log_2-fold change up to 5.0). Additionally, some of the acyl-CoA dehydrogenases, 3-hydroxyacyl-CoA dehydrogenases and 3-ketoacyl-CoA thiolases, which are responsible for catalysing the remaining reaction steps of the β-oxidation pathway, exhibited increased expression in the producer strain (**Fig. 9**). It has also been noticed that a few copies of acyl-CoA dehydrogenases were missing, indicating changes in form of deletions in the genome of mutagenized *S. rimosus* HP126. These remarks bring up the impression of increased supply of acetyl-CoA through heightened degradation of fatty acids. Evaluation of the genes associated with biosynthesis of fatty acids suggested slight downregulation of this anabolic process. The most prominent affect was seen in the expression of 3-ketoacyl-ACP synthases III, enzymes engaged in the initial condensation reaction, where most of them displayed lowered expression levels (log_2-fold change up to -8.2). Moreover, three copies of 3-ketoacyl-ACP reductases, were deleted from the genome of the classically mutagenized strain (**Fig. 9**). Increased activity of lipases (*SRIMR7_21840*, *SRIMR7_32745*; log_2-fold changes = 2.5 and 2.0, respectively) suggests enhanced breakdown of complex lipids to fatty acids that can be subjected to β-oxidation.

One of the most pronounced changes in expression levels at the beginning of stationary phase in the mutagenized *S. rimosus* strain was noticed in genes involved in lipid metabolism (**Fig. 9**). Namely, activation of numerous long chain fatty acyl-CoA synthases, acyl-CoA dehydrogenases, enoyl-CoA hydratases and thiolases is

indicative of overall activation of ß-oxidation of fatty acids, providing further influx of acetyl-CoA in *S. rimosus* HP126. Positive correlation between degradation of storage lipids, such as triacylglycerols (TAGs) and production of polyketides in *Streptomyces* was recently elucidated (Wang and Zhao, 2020; Wang et al., 2020b). As a result, overexpression of fatty acyl-CoA synthases is becoming a common approach in metabolic engineering of streptomycetes for boosting the titres of pharmaceutically relevant polyketides, such as avermectin B_{1a}, actinorhodin, jadomycin B and also oxytetracycline (Wang and Deng, 2020). Although some copies of genes of ß-oxidation pathway in *S. rimosus* HP126 were down-regulated or even deleted, we believe that the strong upregulation of other copies is sufficient to promote accelerated degradation of fatty acids and support magnified production potential of oxytetracycline. Moreover, overexpression of several lipases in *S. rimosus* HP126 gives the idea of mobilisation of complex lipids, like TAGs, for ß-oxidation and subsequent oxytetracycline synthesis. On the other hand, reduced expression of several and deletion of one of *fabH* (3-ketoacyl-ACP synthase III), which are catalysing the initial condensation reaction of acetyl-CoA and malonyl-ACP during biosynthesis of fatty acids is suggestive of inhibition of the competing acetyl-CoA-consuming pathway in *S. rimosus* HP126. As endogenous fatty acid and oxytetracycline synthesis share the common starter unit, this facilitates channelling of flux of acetyl-CoA towards production of oxytetracycline. Native fatty acid synthesis is often a target of metabolic engineering strategies for strain improvement and optimisation of polyketide production (Milke and Marienhagen, 2020). Indeed, titres of malonyl-CoA-derived naringenin, resverastrol and pinosylvin were increased as a result of down-regulation of genes responsible for fatty acid synthesis in *E. coli* (Wu et al., 2014; Contreras et al., 2015; Yang et al., 2015). Furthermore, reducing equivalents and ATP formed during ß-oxidation of fatty acids, in turn additionally inhibits TCA cycle and likely redirected acetyl-CoA flux to synthesis of oxytetracycline.

3.2.6. Expression of genes associated with cell wall biogenesis

Although expression levels of genes encoding the enzymes involved into synthesis of teichoic acids (TAs) were not altered in *S. rimosus* HP126, their incorporation into the cell wall was impaired through strong downregulation of TA exporters (log_2-fold change up to -5.8) (**Table S2**), affecting the structural integrity of the cell wall. Composition of the glue-like extracellular matrix (EM) of the cell wall seems to also be impacted. Namely, the mutagenized strain exhibited reduced expression of a gene for cellulose

synthase (UDP-forming) (*SRMR7_25990*), likely responsible for the synthesis of the cellulose-like component of the EM. In contrast, expression of poly-ß-1,6-N-acetylglucosamine (PNAG) synthase (*SRIMR7_38545*) that produces PNAG part of the EM was enhanced. Increased expression of several chitinases (log_2-fold change up to 2.2) is suggestive of cell wall degradation in *S. rimosus* HP126 by endogenous cell wall degrading enzymes (CWDE). Enhanced activity of murein DD-endopeptidase MepM (*SRIMR7_24075*) additionally contributes to degradation of the cell wall (**Table S2**).

As demonstrated in this study, *S. rimosus* HP126 does not form compact mycelial pellets in liquid culture, but rather loose hyphal networks (**Fig. 8**), called mats. Typically, growing hyphae aggregate into multicellular pellets by producing glue-like extracellular matrix (van Dissel, Claessen & van Wezel, 2014; Petrus & Claessen, 2014). The matrix is, among other components, made up from PNAG (encoded by *matAB* locus) (van Dissel et al., 2015; van Dissel et al., 2018) and cellulose-like polymeric substances (encoded by *cslA*) (Xu et al., 2008). Previously, it was demonstrated that deletion of either *matAB* locus, or *cslA* (van Dissel et al., 2018) was sufficient to induce disintegration of *Streptomyces* pellets in liquid environment. Therefore, it is possible that reduced expression of cellulose synthase contributed (**Table S2**) to hindered pellet aggregation in *S. rimosus* HP126. Furthermore, incorporation of TAs seems to be important for maintaining structural integrity of the cell wall by binding the extracellular glycan polymers to the peptidoglycan layer the cell wall (Ultee et al., 2020). Therefore, not only was expression of the cellulose-like component of the extracellular matrix reduced, but also anchoring of the polymers by TAs was impaired through their reduced export in the producer strain (**Table S2**). In this study, we showed downregulation of several chaplin-encoding genes, which are also thought to be important players in pellet formation of *Streptomyces* (van Dissel et al., 2018). Hereby, our findings suggest that it is possible to tailor morphology of *Streptomyces* by means of engineering of genes involved in regulation of the microbes' morphology in liquid culture. It is difficult to elucidate if dispersed growth of the strain is a result of impaired export of TAs, synthesis of cellulose-like component of EM and chaplins, as well as activated synthesis of chitinases and endopeptidases together, or if manipulation with just single one factor would be enough to achieve dispersed growth of *S. rimosus*. As the increased production potential of *S. rimosus* HP126 is a result of numerous mutations and changes in expression levels of nearly 28% of the gens, it is

difficult with clear certainty to tell if dispersed growth indeed contributed to boosted production the mutagenized strain. However, it is an interesting speculation, especially since (Kuhl et al., 2021) managed to increase production of oxytetracycline by supplementing talc microparticles to the cultures of wild type *S. rimosus*.

3.2.7. Availability of intracellular CoA-thioesters

To compare the availability of oxytetracycline precursors, the intracellular pools of free coenzyme A (CoA) and CoA-thioesters were quantified at five time points during the cultivation for both strains. The wild type contained ten different CoA-thioesters plus a substantial amount of free CoA. Succinyl-CoA was the most abundant derivative, followed by free CoA, acetyl-CoA, malonyl-CoA, and methylmalonyl-CoA. The remaining CoA-thioesters made less than 3% of the total spectrum, with crotonyl-CoA being present only in traces (**Fig. 11A, C)**.

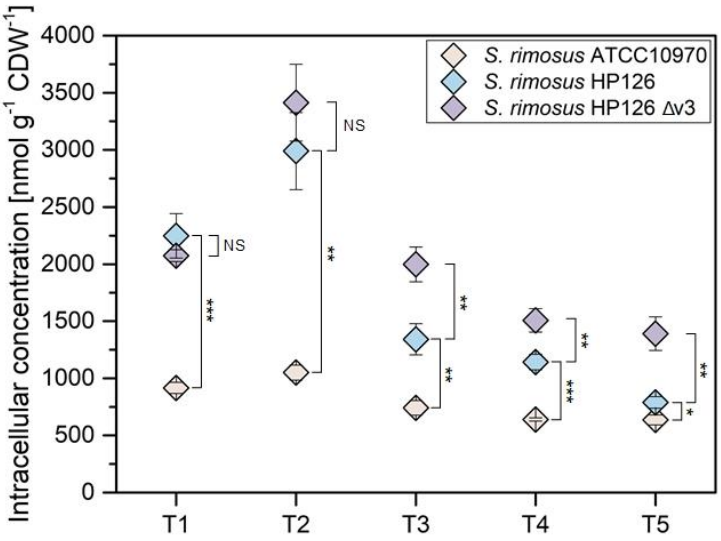

Figure 10. Total pools of intracellular CoA-thioesters and free CoA in oxytetracycline producing *S. rimosus*. The absolute quantification of the metabolites was conducted at five different time points, namely 8 h (T1), 16 h (T2), 40 h (*S. rimosus* ATCC 10970 and *S. rimosus* HP126 Δv3) and 36 h (*S. rimosus* HP126) (T3), 52 h (*S. rimosus* ATCC 10970 and *S. rimosus* HP126 Δv3) and 49 h (*S. rimosus* HP126) (T4), 60 h (*S. rimosus* ATCC 10970), 55 h (*S. rimosus* HP126) and 72 (*S. rimosus* HP126 Δv3) (T5). The statistical significance for observed differences in concentrations of CoA-thioesters is highlighted (t-test; NS, not significant; $p < 0.05$, *; < 0.01, **). n = 3

Overall, the pools slightly increased during the initial phase of growth, whereby CoA-thioesters with four and five carbon atom side chains showed the most prominent increase. With the onset of the stationary phase, the reservoirs of intracellular CoA-thioesters decreased and stabilized, towards the end of cultivation (**Fig. 10, 11A, C**). In contrast, *S. rimosus* HP126 revealed substantially activated CoA-ester metabolism. Qualitatively, it contained the same spectrum of derivatives, but these were notably increased in abundance. Compared to the parent wild type, the mutant accumulated up to almost three-fold more CoA-thioesters and free CoA (**Fig. 10**). Furthermore, the ratios between individual CoA-thioesters were strongly perturbed: ethylmalonyl-CoA showed the highest concentration, followed by butyryl-CoA, methylsuccinyl-CoA, free CoA, succinyl-CoA, and malonyl-CoA. Other CoA-thioesters constituted less than 5% of the total pool. Crotonyl-CoA was present again only in small amount. Notably, the concentration of the individual CoA-thioesters markedly decreased throughout the cultivation, whilst the amount of free CoA increased and finally even was the most abundant CoA derivative in the cell (up to 71%) (**Fig. 11B, D**).

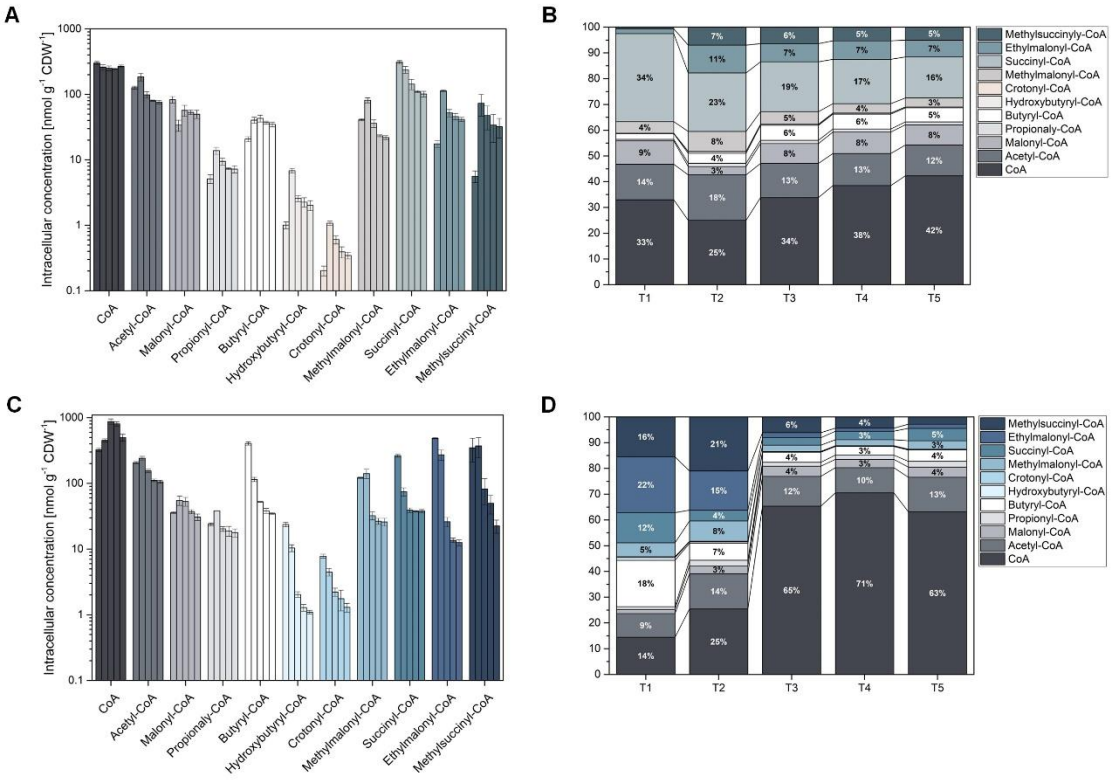

Figure 11. Dynamics of intracellular CoA-thioesters and free CoA in *S. rimosus* ATCC10970 and *S. rimosus* HP126. The data comprise of absolute levels of individual CoA-thioesters and free CoA (**A**, **C**) and their abundances (**B**, **D**) in *S. rimosus* ATCC 10970 (**top**) and *S. rimosus* HP126 (**bottom**). n = 3

Contrary to expectations, *S. rimosus* HP126 does not have more of malonyl-CoA on disposal (**Fig. 11C**), compared to the wild type. Lower concentrations of malonyl-CoA measured in the later stages of production could likely be contributed to stronger flux through the oxytetracycline biosynthetic pathway. Interestingly, the pool of malonyl-CoA was not entirely depleted, indicating that there is no bottleneck in supply of the precursors during the major production phase.

Surprisingly, an increase in the pool of CoA-thioesters and free CoA was observed in both the wild type and the producer strains, even after the provided phosphate was depleted. However, during the stationary phase, the total pools of CoA-thioesters progressively decreased over time, where *S. rimosus* HP126 displayed sharper depletion (**Fig. 10**). The initially observed build-up of CoA/thioesters, that constitute the repertoire of products of primary metabolism, could be contributed to utilisation of internal sources of phosphate. When exposed to phosphate limitation, streptomycetes are known to undergo massive cellular reprogramming (Rodríguez-García et al., 2007; Martín and Liras, 2021), including the composition of the cell wall glycopolymers. Namely, phosphate-rich teichoic acids, are replaced by phosphate-free teichuronic acids (Martín et al., 2017). Indeed, the export of teichoic acids was strongly down-regulated in *S. rimosus* HP126, compared to the parental wild type strain (**Table S2**). Therefore, it can be assumed that reduced export of these phosphorylated cell wall glycopolymers led to accumulation of additional intracellular sources of phosphate for the microbe, which can support the boosted synthesis of CoA-thioesters.

Overall, supply of acetyl-CoA in the mutagenized *S. rimosus* HP126, in comparison to the wild type strain was elevated (**Fig. 11C**). Considering that acetyl-CoA is a key metabolite that stands on the crossroad between the central metabolism and secondary metabolite production (Ku et al., 2020), it is rational to assume that metabolic engineering of pathways that increase carbon flux towards acetyl-CoA represents possible bottlenecks for optimising production of essentially acetyl-CoA-derived oxytetracycline. Conducted differential gene expression analysis enabled us to get more profound understanding of the effects of performed random mutagenesis in *S. rimosus* HP126 on production of acetyl-CoA.

Firstly, this strain showed overexpression of *zwf* (glucose 6-phosphate dehydrogenase) and *eda* (KHG/KDPG aldolase) genes, suggesting increased supply of pyruvate through Entner-Doudoroff (ED) pathway (**Fig. 9**). Pyruvate is known

allosteric activator of pyruvate dehydrogenase, a component of pyruvate dehydrogenase complex (PDC), catalysing a rate-limiting acetylation reaction in the overall conversion of pyruvate to acetyl-CoA (de Kok et al., 1998). Therefore, redirecting glycolysis into ED route, through activation of *zwf* and *eda* genes, reduces carbon loss and enables enhanced conversion of carbon into pyruvate and subsequent acetyl-CoA. Overexpression of *zfw* and *eda*, has already shown to be beneficial for increased supply of acetyl-CoA in poly-3-hydroxybutyrate-producing *Escherichia coli* (Zhang et al., 2014). In addition, upregulation of ED glycolytic route results in boosted production of NADPH, the reduction equivalent required for the synthesis of oxytetracycline. As oxytetracycline biosynthetic route is highly NADPH demanding (Petković et al., 2017), increasing its supply represents important step in establishing conditions for reaching high titres of oxytetracycline. Whilst overexpression of *zwf* itself did not intensify production of oxytetracycline in *S. rimosus* M4018 (Tang et al., 2011), it is possible that joint overexpression of *zfw* and *eda* leads to amplified supply of pyruvate (and downstream acetyl-CoA) and NADPH, which together are favourable for high production levels of oxytetracycline.

Second way in which acetyl-CoA flux is redirected to production of oxytetracycine in *S. rimosus* HP126 is through overall down-regulation of genes involved in tricarboxylic acid (TCA) cycle (**Fig. 9**). Although one copy of citrate synthase, an enzyme which is involved in recruitment of acetyl-CoA into TCA cycle was up-regulated, reduced expression of aconitate hydratase, succinate-CoA ligase, several subunits of succinate dehydrogenase and fumarate reductase complexes, one copy of methylmalonyl-CoA mutase, as well as nearly fourfold lower concentration of succinyl-CoA, suggest easing of acetyl-CoA drain through TCA cycle. Consequently, this enriches the pool of acetyl-CoA for conversion to malonyl-CoA, the precursor of oxytetracycline. As a matter of fact, engineering of TCA cycle to achieve improved production of compounds that use acetyl-CoA as a major or indirect precursor, has been an attractive target in other microbes such as *Corynebacterium glutamicum* and *E. coli* (Milke and Marienhagen, 2020). For instance, have successfully increased production of naringenin, coumaroyl-CoA and malonyl-CoA derived polyphenol, in actinobacterium *C. glutamicum* by deletion of succinate dehydrogenase complex (*sdhCDAB* operon). Likewise, elimination of *sdhCDAB* operon in *E. coli* resulted in enhanced synthesis of flavanone (Fowler et al., 2009). Our findings confirm that tunning of metabolism towards reduced

carbon flux through TCA cycle, is a valuable point for channelling flux of acetyl-CoA in the direction of secondary metabolite production.

Finally, increased expression of phenylacetate-CoA ligase and several subunits of 1,2-phenylacetyl-CoA-epoxidase amplifies rate of degradation of L-phenylalanine, providing auxiliary source of acetyl-CoA and succinyl-CoA (**Fig. 9**). This supplemental inflow of acetyl-CoA can be beneficial for supporting increased precursor demand in *S. rimosus* HP126. On the other hand, succinyl-CoA can facilitate maintenance of TCA cycle. Also, enhanced degradation of BCAAs (**Fig. 9**) provides additional influx of butyryl-CoA, which can subsequently be converted to crotonyl-CoA and ethylmalonyl-CoA and help replenishing of pools of downstream CoA-thioesters. Taken together, these findings show that supplementation of BCAAs and L-phenylalanine, could support increased production capacity of this strain.

3.2.8. Effects of deletion of the oxytetracycline cluster from *S. rimosus* HP 126

Finally, *S. rimosus* HP126 Δv3, derivative of the classical mutant lacking the oxytetracycline biosynthetic gene cluster, was examined. During the cultivation period of 121 h, the strain firstly grew exponentially until 8th h, with the same growth rate as its' parental strain (μ = 0.19 ± 0.01 h^{-1}). However, the exponential phase was not proceeded by the phase of reduced growth, like in the oxytetracycline producing strains, but rather with a pseudo-stationary that lasted until the end of cultivation time (**Fig. 12A**). Absolute quantification of CoA-thioesters showed the presence of the same CoA-thioesters, in similar concentrations, as in *S. rimosus* HP126. Over time, the strain accumulated malonyl-CoA and butyryl-CoA and showed recovery of pools of succinyl-CoA (**Fig. 12B, C**).

However, insights into differential gene expression of the oxytetracycline deletion strain revealed reduced expression of alpha, beta and lipoamide subunits of BCAA dehydrogenase complex, in comparison to the classical producer strain (**Fig. 13**). Likewise, phenylacetate-CoA ligase, phenylacetate-CoA epoxidase A, D and E subunits were downregulated. Lower expression levels of these genes suggest reduced inflow of acetyl-CoA, succinyl-CoA and butyryl-CoA through degradation of amino acid. Noticed replenishing of succinyl-CoA pools was accompanied by similar levels of expression of most of the genes of TCA cycle. Moreover, synthesis of fatty

acids in the deletion strain was slightly impaired through downregulation of several copies of 3-oxoacyl-ACP synthase III. On the other hand, degradation of fatty acids through β-oxidation seems to be activated in the oxytetracycline deletion strain. Besides upregulation of some of the copies of long chain fatty acid-CoA ligases, acyl-CoA dehydrogenases and enoyl-CoA hydratases, duplication of two copies of long chain fatty acid-CoA ligases and three copies of acyl-CoA dehydrogenases likely contributed to the activation of β-oxidation pathway, which in turn provided additional route of acetyl-CoA supply (**Fig. 13**).

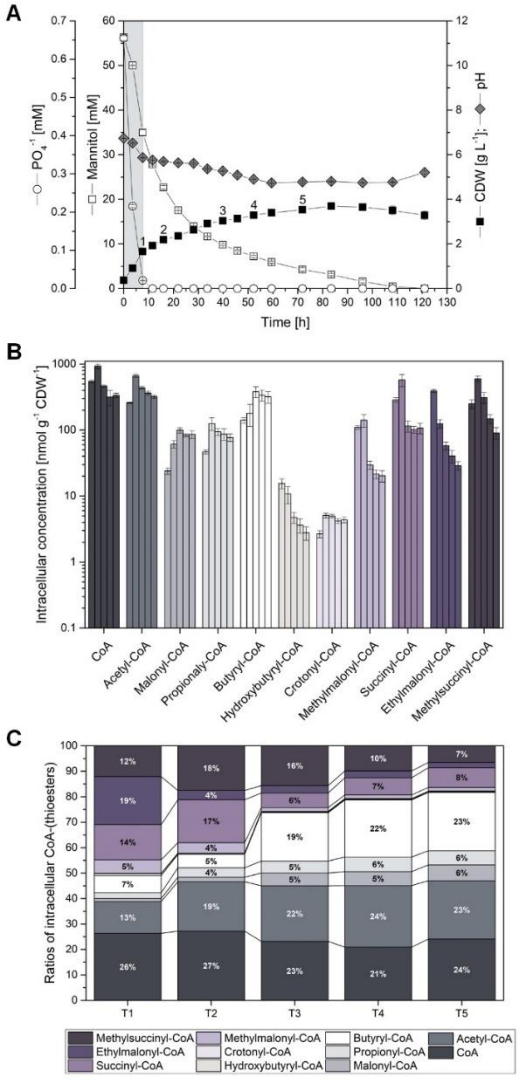

Figure 12. Growth profile and absolute quantification of intracellular CoA-thioesters and free CoA in *S. rimosus* HP126 Δv3. *S. rimosus* HP126 Δv3 was cultivated in mannitol-based mineral salt medium in shake flasks at 30°C until complete uptake of the substrate. The growth profile shows consumption of mannitol and phosphate, formation of biomass and change of pH over time. The exponential phase is shown in light grey, while the pseudostationary phase is presented in dark grey colour (**A**). Dynamics of the absolute levels of the individual intracellular CoA-thioesters and free CoA, and their abundances are shown in subfigures **B** and **C**. n = 3

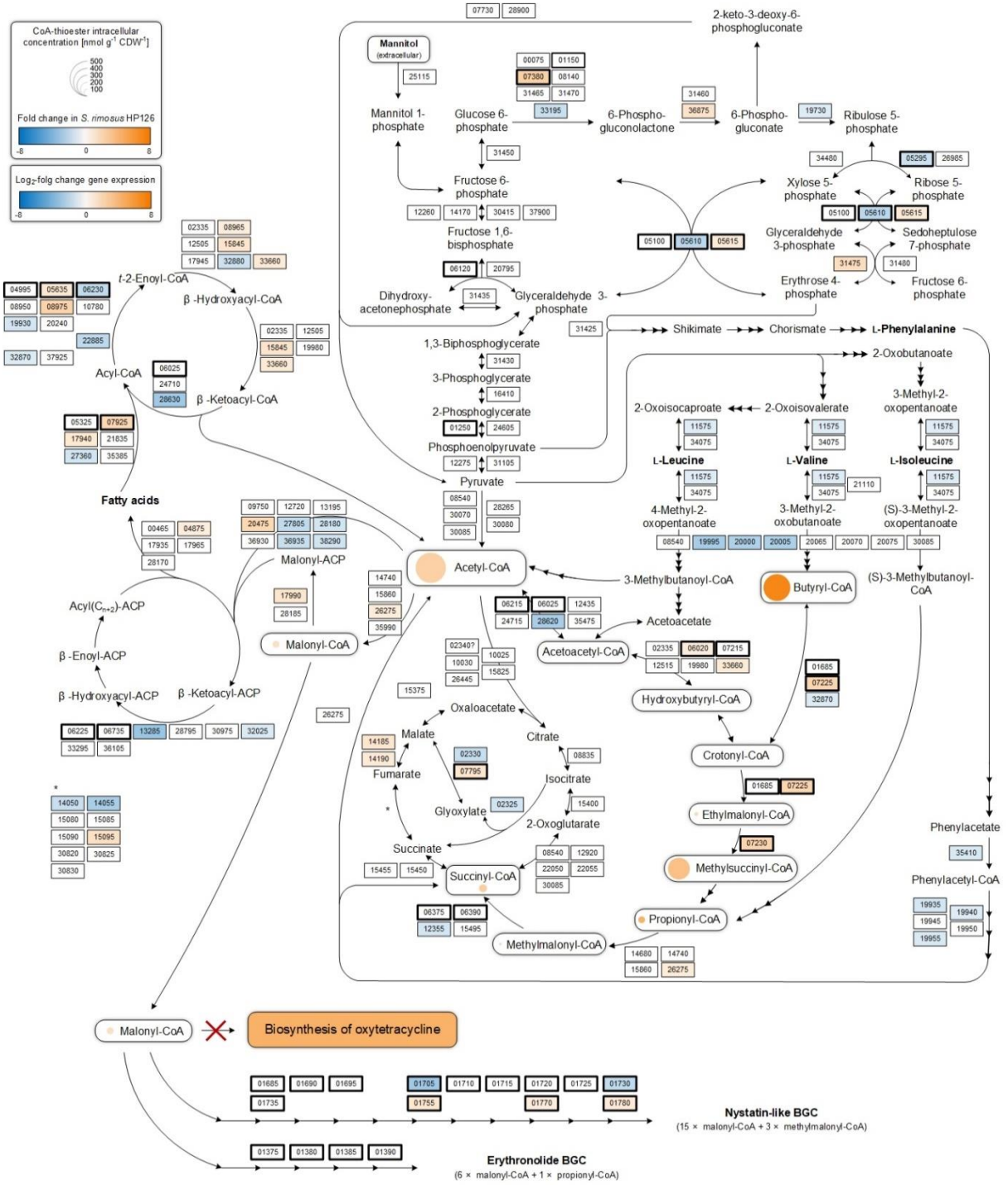

Figure 13. Multiomics profiling of the *S. rimosus* HP126 Δv3. Log_2-fold changes in expression of genes encoding enzymes that catalyze reactions of major catabolic and anabolic pathways, as well as biosynthesis malonyl-CoA-derived secondary metabolites during early stationary phase (24 h), are depicted in rectangulars. The producer *S. rimosus* HP126 was used as a reference. Genome sequencing of the strain revealed additional duplication or multiplication of some genes. Thicker frame around the rectangular represents duplication or multiplication of the given gene. Bubble charts represent concentrations of CoA-thioesters, and their changes compared to *S. rimosus* HP126. Enzymes were assigned to certain reaction based on search of the Kyoto Encyclopedia of Genes and Genomes (KEGG) pathway maps and gene annotations obtained during RNAseq.

3.3. Conclusions and outlook

Classical strain development relies on creating genetic diversity in the bacterial host through mutagenesis. Iterative cycles of mutagenesis are followed by screening of clones with desired phenotype. Some typical mutagens include UV irradiation, chemicals, biological agents, and intercalating agents. Once the screening process is completed, changes on all “omics” levels that eventually sustain the selected phenotype, are typically not know. However, these mechanisms represent valuable biological knowledge, as they can be applied for rational strain development.

In this work, multi-omics systems biology tools were applied to unravel changes in *S. rimosus* HP126, the industrial oxytetracycline producer, previously developed by multiple rounds of classical mutagenesis. In industrial setup, oxytetracycline is produced in a heavily complex medium, containing starch, soy bean flour, and corn steep liquor, among others. These medium components make “omics”-studies incredibly problematic. In that regard, a chemically defined medium was a first step towards systems studies of the classical oxytetracycline mutant. Elaborate screening of simple carbon sources was carried out in mineral salt medium with low concentration of phosphate. Alcohol sugar mannitol supported the highest production of oxytetracycline in the chemically defined medium without any complex additives. Subsequent batch cultivation experiments were carried out using mannitol. In the created setup, the classical producer *S. rimosus* HP126 accumulates 340 mg L^{-1} oxytetracycline, 12-fold more than the parental wild type, demonstrating its’ exceptional production capacity. Microscopic inspection of the submerged cultures revealed that the wild type and classical mutant strongly differ in cellular morphology. Thereby, the wild type forms compact pellets, which showed incredible heterogeneity in size.

Transcriptome analysis of the wild type and the producer showed that the classical mutagenesis led to global changes in gene expression in *S. rimosus* HP126. Substantial activation of the oxytetracycline biosynthetic gene cluster and highly modulated CoA-thioester-supporting pathways were apparent. The oxytetracycline biosynthetic genes showed up to 3-fold elevated levels of transcripts than the ancestor wild type, indicating strong activation of the BGC. Not only did the classical mutagenesis led to notable activation of the oxytetracycline BGC, it also resulted in reduced mRNA levels of genes associated with other putative secondary metabolites. Thereby, other malonyl-CoA-consuming pathways were silenced. This was also true

for fatty acid synthesis, where multiple genes related to this primary metabolic route showed diminished expression levels, as compared to the wild type. Obviously, decreased flow of acetyl-CoA and malonyl-CoA into biosynthesis of fatty acids contributed to enriching of acetyl-CoA pool in the producer. On the other hand, *S. rimosus* HP126 did not show increased concentration of malonyl-CoA, likely due to the pronounced withdrawal by the oxytetracycline BGC. Next, accelerated ß-oxidation of fatty acids, and catabolism of L-phenylalanine underpins the build-up of acetely-CoA and succinyl-CoA. Overall, metabolism of *S. rimosus* HP126 is modulated towards elevated synthesis of CoA-activated thioesters and downstream oxytetracycline. Notably, deletion of the oxytetracycline cluster from *S. rimosus* HP 126 reveals the metabolic burden of production and its impact on cellular regulation. It appears noteworthy that classical mutagenesis also introduced massive changes on genome level, whereby numerous genes seemed to be deleted or present in multiple copies, indicating significant genome instability of the mutant strain.

Systems level investigation of *S. rimosus* wild type and the industrial oxytetracycline producer demonstrates the value of modulating precursor supply and activation of the biosynthetic genes for upgraded product formation. Thereby, diminished activity of precursor-withdrawing, and boosted activity of precursor-forming pathways plays a central role. These key findings confirm that precursor supply is an exceptionally valuable target during rational, targeted strain development.

Furthermore, elimination of oxytetracycline background from the industrial producer creates highly attractive cell platform for production of other secondary metabolites. Rich pool of CoA-thioesters allows secondary metabolites derived from diverse CoA-thioesters such as: methylmalonyl-CoA, ethylmalonyl-CoA, succinyl-CoA, and malonyl-CoA-derived pamamycins; acetyl-CoA and malonyl-CoA-derived bhimamycin, and malonyl-CoA-derived flaviolin. *S. rimosus* HP126 Δv3 is a promising chassis for high-level production of secondary metabolites.

4. Metabolic engineering of *C. glutamicum* for the production of curcumin

4.1. Material and Methods

4.1.1. Microorganisms and plasmids

C. glutamicum ATCC 13032 (DSM 20300) was obtained from the Deutsche Stammsammlung für Mikroorganismen und Zellkulturen (DSMZ, Braunschweig, Germany). *E. coli* DH10B (Life GmbH, Darmstadt, Germany) and NM522 (Invitrogen, Carlsbad, CA, USA) were used for the propagation of plasmids. *E. coli* NM522 co-expressed the plasmid pTC expressing a *C. glutamicum*-specific DNA-methyltransferase for methylation of plasmid DNA (Kind et al., 2010). For plasmid-based expression of genes, the episomal vector pClik 5α plasmid was used (Buschke et al., 2011). For genome-based modification, including the deletion and integration of genes, the integrative pClik int *sacB* plasmid was applied (Becker et al., 2005; Kind et al., 2010). All strains and plasmids, including newly created derivatives, were maintained in 30% glycerol at -80°C. They are listed in table 1.

Table 1. Bacterial strains and plasmids used in this study.

Strain or plasmid	Characteristics	Reference
C. glutamicum		
ATCC 13032	Wild type strain	American Type Strain and Culture Collection, Manassas, VA, USA
CUR-1	ATCC 13032 derivative with deletion of *phdBCDE*	This work
CUR-2_nat	CUR-1 harbouring the pClik 5α MCS_OsCUS_nat	This work
CUR-2_co	CUR-1 harbouring the pClik 5α MCS_OsCUS_co	This work
CUR-3_nat	CUR-1 harbouring the pClik 5α MCS_SbCUS_nat	This work

CUR-3_co	CUR-1 harbouring the pClik 5α MCS_SbCUS_co	This work
CUR-4_nat	CUR-1 harbouring the pClik 5α MCS_ClDCS_CURS1_nat	This work
CUR-4_co	CUR-1 harbouring the pClik 5α MCS_ClDCS_CURS1_co	This work
CUR-5_nat	CUR-1 harbouring the pClik 5α MCS_At_4CL_ClDCS_CURS1_nat	This work
CUR-5_co	CUR-1 harbouring the pClik 5α MCS_At_4CL_ClDCS_CURS1_co	This work
CUR-6	ATCC13032 harbouring the pClik 5α MCS_ClDCS_CURS1_nat	This work
CUR-7	CUR-1 derivative with deletion of *phdR*	This work
CUR-8	CUR-7 harbouring pClik 5α MCS_ClDCS_CURS1_nat	This work
CUR-9	ATCC 13032 derivative with the deletion of the *phdRBCDE* and exchange of native promoter of *phdAT* with the *tuf* promoter	This work
CUR-10	CUR-7 derivative with the deletion of *phdR* and replacement of native promoter of *phdA* with the *tuf* promoter	This work
CUR-11	CUR-6 derivative with ATG start codon of citrate synthase replaced with GTG	This work
CUR-12	CUR-11 derivative harbouring pClik 5α MCS_ClDCS_CURS1_nat	This work
CUR-13	CUR-7 derivative with accBC *fasO* site mutated	This work
CUR-14	CUR-13 derivative with accD1fasO site mutated	This work
CUR-15	CUR-14 derivative harbouring pClik 5α MCS_ClDCS_CURS1_nat	This work

E. coli

DH10B	F- mcrA Δ(*mrr-hsd*RMS-*mcr*BC) Φ80d*lac*ZΔM15 Δ*lac*X74 *end*A1 *rec*A1 *deo*R Δ(*ara*,*leu*)7697 *ara*D139 *gal*U *gal*K *nup*G *rps*L λ-	Invitrogen, Carlsbad, CA, USA
NM522	*sup*E, *thi*, Δ(*lac-pro*AB), *hsd*5 (r^-, m^-)	Invitrogen, Carlsbad, CA, USA
Plasmids		
pClik 5α MCS	Episomal transformation vector *for C. glutamicum* with *E. coli* and *C. glutamicum* MCS and ORI, and Kan^R and *sacB* as selection markers	(Becker et al., 2011)
pClik 5α MCS_ClDCS_CURS1_nat	pClik 5α MCS with native *C. longa* DCS and CURS1 genes	GenScript Biotech, Rijswijk, Netherlands
pClik 5α MCS_ClDCS_CURS1_co	pClik 5α MCS with *C. longa* DCS and CURS1 genes codon-optimized for *C. glutamicum*	GenScript Biotech, Rijswijk, Netherlands
pClik 5α MCS_At4CL_ClDCS_CURS1_nat	pClik 5α MCS with native *Arabidopsis thaliana* 4CL and *C. longa* DCS and CURS1 genes	GenScript Biotech, Rijswijk, Netherlands
pClik 5α MCS_At4CL_ClDCS_CURS1_nat	pClik 5α MCS with *A. thaliana* 4CL and *C. longa* DCS and CURS1 genes codon-optimized for *C. glutamicum*	GenScript Biotech, Rijswijk, Netherlands
pClik 5α MCS_OsCUS_nat	pClik 5α MCS with native *Oryza sativa* CUS gene	GenScript Biotech, Rijswijk, Netherlands
pClik 5α MCS_OsCUS_co	pClik 5α MCS with *O. sativa* CUS gene codon-optimized for *C. glutamicum*	GenScript Biotech, Rijswijk, Netherlands
pClik 5α MCS_SbCUS_nat	pClik 5α MCS with native *Sorghum bicolor* putative curcumin synthase	GenScript Biotech, Rijswijk, Netherlands
pClik 5α MCS_SbCUS_co	pClik 5α MCS with *S. bicolor* putative curcumin synthase codon-optimized for *C. glutamicum*	GenScript Biotech, Rijswijk, Netherlands
pClik int *sacB*	Integrative transformation vector for *C. glutamicum* with *E. coli* MCS and ORI, and Kan^R and *sacB* as selection markers	(Becker et al., 2011)
pClik int *sacB*_Δ*phdBCDE*	pClik int *sacB* for the deletion of the *C. glutamicum phdBCDE* genes	This work

pClik int *sacB*_Δ*phdR*	pClik int *sacB* for the deletion of the *C. glutamicum phdR* gene	This work
pClik int *sacB* Δ*phdRBCDE_phdAT*$_{Ptuf}$	pClik int *sacB* for the deletion of the *C. glutamicum phdR*BCDE genes and the replacement of the native *C. glutamicum phdAT* promoter with the *C. glutamicum* structural *tuf* promoter	This work
pClik int *sacB_phdA*$_{Ptuf}$	pClik int *sacB* for the deletion of the *C. glutamicum* phdR gene and replacement of the native *C. glutamicum phdA* promoter with the *C. glutamicum* structural *tuf* promoter and reversed orientation of the *phdA* gene	This work
pClik int *sacB_cs*$_{GTG}$	pClik int *sacB* for the exchange of the *C. glutamicum* citrate synthase ATG start codon with GTG	*
pClik int *sacB_accBC*_fasO_mut	pClik int *sacB* for the mutation of the *fasO* site of the *C. glutamicum accBC* gene	This work
pClik int *sacB_accD1*_fasO_mut	pClik int *sacB* for the mutation of the *fasO* site of the C. glutamicum *accD1* gene	This work

*The plasmid was kindly provided from the in-house strain collection at the Institute for Systems Biotechnology (University of Saarland, Saarbrücken, Germany).

4.1.2. Genetic engineering work

Cloning strategies were designed using the SnapGene software (GSL, Biotech, LLC, Insightful Science, Chicago, IL, USA). DNA fragments were amplified by PCR (2x Phusion High-Fidelity PCR Master Mix with GC Buffer, Thermo Fischer Scientific, Waltham, MA, USA) using specific primers (**Table S3**). DNA with heterologous genes for curcumin expression was synthetized in either native or codon-optimized form (**Table S4**). The cloning vector was linearized using SmaI restriction digestion (FastDigest, Thermo Fischer Scientific). The linearized plasmid and the DNA fragments of interests were purified (Wizard SV Gel, PCR Clean-UP System, Promega, Mannheim, Germany) and then assembled *in vitro* (Rohles et al., 2016).

The assembled plasmids were transformed into *E. coli* DH10B using heat shock and verified for correctness using analytical PCR (2x Phire Hot Start II DNA-polymerase, Thermo Fischer Scientific), isolated (QIAprep Spin Miniprep Kit, Qiagen, Hilden, Germany), and verified by sequencing (Azenta Life Sciences, Genewiz Germany, Leipzig, Germany) (Becker et al., 2010). Integrative plasmids were additionally transformed into *E. coli* NM522 pTC for the generation of the *C. glutamicum*-specific methylation pattern (Kind et al., 2010). Subsequently, the plasmid were transformed into *C. glutamicum* by electroporation, and the desired mutants were obtained by homologous recombination as described earlier (Becker et al., 2010; Kind et al., 2010; Rohles et al., 2022). All recombinant strains were verified by PCR and sequencing.

4.1.3. Media

For cell propagation during cloning and pre-culturing for curcumin production, the cells were grown in complex BHI medium (37 g L^{-1}, brain heart infusion, Becton Dickinson, Franklin Lakes, NJ, USA). For plate cultures, the BHI medium was solidified by the addition of 15 g L^{-1} of agar (Becton Dickinson). For plasmid maintenance, growth media were supplemented with kanamycin (25 - 50 µg mL^{-1}) and tetracycline (12.5 µg mL^{-1}). In addition, a glucose-based minimal medium was used for the cultivation of *C. glutamicum*. The medium contained per litre: 30 g of glucose, 15 g of $(NH_4)_2SO_4$, 1 g of NaCl, 0.2 g of $MgSO_4 \cdot 7H_2O$, 0.055 g of $CaCl_2$, 34.8 g of K_2HPO_4, 27.2 g of KH_2PO_4, 2 mg of $FeCl_3 \cdot 6H_2O$, 2 mg of $MnSO_4 \cdot H_2O$, 0.5 mg of $ZnSO_4 \cdot H_2O$, 0.2 mg $CuCl_2 \cdot 2H_2O$, 0.2 mg of $Na_2B_4O_7 \cdot 10H_2O$, 0.1 mg $(NH_4)_6Mo_7O_{24} \cdot 4H_2O$, 20 mg $FeSO_4 \cdot 7H_2O$, 1 mg of thiamine-HCl, 1 mg of Ca-pantothenate, 0.5 mg of biotin and 30 mg of 3,4-dihydroxybenzoic acid (Rohles et al., 2022; Weiland et al., 2023). In addition, ferulate was added as substrate for curcumin production, as given below.

4.1.4. Batch cultivation in shake flasks

C. glutamicum was incubated in an orbital shaker (Multitron, Infors AG, Bottmingen, Switzerland) at 30°C, 230 rpm, and 80% humidity, using non-baffled shake flasks (10% filling volume). Regarding the light-sensitivity of curcumin (Mondal et al., 2016), the glass window of the incubator was covered with aluminium foil to enable cultivation in the dark. The cultivation involved two subsequent pre-cultures, followed by the main

culture. The first pre-culture (10 mL BHI medium) was inoculated in with a single colony from a BHI-agar plate, pre-grown for 48 h at 30°C and incubated 12 h. Then, the cells were harvested (6,000 x *g*, 20°C, 3 min), washed twice with minimal glucose medium, and used to inoculate the second pre-culture (50 mL minimal glucose medium) which was grown for another 7 h. Finally, the main culture in minimal glucose medium (50 mL) was inoculated from the second pre-culture as described above. The main culture was inoculated to an initial optical density (OD_{660}) of 1.0. For the production of curcumin, ferulate was added only to the main culture. All experiments were conducted in biological triplicate.

4.1.5. Screening of curcumin producers and medium tests in reagent tubes

Small scale screening experiments of curcumin-producing strains and tests for medium optimization were performed in glass reagent tubes (25 mL) filled with 5 mL of inoculated main culture medium (see above). Different combinations of glucose (10, 20, 30, and 40 g L^{-1}, corresponding to 55, 110, 165, and 220 mM) and ferulate (1, 2, 3, 4, and 5 mM) were tested.

4.1.6. Batch fermentation in stirred tank bioreactor

For selection of appropriate aeration and pH, curcumin production was carried out in batch mode in 1 L stirred-tank reactors (SR0700DLS, DASGIP AG, Jülich, Germany) under different pH and oxygen saturation. To start the process, a BHI pre-culture (100 mL supplemented with 25 µg mL^{-1} kanamycin) was inoculated and cultivated at 30°C. The cells were harvested (5,000 × g, 5 min, room temperature) and used to inoculate a second pre-culture in a chemically defined medium containing 25 µg mL^{-1} kanamycin (Chapter 4.1.3.). The second pre-culture was grown for 10 hours. The exponentially growing cells were harvested (5,000 × g, 5 min, room temperature) and resuspended in batch medium. The inoculum was injected through the septum of the bioreactor, and inoculated in 300 mL of batch medium to OD_{660} = 2.0. Fermentation was carried out under three process conditions: 20% dO_2, pH = 6.8; 2.5% dO_2, pH = 6.8; and 2.5% dO_2, pH = 6.0. The batch medium had the composition as described above (Chapter 6.3.), with increased glucose concentration to 90 g L^{-1}, and 2.5 g L^{-1} yeast extract. The pH was monitored online using a pH electrode (Mettler Toledo 405-DPAS-SC-

K8S/225, Mettler Toledo, Giessen, Germany). 6 M NaOH and 6 M HCl were used to maintain pH value of 6.8 (MP8 pump system, Eppendorf, Hamburg, Germany). Oxygen was also monitored online (Hamilton, Höchst, Germany), and saturation of 2.5% and 20% was maintained by automatic adjustments of agitation and gas inflow. DASGIP control software (DASGIP AG) was applied for data acquisition and process control. Ferulate feed phase was initiated manually by injecting 15 mM ferulate from a 500 mM stock after 4 h of growth.

4.1.7. Fed-batch fermentation in stirred tank reactors

The selected curcumin producer was further evaluated in stirred tank 1 L bioreactors (SR0700DLS, DASGIP AG) in a fed-batch mode. The preparation of first and second pre-cultures was carried out as described above (Chapter 4.1.6.). The initial batch medium had composition as described above (Chapter 4.1.3.), whereby glucose was supplemented in concentration of 30 and 20 g L^{-1}, and kanamycin was omitted (small scale test tube test revealed no statistical difference in curcumin production with and without supplementation of kanamycin (**Fig. S14**). Two different sizes of inoculum were tested (OD_{660} = 2 and OD_{660} = 8, corresponding to low and high cell density inoculum, respectively). The process was maintained at 30°C, 20% dO_2 (dissolved oxygen), and pH = 6.8. Ferulate feed phase was initiated manually by injecting 5 mM ferulate from a 500 mM stock after 4 h of batch phase. Ferulate and glucose concentrations were monitored using HPLC (Agilent Technologies). Glucose and ferulate feeds were given manually upon exhaustion of the provided substrates. Thereby glucose feed was given from a 550 mM stock of glucose monohydrate solution.

4.1.8. Quantification of cell concentration

The cell concentration was inferred from spectrophotometric analysis of the optical density at 660 nm (OD_{660}). A previously established correlation was used to convert OD-readings into cell dry weight (CDW) levels: CDW [g L^{-1}] = 0.32 x OD_{660} (Becker et al., 2009).

4.1.9. Quantification of substrates and products

Glucose and lactate were quantified by isocratic HPLC (Agilent 1260 Infinity Series, Agilent Technologies, Waldbronn, Germany). The analytes were separated using a reversed phase column (Aminex HPX-87H, 300 × 7.8 mm, Bio-Rad, Hercules, CA, USA) at 40°C as the stationary phase, and 3.5 mM H_2SO_4 at a flow rate of 0.50 mL min^{-1} as the mobile phase. Detection was based on refractive index measurement at 55°C (Agilent 1260 RID, G1362A, Agilent Technologies). External standards were applied for quantification.

Ferulate was quantified by gradient HPLC (Agilent 1260 Infinity Series, Agilent Technologies), using separation done at 25°C (Nucleodur EC 4/3 C18 Isis, 3 µm x 4 mm, Nucleodur EC 100/3 C18 Isis, 3 µm x 100 mm, Macherey-Nagel, Düren, Germany) and following gradient of 0.025% H_3PO_4 (eluent A) and acetonitrile (eluent B) at a continuous flow rate of 1.0 mL min^{-1}: 0 - 13.8 min, 99 - 67% A; 13.8 - 14.3 min, 67 - 0% A; 14.3 - 17.3 min, 0% A; 17.3 - 17.8, 0 -99% A; 17.8 - 24.3 min, 99% A. Ferulate was detected by UV absorption at 325 nm (Agilent 1260 DAD, G4212B, Agilent Technologies) and quantified using external standards.

Curcumin was quantified by gradient HPLC (Agilent 1260 Infinity Series, Agilent Technologies). For this purpose, 50 to 500 µL of cell broth was acidified to pH 3.0 (6 M HCl), subsequently mixed with two volumes of ethyl acetate, followed by phase separation (15,000 x *g*, 4°C, 2 min). The organic phase was transferred into a fresh tube. The extraction of the sample was repeated until the obtained organic phase appeared no longer yellow. All extracts were combined, dried under a stream of nitrogen, dissolved in 200 µL of acetonitrile, and analyzed by HPLC. In short, 10 µL sample was injected and separated on reversed phase column (Nucleodur EC 100/3 C18 Isis, 3.5 µm x 100 mm, Macherey Nagel) at 25°C, using a gradient of 0.025% H_3PO_4 (eluent A) and acetonitrile (eluent B) at a constant flow rate of 1.0 mL min^{-1}: 0 - 22.0 min, 100-0% A; 22 - 22.5 min, 27.4 - 72.6% A; 22.5 - 24.5 min, 0-100% A; 24.5 - 27.0 min, 100% A. Curcumin was detected by UV absorption at 426 nm (Agilent 1290 DAD, G4212A, Agilent Technologies). External standards were applied for quantification.

4.1.10. Quantification of intracellular CoA-thioesters

The protocol for the quantification of intracellular CoA-thioesters was adapted from previous work (Gläser et al., 2020). Briefly, culture samples (10 mg CDW) were quenched with an adequate amount of quenching and extraction buffer (25 mM formic acid, 95% acetonitrile, -20°C). Extraction of the intracellular CoA-thioesters was achieved through mixing and cooling steps on ice for 10 minutes, followed by centrifugation (15,000 × *g*, 4°C, 10 min) and collection of the obtained supernatant into 10 mL ice-cold deionized water. The cell pellets were washed two times with 8 mL of ice-cold water, and all supernatants were combined afterwards. The extract was frozen in liquid nitrogen, freeze-dried, and subsequently resuspended in 500 µL of pre-cooled buffer (25 mM ammonium formate, 2% MeOH, pH 5.6, 4°C). Prior to analysis, the buffered extract was clarified from debris by centrifugation (15,000 × *g*, 4°C, 10 minutes).

The analysis was carried out using a triple quadrupole MS (QTRAP 6500+, AB Sciex, Darmstadt, Germany), coupled to an LC system (Agilent 1290 Infinity System, Agilent). The analytes of interest were separated on a reversed phase column (Gemini, C18, 100 mm × 2.1 mm, 1.5 µm, 110 Å, Phenomenex, Aschaffenburg, Germany) at 40°C and a flow rate of 0.60 mL min^{1}, using a gradient of eluent A (50 mM formic acid, pH 8.1) and eluent B (methanol). The fraction of eluent B was as follows: 0-12 min, 0-15%; 12-16 min, 15-100%; 16-18 min, 100%; 18-20 min, 100-0%; 20-25 min, 0%.

For absolute quantification, ^{13}C-labelled cell extracts were used as internal standard (Gläser et al., 2020). For this purpose, *C. glutamicum* ATCC 13032 was grown on 99% [$^{13}C_6$] glucose (Omicron, Biochemicals, South Bend, United States). To obtain fully ^{13}C-enriched cell extracts, the inoculum size for both the second pre-culture, as well as for the main culture, was kept below 1% of the finally harvested cell concentration (Wittmann, 2007). Extraction of the ^{13}C CoA-thioesters was conducted as described above. The concentration of individual ^{13}C CoA-thioesters was determined using synthetic standards. For subsequent absolute quantification, an appropriate amount of ^{13}C extract was added to the samples during the initial quenching step (Gläser et al., 2020).

4.1.11. Transcriptome profiling

Global gene expression profiling of curcumin producing and non-producing C. glutamicum was carried out by applying one-color DNA microarrays, as described before (Christmann et al., 2023; Gasovic et al., 2023). Briefly, custom-made microarrays (8 × 15 K) with 8990 probes were designed using the eArray online tool (Agilent Technologies). The array contained probes for the complete genome of *C. glutamicum* wild type ATCC 13032, and 60 Agilent-based quality control (QC) probes (SurePrint G3 Custom GE 8 × 60 K, Agilent Technologies). For each gene, three different 45-60 bp probes were designed. Each probe was present in 6 technical replicates, randomly distributed across the microarray chip. Subsequently, 50 ng of extracted RNA was purified from the remaining DNA using TURBO DNA-free Kit (Thermo Fischer Scientific). Purified RNA was reverse-transcribed into Cy3-labeled cDNA and hybridized onto the microarrays (Low Input Quick Amp WT Labeling preparation protocol, Agilent Technologies). Subsequently, labelled cDNA was fragmented and hybridized on the microarray slide (Gene Expression Hybridization Kit, Agilent Technologies). Hybridization took place in a hybridization over at 65°C for 17 h (G2545A, Agilent Technologies). Upon hybridization, the microarray slides were washed and scanned (SureScan Microarray Scanner G4900DA, Agilent Technologies). Feature Extraction Software (Agilent Technologies) was applied for feature extraction from the scans. Data visualisation was done using the GeneSpring software (version 14.9, Agilent Technologies). The data were normalized by applying the percentile shift method. Statistical evaluation was carried out with 3-way ANOVA test. The fold change cut-off was set to 2, whereas P value significance threshold was set to ≤ 0.05.

For RNA extraction, 1-2 mL culture broth was centrifuged (30 seconds, 13,000 × *g*, room temperature). Cells were harvested and immediately frozen in liquid nitrogen. Subsequently, RNA was purified following the RNeasy Mini Kit (Qiagen, Hilden, Germany). NanoDrop 1000 (PEQLAB Biotechnology GmbH, Erlangen, Germany) was used to determine the concentration and purity of the extracted RNA. Finally, the integrity was assessed using the semi-automized chi-based electrophoresis (RNA 6000 Nano Kit, 2100 Bioanalyzer).

4.2. Results and Discussion

4.2.1. Development of the *C. glutamicum* chassis for curcumin production

In its natural host turmeric, curcuminoids are produced by PKS III from the intermediates of the phenylpropanoid pathway: *p*-coumarate and ferulate (Ramirez-Ahumada et al., 2006). The previously characterized phenylpropanoid degradation (*phd*) gene cluster, enabled *C. glutamicum* to utilize these lignin-derived molecules as a sole energy and carbon source (Kallscheuer et al., 2016a). This competence made *C. glutamicum* an exceptionally interesting candidate for heterologous production of curcumin, and related curcuminoids. In order to reap the benefits of its inherent tolerance towards toxic aromatic phenylpropanoids (Chen et al., 2017; Kallscheuer and Marienhagen, 2018; Lin et al., 2022; Virklund et al., 2023), the first step was the elimination of competing genes within the *phd* operon.

The potential of *C. glutamicum* to be used as a host for heterologous production of plant-derived polyphenols has already been recognized (Kallscheuer et al., 2017; Kogure and Inui, 2018; Milke et al., 2019; Wu et al., 2022; Zha et al., 2023). In this context, deletion of *phdBCDE* genes was indeed a norm for creating a platform strain for the production of plant polyphenolic compounds (Kallscheuer et al., 2016b). The successful production of polyphenols such as naringenin, eriodictyol (Kallscheuer et al., 2017), pinosylvin, resveratrol, and piceatannol (Kallscheuer et al., 2016b), was promising.

Additionally, the curcumin precursor ferulate, is a hydroxycinnamic acid present in lignin preparations from monocot grasses such as wheat, rice, rye, maize stems, barley straws, and a fast-growing dicot tree, poplar wood (Xu et al., 2005). The valorisation of lignin, the second most abundant polymer in nature, into value-added chemicals, has been drawing increasing attention (Becker and Wittmann, 2019). Thereby, ferulate has been a precursor of choice in biotechnological production of the nature-identical fragrance vanillin. Namely, ferulate extracted from sugar beet pulp has been used for enzymatic production of vanillin by Novozymes (Bagsvaerd, Denmark) (Banerjee and Chattopadhyay, 2019). Microbial-based production of vanillin has been established in *Streptomyces* sp. (Hua et al., 2007), *Amycolatopsis* sp. (Fleige et al., 2016), and *Pseudomonas putida* (Graf and Altenbuchner, 2014). In addition, *E. coli* BL21 (DE3) (Li et al., 2019), *Streptomyces setonii* (Max et al., 2012), and Bacillus pumilus (Lee et

al., 1998) have been applied for production of 4-vinylguaiacol. Moreover, Katsuyama et al. (2008) managed to employ ferulate-containing rice bran pitch, a waste stream formed during industrial production of rice oil. These successful examples highlight the versatility of ferulate as a precursor for production of value-added compounds. This work aims rendering *C. glutamicum* capable of bio-transforming the industrially relevant precursor ferulate, into a multipotent biologically active curcumin. The first step towards realizing this challenge was addressing the in-built pathway for degradation of ferulate and related phenylpropanoids in *C. glutamicum*.

4.2.2. Elimination of competing phenylpropanoid catabolic pathway

In total, seven genes comprise the *phd* cluster (*phdTARBCDE*) (Kallscheuer et al., 2016a) (**Fig. S2**). Among them, *phdT* and *phdA*, encoding a membrane transporter and a acyl:CoA ligase, respectively, are involved in the uptake and CoA-mediated activation of phenylpropanoids. Their activity would not interfere with heterologous synthesis of phenylpropanoid-derived plant polyphenols. On the contrary, it can be exploited for their anabolism, as native the *phdT* would facilitate uptake, and *phdA* would catalyse CoA-mediated activation of phenylpropanoids. This eliminates the need for heterologous expression of the transporter and the acyl:CoA ligases, thereby reducing the metabolic burden on the host.

These built-in properties of *C. glutamicum* offer another advantage over other expression hosts. For instance, *E. coli* as a flagship bacterium in molecular biology and biotechnology, is not known to possess native transporters and acyl:CoA ligases that accept phenylpropanoids as substrates (Horinouchi, 2009).

The *phdBCDE* genes, coding for 3-hydroxyacyl-CoA dehydrogenase, metal-dependent hydrolase, acyl-CoA dehydrogenase, and enoyl-CoA hydratase (Kallscheuer et al., 2016a), are expected to represent a major bottleneck for efficient biotransformation of phenylpropanoids to aromatic plant polyphenols (Kallscheuer and Marienhagen, 2018). Namely, these enzymes catalyse conversion of phenylpropanoids via β-oxidative, CoA-dependent pathway into benzoate derivates, which are further degraded via β-ketoadipate pathway to acetyl-CoA and succinyl-CoA. These are then channelled to the central carbon metabolism (Kitade et al., 2020). As such, the native catabolism of phenylpropanoids would compete with heterologous pathways utilizing same intermediates in *C. glutamicum*.

In an effort to delete *phdBCDE* genes at once, 485 bp sequence upstream from *phdB* gene and 608 bp sequence downstream from *phdE* gene were cloned into the non-replicative plasmid pClik_IntsacB_Δ*phdBCDE*. Methylated plasmid was used to transform *C. glutamicum* ATCC 13032 to kanamycin resistance, indicating successful first recombination and integration of the plasmid into the wild type genome. For markerless deletion and removal of the vector backbone, one positive merodiploid underwent the second recombination step. From approximately 50 clones analysed by PCR, 12 appeared to have *phdBCDE* genes deleted, indicated by truncated PCR product (289 bp, compared to 3841 bp in the wild type) (**Fig. S3**). One selected clone was further confirmed by sequencing, and designated as *C. glutamicum* CUR-1.

In order to assess the effects of genomic removal of the *phdBCDE* genes, the CUR-1 chassis strain was cultivated on minimal media agar plates supplemented individually with 5 mM *p*-coumarate, caffeate, and ferulate as a sole carbon and energy source. As expected, the growth of the CUR-1 strain was entirely abolished on all tested phenylpropanoids (**Fig. 14**). The observed growth phenotype is in line with previous findings, where even single deletions of *phdBCDE* genes were sufficient to abrupt the growth of *C. glutamicum* on *p*-coumarate, caffeate, and ferulate in CGXII minimal medium (Kallscheuer et al., 2016a).

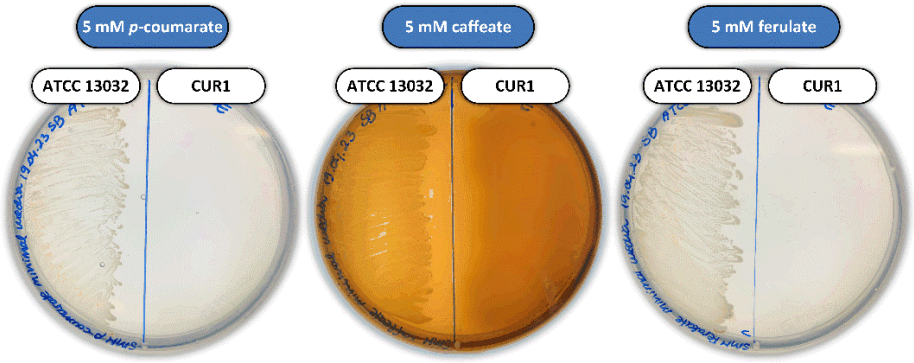

Figure 14. Growth performance of *C. glutamicum* 13032 wild type and CUR-1 strains on phenylpropanoid-based minimal medium agar plates. The strains were inoculated from their corresponding glycerol stocks and incubated on minimal medium agar plates supplemented with 5 mM *p*-coumarate, caffeate, and ferulate as a sole carbon and energy source. The plates were incubated at 30°C for 72h. As indicated by the line, the wild type was streaked out on the left side, while the CUR-1 strain was inoculated on the right half of the same plate. Each condition was tested in triplicates. Single examples are shown here.

Although, *C. glutamicum* CUR-1 was not able to utilize *p*-coumarate, caffeate, or ferulate as a growth substrate, its fitness in glucose based minimal medium was rather not affected (**Fig. 15**). The CUR-1 strain exhibited similar growth behaviour like its parental wild type strain. Both strains consumed entire 10 g of glucose within 9.5 hours without significant change in maximum growth rate. The wild type reached μ_{max} of 0.39 ± 0.02 h^{-1}, while the strain lacking the *phdBCDE* genes grew with comparable growth rate of 0.36 ± 0.02 h^{-1}. Biomass yield and specific glucose uptake rates were also without notable difference (**Table 2**).

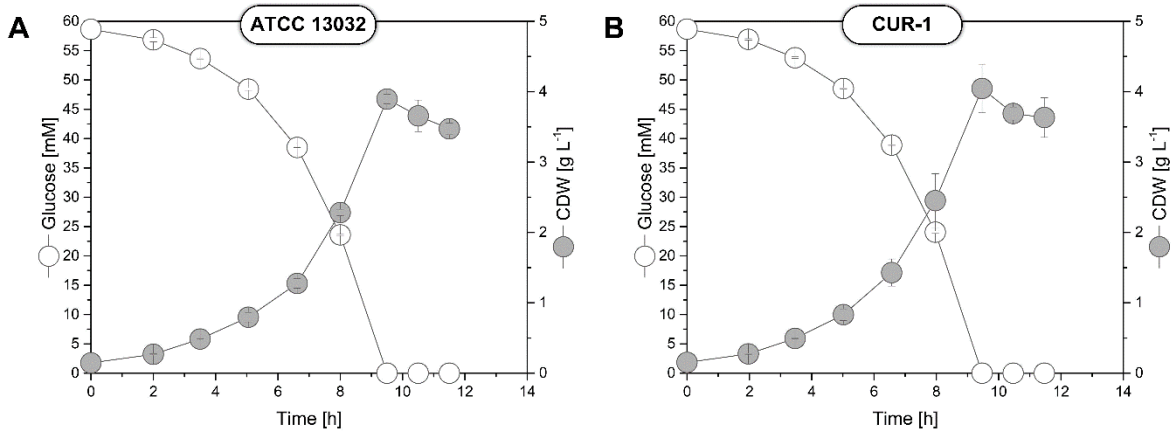

Figure 15. Growth profile of the wild type and CUR-1 strains during batch cultivation in shake flasks. The data represent cultivation profiles of *C. glutamicum* ATCC13032 and CUR-1 strain in minimal medium with 10 g L^{-1} glucose (55 mM). Increase of biomass (g L^{-1} of CDW) and consumption of glucose (mM) over time are displayed. All experiments were carried out in biological triplicates. Their respective mean values and standard deviations are shown.

Table 2. Growth performance of *C. glutamicum* wild type and CUR-1 strains in glucose-based minimal medium during batch cultivation in shake flasks. The data comprise of maximum growth rate (μ_{max}), biomass yield ($Y_{X/Glc}$), and specific glucose uptake rate (q_{Glc}). Errors represent standard deviations from three biological replicates.

Strain	μ_{max} [h^{-1}]	$Y_{X/Glc}$ [g mol^{-1}]	q_{Glc} [mmol g^{-1} h^{-1}]
ATCC 13032	0.39 ± 0.02	66.13 ± 7.07	5.90 ± 0.69
CUR-1	0.36 ± 0.02	66.13 ± 6.82	5.49 ± 0.78

The newly generated *phdBCDE* mutant was further assessed in minimal medium containing glucose and additional 5 mM ferulate. When exposed to ferulate, the wild type experiences a 1.5-fold decrease in its maximum growth rate, as opposed to cultivation with glucose as the only carbon source. Furthermore, in the presence of

ferulate, the glucose uptake rate is also reduced, effectively leading to nearly two hours of extended growth to consume the provided 10 g of glucose. Utilization of glucose was completed within 11.45 h. It is notable, that during this time, only 2 mM of ferulate were consumed with a rate of 0.18 mmol h^{-1}. When glucose was exhausted, the remaining 3 mM ferulate were consumed within one hour (**Fig. 16A, Table 3**). The observed slow uptake of ferulate while glucose is still present in the medium, can be attributable to carbon catabolite repression. For most of bacteria, glucose is often preferred growth substrate from the mixture of different carbon sources. Under this scenario, glucose prevents, or strongly inhibits the use of other, secondary carbon sources (Görke and Stülke, 2008). The cultivation profile of the wild type in the medium containing the mixture of glucose and ferulate (**Fig. 16A**) demonstrates the case of the carbon catabolite repression.

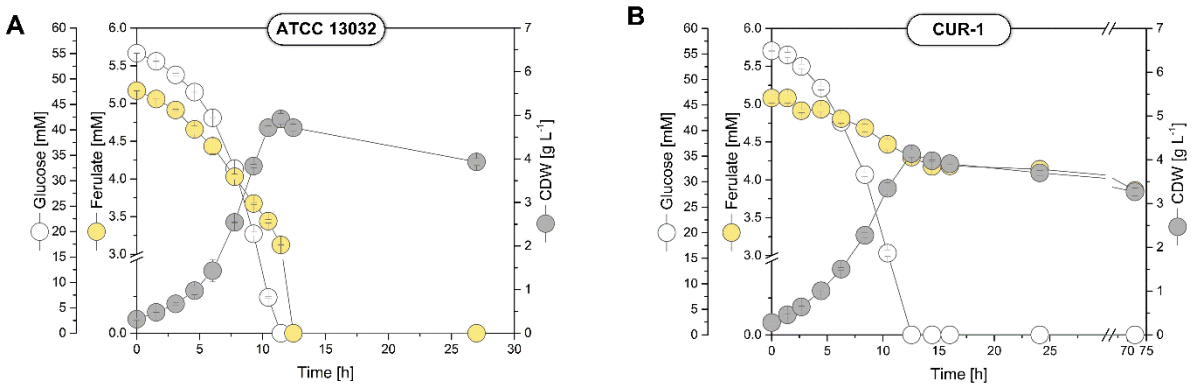

Figure 16. Ferulate utilization by wild type *C. glutamicum* and *phdBCDE* deletion mutant during batch cultivation in shake flaks The data displays cultivation profiles in minimal medium with 10 g L^{-1} of glucose (55 m) and 5 mM ferulate of: *C. glutamicum* ATCC 13032 wild type (**A**); CUR-1 strain lacking the *phdBCDE* genes (**B**). Increase of biomass (g L^{-1} of CDW) and consumption of glucose (mM), and ferulate (mM) over time are displayed. The data comprise mean values and standard deviations from three biological replicates.

The *phd* operon, which is responsible for catabolism of ferulate and other phenylpropanoids, is transcriptionally controlled by *phdR*, a MarR-type repressor (Kallscheuer et al., 2016a). PhdR-mediated repression is relieved once glucose is no longer present. Similarly, in the presence of glucose, the RamB repressor becomes activated through an unidentified mechanism and inhibits expression of genes that are associated with catabolism of acetate and ethanol (Gerstmeir et al., 2004; Arndt and Eikmanns, 2007).

The deletion of *phdBCDE* genes moderately impacted growth of *C. glutamicum*. Specifically, the CUR-1 strain exhibited a decreased maximum growth rate of 0.20 ± 0.0 h^{-1}, and glucose uptake rate of 4.88 ± 0.06 mmol h^{-1}, compared to the wild type (*P*: .0035 and .0036, respectively) (**Fig. 16B, Table 3**). It is apparent that the deletion of *phdBCDE* genes also resulted in reduced biomass formation (**Fig. 16**). Notably, deletion of the ferulate-catabolizing genes did not entirely abolish utilization of ferulate. Although at a significantly reduced rate, the CUR-1 strain consumed nearly 0.7 mM during first 12.5 hours while glucose was available. Subsequently, upon complete exhaustion of glucose, and until 72 hours of cultivation, the level of ferulate in the medium remained close to 4 mM (**Fig. 16B**).

The observed utilization of ferulate by *C. glutamicum*, even after the deletion of the *phdBCDE* genes, can be related to unspecific conversion by 4-hydroxybenzoate-3-hydroxylase PobA and protocatechuate dioxygenase PcaGH (Kallscheuer et al., 2016b). These enzymes have natural substrates that are structurally similar to phenylpropanoid intermediates (Hammer et al., 1996; Chang and Zylstra, 2008; Kallscheuer et al., 2016b). Additional decrease during stationary phase is likely due to abiotic oxidation. Related phenylpropanoids, such as caffeate, have been shown to undergo spontaneous oxidation (Weiland et al., 2023). However, the extent of potential abiotic oxidation is relatively small, and should not significantly hinder its biotransformation to curcumin.

Table 3. Growth performance of *C. glutamicum* wild type and CUR-1 strains in minimal medium supplemented with 55 mM glucose and 5 mM ferulate during batch cultivation in shake flasks. The data comprise of maximum growth rate (μ_{max}), glucose uptake rate (Q_{Glc}), and ferulate uptake rate (Q_{Fer}). Errors represent standard deviations from three biological replicates.

Strain	μ_{max} [h^{-1}]	Q_{Glc} [mmol h^{-1}]	Q_{Fer} [mmol h^{-1}]
ATCC 13032	0.26 ± 0.00	5.10 ± 0.43	0.18 ± 0.00
CUR-1	0.20 ± 0.00	4.88 ± 0.06	0.04 ± 0.00

In this context, the observed growth status of the CUR-1 strain in glucose-based minimal medium, with and without supplementation of ferulate, indicated good fitness albeit deletion of the *phdBCDE* genes. Therefore, the first chassis strain CUR-1 was selected as a host for further screening of curcumin biosynthetic gene clusters.

4.2.3. Screening of curcumin biosynthetic gene clusters

The primary objective of this group of experiments was to identify the most suitable biosynthetic gene cluster for curcumin production. In total, four different clusters were designed and heterologously expressed in *C. glutamicum* CUR-1 (**Fig. 17A**). Each cluster was tested in both native sequence and *C. glutamicum*-adapted codon form (**Table S4**). All genes were under transcriptional control of the native, strong constitutive *tuf* promoter, controlling the expression of translational elongation factor gene (Shang et al., 2018). In the designs with multiple genes, promoter sequence was positioned in front of the first gene, while the rest contained its own ribosomal binding site (RBS) (the last 20 bp from the *tuf* promoter sequence) (**Fig. 17A**).

In order to ensure sufficient copy number, the biosynthetic genes were not integrated into the host's genome, but rather episomally expressed from the low-copy pClik5α plasmid. The rationale behind this choice were previous findings where the expression of 1-deoxy-D-xylulose 5-phosphate (DXP) synthase led to threefold increase in lycopene (red carotenoid pigment) production in *E. coli* cultures expressing the gene from a low-copy plasmid, compared to cultures expressing single, chromosomally integrated gene copy (Jones et al., 2000). In the context of heterologous compound production, high-copy plasmids are often sought after to achieve maximum expression levels (Cao et al., 2016). However, possible concomitant metabolic burden arising from the presence of too many plasmid copies may adversely impact overall productivity and cell vitality (Keasling, 1999). In the same study by Jones et al. (2000), cell growth and lycopene production were decreased upon switching to high-copy plasmid. These inhibitory effects of high copy numbers of DXP synthase can be ascribed to the bactericidal effects that lycopene exerts against *E. coli* (Lee and Lee, 2014; Amorim et al., 2018). Likewise, curcumin which also exerts antimicrobial properties (De et al., 2009; Adahoun et al., 2017; Adamczak et al., 2020; Araújo et al., 2023; Liu et al., 2023), may have negative effects on cell growth and curcumin production if the biosynthetic genes are present in an excessively high copy number. In order to mitigate possible undesired effect of high-copy plasmids, the low-copy number pClik5α was used as an expression vector.

The first variant of biosynthetic gene cluster comprised of a single *cus* gene from rice (*O. sativa*) (**Fig. 17A**). This gene encodes curcuminoid synthase (CUS) (GenBank accession number: LOC4342896) that can catalyse the "one-pot" synthesis of

curcumin (Katsuyama et al., 2008), bisdemethoxycurcumin (Morita et al., 2010; Fang et al., 2018), and dicinnamoylmethane (Katsuyama et al., 2008; Kim et al., 2017; Chu et al., 2020; Wang et al., 2020a). CUS exhibits substrate-dependent specificity. The preferred substrate is *p*-coumaroyl-CoA, leading to the synthesis of bisdemethoxycurcumin through the condensation of two molecules of *p*-coumaroyl-CoA and one molecule of malonyl-CoA. Although it displays lower specificity, the enzyme can also accept feruloyl-CoA and cinnamoyl-CoA as precursors, catalysing the synthesis of curcumin and dicinnamoylmethane, respectively.

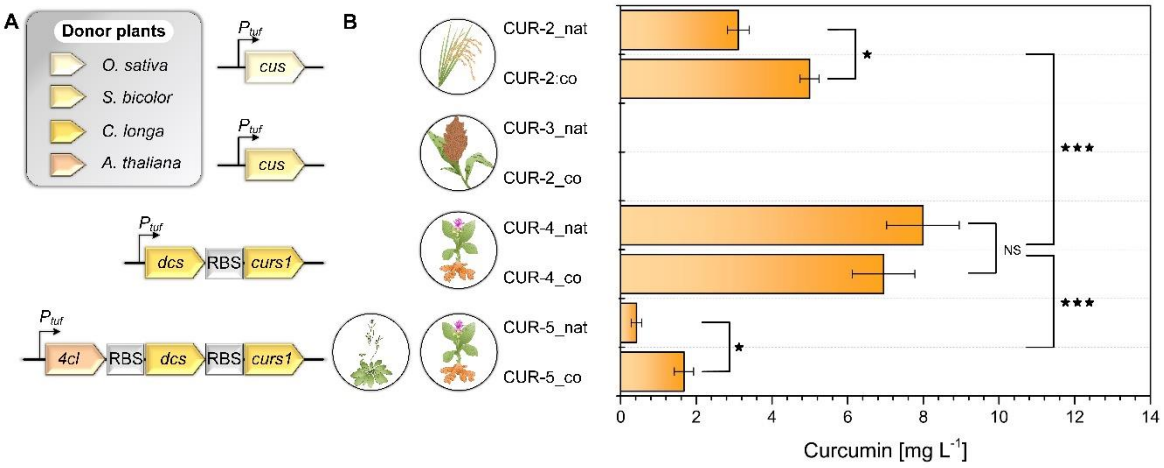

Figure 17. Screening of curcumin biosynthetic gene clusters in genetically engineered *C. glutamicum*. The data comprise structure of four heterologous gene clusters for synthesis of curcumin (**A**); curcumin titres in *C. glutamicum* CUR-1 derivatives harbouring the corresponding gene clusters cultivated in test tubes in minimal medium supplemented with 10 g L^{-1} glucose (55 mM) and 5 mM ferulate (**B**). Heterologous genes were expressed on the episomal plasmid pClik5α, and selected for kanamycin resistance. Abbreviations: nat: native gene sequence from the donor plant; co: codon-optimized sequence, adapted for *C. glutamicum*. The data comprise mean values and standard deviations from three biological replicates

Although curcuminoids have not been naturally reported in rice (Rodrigues et al., 2015b), the CUS gene has been successfully employed for heterologous production of curcumin and other curcuminoids in several hosts such as *E. coli* (Katsuyama et al., 2008; Rodrigues et al., 2015a), *Saccharomyces cerevisiae* (Rainha et al., 2022a), and *Aspergillus oryzae* (Kan et al., 2019). Notably, the CUS from rice facilitates the one-step synthesis of curcuminoids, in contrast to two enzymes diketide synthase (DCS) and curcumin synthase (CURS) present in turmeric, which catalyse biosynthesis of curcuminoids through three separate enzymatic reactions (**Fig. 6**) (Rodrigues et al., 2015b). Moreover, CUS from rice was identified and employed for heterologous

production of bisdemethoxycurcumin, dicinnamoylmethane, and curcumin in *E. coli* (Katsuyama et al., 2008) even before DCS and CURS from turmeric were identified (Katsuyama et al., 2009a).

In the current work, cultivation of *C. glutamicum* CUR-2_nat and CUR-2_co, derivatives of *C. glutamicum* CUR-1 expressing the *Os*CUS cluster in native and codon-optimized form respectively, resulted in curcumin titres of 3 and 5 mg L^{-1}, in the same order as first mentioned (**Fig. 17B**). The codon-optimized form exhibited slightly higher titre of curcumin (*P*= .001). The use of codon-optimized genes has previously demonstrated enhancements in production of lysostaphin in *E. coli* (Wang et al., 2022), enzymes prochymosin in *E. coli* (Menzella, 2011), β-fructofuranosidase in *Pichia pastoris* (Coetzee et al., 2022), and 1,2-dioxygenase in *S. cerevisiae* (Lanza et al., 2014).

Heterologous expression of a single gene can alleviate metabolic burden imposed upon the host. As such, it can be advantageous compared to expression of multiple genes. In that regard, a blast search was conducted to identify additional homologous of curcumin synthase 1 (CURS1) from turmeric. The search for additional homologous protein sequences of CURS1 revealed putative bisdemethoxycurcumin synthase from great millet (*S. bicolor*) (E-value: 0.0; identity: 72.26%; GenBank accession number: XP_002462898) (**Fig. S5**). Despite expressing both the native and codon-optimized form of the *Sbcus* gene, *C. glutamicum* CUR-3_nat or CUR-3_co, did not produce any curcumin (**Fig. 17B**).

The next cluster variant contained two type III PKS genes responsible for curcumin synthesis in turmeric (*C. longa*): diketide synthase (*dcs*) and curcumin synthase 1 (*curs1*) (GenBank accession numbers: AB495006 and KM880189, respectively) (**Fig. 17A**) (Rainha et al., 2022b). Briefly, the DCS enzyme catalyses synthesis of feruloyl-diketide-CoA, from one molecule feruloyl-CoA and malonyl-CoA. The CURS1 enzyme exerts dual function during biosynthesis of curcumin. Firstly, it hydrolases feruloyl-diketide-CoA in a corresponding keto acid, and second extends it with another molecule of feruloyl-CoA, to yield one molecule of curcumin (Katsuyama et al., 2009a). The two genes have been often selected for production of curcumin in *E. coli* (Rodrigues et al., 2015a; Couto et al., 2017; Rodrigues et al., 2020; Wu et al., 2020) and *S. cerevisiae* (Rainha et al., 2022a).

In the present work, cultivation of *C. glutamicum* CUR-4_nat resulted in a titre of 8 mg L^{-1} curcumin. On the other hand, 7 mg L^{-1} of curcumin was produced by the strain expressing the cluster in the codon-adapted form, *C. glutamicum* CUR-4_co (**Fig. 17B**). In contrast to the first cluster variant expressing the *cus* gene from rice, the combination of *dcs* and *curs1* from turmeric performed better in the native codon sequence. However, the difference between the two sequence types was not statistically significant (*P*: .23). Although codon-optimizations aim to improve the expression of a donor gene in a new host, it is necessary to consider that it can lead to impaired co-translational protein folding kinetics and suboptimal production (Rehbein et al., 2019). In such cases, different codon-optimization strategies or native sequence should be considered.

In addition to *dcs* and *curs1* genes from *C. longa*, the final cluster variant contained a copy of *p*-coumaroyl:CoA ligase (*4cl1*) gene from tale cress (*A. thaliana*) (GenBank accession number: NC_003070.9) (**Fig. 17A**). In *A. thaliana*, there are four isoforms of *4cl* genes, and they play indispensable role in directing carbon flow from primary metabolism to different routes of secondary metabolism. Specifically, they catalyse activation of phenylpropanoids into corresponding CoA-thioesters that are used in downstream synthesis of numerous secondary metabolites (Li et al., 2015). Among the four isoforms, *4cl1* displays the highest affinity for ferulate (Ehlting et al., 1999), and was selected as an additional source of feruloyl-CoA-synthetizing enzyme. Despite supplemental source of enzyme that can perform CoA-activation of ferulate, *C. glutamicum* CUR-5_nat and CUR-5_co did not produce more curcumin than the strain with only endogenous acyl:CoA ligase (*phdA*) (*C. glutamicum* CUR-4_nat and CUR-4_co). Overall, the strains *C. glutamicum* CUR-5_nat and CUR5_co produced 0.4 and 1.6 mg L^{-1} of curcumin, respectively (**Fig. 17B**).

After conducting screening of four biosynthetic gene clusters, it has been determined that the combination including the *dcs* and *curs1* genes from *C. longa* in their native sequence showed supreme performance compared to other cluster combinations. For this reason, this cluster variant has been chosen as the most suitable candidate for curcumin production. The curcumin titres obtained with initial cluster screening in the present work are rather low compared to the highest one reached by Rodrigues et al. (2020). Nevertheless, the following experiments aimed to close and even surpass this gap.

4.2.4. Deletion of *phdR* repressor for deregulation of ferulate uptake

As a soil-borne bacterium, *C. glutamicum* is known for its inherent ability to effectively metabolize lignin derived aromatics (Weiland et al., 2022), such as ferulate and *p*-coumarate. As mentioned earlier, ferulate serves as a prime building block of the curcumin molecule. It appears noteworthy, that *C. glutamicum* can withstand and grow in the presence of up to 30 mM ferulate supplemented to the glucose-based (55 mM) minimal medium (Weiland et al., 2023). Nevertheless, at this high concentration of ferulate, the growth of *C. glutamicum* appears to be impaired. Therefore, a reduced level of 5 mM ferulate was selected as a starting concentration for biotransformation of ferulate to curcumin in a glucose-based (55 mM) minimal medium by genetically engineered *C. glutamicum*.

In both CUR-6, the wild type derivative heterologously expressing the *dcs* and *curs1* genes from *C. longa*, and CUR-4_nat, the maximum growth rate was further slowed to 0.16 and 0.17 h^{-1}, respectively. Both strains exhibited comparable rates of glucose consumption, approximately 3.8 mmol h^{-1}. Furthermore, the uptake rate of ferulate demonstrated a significant reduction by 3.6-fold in *C: glutamicum* CUR-6, as compared to the wild type strain (**Fig. 18, Table 4**). Interestingly, the uptake rate of ferulate remained unaffected upon expression of an empty pClik5α plasmid in the wild type (*P*: .341). Additionally, glucose consumption showed a moderately reduced rate of 4.85 ± 0.04 (*P*: .0019) (**Fig. S4**).

Table 4. Growth performance of curcumin producing *C. glutamicum* CUR-4_nat and CUR-6 during batch cultivation in shake flasks. The data comprise of maximum growth rate (μ_{max}), glucose uptake rate (Q_{Glc}), ferulate uptake rate (Q_{Fer}), and curcumin titre of CUR-4_nat and CUR-6 in minimal medium with 10 g L^{-1} glucose (55 mM) and 5 mM ferulate. Errors represent standard deviations from three biological replicates.

Strain	μ_{max} [h^{-1}]	Q_{Glc} [mmol h^{-1}]	Q_{Fer} [mmol h^{-1}]	Curcumin titre [mg L^{-1}]
CUR-4_nat	0.16 ± 0.0	3.83 ± 0.07	0.05 ± 0.0	6.33 ± 0.17
CUR-6	0.17 ± 0.0	3.84 ± 0.02	0.05 ± 0.0	2.47 ± 0.17

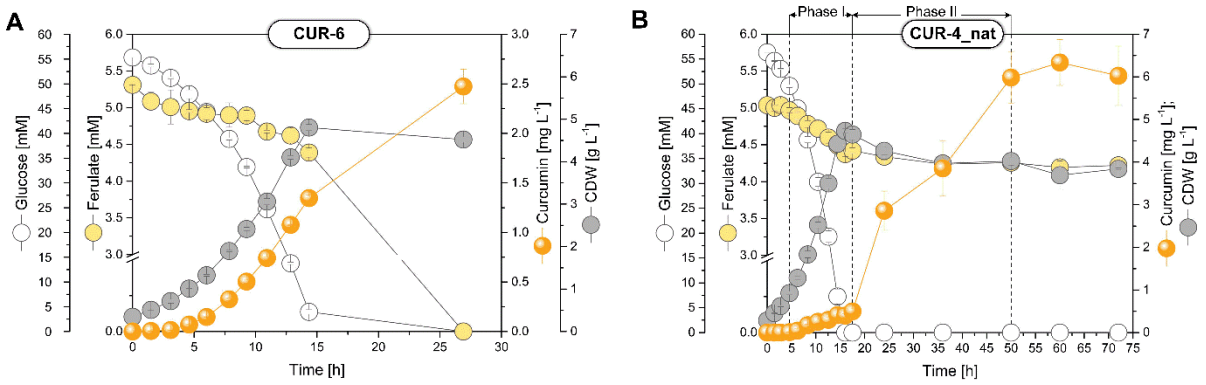

Figure 18. Curcumin production by engineered *C. glutamicum* strains from ferulate during batch cultivation in shake flaks The data displays cultivation profiles in minimal medium with 10 g L^{-1} of glucose (55 m) and 5 mM ferulate of CUR-6, of the wild type derivative expressing *dcs* and *curs1* genes from *C. longa* (**A**); and CUR-4_nat, a *phdBCDE*-deficient strain expressing the *dcs* and *curs1* genes from *C. longa* (**B**). Increase of biomass (g L^{-1} of CDW), consumption of glucose (mM) and ferulate (mM), and formation of curcumin (mg L^{-1}) over time are displayed. The data comprise mean values and standard deviations from three biological replicates.

In this work, antibiotic kanamycin was utilized as a selection marker for the maintenance of pClik5α_ClDCS_CURS1_nat plasmid. Antibiotics are commonly employed during bacterial fermentation to select for the cells carrying the desired plasmid (Mignon et al., 2015). However, addition of antibiotics can lead to delay in growth of bacterial cells (Rozkov et al., 2004), here reflected by decreased uptake rate of glucose in *C. glutamicum* ATCC 13032 :: pClik5α (**Fig. S4**). Nevertheless, once the strain was adapted to the presence of the antibiotic, it displayed a comparable maximum growth rate of 0.25 ± 0.01 h^{-1}. Moreover, results suggest that the observed substantial reduction in the uptake rate of ferulate in the CUR-6 strain, as compared to the plasmid-free wild type, is not linked to the kanamycin-imposed selection pressure. Instead, it is primarily related to the expression of the *dcs* and *curs1* genes and formation of curcumin.

In the wild type derivative expressing the pClik5α_ClDCS_CURS1_nat plasmid (CUR-6), the production of curcumin was growth coupled, with initial traces of the product detectable as early as 1.5 hour of cultivation (**Fig. 18A**). After 27 hours of cultivation, the final titre of curcumin achieved by this strain was 2.5 mg L^{-1}, coinciding with the depletion of ferulate from the medium. On the other hand, two distinct phases were observed in the production profile of *C. glutamicum* CUR-4_nat, with deleted *phdBCDE* genes. The first phase commenced after a brief non-productive period (first 2.75 hours) and persisted until the beginning of the stationary phase, achieving a peak titre of 0.5

mg L^{-1}. Subsequent second production phase, spanning from 17.5 to 72 hours (**Fig. 18B**), was characterized by approximately 3-fold higher volumetric and specific productivity rate, resulting in a maximum titre of 6 mg L^{-1} of curcumin. Throughout the production process, the concentration of unutilized ferulate remained close to 4 mM, indicating that considerable amount of the curcumin precursor remains untouched. Evidently, greater part of curcumin was formed during the stationary phase, after the supplied glucose as the primary growth substrate was exhausted. Formation of curcumin from existing pools of feruloyl-CoA and malonyl-CoA was clearly not able to sustain high-level curcumin production. Given the presence of unconsumed ferulate and delayed production of majority of curcumin, elimination of the PhdR-mediated repression of ferulate catabolism, emerged as the next promising target for strain optimization.

With the intention of deleting *phdR* gene, the non-replicative plasmid pClik_intSacB_Δ*phdR* was made. The plasmid harboured 521 and 551 bp fragments homologous to the upstream and downstream sequences flanking the *phdR* gene in the CUR-1 background. Methylated form of plasmid was transformed in *C. glutamicum* CUR-1. First recombination transformants were selected against kanamycin resistance markers, encoded within the plasmid backbone. One isolated clone was subjected to second recombination via *sacB*-mediated counter selection. From approximately 50 clones analysed by colony PCR, 19 had abbreviated PCR products (431 bp compared to 1129 bp in CUR-1 background), indicating deletion of the *phdR* gene. One of the clones was further validated by sequencing, and named as CUR-7 strain. Derivative of the CUR-7 strain expressing the episomal plasmid with *dcs* and *curs1* genes was designated as CUR-8 strain. With the aim of evaluating the effect of *phdR* deletion in CUR-1 strain background, the CUR-8 strain was cultivated in minimal medium containing glucose and ferulate, in the same biotransformation set-up as its ancestor CUR-4_nat.

In the growth profile of CUR-8 strain three individual phases were notable (**Fig. 19**). First phase, representing early curcumin production phase, manifested with low curcumin productivity and titre. During this phase that lasted first 16 hours less than 5 mg L^{-1} of curcumin were formed. Interestingly, early curcumin production phase fully overlapped with extended lag phase. As most of curcumin was formed during second phase, this period was designated as major production phase. Notably, it commenced

with the beginning of exponential growth. During this stage, greatest portion of supplemented ferulate was consumed (close to 3 mM). Upon exhaustion of glucose ferulate uptake considerably ceased. Only minor fractions were utilized during the final third phase, distinguished by reduced curcumin productivity, as compared to the previous major production phase. Nevertheless, maximum titre of 110 mg L^{-1}, a 13-fold increase as compared to the parental strain with intact regulation of ferulate uptake.

Elimination of PhdR-mediated regulation of ferulate catabolism resulted in remarkable upgrade of curcumin production in metabolically engineered *C. glutamicum*. Notably, this increase occurred at the expense of cellular fitness, here demonstrated by prolonged lag phase. Nonetheless, platform strain with deleted *phdRBCDE* genes, was employed as host in upcoming cultivation experiments.

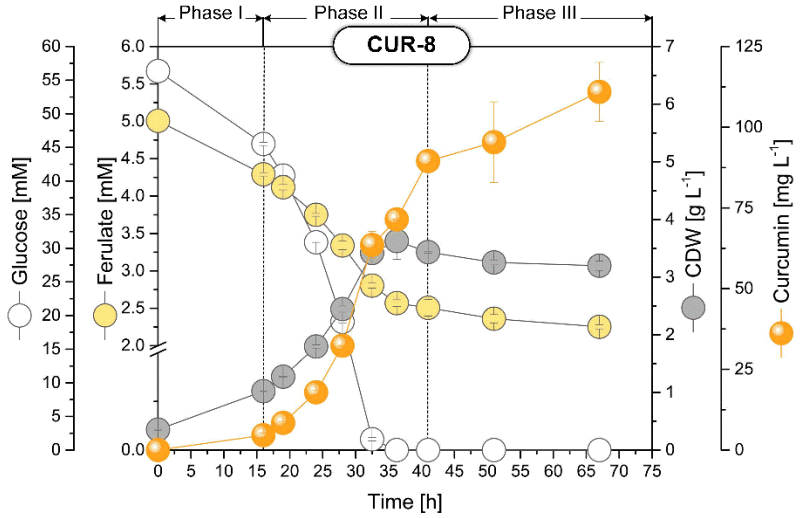

Figure 19. Curcumin production by engineered *C. glutamicum* CUR-8 from ferulate during batch cultivation in shake flaks The data displays cultivation profile in minimal medium with 10 g L^{-1} of glucose (55 m) and 5 mM ferulate of CUR-8 strain expressing the *dcs* and *curs1* genes from *C. longa*, with deletion of *phdRBCDE* genes. Increase of biomass (g L^{-1} of CDW), consumption of glucose (mM) and ferulate (mM), and formation of curcumin (mg L^{-1}) over time are displayed. The data comprise mean values and standard deviations from three biological replicates.

4.2.5. Promoter engineering of *phdT* and *phdA*

As described in previous chapters, *phdT* and *phdA* genes are part of the *phd* operone, involved into catabolism of phenylpropanoids in *C. glutamicum* (Kallscheuer et al., 2016a; Kitade et al., 2020). Briefly, PhdT is a membrane-bound transporter, facilitating the uptake of phenylpropanoids. Given that the *phdT*-deficient strain still exhibited growth in minimal medium containing ferulate as only carbon source, it is probable that

phenylpropanoids can enter the cell through yet undiscovered transporters, or by passive diffusion when present at increased levels (Kallscheuer et al., 2016a). PhdA functions as an acyl:CoA ligase, which catalyzes conversion of phenylpropanoids into their corresponding CoA-thioesters. In the native operon architecture, *phdT* and *phdA* are interspersed with a short segment of 38 bp, while each contain their own start codon (ATG). Their transcription is regulated by a promoter positioned upstream of the *phdA* gene. (**Fig. 20A**).

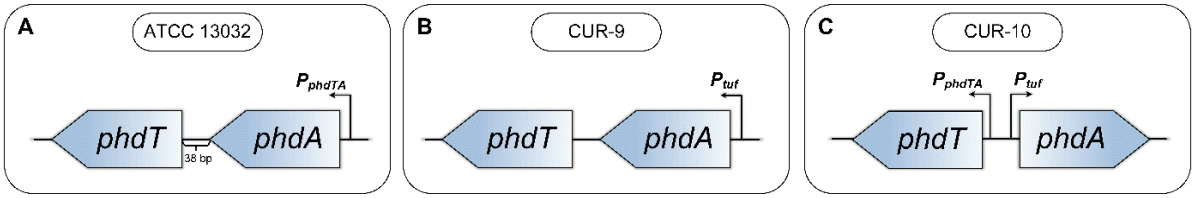

Figure 20. Promoter engineering strategies for increased expression of the *phdTA* genes. Wild type genetic structure of the *phdTA* genes from the *phd* operone (**A**). Replacement of the native *phdTA* promoter with the *tuf* promoter in CUR-9 strain (**B**). In CUR-10 strain, the native *phdTA* promoter was placed directly in front of the *phdT* gene, while the sequence of the *phdA* gene was reversed and placed under transcriptional control of the *tuf* promoter (**C**).

With the objective of achieving consistent and robust expression of the *phdTA* genes, along with increasing the rate of ferulate uptake and synthesis of the curcumin precursor, feruloyl-CoA, overexpression of the *phdTA* genes appeared as a relevant genetic engineering target. The overexpression was accomplished by replacing the original *phdTA* promoter with the strong, constitutive *tuf* promoter along (**Fig. 20B**) with simultaneous deletion of *phdRBCDE* genes in the wild type. The *tuf* promoter is widely utilized to increase the expression of several genes in *C. glutamicum*, such as fructose 1,6-biphosphatasev- *fbp* (Becker et al., 2005; Becker et al., 2011), 5-aminovalerate transaminase – *gabT*, and glutarate semialdehyde dehydrogenase - *gabD* (Rohles et al., 2018).

The new strain *C. glutamicum* Δ*phdRBCDE_phdTA*$_{Ptuf}$ was designated as CUR-9 strain. When cultured in a microbioreactor, it exhibited an exceptionally prolonged lag phase of nearly 60 hours during growth on the mixture of glucose and ferulate. In addition to delayed growth, the strain display overall reduction in biomass formation (**Fig. 21B**). This growth behaviour was not observed in the medium containing only glucose. The absence of ferulate in the medium completely restored the typical growth phenotype, which closely resembles that of its ancestor wild type strain (**Fig. 21A**).

Hence, it appears that only in the presence of ferulate, the growth is severely impaired. These results lead to the conclusion that the *tuf* promoter exerts overly strong transcriptional control, enhancing the uptake of ferulate and synthesis of feruloyl-CoA at the expense of strain fitness. Although to a far less extent, amplified expression of membrane transporters, such as vanilate *vanK* (Weiland et al., 2023) and glutarate *gabP* permeases in *C. glutamicum* (Rohles et al., 2018), also led to decreased growth rate.

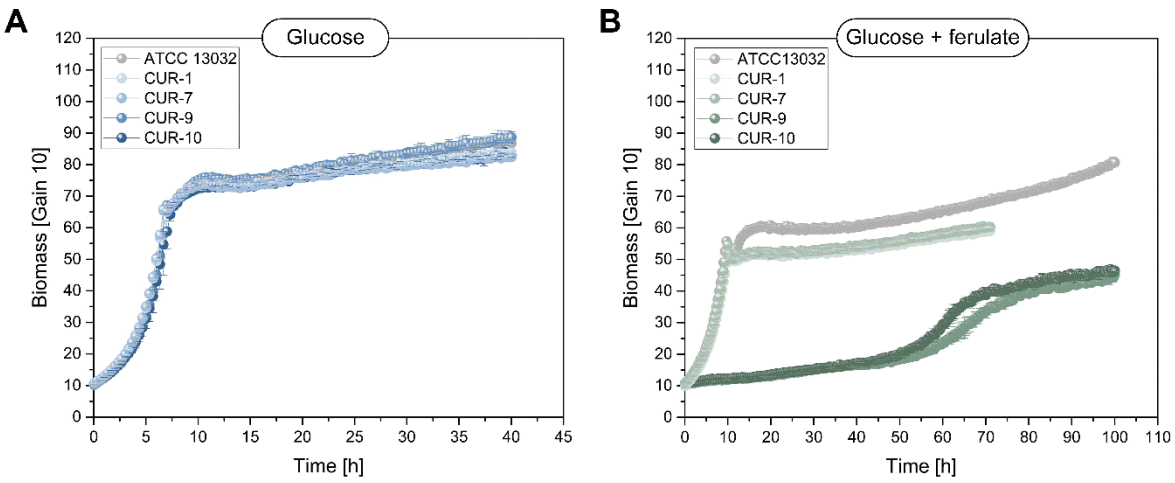

Figure 21. Vitality assessment of the engineered *C. glutamicum* strains in microbioreactors. The data displays detected biomass signal for the growth of *C. glutamicum* ATCC 13032, CUR-1, CUR-7, CUR-9, and CUR-10 (gain 10) during the growth in minimal media supplemented with 55 mM glucose (**A**); and 55 mM glucose and 5 mM ferulate (**B**). The data comprise mean values and standard deviations from three biological replicates.

Therefore, an alternative, less vigorous approach was taken to boost the activity of the *phdTA* genes. In this second metabolic engineering design, the original *phdTA* promoter was positioned in front of the *phdT* gene, while the orientation of the *phdA* gene was reversed, and the gene was placed under transcriptional control of the *tuf* promoter (**Fig. 20C**). Genetic engineering was performed using CUR-1 as a parental strain, and the newly obtained strain was designates as CUR-10. The genetic modification has only marginally lessened the effect of ferulate on growth, shortening the lag phase to approximately 55 hours (**Fig. 21B**). Similar to the previous approach, the growth in the medium containing only glucose, remained comparable to that of the wild type (**Fig. 21A**).

Precursor supply undoubtedly plays an important role in achieving high-level production of the desired compounds (Nielsen and Jewett, 2008; van der Hoek et al., 2022; Bi et al., 2023). Therefore, precursor pathways are often targets for metabolic engineering-driven strain optimization (Li et al., 2021a). For instance, production of polyphenols naringenin and eriodictyol from *p*-coumarate and caffeate in *C. glutamicum* was increased by almost 30% through an additional expression of chromosomally integrated *4cl* gene from parsley (*Petroselinum crispum*) under the control of the T7 promoter (Kallscheuer et al., 2016b).

Furthermore, production of monoterpene geraniol in *S. cerevisiae* (Liu et al., 2013), carotenoid lycopene in *E. coli* (Rodríguez-Villalón et al., 2008), polyketide rapamycin in *Streptomyces hygroscopicus* (Jung et al., 2011), antihelmintic polyketide avermectin in *S. avermitilis* (Hao et al., 2022), diamine putrescine in *E. coli*, (Qian et al., 2009), vitamin riboflavin in *Ashbya gossypii* (Monschau et al., 1998), indigo dye in *E. coli* (Berry et al., 2002), and polyketide antibiotic oxytetracycline in *S. rimosus* (Li et al., 2021a), was successfully enhanced through increased supply of their respective precursors.

However, growth of both of the newly generated CUR-9 and CUR-10 strains in the medium containing ferulate was manifested with more than two days long lag phase and reduced biomass formation by almost 30%. The observed growth defects were indicators of drastically decreased cellular fitness. Hence, the undesired reduced cellular viability pointed out that the overexpression of *phdTA* genes using the strong, constitutive *tuf* promoter was not the most suitable strategy to increase supply of ferulate and shows confied likelihood for the improvement of the strain performance.

Although strong, constitutive promoters ensure stable high-level gene expression during all growth phases unaffected by transcriptional regulators, they are not the most appropriate choice when it comes to expression of toxic proteins (Ma et al., 2018). PhdT and PhdA are not toxic proteins themselves, but they do mediate uptake and catabolism the toxic compound ferulate (Luo et al., 2019). Having in mind that curcumin itself exerts antimicrobial activity that could cause additional growth defects, CUR-9 and CUR-10 strains were not further considered for the production of curcumin.

4.2.6. Optimization of minimal medium formulation

During the past decade, heterologous biosynthesis of curcumin using microbial systems has been at the centre of atention of several studies. Various strategies for enhancing curcumin production have been explored, including screening of different expression systems (Kang et al., 2018), membrane engineering (Wu et al., 2020), and medium optimization (Couto et al., 2017). Medium optimization represents a crucial aspect during bioprocess development for heterologous production of the desired products (Jorge et al., 2016). One of the central parameters to be considered, is balancing between cell growth and product formation. (Braga et al., 2018). In terms of curcumin production, this balancing can be achieved by optimization of concentration of glucose, as the growth substrate, and ferulate, as the biotransformation substrate.

In so-far, 110 mg L^{-1} of curcumin was produced in a biotransformation setup with 10 g L^{-1} of glucose and 5 mM ferulate in a minimal medium by the CUR-8 strain. For industrially feasible productivity, higher cell densities are often desired (Henke and Wendisch, 2019). Considering the fact that rate of enzymatic reactions depends on substrate concentrations (Wegner et al., 2015), it appeared relevant to investigate impact of different concentrations of ferulate as well. In that regard, the initial glucose concentrations tested were set to 10, 20, 30, and 40 g L^{-1}. Each alternative was tested in a combination with a varying starting concentration of ferulate (1, 2, 3, 4, and 5 mM), comprising in total 20 different screening conditions. Given the elevated production capacity of CUR-8 strain, the screening was carried out using this strain.

Among the tested conditions, a combination of 30 g L^{-1} glucose and 5 mM ferulate resulted in the highest curcumin titre of 244 mg L^{-1}. Furthermore, a distinct trend in the production pattern was observed. When glucose was supplemented in concentrations of 10, 30, and 40 g L^{-1}, an increase in the initially provided ferulate from 1 to 5 mM, matched with the increase in final curcumin titre. The condition with 20 g L-1 glucose was the only exception. Hereby, the supplementation with 4 mM ferulate resulted in higher curcumin titre when compared to 5 mM, albeit without statistical difference (*P*: .37). Despite the natural antimicrobial activity of ferulate (Sova, 2012; Zduńska et al., 2018), curcumin production was more boosted at the elevated concentrations of the biotransformation substrate (**Fig. 22**).

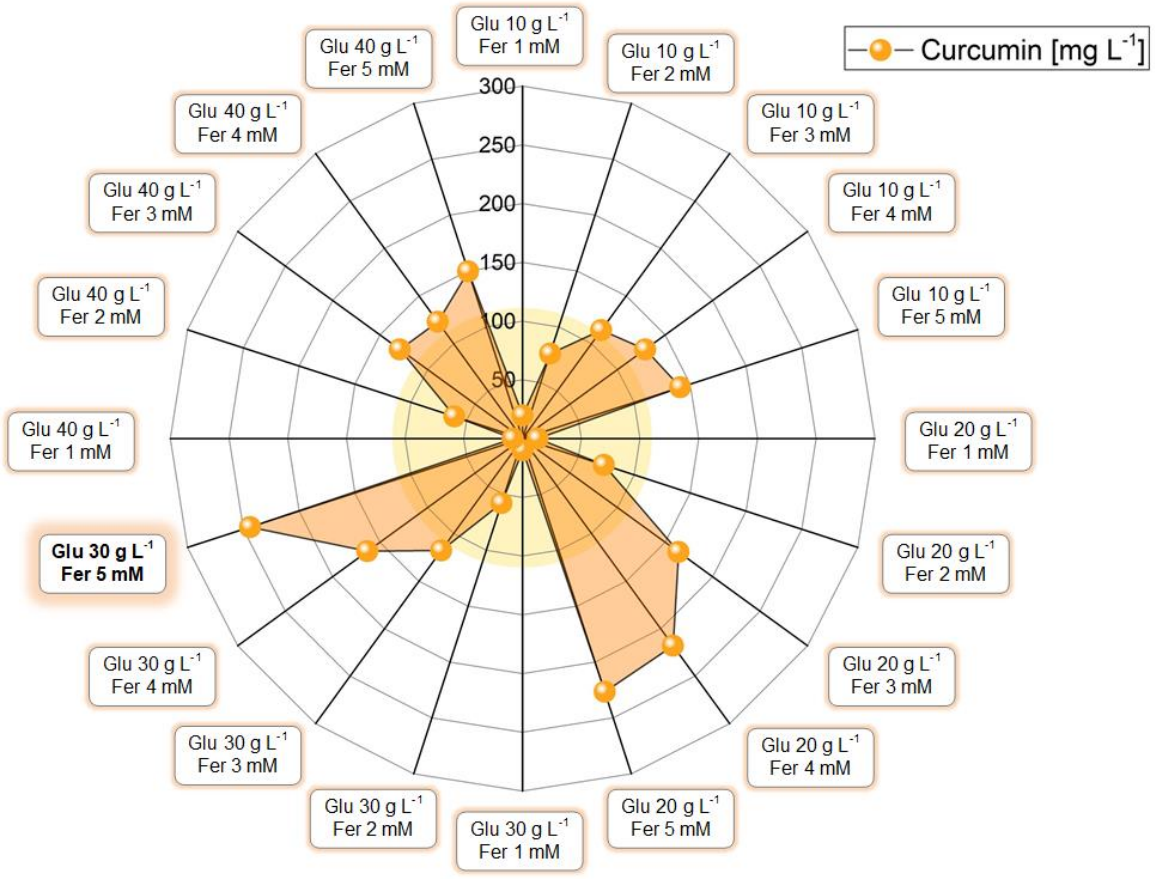

Figure 22. Optimization of growth and biotransformation substrate concentration for curcumin production by genetically engineered *C. glutamicum*. CUR-8 strain was cultured in minimal medium with varying starting concentrations of glucose (10, 20, 30, and 40 g L^{-1}) and ferulate (1, 2, 3, 4, and 5 mM) in glass test tubes. The curcumin titres were compared based on the end-point sampling and extraction after 72 hours of cultivation. The data represent average values from three biological replicates.

Overall, curcumin levels increased from 172, to 226, and 244 mg L^{-1} at 10, 20, and 30 g L^{-1} glucose respectively, but then sharply decreased to 149 mg L^{-1} at 40 g L^{-1} glucose (**Fig. 22**). It is appears noteworthy, that due to its pronounced lipophilic nature, curcumin anchors deep into the cell membrane in a transbilayer orientation (Barry et al., 2009) (**Fig. S7**). Therefore, the increase in curcumin production in biotransformation setups with 10 to 30 g L^{-1} glucose can be associated with increased formed biomass that can accommodate membrane-bound curcumin. Similarly, production of membrane-bound β-carotene astaxanthin by *C. glutamicum* was increased under high glucose concentration at 40 g L^{-1}, compared to 20 g L^{-1} (Henke and Wendisch, 2019). However, the titres decreased at more elevated glucose concentration of 40 g L^{-1}. The decrease could potentially be attributed to stronger

channelling of metabolic resources towards cell proliferation, thereby reducing the flux towards curcumin biosynthesis.

These results showed that adapting concentrations of glucose and ferulate had a pronounced effect on the production of curcumin, indicating the importance of balancing the levels of growth and biotransformation substrate for optimal curcumin formation. Taking into account the fact that 30 g L^{-1} glucose in combination with 5 mM ferulate resulted in 2.2-fold enhanced production of curcumin, when compared to initial biotransformation setup with 10 g L^{-1} glucose and 5 mM ferulate, subsequent cultivations were carried out in the optimized minimal medium containing 30 g L^{-1} glucose and 5 mM ferulate.

4.2.7. Profiling of the advanced curcumin producer strains

In addition to ferulate, biosynthesis of curcumin requires malonyl-CoA, which serves as an extender substrate during the decarboxylative elongation of feruloyl-CoA starter unit. In total, two molecules of feruloyl-CoA, derived from ferulate by CoA-mediated activation, and one molecule of malonyl-CoA, are the building blocks of one molecule of curcumin (Katsuyama et al., 2009a).

Malonyl-CoA is an indispensable metabolite that is primarily utilized as an extender unit during synthesis of fatty acids. However, it also serves as a substrate for synthesis of plentiful of polyketides, such as oxytetracycline (Yu et al., 2012), noreugenin (Milke and Marienhagen, 2020), naringenin (Zhang et al., 2022), lovastatin (Hasan et al., 2018), 4-hydroxyphenylbutan-2-one “raspberry ketone” (Schröder, 1999), flaviolin (Yang et al., 2018), and 6-methylsalicylic acid (Wen et al., 2020). Given the functions it fulfils, malonyl-CoA sits at the crossroad between primary and secondary metabolism (Laakel et al., 1994). Therefore, it comes to no surprise that enrichment of malonyl-CoA supply in several microbial platform strains, such as *C. glutamicum* (Kaku et al., 2022; Wu et al., 2022), *E. coli* (Zha et al., 2009; Yang et al., 2015; Zhou et al., 2021) and *S. cerevisiae* (Wattanachaisaereekul et al., 2008; Shin et al., 2012; Guo et al., 2016), has been the focus of numerous studies. Herein, it is important to highlight that malonyl-CoA is a product of carboxylation reaction of acetyl-CoA by acetyl-CoA carboxylases (ACCs) (Saha and Ruderman, 2003).

Regarding the metabolic engineering strategies for increasing the pools of intracellular malonyl-CoA, two major approaches can be distinguished: enhancing the activity of malonyl-CoA or acetyl-CoA supporting pathways and reducing activity of malonyl-CoA or acetyl-CoA withdrawing pathways (Milke and Marienhagen, 2020). Numerous successful attempts in which metabolic engineering of acetyl-CoA or malonyl-CoA pathways enabled increased production of malonyl-CoA-derived compounds, further motivated engineering of the malonyl-CoA supply in *C. glutamicum* for enhanced production of curcumin in this work. In that regard, two different strategies were implemented.

First approach intended to tone down the influx of acetyl-CoA into the TCA cycle. With that objective, the native ATG start codon of citrate synthase, encoded by *gltA* gene, was exchanged with the rare GTG codon in the CUR-7 strain, which is devoid of the *phdRBCDE* genes. Modification of the start codon is a tool that can be used to lessen the gene expression levels. Thereby the exchange of the most abundant ATG start codon with rare GTG and TTG variants, attenuates translational efficiency and enzyme activity in *C. glutamicum* (Becker et al., 2018a; Kim et al., 2021). As an example, replacement of the ATG start codon with the less frequent GTG codon, reduced activity of isocitrate dehydrogenase in *C. glutamicum* by 20% (Becker et al., 2009). The exchange of the start codon in *gltA* gene was accomplished by two rounds of *sacB*-mediated counter-selection, and one positive clone, confirmed by PCR and sequencing, was designated as CUR-11 strain. Derivative of CUR-11 strain expressing the pClik5α_ClDCS_CURS1 curcumin biosynthetic cluster was named as CUR-12 strain.

In parallel to the strategy that aimed to decrease withdrawal of acetyl-CoA by the TCA cycle, a second approach focusing rather on strengthening the malonyl-CoA-forming pathway was pursued. Carboxylation of acetyl-CoA to malonyl-CoA is catalysed by the multi-enzyme acetyl-CoA carboxylase complex, which is in case of *C. glutamicum* comprised of a ATP-dependent biotin carboxylase and biotin carboxyl carrier protein that form the α-subunit, carboxyltransferase that makes the β-subunit, and the carboxylase-associated ε-subunit, encoded by the *accBC*, *accD1*, and *accE* genes, respectively (Gande et al., 2007; Fränzel et al., 2010). Expression of *accBC* and *accD1*, as well as of the fatty acid synthase I (*fasA*) and II (*fasB*), is regulated by FasR, a TetR-type transcriptional repressor. Typical for a TetR-type regulator, FasR directly

binds to the promoter regions of *accBC* and *accD1*, designated as *fasO* sites, thereby inhibiting their transcription (Nickel et al., 2010). Although a consistent model of FasR-mediated transcriptional control in *C. glutamicum* is not available (Nickel et al., 2010), de-regulation of FasR-imposed repression of *accBC* and *accD1* emerged as a relevant target for increasing the availability of intracellular malonyl-CoA.

In that regard, point mutations were introduced into *fasO* sites of *accBC* and *accD1* genes in CUR-7 strain. Specific nucleotide changes are depicted in the supplementary figure S6. The exchange of nucleotides was accomplished step-wise, by first replacing the nucleotides in the *fasO* site of *accBC* gene, thereby using the CUR-7 as a parental strain. After two rounds of *sacB*-mediated counter-selection, one positive clone, validated by PCR and sequencing, named CUR-13, was used as a parent strain to introduce mutations in the *fasO* site of *accD1* gene in the same manner, by using the *sacB* counter selection. A correct clone, obtained by two round of homologous recombination, and proven by PCR and sequencing, was named as CUR-14 strain. Derivative of CUR-14 strain expressing the pClik5α_ClDCS_CURS1 curcumin biosynthetic cluster was designated as CUR-15 strain.

In the interest of investigating the effects of introduced genetic mutations, CUR-12, CUR-15, as well as CUR-8, an ancestor in the strain lineage, were cultivated in shake flasks in minimal medium with supplementation of 30 g L^{-1} glucose and 5 mM ferulate.

First insight into production performance of the tested strains revealed increased curcumin titre in the cultures of CUR-12 strain. Specifically, the strain produced 203 mg L^{-1} curcumin, which is 13 mg more than the CUR-8 strain (curcumin producer in which start codon of citrate synthase as unchanged) (**Table 5**), demonstrating the value of engineering supply of acetyl-CoA in production of curcumin. CUR-15 strain, the curcumin producer with deregulated expression of *accBCD1* genes, produced slightly less, 187 mg L^{-1} (**Table 5**). At the first sight, genetic engineering of acetyl-CoA and malonyl-CoA pathways had only a minor influence on production of curcumin. However, detailed inspection of growth and production performances, as well as dynamics of intracellular CoA-thioesters over time, revealed exact consequences of engineering acetyl-CoA and malonyl-CoA metabolism in curcumin producing *C. glutamicum*.

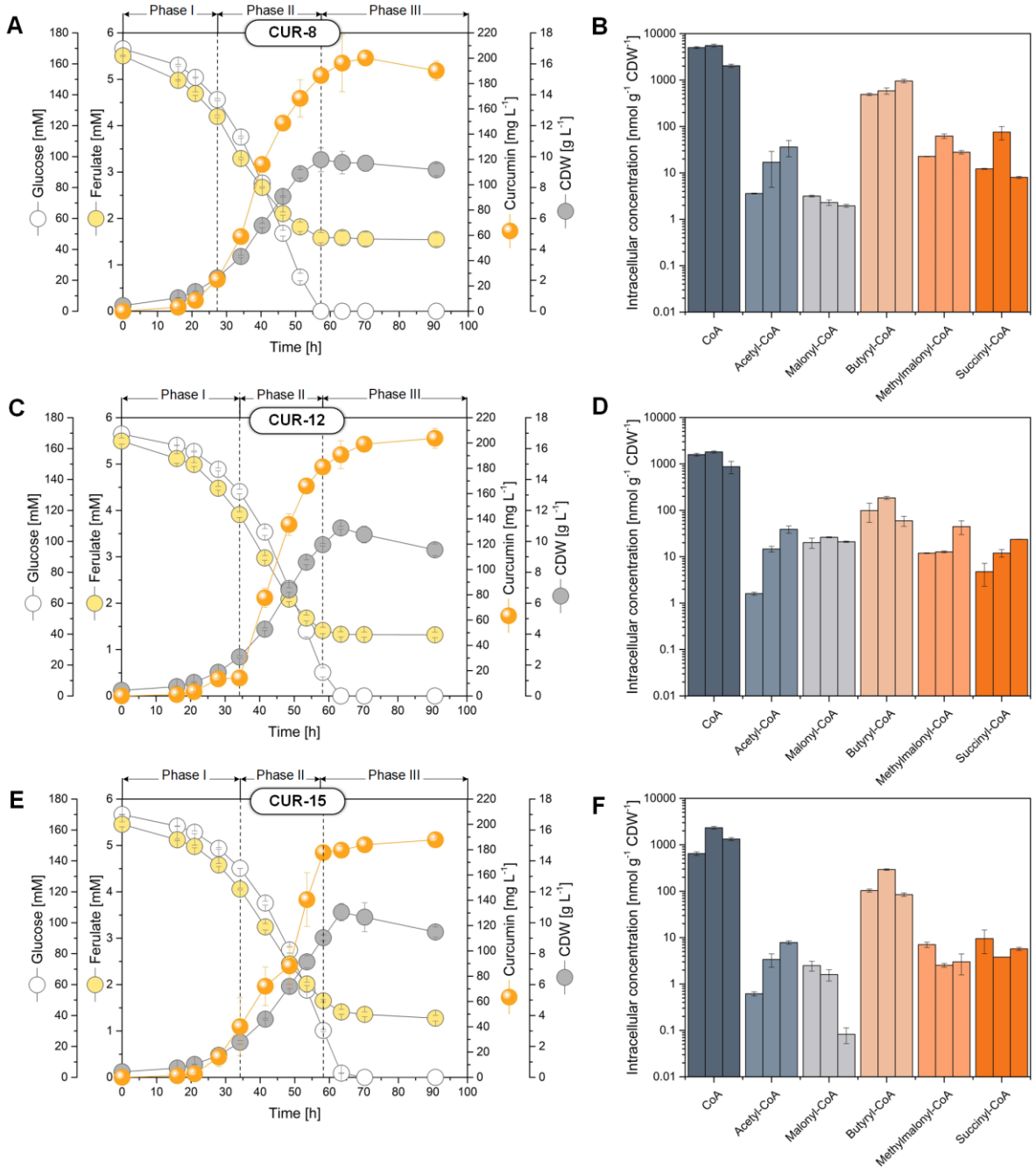

Figure 23. High-level curcumin production by engineered *C. glutamicum* strains from ferulate during batch cultivation in shake flaks The data displays cultivation profiles in minimal medium with 30 g L^{-1} of glucose (55 m) and 5 mM ferulate of CUR-8, CUR-12, and CUR-15 (**A**, **C**, **E**, respectively); and their respective dynamics of intracellular CoA-thioester concentrations (**B**, **D**, **F**). Increase of biomass (g L^{-1} of CDW), consumption of glucose (mM) and ferulate (mM), and formation of curcumin (mg L^{-1}) over time are displayed. Samples for the absolute quantification of CoA-thioesters were taken at the beginning, in the middle, and at the end of the exponential growth, here indicated as phase II. The data comprise mean values and standard deviations from three biological replicates.

First, a substantially long lag phase was apparent in growth profiles of all three strains, whereby first doubling of CUR-12 and CUR-15 strains occurred 16 hours after main cultures were inoculated. At this point, CUR-8 strain formed around 1.4-fold more

biomass, when compared to CUR-12 and CUR-15 curcumin producers (**Fig. 23A, C, E**). Slightly higher biomass formation at this stage of cultivation is likely linked to the exchange of start codon in *gltA* gene and derepression of *accBCD1* transcriptional control. These mutations perturbed native influx of acetyl-CoA into the TCA cycle and acetyl-CoA carboxylation rate, respectively. Once the strains adapted to the mutations, they caught up with the ancestor strain in terms of growth rate and maximum biomass formed.

Table 5. Growth performance of curcumin producing *C. glutamicum* CUR-8, CUR-12 and and CUR-15 during main curcumin production phase in shake flasks. The data comprise of maximum growth rate (μ_{max}), glucose uptake rate (Q_{Glc}), ferulate uptake rate (Q_{Fer}), specific glucose uptake rate (q_{Glc}), specific curcumin formation rate (q_{Cur}), volumetric productivity (P_{vol}), specific productivity (P_{spec}), biomass yield ($Y_{X/Glc}$), curcumin yield ($Y_{Cur/Glc}$ and $Y_{Cur/Fer}$), and curcumin titre (T_{Cur}) of CUR-8, CUR-12, and CUR-15 in minimal medium with 30 g L^{-1} glucose (165 mM) and 5 mM ferulate. Main production phase refers to the phase II in the cultivation profiles in Fig. 10. Errors represent standard deviations from three biological replicates.

Strain	CUR-8	CUR-12	CUR-15
Rates			
μ [h^{-1}]	0.04 ± 0.00	0.05 ± 0.00	0.05 ± 0.00
Q_{Glc} [mmol h^{-1}]	4.99 ± 0.01	5.42 ± 0.08	4.92 ± 0.04
Q_{Fer} [mmol h^{-1}]	0.07 ± 0.00	0.09 ± 0.01	0.10 ± 0.01
q_{Glc} [g g^{-1} h^{-1}]	0.14 ± 0.01	0.15 ± 0.00	0.15 ± 0.00
q_{Cur} [mg g^{-1} h^{-1}]	0.85 ± 0.04	0.94 ± 0.10	1.10 ± 0.10
P_{vol} [mg L^{-1} h^{-1}]	3.25 ± 0.07	3.11 ± 0.11	3.05 ± 0.03
P_{spec} [mg g^{-1} h^{-1}]	0.33 ± 0.02	0.32 ± 0.01	0.34 ± 0.01
Yields			
$Y_{X/Glc}$ [g g^{-1}]	0.31 ± 0.02	0.34 ± 0.01	0.35 ± 0.02
$Y_{Cur/Glc}$ [mg g^{-1}]	6.00 ± 0.45	6.41 ± 0.64	7.45 ± 0.51
$Y_{Cur/Fer}$ [mg $mmol^{-1}$]	74.42 ± 2.03	66.85 ± 4.30	65.70 ± 2.14
Titres			
T_{Cur} [mg L^{-1}]	190.09 ± 7.47	203.74 ± 7.82	187.65 ± 1.37

In all three cultivated strains, three distinct productivity phases were apparent. First, phase I, an early production phase, which lasted until the strains began to grow exponentially. This took place after 27 hours in case of CUR-8, and slightly later, after 34 hours in case of CUR-12 and CUR-15 (**Fig. 23A, C, E**). For all three strains, specific curcumin formation rate (q_{Cur}) and volumetric productivity (P_{vol}) were lower during the early production phase (**Table 5**). Notably, this was most prominent in CUR-12 strain. The CUR-8 strain exhibited superior specific (P_{spec}) and volumetric productivity (P_{vol}) during this phase, when compared to CUR-12 and CUR-15 (**Table S5**), indicating potentially reduced fitness of acetyl-CoA and malonyl-CoA-engineered strains during an early stage of cultivation. Partially impaired cellular vitality of CUR-12 and CUR-15 was additionally demonstrated by less efficient utilization of glucose. This was reflected by reduced specific glucose uptake rate (q_{Glc}) (**Table S5**).

Next, close to 80% of curcumin was produced during second phase, designated as major production phase. It coincided with the exponential growth phase, and lasted until the ferulate consumption rate ceased. Interestingly, in neither of tested strains, 5 mM ferulate were not completely depleted. Around 1.5 mM still remained untouched by the end of cultivation (**Fig. 23A, C, E**). Moreover, uptake of ferulate in CUR-12 and CUR-15 strains diminished even before glucose was entirely consumed. Notably, curcumin productivity rates (P_{vol} and P_{spec}) were indistinguishable among the strains during the major production phase, whereby volumetric productivity was up to 7-fold higher, in comparison to the previous early production phase (**Table 5**).

Finally, phase III, a late production phase, which manifested with lower volumetric and specific curcumin productivity than the previous phase. Production of curcumin plateaued during phase III (**Fig. 23A, C, E**). Notably, in cultures of CUR-8 strain, with unmodified acetyl-CoA and malonyl-CoA pathways, levels of curcumin began to slightly drop towards the end of cultivation, indicating possible product degradation over time. However, in CUR-12 and CUR-15 strains curcumin degradation was not apparent. In contrast, the strains demonstrated moderate increase in concentration towards the last hours of cultivations. The marginally extended increase in produced curcumin was more evident in CUR-12 strain. It is during this stage that CUR-12 surpassed CUR-8 strain in terms of maximum titre, likely due to the increased concentration of intracellular malonyl-CoA, as demonstrated by the absolute quantification of intracellular-CoA thioesters (**Fig. 23B, D**).

Sampling for the measurement of intracellular CoA-thioesters was carried out consistently at the beginning, in the middle, and at the end of exponential growth of all three cultivated strains. Evidently, expression of curcumin BGC strongly impacted levels of acetyl-CoA, malonyl-CoA, succinyl-CoA, and butyryl-CoA in the CUR-8 producer, as compared to the wild type expressing the empty pClik5α plasmid (**Fig. S10**). Thereby concentration of malonyl-CoA plummeted by 20-fold during the major production phase. Diminished availability of the acetyl-CoA and ongoing channelling of malonyl-CoA into curcumin biosynthetic machinery, contributed to the dramatically reduced levels of one of the curcumin precursors. Disparate picture was seen in the levels of butyryl-CoA, which showed up to nearly 300-fold boost. Concentration of feruloyl-CoA was elevated by nearly 80% during at the beginning of the exponential growth phase, but declined sharply by the onset of the major production phase (**Fig. S11**).

As demonstrated by enriched pools of malonyl-CoA in the CUR-12 curcumin producer, weakening the flow of acetyl-CoA in the TCA cycle, was beneficial for improving its supply and curcumin titre. The most notable increase of 11-fold was measured during mid-exponential phase (**Fig. S10**). Overall, pools of butyryl-CoA in the CUR-12 strain were decreased, when compared to the CUR-8. The most prominent reduction of 16-fold was recorded at the end of exponential growth phase. Lower availability of butyryl-CoA in the samples from the TCA cycle-defective mutant can be potentially linked to replenishing of succinyl-CoA, the TCA cycle intermediate downstream from citrate, through methylmalonyl-CoA node. According to the Kyoto Encyclopaedia of Genes and Genomes (KEGG database), butyryl-CoA is catabolised to methylmalonyl-CoA, although the enzymes responsible to catalyse these reactions are not fully characterized (**Fig. S9**). Methylmalonyl-CoA is further converted to succinyl-CoA in a reversible reaction catalysed by methylmalonyl-CoA mutase.

Downregulation of the CS and reduced consumption of acetyl-CoA by the TCA cycle was shown to support increased production of curcumin by *C. glutamicum*. This positive effect can be attributed to the fact that the TCA cycle is well-known to be the main drain of acetyl-CoA (Tovilla-Coutiño et al., 2020). As an amphibolic pathway, TCA cycle is a central metabolic hub in *C. glutamicum* providing reducing equivalents (NADH) for respiration, generating ATP (or GTP) by substrate-level phosphorylation, and producing glutamate- and aspartate-family precursors, 2-oxoglutarate and

oxaloacetate, respectively (Eikmanns, 2005; Bott, 2007; Ciccarone et al., 2017). Condensation of acetyl-CoA and oxaloacetate to produce citrate is catalysed by the *gltA*-encoded enzyme, citrate synthase (CS) (Eikmanns et al., 1994).

When cultured on glucose, the CS in *C. glutamicum* ATCC 21526 exhibited relative flux of 53%, indicating that significant amount of carbon was diverted to TCA cycle for formation of energy (Kiefer et al., 2004; Wittmann et al., 2004). Notably, in presence of propionate, condensation of acetyl-CoA and oxaloacetate in *C. glutamicum* is catalysed by two methylcitrate synthases (MCS; encoded by *prpC1* and *prpC2*) instead (van Ooyen et al., 2012). As this is the entry reaction of the TCA cycle, CS is considered to be the rate-limiting enzyme determining the flux through the cycle (Krivoruchko et al., 2015). Accordingly, CS competes with any other acetyl-CoA consuming pathway, and represents a promising target for metabolic engineers to improve the availability of intracellular acetyl-CoA (Tovilla-Coutiño et al., 2020) for the downstream synthesis of malonyl-CoA.

Given its fundamental role in central carbon metabolism, deletion of CS completely abolished growth of *C. glutamicum* on glucose (van Ooyen et al., 2012). Although deregulation of PrpR-mediated repression of *prpC2*-encoded MCS restored growth of *gltA* deletion strain on glucose, these “regain-of-function” mutants were still characterized by reduced growth (Radmacher and Eggeling, 2007). Therefore, completely impeding the CS activity has negative impact on growth and biomass yield (Milke and Marienhagen, 2020).

The issue of detrimental effect that *gltA* deletion has on growth of *C. glutamicum* can be addressed by replacing the native CS promoter with a weaker one. This approach has been proven to be successful in increasing production of polyphenol naringenin in *C. glutamicum*, where the native promoter of *gltA* was replaced with synthetic variants of dihydrodipicolinate synthase (*dapA*) promoters. In this manner, the expression of *gltA* was gradually downregulated, resulting in 90% reduced activity of CS, whereby growth rate maintained at 70% level of the reference strain (Milke et al., 2019). In this work, downregulation of CS was also accompanied with slightly reduced growth rate during the initial stage of cultivation. However, once attuned to the modified influx of acetyl-CoA into the TCA cycle, the CUR-12 strain exhibited even higher growth rate than CUR-8, the ancestor with unmodified CS activity. Like in the work by Milke et al. (2019), both CS engineered and un-engineered strain reached same final cell dry

weight. Increased production of curcumin and naringenin as a result of reduced activity of CS, highlight the importance of tailoring acetyl-CoA pathways for high-level production of malonyl-CoA-derived products.

With regards to the second malonyl-CoA enrichment strategy, deregulation of FasR-mediated transcriptional repression of *accBC* and *accD1* genes by mutating FasO binding sites was prove to be beneficial in increasing the concentration of available malonyl-CoA in *C. glutamicum* C7 strain, and supported enhanced production of malonyl-CoA-derived plant flavonoid noreugenin (Milke et al., 2019). These results contrast to the findings in the current study. However, there were two differences in the present work and in the previously mentioned study. Notably, Milke et al. (2019) used C. glutamicum C7 as a heterologous host, whereas ATCC 13032 wild type was employed in this work, pointing out to strain-specific regulation of malonyl-CoA metabolism. Secondly, magnified supply of malonyl-CoA in study by Milke et al. (2019) was demonstrated in the strain without the noreugenin BGC, thereby eliminating the influence of the malonyl-CoA-withdrawing cluster on the intracellular concentration of the acetyl-CoA-carboxylation CoA-thioester.

Levels of malonyl-CoA in the CUR-15 strain remarkably subsided, when compared to the CUR-8 curcumin producer (**Fig. S10**). Eminently, association of the ε-subunit with the α_3-β_5 complex in the related actinobacteria *M. tuberuculosis*, stimulated the rate of acetyl-CoA carboxylation reaction. Thereby, optimal molar ration between α_3, β_5, and ε subunits is 1:1:2 (Daniel et al., 2007). This fine-tuned balance between the three ACC subunits, points out on the implications of the ε-subunit on the efficiency of carboxylation by the α and β complex in *C. glutamicum* in the like manner. Clearly, deregulation of the α and β subunit-encoding genes has potential to perturb the optimal molar ratio between the subunits, and thereby the intracellular concentrations of malonyl-CoA, the product of their enzymatic activity.

4.2.8. Impact of curcumin production on fatty acid composition

As mentioned in earlier chapters, curcumin in highly hydrophobic compound, and as such intercalates between membrane phospholipids, causing segmental ordering (Duda et al., 2020). Furthermore, it has been demonstrated that curcumin exerts its antimicrobial activity, among other mechanisms, by triggering a cascade of apoptosis-

specific events, including depolarization of membrane and influx of calcium ions (Ca^{2+}) in *E. coli* (Yun and Lee, 2016). In the context of heterologous production of curcumin, these factors need to be taken into consideration. Therefore, it appears essential to examine the impact of curcumin production on the composition of membrane-building fatty acids in *C. glutamicum*. For this purpose, samples from the cultures of wild type *C. glutamicum* expressing the pClik5α plasmid and CUR-8 strain cultivated on 30 g L^{-1} glucose and 5 mM ferulate, were collected during the exponential growth phase at the OD_{660} of 15 (**Fig. 23A; Fig. S12**). Extraction and GC-MS analysis of fatty acids were kindly carried out by DSMZ (Deutsche Sammlung von Mikroorganismen und Zellkulturen).

Fatty acid profile of the wild type strain revealed by 2.9 percentiles higher abundance of unsaturated fatty acids, compared to saturated fatty acids. Oleate (18:1*ω*9*c*) and palmitate (16:0) (with 51% and 46.4%, respectively) accounted for majority of total fatty acids in the wild type. Relative abundance of myristate (14:0), palmitoleate (16:1 *ω*9*c*), stearate (18:0), and methyl stearate (10Me 18:0) was less than 1% each (**Fig. 24**). This fatty composition is comparable to the one previously obtained from *C. glutamicum* wild type grown on glucose solely (Radmacher et al., 2005).

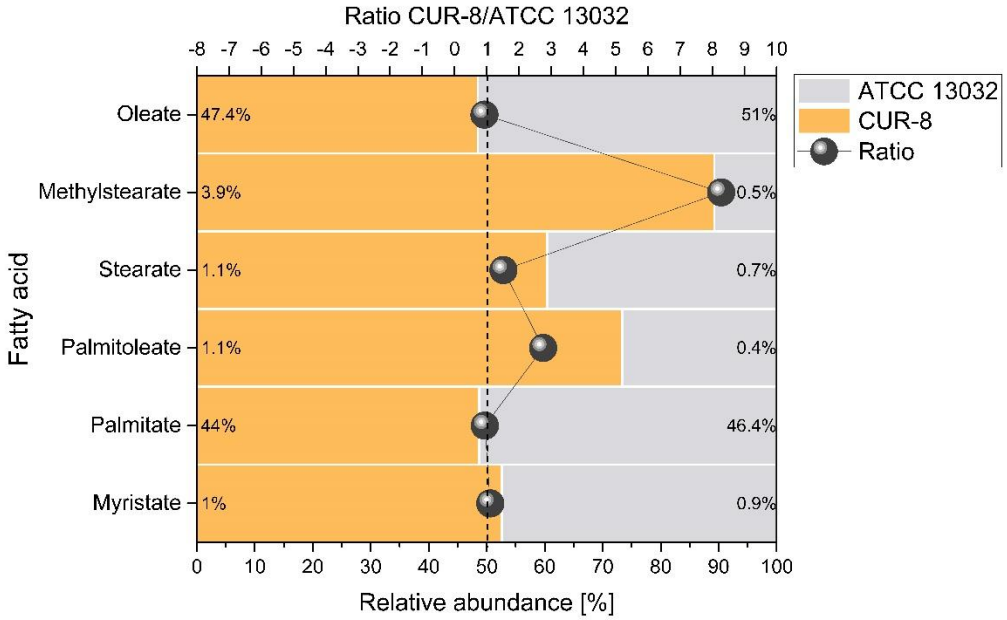

Figure 24. Composition of fatty acids in the wild type *C. glutamicum* and curcumin producing CUR-8. The data displays relative quantities of the detected fatty acids in ATCC13032_pClik5α and CUR-8, represented in percentages at the far right and left part of the bar charts, and ratios in abundance between the tested strains.

Heterologous production of curcumin shifted ratio of total fatty acids in direction of saturated fatty acids. However, at the individual level, abundance of palmitoleate increased by 2.75-fold, while oleate reduced by nearly 4 percentiles. Methyl stearate exhibited the most notable change of 8.4-fold increase, when compared to reference samples from the wild type (**Fig. 24**). Methyl stearate, also known as tuberculostearate, is a branched chain, signature fatty acid of *Mycobacterium* genus and finite number of related actynomycetes (Smith et al., 2000; Quezada et al., 2007; Liu and Larrouy-Maumus, 2022). In clinical practice, tuberculostearate is used as one of biomarkers for diagnosis of tuberculosis, an infectious disease caused by *Mycobacterium tuberculosis* (Traunmüller et al., 2003).

Branched chain fatty acid are known to have prominent influence on fluidity of the cellular membrane (Mostofian et al., 2019). Membrane fluidity refers to lateral mobility of lipid and protein molecules across the plane of the lipid bilayer (Ballweg et al., 2020). It is defined by a ratio of saturated and unsaturated fatty acids (Loffeld and Keweloh, 1996; Choi et al., 2003), whereby less fluid membranes are characterized by higher proportion of rigid, saturated fatty chains (Kates et al., 1984). In contrast, unsaturated fatty acids create more fluid membrane environment (Ballweg and Ernst, 2017). Bacteria can adapt their membrane fluidity in a process called homeoviscous adaptation (Hazel, 1995). For instance, *Bacillus subtilis* and *Lysteria monocytogenes*, adapt their membrane fluidity in response to low temperature, by desaturation of saturated fatty acids in existing phospholipids, or by producing branched-chain fatty acids (Yang et al., 2020). Membrane fluidization by branching is believed to be analogous to process of unsaturation (Nickels et al., 2017).

It has been already pointed out that due to is positioning within the membrane, curcumin seems to affect its fluidity (Jaruga et al., 1998). Namely, exposure of *E. coli* to curcumin resulted in reduced membrane fluidity, which could be partially restored by a pre-treatment of bacterial cells with an unsaturated palmitoleic acid (Wu et al., 2020). In the same study, supplementation of unsaturated fatty acids palmitoleate and oleate has been shown to boost production of curcumin in *E. coli*, whereas addition of saturated fatty acids palmitate and stearate had adverse effects. These findings indicated positive correlation between increased unsaturation rate and increased curcumin production, likely due to increased membrane fluidity that confers enhanced tolerance to curcumin (Wu et al., 2020).

Therefore, it is possible to draw a connection between heterologous production of curcumin, and changes in favour of the unsaturated fatty acid palmitoleate and branched chain fatty acid methyl stearate in the fatty acid profile of the CUR-8 curcumin producer. Prominent increase in the abundance of the given fatty acids is likely an adaptation of the curcumin-producing *C. glutamicum* to heterologously produced curcumin. In this way, the strain counteracts the adverse effects that curcumin has on the membrane integrity and fluidity, and overall mitigates its antimicrobial activity.

4.2.9. Transcriptome analysis of curcumin producing *C. glutamicum*

With an aim of getting more profound understanding of how *C. glutamicum* responds to curcumin production, global transcriptome analysis was carried out. For this purpose, a custom-made DNA array was designed. Samples for RNA extraction were harvested at the beginning and in the middle of exponential phase, reflecting the time point of early (low) and late (high) curcumin production. Additionally, these time points correspond to the same time points for CoA-thioester sampling (**Chapter 4.1.10.**).

In order to obtain transcriptome changes that reflect solely effects of high-level curcumin production, the CUR-8 strain, with unmodified supply of acetyl-CoA and malonyl-CoA, was selected as an appropriate candidate for the analysis. The wild type, curcumin-non-producing *C. glutamicum* served as a reference. In total, 12 datasets were obtained, and principal component analysis (PCA) was applied to assess the quality of data. PCA revealed clustering of three biological replicates, indicating good quality of the data (**Fig. 25**). The only exception from this general picture was the sample corresponding to replicate C from the wild type culture in the late production phase. Therefore, this replicate was excluded from the further data analysis. Given the close clustering of the remaining wild type samples from both time points, they were used collectively as a “wild type” reference during the differential gene expression analysis.

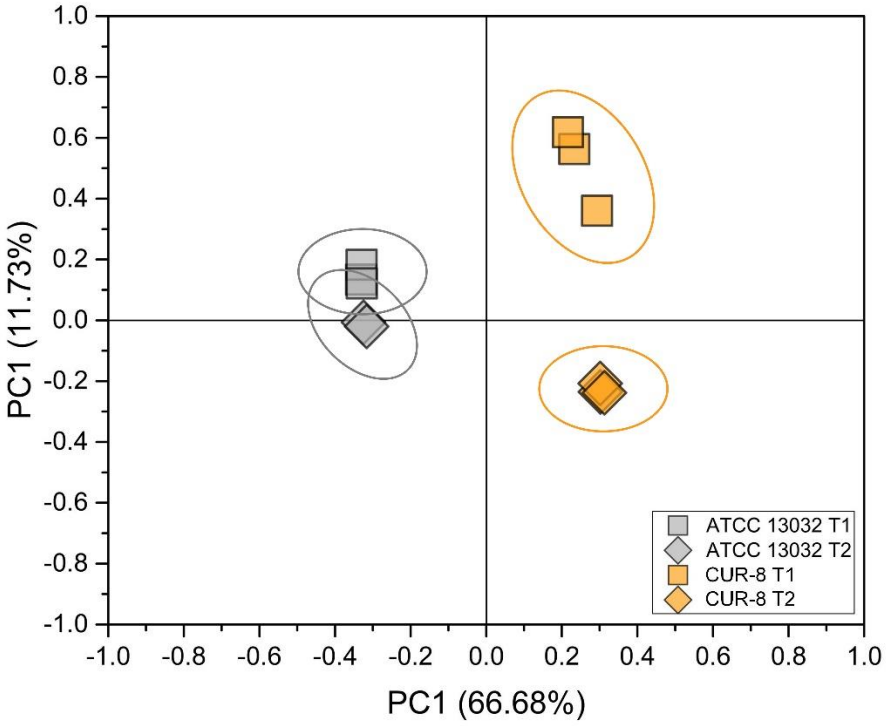

Figure 25. Statistical analysis of global gene expression data. PCA of the raw signals obtained from the custom-made DNA microarray correspond to curcumin producer *C. glutamicum* CUR-8 and wild type ATCC 13032 at the beginning of (T1), and in the middle (T2) of the exponential phase, corresponding to early and late curcumin production phase. Three biological replicates are shown, whereby only ATCC 13032 C2 sample is excluded.

Differential gene expression (DEG) analysis involving native *C. glutamicum* genes revealed quite a few differentially expressed genes. Out of more than 3000 genes, 724 (23.47%) were differentially expressed in the CUR-8 strain at the beginning of exponential phase, when curcumin production was still low. The number of genes affected by curcumin production increased as a production progressed further. Precisely, 967 genes (31.35%) were differentially expressed at the second time point, which corresponds to high level of curcumin production. At both time points, the number of upregulated genes in the CUR-8 strain was more than 600, while number of downregulated genes substantially increased from 63 to 275, from low to high curcumin production phase (**Fig. 26**). The scope of transcriptional changes in curcumin-producing *C. glutamicum* was considerably higher than the previously observed in antibiotic pediocine-producing *C. glutamicum* (Christmann et al., 2023). These results clearly imply strong impact of curcumin production on the native metabolism of *C. glutamicum*.

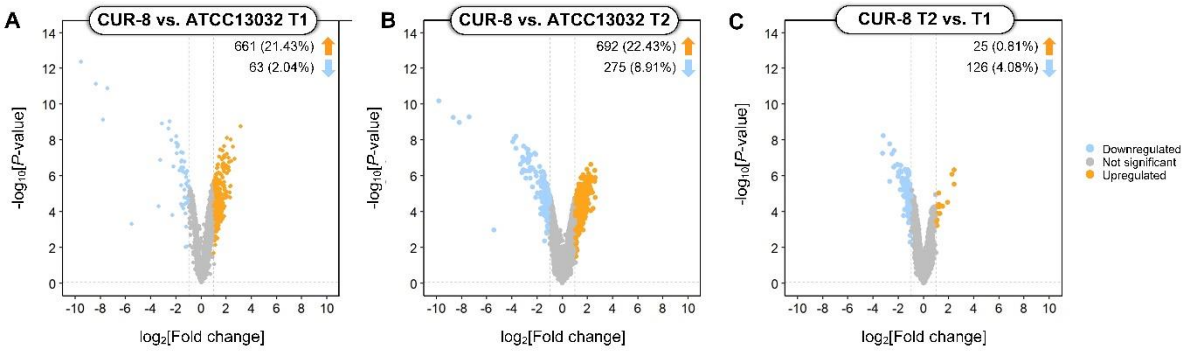

Figure 26. Identification of differentially expressed genes. Volcano plots depicting differentially expressed genes between the curcumin producer and *C. glutamicum* wild type in early production phase – T1 (**A**); and late production phase – T2 (**B**); late and early production phase (T2 vs. T1) in the cultivation profile of the CUR-8 producer strain (**C**). The time points refer to the cultivation profile of the CUR-8 strain and the wild type shown in Fig. 23 and Supplemental Fig. 12, respectively. Number of DEGs and their ratio with respect to complete set of the wild type *C. glutamicum* genome are also represented. Downregulated: $\log_2$[Fold change] < -1, *P*-value >0.05; Upregulated $\log_2$[Fold change] > 1, *P*-value >0.05.

4.2.9.1. Expression of carbon metabolism genes

Relative to the expression levels in the wild type, expression of genes involved in carbon metabolism (Embden-Meyerhof-Parnas (EMP) pathway, pentose phosphate pathway (PPP), TCA cycle, glyoxylate shunt, and anaplerotic reactions), were predominantly downregulated in CUR-8 strain (**Fig. 14**). In addition, *ptsI*, *ptsG*, and *ptsS* genes, encoding phosphotransferase system for glucose uptake, were significantly downregulated. Among them, *ptsI* exhibited the strongest decrease in transcript levels ($\log_2$ fold-change ($\log_2$FC): -3.19). Several other genes annotated as sugar transporters were also downregulated (*NCgl2373*, *NCgl2374*, *NCgl2377*, and *NCgl2894*) (**Table S10**). Reduced expression levels of genes associated with glucose catabolism are in accordance with growth behaviour of the CUR-8 strain, which exhibited nearly 4-fold slower growth rate and glucose uptake rate, during the early production phase than the reference wild type. Moreover, anaplerosis of oxaloacetate intermediate of the TCA cycle was reduced, since the expression of pyruvate carboxylase (*pyc*) and phosphoenolpyruvate carboxylase (*ppc*) was downregulated. Notably, expression of *pyc* and *ppc* genes was more reduced during the late curcumin production phase (**Fig. 27**). In contrast, *dctM*, *dctX*, *dctP*, and *NCgl2506* genes encoding transporters that mediate uptake of C4-dicarboxylates (malate, succinate, and fumarate) (**Table S10**), were upregulated throughout low and high curcumin production phase. Elevated expression of these transporters could potentially be an

adaptation strategy of the strain to replenish C4-dicarboxylate intermediates of the TCA cycle.

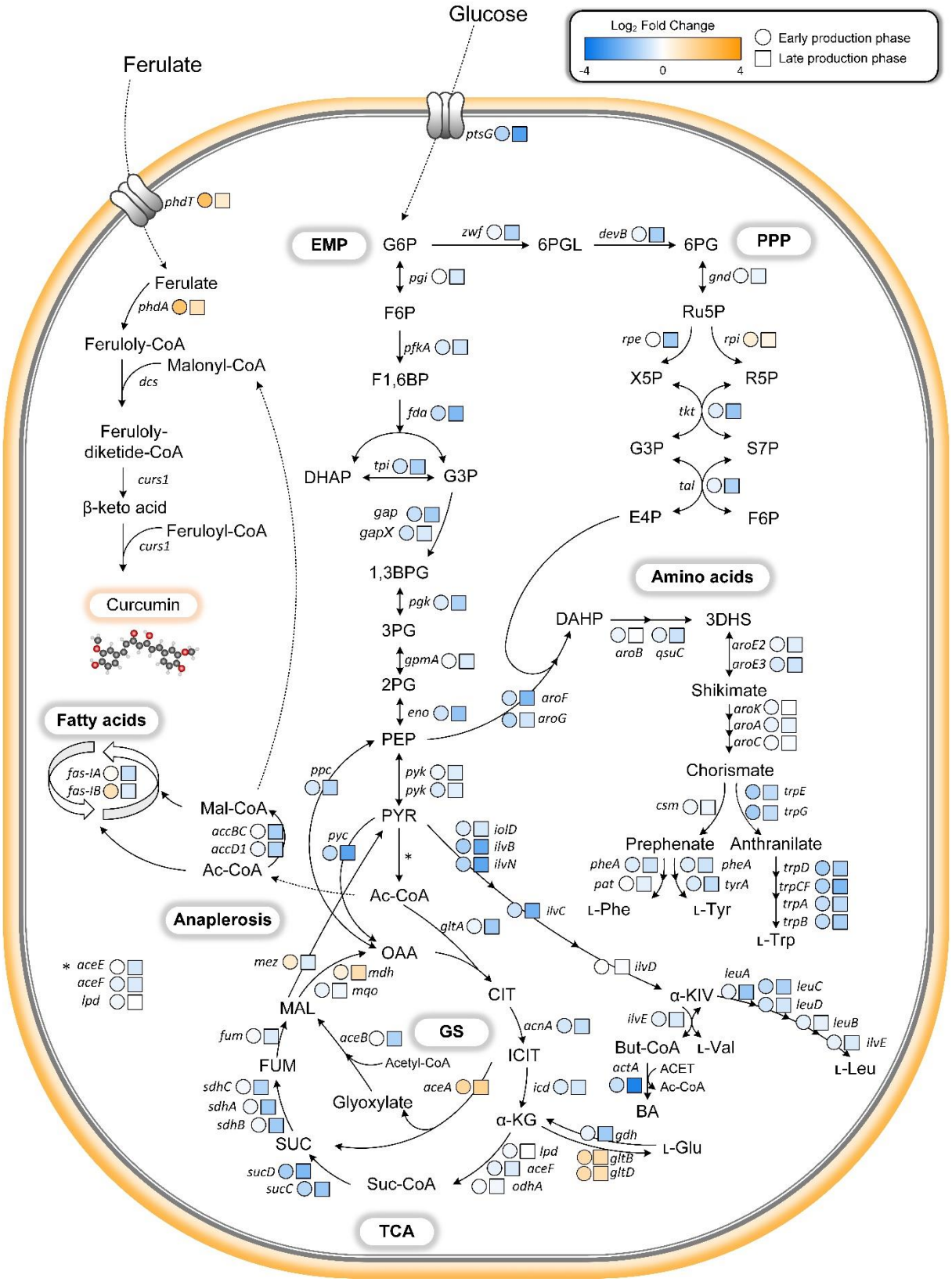

Figure 27. Dynamics of transcriptional changes in primary metabolic pathways in the metabolically engineered *C. glutamicum* CUR-8 during production of curcumin. EMP pathway, PPP, TCA cycle, glyoxylate shunt, analplerotic reactions, synthesis of fatty acids, synthesis of aromatic amino acids, branched-chain amino acids (L-valine and L-leucine), and L-glutamate, degradation of L-valine, and heterologous curcumin biosynthetic pathway are displayed. Gene expression levels are represented as comparative changes (log_2FC) between the CUR-8 curcumin producer and the wild type *C. glutamicum* during early and late production phase (indicated by a circle and square symbol, respectively). KEGG and BioCyc databases were used to reconstruct the metabolic pathways. Abbreviations: *ptsG*: phosphoenolpyruvate-dependent sugar phosphotransferase (PTS) system, glucose-specific EIIBCA component; *pfkA*: 6-phosphofructo kinase; *fda*: fructose-bisphosphate aldolase; *tpi*: triosephosphate isomerase; *gap*: glyceraldehyde-3-phosphate dehydrogenase; *gapX*: glyceraldehyde-3-phosphate dehydrogenase; *pgk*: 3-phosphoglycerate kinase; *gpmA*: phosphoglycerate mutase 1; *eno*: enolase; *pyk* (*NCgl2008*): pyruvate kinase; *pyk* (*NCgl2809*): pyruvate kinase; *aceE*: pyruvate dehydrogenase complex E1 component; *aceF*: pyruvate dehydrogenase complex component E2; *lpd*: dihydrolipoyl dehydrogenase; *ppc*: phosphoenolpyruvate carboxylase; *pyc*: pyruvate carboxylase; *gltA*: citrate synthase; *acnA*: aconitase; icd: isocitrate dehydrogenase; *odhA*: 2-oxoglutarate dehydrogenase E1/E2 component; *sucD*: succinyl-CoA synthetase α subunit; *sucC*: succinyl-CoA synthetase β subunit; *sdhA*: succinate dehydrogenase, flavoprotein subunit; *sdhB*: succinate dehydrogenase, iron-sulfur subunit; *sdhC*: succinate dehydrogenase, membrane-achoring protein; *fum*: fumarase; *mdh*: malate/lactate dehydrogenase; *mqo*: malate quinone oxidoreductase; *mez*: malic enzyme; *zwf*: glucose-6-phosphate 1-dehydrogenase; *devB*: 6-phosphogluconolactonase (glucosamine-6- phosphate isomerase/deaminase); *gnd*: 6-phoshogluconate dehydrogenase; *rpe*: pentose-5-phosphate-3-epimerase; *rpi*: ribose 5-phosphate isomerase; *tkt*: transketolase; *tal*: transaldolase; *accBC*: acetyl/propionyl/methylcrotonyl-CoA carboxylase subunit α; *accD1*: acetyl-CoA carboxylase β subunit; *fas-IA*: fatty acid synthase I; *fas-IIB*: fatty acid synthase II; *aceA*: isocitrate lyase; *aceB*: malate synthase B; *aroF*: 3-deoxy-D-arabino-heptulosonate 7-phosphate (DAHP) synthase; *aroG*: 3-deoxy-D-arabino-heptulosonate 7-phosphate (DAHP) synthase; *aroB*: 3-dehydroquinate synthetase; *qsuC*: type II dehydroquinate dehydratase; *aroE2*: shikimate 5-dehydrogenase; *aroE3*: shikimate 5-dehydrogenase; *aroK*: shikimate kinase; *aroA*: 5-enolpyruvylshikimate-3-phosphate synthase; *aroC*: chorismate synthase; csm: chorismate mutase: *trpE*: anthranilate/para-aminobenzoate synthases component I; *trpG*: anthranilate/para-aminobenzoate synthases component II; *pheA*: prephenate dehydratase; *pat*: L-phenylalanine aminotransferase; *tyrA*: prephenate dehydrogenase; *trpD*: anthranilate phosphoribosyltransferase; *trpCF*: indole-3-glycerol phosphate synthase; *trpA*: L-tryptophan synthase α chain; *trpB*: L-tryptophan synthase β chain; *iolD*: putative acetolactate synthase; *ilvB*: acetolactate synthase large subunit; *ilvN*: acetolactate synthase small subunit; *ilvC*: ketol-acid reductoisomerase; *ilvD*: dihydroxyacid dehydratase/phosphogluconate dehydratase; *leuA*: isopropylmalate/homocitrate/citramalate synthase; *leuC*: 3-isopropylmalate dehydratase large subunit; *leuD*: 3-isopropylmalate dehydratase small subunit; *leuB*: Isocitrate/isopropylmalate dehydrogenase; *ilvE*: branched-chain amino acid aminotransferase/4-amino-4-deoxychorismate lyase; *actA*: acetyl-CoA hydrolase/transferase family protein; *gdh*: L-glutamate dehydrogenase/leucine dehydrogenase; *gltB*: L-glutamate synthase α subunit; *gltD*: L-glutamate β subunit; *dcs*: diketide synthase; *curs1*: curcumin synthase 1; *phdT*: phenylpropanoid transporter; *phdA*: acyl:CoA ligase; TCA: tricarboxylic acid; PPP: pentose phosphate pathway; GS: glyoxylate shunt; EMP: Embden-Meyerhof-Parnas; G6P: glucose 6-phosphate; F6P: fructose 6-phosphate; F1,6BP: fructose 1,6-biphosphate; DHAP: dihydroxyacetone phosphate; G3P: glyceraldehyde 3-phosphate; 1,3BPG: 1,3-biphosphoglycerate; 3PG: 3-phosphoglycerate; 2PG: 2-phosphoglycerate; PEP: phosphoenolpyruvate; PYR: pyruvate: Ac-CoA: acetyl-CoA; CIT: citrate; ICT: isocitrate: α-ketoglutarate; Suc-CoA: succinyl-CoA; SUC: succinate; FUM: fumarate; MAL: malate; OAA: oxaloacetate; Mal-CoA: malonyl-CoA; 6PGL: 6-phospho-gluconolactone; 6-PG: 6-phospho-gluconate; Ru5P: ribulose 5-phosphate; X5P: xylose 5-phosphate; R5P: ribose 5-phosphate; S7P: sedoheptulose 7-phosphate; E4P: erythrose 4-phosphate; DAHP: 3-Deoxy-D-arabinoheptulosonate 7-phosphate; 3DHS: 3-dehydroshikimate; L-Phe: L-phenylalanine; L-Tyr: L-tyrosine; L-Trp: L-tryptophane; L-Val: L-valine; L-Leu: L-leucin; L-Glu: L-glutamate; ACET: acetate; α-KIV:α-keto-isovaleric acid; BA: butyric acid.

4.2.9.2. Expression of amino acid metabolism genes

Concerning the amino acid metabolism, genes catalysing the steps of metabolic route towards the proteinogenic aromatic amino acids (AAA) L-tryptophan, L-phenylalanine, and L-tyrosine, are generally downregulated in the producer strain, as compared to the control wild type strain. Biosynthesis of all three AAA involves shikimate pathway, which starts with condensation of one molecule of erythrose 4-phosphate, the PPP intermediate, and one molecule of phosphoenolpyruvate, the EMP pathway intermediate, in a reaction catalyzed by 3-deoxy-D-arabino-heptulosonate 7-phosphate (DAHP) synthase (Sprenger, 2007). The pathway includes six subsequent enzymatic steps, and proceeds via shikimate to chorismate, a last common precursor of all three AAA (Pittard and Yang, 2008). The rate-limiting step of the shikimate pathway is synthesis of DAHP, which is in *C. glutamicum* catalysed by *aroG* and *aroF* genes (Neshat et al., 2014). Notably, expression of *aroF* gene was significantly downregulated in the curcumin producer during late production phase (log_2FC: -1.73). From chorismate, biosynthesis further proceeds via two branches (Sprenger, 2007). First, L-phenylalanine and L-tyrosine are produced from prephenate, while biosynthesis of L-tryptophane starts from anthranilate. The branch leading from chorismate to L-tryptophane was notably downregulated, given that genes (*trpG*, *trpD*, *trpCF*, *trpA*, and *trpB*) encoding enzymes catalysing each step of this metabolic route (Brune et al., 2007), had reduced transcript levels (**Fig. 27**).

Next, *ilvB* and *ilvN*, encoding acetohydroxyacid synthase (AHAS) (Keilhauer et al., 1993), an enzyme catalysing first committed step in biosynthesis of the branched-chain amino acids L-valine and L-leucine (Pátek, 2007), were downregulated (**Fig. 27**). In addition, *leuA*, coding for isopropylmalate synthase (IPMS), an enzyme that catalyses first reaction in L-leucine-specific pathway using 2-ketoisovalerate as substrate (Pátek, 2007), was downregulated as well. Transcript levels of carbamoylphosphate synthases (CPS), encoded by *carA* and *carB* were also reduced in the producer strain. Thereby, CPS catalyses first step in biosynthesis of L-arginine via hydrogen carbonate route (Glansdorff and Xu, 2007). Moreover, expression of 5-methyltetrahydropteroyltriglutamate homocysteine S-methyltransferase *metE*, glutamate-5-semialdehyde dehydrogenase *proA*, genes encoding enzymes involved in biosynthesis of L-methionine (Rückert et al., 2003), and L-proline (Ankri et al., 1996), respectively, was downregulated in CUR-8 strain. It appears noteworthy that transport of L-glutamate was significantly downregulated, given that *gluA* (L-glutamate ABC-type

transporter, ATP –binding protein) (Haußmann et al., 2009), *gluB* (L-glutamate ABC-type transporter, periplasmic, L-glutamate-binding component) (Michel et al., 2015) , and *gluC* (L-glutamate ABC-type transporter, permease) (Silberbach et al., 2005) had reduced transcripts level in the curcumin producer (**Table S6**). In contrast, genes encoding L-glutamate synthase α and β subunits (*gltB* and *gltD*) (Beckers et al., 2001) appeared to have elevated levels of transcripts (**Fig. 27**), whereas the reaction in opposite direction, leading back to the L-glutamate precursors (α-ketoglutarate), which is catalysed by the glutamate dehydrogenase (*gdh*) (Tesch et al., 1999), was downregulated. These set of observations suggest activation of L-glutamate synthesis, and tonning down of L-glutamate consuming reactions. Notably, L-glutamate is needed for biosynthesis of glutathione, tripeptide involved in scavenging of free radicals during oxidative stress (Tsutsui et al., 2021).

Gnes involved in the biosynthesis of L-tyrosine, L-tryptophane, and L-methionine, were previously shown to be downregulated in yeast strain overproducing *p*-coumarate (Rodriguez et al., 2017), phenylpropanoid precursor for biosynthesis of other curcuminoids, demethoxycurcumin and bisdemethoxycurcumin. Diminishment in protein biosynthesis has been considered as an adaptation during exposure to oxidants, such as hydrogen peroxide. This strategy is believed to put a stop to continuous protein biosynthesis during error-prone conditions, such as oxidative stress (Shenton and Grant, 2003). This notion motivated further investigation of genes closely associated with oxidative stress response, and other steps of central molecular dogma leading to protein biosynthesis.

4.2.9.3. Expression of oxidative stress-response genes

DEG analysis revealed additional markers of oxidative stress in curcumin-producing *C. glutamicum* CUR-8. Upregulation of organic peroxide resistance protein (*NCgl0023*), peroxide stress protein YaaA (*NCgl1920*), Dyp-type peroxidase (*NCgl1608*), and predicted glutathione S-transferase (*NCgl1216*), suggests activation of oxidative stress response in the CUR-8 strain (**Table S7**). Peroxidases are ubiquitous enzymes performing vital function in elimination of peroxides, the oxidative stress causing agents (Bindoli and Rigobello, 2013; Watanabe and Nakajima, 2016). Essentially, peroxidases catalyse reduction of hydrogen or organic peroxides to water, thereby oxidising a range of substrates, such as halide ions, aromatic azo compounds,

and hydroquinones (Everse, 2013). Additionally, s-glutathionylation is a universal regulatory system in all domains of living organisms. Its purpose is post-translational modification of protein cysteine residues, as a protective mechanism against oxidation of protein thiol groups (Shenton and Grant, 2003; Dalle-Donne et al., 2009). Indeed, curcumin is known to trigger production of reactive oxygen species in carcinoma cell lines, thereby sensitizing them to radiation toxicity (Mortezaee et al., 2019). Moreover, pyridoxal 5'-phosphate (PLP) synthases *pdxT* and *pdxS*, genes involved in biosynthesis of an essential cofactor vitamin B6, were significantly downregulated in low and high curcumin production phase (**Table S7**). PLP deficient mutants of Gram-positive *Actinobacillus pleuropneumoniae* were more susceptible to hydrogen peroxide-induced oxidative stress and showed reduced cell count (Xie et al., 2017). On a first glance, lack of *pdxT* and *pdxS* renders cells more prone to hydrogen peroxide-induced cell death. However, downregulation of these genes has been considered as a marker of metabolic shift during SOS response in *C: glutamicum* (Jochmann et al., 2009). Clearly, role of *pdxT* and *pdxS* in oxidative stress response in *C. glutamicum* is complex, and requires further investigation.

Implications of glyoxylate shunt (GS) isocitrate lyase (*aceA*) and the second GS enzyme malate synthase (*aceB*) in oxidative stress response is not straightforward. *AceA* gene was consistently upregulated, whereas expression of the second GS enzyme malate synthase (*aceB*) was close to basal levels, or slightly downregulated during high curcumin production phase (**Fig. 27**). Identical picture has been previously observed in *P. aeruginosa* cultures treated with hydrogen peroxide (H_2O_2) (Ha et al., 2018). The role of *aceA* in oxidative stress response is poorly understood. Nevertheless, GS genes are associated with response to various forms of environmental stress, including redox stress, iron limitation, and exposure to antibiotics (Dolan and Welch, 2018). Implications of curcumin in promoting formation of reactive oxygen species (ROS) have been widely studied before, and there is strong association between treatment with curcumin an oxidative stress in Gram-negative and Gram-positive bacteria, such as *E. coli* and *Staphylococcus aureus*, respectively (Adeyemi et al., 2020). Therefore, triggering of oxidative stress and consequential DNA damage are considered to be part of the curcumin antimicrobial arsenal (Dai et al., 2022).

It appears noteworthy that certain genes associated with SOS response, such as 3-methyladenine DNA glycosylase (*NCgl2739*), involved into repair of methylating agent-induced DNA damage (Lindahl et al., 1988), RecA recombinase (*NCgl1880*), a universal enzyme in stress-induced DNA damage repair (Kaushik et al., 2022), and iron-sulphur cluster assembly proteins involved in disulphide stress response, s*ufC*, *sufB*, and *sufD* (Nakunst et al., 2007), were found to be have reduced levels of transcripts in CUR-8 when compared to the reference strain (**Table S7**). Herein, it is important to point out that in addition to inducing production of reactive species in bacteria, curcumin can, at the same time, inhibit activation of several SOS response associated genes. This inhibition of stress response is yet another way in which curcumin could reduce vitality of bacterial cells (Dai et al., 2022). With regards to SOS response, differentially expressed genes indicate a complex transcriptional response of *C. glutamicum* during curcumin production, showing attempts to mitigate the effects of oxidative stress.

4.2.9.4. Expression of genes associated with transcription, translation and ribosome structure

DEG analysis of curcumin producing *C. glutamicum* additionally revealed reduced transcripts of genes associated with transcription, translation, and ribosome structure, as compared to the wild type strain (**Table 6, S8**). Degree of downregulation particularly increased during high curcumin production phase, suggesting that elevated concentrations of curcumin have more pronounced effect on expression of genes involved in transcription and translation, processes that are essentially at the crux of all living organisms.

Table 6. Gene expression data of the selected genes related to ribosome biogenesis, transcription, and translation during curcumin production in genetically engineered *C. glutamicum*. The data represents log_2FC of genes involved in formation of ribosomes, transcription, and translation in the CUR-8 strain, as compared to the curcumin non-producing *C. glutamicum* ATCC 13032_pClik 5α during the early production (T1) and major production phase (T2).

Locus tag	Gene ID	Product	Log_2FC T1	Log_2FC T2
		Transcription and translation		
NCgl0540	*rpoA*	DNA-directed RNA polymerase subunit α	-0.48	-1.14
NCgl0471	*rpoB*	DNA-directed RNA polymerase subunit β	-0.46	-1.16
NCgl0472	*rpoC*	DNA-directed RNA polymerase subunit β	-0.66	-1.22

NCgl1543	*rpoZ*	DNA-directed RNA polymerase subunit ω	-0.43	-1.05
NCgl0946	*greA*	Transcription elongation factor	-0.50	-1.19
NCgl0536	*infA*	Translation initiation factor IF-1	-0.36	-1.08
NCgl1910	*infB*	Translation initiation factor IF-2	-0.67	-1.39
NCgl1324	*infC*	Translation initiation factor IF-3	-0.35	-1.33
NCgl1949	*tsf*	Translation elongation factor Ts	-0.72	-1.12
NCgl0725	*raiA*	Ribosome-associated translation inhibitor	-0.59	-1.21
		50S ribosomal proteins		
NCgl2993	*rpmH*	50S ribosomal protein L34	-0.35	-1.46
NCgl0556	*rplM*	50S ribosomal protein L13	-0.65	-1.42
NCgl0487	*rplC*	50S ribosomal protein L3	-0.43	-1.41
NCgl0520	*rplO*	50S ribosomal protein L15	-0.69	-1.40
NCgl0490	*rplB*	50S ribosomal protein L2	-0.52	-1.39
		30S ribosomal proteins		
NCgl0493	*rpsC*	30S ribosomal protein S3	-0.51	-1.44
NCgl0518	*rpsE*	30S ribosomal protein S5	-0.54	-1.32
NCgl0477	*rpsG*	30S ribosomal protein S7	-0.54	-1.38
NCgl0515	*rpsH*	30S ribosomal protein S8	-0.44	-1.16
NCgl0557	*rpsI*	30S ribosomal protein S9	-0.66	-1.41

Expression of notable number of 43 ribosomal proteins was downregulated in the CUR-8 strain when compared to the reference wild type strain (**Table S8**), proposing reduced ribosome formation and impaired translational machinery. Literature on direct inhibition of transcription and translation processes by curcumin is scarce, but there is growing body of research related to impact of oxidative stress on every stage of central dogma. Indeed, several ribosome proteins were found to be downregulated in *E. coli* cells upon treatment with hydrogen peroxide (Zheng et al., 2001). Ribosomes are organelles formed by rRNA and ribosomal proteins, which are organised into two subunits, 50S and 30S subunit (Martín et al., 2003). They are present in enormous number (~30,000 μm^{-3} during exponential growth of *C. glutamicum*), (Susana et al., 2021) whereby rRNA accounts for up to 80% of the total RNA and ribosomal proteins 10% of total cell proteome (Martín et al., 2003). Therefore, ribosome biogenesis is tremendously energy costly for the cell (Davis and Williamson, 2017), and recycling of ribosomes upon oxidative damage is additional burden for the microbe (Fasnacht and Polacek, 2021). Overall, diminished rate of ribosomal biogenesis can be an adaptation strategy as part of the survival during stress conditions (Njenga et al., 2023).

Another adaptation strategy to stress conditions is inhibition of translation. Although only elongation process was previously been reported to be affected by oxidative stress in *E. coli* (Fasnacht and Polacek, 2021), here a collective downregulation of translation initiation (*infA*, *infB*, *infC*) and elongation (*tsf*) factors was observed (**Table 6**). Additionally, transcription-related genes were not spared. Namely, RNA polymerase subunits (*rpoA*, *rpoB*, *rpoC*, and *rpoZ*) and transcription elongation factor (*greA*) were downregulated in the CUR-8, as compared to the wild type (**Table 6**)**.** Overall, heterologous production of curcumin seemed to severely impact processes of central dogma processes, including initiation and elongation of transcription and translation, and ribosome biogenesis.

4.2.9.5. Expression of transcription factors

Regarding the regulatory transcription network, transcription factors from various families were differentially expressed in the curcumin producing strain (PadR, WhiB, TetR, LuxR, IclR, LysR, GntR, AraC, AbrB, LacI, Lrp/AsnC, ArgP/LysG, Crp/Fnr, BlaI/MecI/CopY, ArsR/SmtB, and XRE) (**Table S9**). Among them, GlxR as a global transcriptional regulator stands out. More than 200 genes are part of the GlxR regulatory network, and they are associated with carbohydrate metabolism, aromatic compound catabolism, biosynthesis of fatty acids, respiration, glutamate and nitrogen metabolism, resuscitation, and stress response (Kohl and Tauch, 2009; Toyoda et al., 2011). GlxR, which was slightly downregulated in the curcumin producer, was previously identified as an activator of glycolytic pathway genes. Herein, glycolytic genes were overall downregulated inthe CUR-8, when compared to the wild type. Similar picture was seen with another global transcriptional regulator RamB, which also had reduced expression levels in the curcumin producer strain. RamB was initially identified as a regulator of acetate (Gerstmeir et al., 2004) and ethanol (Arndt and Eikmanns, 2007) metabolism genes. However, genome-wide transcriptome analysis identified additional genes as part of the RamB regulon (Auchter et al., 2011). For instance, RamB was proposed to activate expression of glucose and fructose transporters *ptsG* (*NCgl1305*), *ptsS* (*NCgl2553*), and pyruvate carboxylase *pyc* (*NCgl0659*) (Auchter et al., 2011) which were notably downregulated in the CUR-8 strain (log2FC: -2.73, -2.56, and -2.61, respectively). Therefore, it is likely that reduced expression of sugar importers *ptsG*, *ptsS*, and *pyc* is connected to downregulation of

their cognate activator RamB. Moreover, RamB has been identified as repressor of citrate synthase *gltA*, *aceA*, and *aceB* (Auchter et al., 2011). In accordance with reduced expression of *ramB*, *aceA* was upregulated, but *gltA* and *aceB* showed reduced expression in the curcumin producer.

Concerning the sigma factors, seven are encoded by the genome of *C. glutamicum* (*sigA*, *sigB*, *sigC*, *sigD*, *sigE*, *sigH*, and *sigM*) (Kalinowski et al., 2003). Only *sigM* was differentially expressed in the curcumin producer (**Table S9**). *SigM* has been previously shown to be upregulated in *C. glutamicum* in response to diamide-caused disulphide stress, but not in response to hydrogen peroxide (Bott, 2007). Therefore, enhanced expression of the sigma factor *sigM* suggests exposure of the CUR-8 strain to disulphide stress. Despite the fact that *sufCBD* genes are part of the *sigM* regulon, and that they are typically activated upon exposure of *C. glutamicum* to disulphide stress (Nakunst et al., 2007), this was not a scenario during curcumin production. As mentioned above, these genes had lower levels of transcripts, as compared to the wild type (**Table S7**).

Furthermore, WhiB family transcriptional regulators *whcE*, *whcB*, and *whcA* were differentially expressed in the CUR-8 strain. WhiB family transcription factors are homologues of WhiB proteins from *Streptomyces coelicolor*, whereby they play central role in development of aerial hyphae (Soliveri et al., 2000). In the related actinomycetes, WhiB-like proteins act as transcription factors, which are implicated in the regulation of various cellular processes, such as cell division (Lee et al., 2018), differentiation (Kim et al., 2012), pathogenesis (Steyn et al., 2002), survival during starvation (Zheng et al., 2012) and stress response (Geiman et al., 2006). WhcE, WhcB, and WhcA contain redox-sensing motifs, which enables them to respond to changes in oxidative status of the cell (Choi et al., 2009). Therefore, they are part of the oxidative stress response system in *C. glutamicum*.

The roles of *whcE*, *whcB*, and *whcA* in the oxidative response network have been established. *WhcB*, which was found to be upregulated in the curcumin producer, stimulates expression of the positive regulator *whcE* (Lee et al., 2013a) that subsequently activates stress response genes (Kim et al., 2005), including *whcA* (Lee et al., 2013a). In contrast, WhcA has an opposing role, and exerts negative control of its regulon (Choi et al., 2009). The repressing effect is mediated by interaction with SpiA protein. During imbalanced oxidative state, SpiA dissociates from WhcA, and its

repressing effect is relieved (Park et al., 2012). Although *whcB* was upregulated during high curcumin production phase, expression of its target gene *whcE* was downregulated. Moreover, transcript levels of *whcA* were reduced in the CUR-8 strain, but NADH oxidase (*NCgl0328*), cysteine desulfurase (*NCgl1022*), alcohol dehydrogenase (*NCgl2053*), quinone reductase (*NCgl2971*), and thioredoxin reductases *trxAB* (*NCgl2984* and *NCgl2874*) (Choi et al., 2009) were not differentially expressed. Notably, both *whcE* and *whcA* contain binding sites of the global transcription factor GlxR (Kohl and Tauch, 2009).

Overall, differential expression of number of transcription factors, including global regulators, in the CUR-8 strain, suggests complex global transcription changes coordinating activity of various metabolic pathways in response to curcumin production in *C. glutamicum*. This was reflected by hundredths of differentially expressed genes in a host that is generally regarded as robust (Wolf et al., 2021).

4.2.9.6. Expression of membrane proteins genes

Significant proportion of the differentially expressed genes (208) in the CUR-8 strain were genes encoding membrane proteins, suggesting strong disturbance of membrane homeostasis during heterologous curcumin production. More than half of these genes encode for transport proteins. Supplemental table 10 gives a comprehensive view of these transporters, whereby they are grouped according to the type of solute they transport.

Transport of amino acids, vitamins, cations, ammonium, aromatic compounds, organic acids, carbohydrates, iron, lipids, phosphate, and peptides seems to be affected. Notably, expression of MMPL family drug transporter (*NCgl0887*), multidrug efflux MFS protein (*NCgl2647*), and *tetA* ATP-binding protein of an ABC transporter (*NCgl1468*), predicted to mediate drug transport, was upregulated. Although curcumin tends to anchor within the membrane, it is likely that some of the produced curcumin is exported outside of the cell, as a way of the microbe to expel curcumin and mitigate its antimicrobial effects. Orange colour of the culture supernatant (**Fig. S13**) confirms that not all curcumin is stored within the cell membrane, but whether this happens due to transport-mediated efflux, or passively, cannot be elucidated.

4.2.9.7. Expression of CoA-thioester metabolism genes

Given that CoA-thioester metabolism generates malonyl-CoA and feruloyl-CoA, as the main building blocks of curcumin, transcript levels of these and other CoA-thioesters identified in extracts of curcumin producing *C. glutamicum* (acetyl-CoA, succinyl-CoA, butyryl-CoA, methylmalonyl-CoA) (**Fig. 23**), were examined further. Here, *aceE*, *aceF*, and *lpd*, encoding pyruvate dehydrogenase complex E1 component, E2 component, and dihydrolipoyl dehydrogenase, enzymes that drive conversion of pyruvate to acetyl-CoA (Guest and Stephens, 1980), were not differentially expressed (**Fig. 27**). On the other hand, acetate kinase *ackA* and phosphotransacetylase *pta*, which catalyse step-wise conversion of acetate to acetyl-CoA in the acetate node (Rajaraman et al., 2016), showed reduced mRNA levels. Nevertheless, pools of acetyl-CoA in the CUR-8 strain showed diminution in size at the beginning and in the middle of exponential growth phase, when compared to the wild type. Importantly, concentration of acetyl-CoA progressively decreased in the wild type, while in the curcumin producer, acetyl-CoA showed increasing dynamics. This observation correlates well with downregulation of *gltA*, *accBC*, and *accD1* (**Fig. 27**, **Table S11**), enzymes that govern withdrawal of acetyl-CoA by TCA cycle (Akram, 2014) and fatty acid biosynthetic module (Hardie, 1989). Therefore, diminished consumption of acetyl-CoA by these central metabolic pathways could enable its accumulation over time. Reduced mRNA levels of *accBC* and *accD1* genes, agrees with up to 20-fold reduced concentration of malonyl-CoA in the producer strain. Importantly, heterologous production of malonyl-CoA-derived curcumin, certainly contributed to depletion of malonyl-CoA.

Concerning the second precursor for biosynthesis of curcumin feruloyl-CoA, *phdA* showed pronounced upregulation at the beginning of exponential phase (early production phase), during which curcumin production was still low. However, during mid-exponential growth phase (late production phase), the gene exhibited minor upregulation, which was statistically not significant (log_2FC: <1.0). The noted dynamics of *phdA* expression is in line with changes in concentration of feruloyl-CoA throughout cultivation profile (**Fig. S11**). During the early production phase, concentration of feruloyl-CoA was 43% higher in the CUR-8 strain than in the wild type. However, as the production proceeded, a sharp decline in pools of feruloyl-CoA was apparent. This can be related to increased productivity of curcumin during late production phase and consequently stronger withdrawal of feruloyl-CoA from the created pool, while at the same time expression of *phdA* ceased.

The synthesis of TCA cycle intermediate succinyl-CoA from 2-oxoglutarate appeared to be downregulated, given that succinyl-CoA synthases *sucC* and *sucD* (Buck et al., 1985) exhibited reduced transcript levels during early and late production phase. In view of decreased expression of methylmalonyl-CoA mutases *mcmA* and *mcmB*, replenishment of succinyl-CoA from methylmalonyl-CoA was also reduced. Notable increase in concentration of butyryl-CoA can be related to significant decrease in expression of butyryl-CoA: acetate CoA-transferase *actA*, an enzyme that catalyses synthesis of short chain fatty acid butanoate and acetyl-CoA, from butyryl-CoA and acetate (Yang et al., 2021b). ActA has been previously associated with lipid and cell envelope synthesis, and showed reduced mRNA levels in *C. glutamicum* upon salt stress (Fränzel et al., 2010).

4.2.9.8. Expression of cell envelope and lipid metabolism related genes

Taking into account considerable number of membrane proteins that were differentially expressed, as well as notable decrease in expression of lipid and cell wall-associated *actA*, genes related to fatty acids, lipids, cell wall, and cell division were investigated further.

In terms of fatty acid synthesis, malonyl-CoA-forming enzymes *accBC* and *accD1*, showed decreased expression during the late production phase, suggesting reduced supply of the fatty acid precursor, malonyl-CoA. Unlike majority of bacteria, which synthesize fatty acids by fatty acid syntheses (FAS) type II, *C. glutamicum* and related species from *Corynebacteriaceae* family employ FAS type I (FAS-I) (Radmacher et al., 2005). Here genome of *C. glutamicum* encodes two fatty acid synthases; *fasA* and *fasB* (Takeno et al., 2013). Expression of *fasB* was slightly upregulated during early production phase (log_2FC: 1.00), however during late production phase both *fasA* and *fasB* exhibited only minor reduction in the levels of mRNA ($0 < log_2FC > -1.0$). Notably, *fasB* is not an essential FAS, as its deletion was not detrimental to *C. glutamicum*. However, *fasA* is a vital FAS, given that the *fasA*-deficient strain could not grow in glucose minimal medium without additional supplementation of oleate (Radmacher et al., 2005). Even under these conditions, palmitoleate and stearate were not detected in the fatty acid profile of the *fasA* mutant, implying that *fasA* catalyses synthesis of palmitoleate and stearate in *C. glutamicum*. These findings partially correlate with the fatty acid phenotype observed in the curcumin producer. Slight downregulation of *fasA*

could explain reduced ratio of oleate in the curcumin producer, but it does not justify increased abundance of palmitoleate. None of the genes that are annotated as desaturases were not differentially expressed in the CUR-8 strain.

Next, upregulation of putative lipase *NCgl1426* during early and late production phases is indicative of degradation of already existing lipids. However, none of the genes annotated as fatty acid: CoA ligase, which would activate fatty acids during β-oxidation degradation of fatty acids were not differentially expressed in the curcumin producers. On the other hand, several genes annotated as acyl-CoA dehydrogenases (*NCgl1229*, *NCgl0974*, and *NCgl0973*), enzymes that catalyse conversion of acyl-CoAs to 2,3-enoyl-CoAs during β-oxidation, showed increased levels of mRNA transcripts (**Table S12**). Overall, there was no clear indication of increased β-oxidation of fatty acids in the CUR-8 strain.

Concerning cell wall biogenesis and cell division, glucosamine-1-phosphate acetyltransferase *glmU*, endolytic transglycosylase *mltG*, septum formation initiator family protein *NCgl0936*, and cell division protein *ftsQ*, showed decreased levels of their corresponding transcripts. GlmU catalyses formation of UDP-N-acetyl-D-glucosamine, a key precursor of cell wall peptidoglycan (Zhang et al., 2008a), whereas MltG controls termination of the nascent peptidoglycan chain (Taguchi et al., 2021). Septum formation is central process during cell division of Gram-positive bacteria (Su et al., 2020). Therefore, downregulation of *glmU*, *mltG*, and *ftsQ* is indicative of impaired cell differentiation in the curcumin producer.

4.2.9.9. Expression of aromatic compound metabolism genes

With regards to ferulate metabolism, *phdT* and *phdA* genes were upregulated during early production phase, whereas their transcript levels dropped during the late production phase. Identical picture was observed for the ferulate importer *phdT* (**Fig. 27**, **Table S13**). Given that rest of the *phd* cluster genes (*phdRBCDE*) were deleted in the CUR-8 strain, their mRNA levels were understandably notably reduced.

Although benzoate was not supplied in the growth medium, genes of the benzoate degradation cluster *benABCDEK* showed elevated expression in the curcumin producer during early and late production phase (**Table S13**). This results is consistent with previous findings where hydrogen peroxide-tolerant *C. glutamicum* strain

developed by adaptive evolution displayed elevated expression of the same genes (Lee et al., 2013b). Therefore, upregulation of genes of the benzoate degradation cluster, could be related to adaptation towards oxidative stress agents. Moreover, transcript levels of protocatechuate degradation pathway *pcaI*, *pcaB2*, and *NCgl1004*, were also found to be de enhanced (**Table S13**). Protocatechuate, also known as 3, 4-dihydroxybenzoate is supplemented in the growth medium, as an iron chelating agents to facilitate uptake of iron. Degradation of protocatechuate via the β-ketoadipate pathway yields in formation of acetyl-CoA and succinyl-CoA (Sgro et al., 2023), and can aid in replenishment of these primary metabolites. Moreover, intermediates of the β-ketoadipate pathway are believed to exert ROS scavenging properties (Lee et al., 2014). Hence, increased degradation of protocatechuate could help the curcumin producer to adapt to oxidative environment.

4.2.10. Process optimization for scale-up of curcumin production

Given the pronounced sensitivity of curcumin to pH and oxygen (Martínez-Guerra et al., 2019), these bioprocess parameters needed to be optimized. This step was motivated by the premise that not all curcumin is stored inside of the cell (**Fig. S13**), and that some portion is present extracellularly. Outside of the lipid bilayer, curcumin would be sensitive to impact of pH and oxygen, and prone to degradation. For this purpose, *C. glutamicum* CUR-8 strain was grown in stirred-tank bioreactors, in three fermentation setups: high oxygen and high pH (20% dO_2; pH=6.8); low oxygen and high pH (2.5% dO_2; pH=6.8), and low oxygen and low pH (2.5% dO_2; pH=6.0). Taking into account that curcumin exhibits increased stability in the acidic environment, only pH values below 7.0 were considered. In each condition, the process started with the initial concentration of 90 g L^{-1} glucose, as growth substrate, and 2.5 g L^{-1} yeast extract, to support the cell vitality at acidic pH. In order to shorten the lag phase observed in cultivation profile of the CUR-8 strain in the shake flask experiments, ferulate was not added at beginning of the fermentation process. Instead, a 15 mM ferulate feed was added after hours of cultivation, which corresponds to two new generations, indicating good cell vitality. The goal of delayed addition of ferulate was to allow the cells to adapt to the conditions in the reactors, thereby reducing the stress from the exposure to the aromatic. In each set-up, kanamycin was added to the cultivation medium.

A highest curcumin titre of 392 mg L^{-1} was obtained in the in the first condition where oxygen saturation was maintained at 20% level and pH at 6.8. It took the producer 88 hours to consume glucose entirely, whereas ferulate was depleted sooner, after 64 hours. Within this time, there was modest accumulation of 4.6 mM lactate (**Fig. 28A**). Notably, the dynamics of ferulate consumption was peculiar. Namely, until 40 hours, the uptake rate was slow (0.17 h^{-1}), suggesting that entire feed of 15 mM would not be utilized by the end of fermentation period. Surprisingly, HPLC measurements after 48 hours showed sharp decrease in the concentration of ferulate in the supernatant of culture broth. The acceleration of ferulate utilization also coincided with the revived growth of the cells that previously stopped already after 22 hours of fermentation. Moreover, maximum formed biomass was 15 g L^{-1}, which is by 33% more than in the other tested conditions. This brings an assumption that the during this fermentation period, a mutation, which allows the *phdRBCDE*-deficient strain to rapidly consume ferulate, occurred.

Lowering the oxygen saturation to 2.5% turned out to be unfavourable for curcumin production, reducing the curcumin titre by 42% to 224 mg L^{-1}. Given that nearly two thirds of the ferulate feed were still present after 65 hours, and that staggering amount of almost 500 mM lactate accumulated within this time, fermentation was terminated at this time point. The growth stopped fairly early after 22 hours, which exactly matches the time when lactate formation surged (**Fig. 28B**). This growth phenotype corroborates with previous findings where under oxygen limiting conditions, lactate was produced from glucose by *C. glutamicum* without growth (Inui et al., 2004). Curcumin production abated when lactate level reached 122 mM.

Combination of oxygen limitation and lower pH had even more detrimental effect on the production, resulting in 161 mg L^{-1} of curcumin formed (**Fig. 28C**). The trends in growth, lactate formation, ferulate utilization, and curcumin production are very alike to the ones in previous condition. However, within the 65 hours period, more than 200 mM glucose remained untouched by the strain, explaining the 2-fold lower accumulation of lactate, when compared to condition with higher pH.

This set of observations suggest that oxygen limitation and low pH are not advantageous for curcumin production. Rather, high oxygen levels and moderately acidic conditions support higher production of curcumin. For this reason, in the

following fermentation experiments, dissolved oxygen and pH were set to 20% 6.8, respectively.

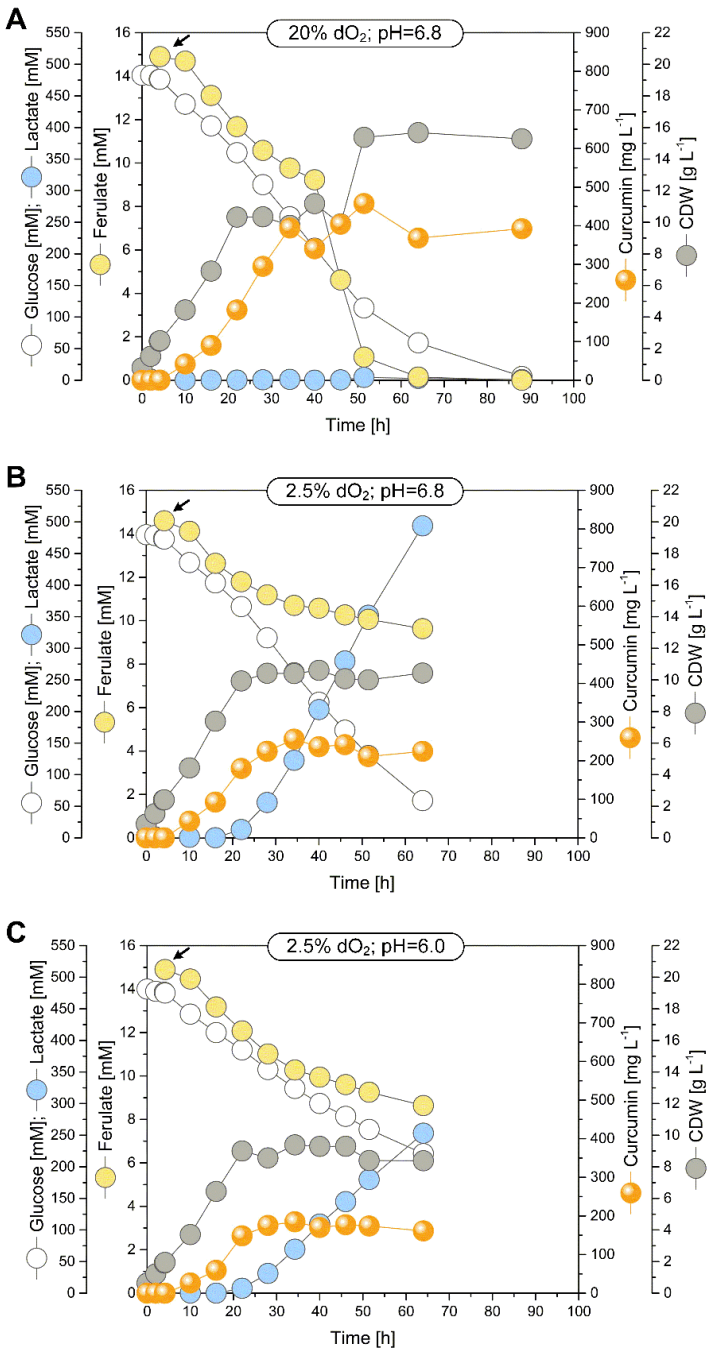

Figure 28. Bioprocess optimization of curcumin production in stirred-tank bioreactors by metabolically engineered *C. glutamicum* CUR-8. The data represents cultivation profiles under high oxygen, low pH (20% dO_2; pH=6.8) (**A**); oxygen limiting, high pH (2.5% dO_2; pH=6.8) (**B**); and oxygen limiting, low pH (2.5% dO_2; pH=6.0) (**C**) conditions. The arrows indicate feeding with ferulate. The data comprises single biological replicates.

4.2.11. Benchmarking of *C. glutamicum* CUR-8 in fed-batch process

Given that increased concentration of glucose and ferulate did not result in considerable increase in the curcumin titre, the second-best performing strain from the shake flask experiments, the CUR-8 strain was further evaluated in a fed-batch process. Here, the CUR-8 strain, and not the best-performing CUR-12 was selected. The rationale behind this was fitter cell vitality of the CUR-8 strain, indicated by shorter lag phase in the cultivation profile. Oxygen saturation and pH were maintained at 20% and 6.8, respectively.

The initial concentration of glucose was set to 30 g L^{-1}, and subsequent pulses of 30 g L^{-1} glucose and 5 mM ferulate were given manually from concentrated stock solutions (500 g L^{-1} and 500 mM, respectively). During the first batch, glucose was consumed within 30 hours with a rate of 6.63 mM h^{-1} (**Fig. 29A**). First ferulate pulse was given after four hours, and was consumed in 26 hours with a rate of 0.22 mM h^{-1}. Notably, ferulate and glucose were co-utilized, and curcumin production set-on immediately after the ferulate feed. Throughout the first batch 338 m L^{-1} of curcumin were produced. The second pulse of glucose was given once the initially provided glucose was depleted, indicated by increase in dissolved oxygen and confirmed by HPLC measurement. Given that the second ferulate pulse was given at the time when glucose was completely exhausted, the strain experienced plateau in growth, but picked up as soon as the second glucose pulse was injected. During the second phase, glucose uptake rate increased to 7.29 mM h^{-1}, whereas ferulate uptake slowed down, demonstrated by reduced rate of 0.13 mM h^{-1}. Glucose and ferulate were still co-consumed, and curcumin formation was growth coupled, reaching 692 mg L^{-1} prior the third feed (**Fig. 29A**). In order to provide strain with a sufficient amount of glucose, a third pulse was injected prior complete exhaustion of the second feed. In the course of third feed consumption of glucose was minors, whereas ferulate concentration did not decrease since the third pulse. Nonetheless, production of curcumin proceeded, likely from already created pools of feruloyl-CoA, reaching 806 mg L^{-1} after 88 hours of cultivation. Notably, this is the highest curcumin titre obtained by microbial fermentation, reported to date.

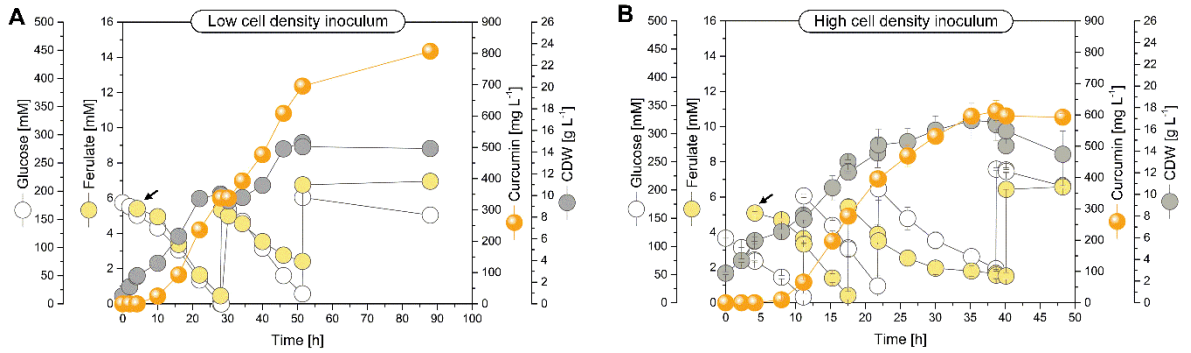

Figure 29. Fed-batch production of curcumin by metabolically engineered *C. glutamicum* CUR-8. Data represents growth and production profiles of the cultures from low cell density (**A**) and high cell density (**B**) inoculums. After depletion of initially provided glucose and ferulate, additional pulses were added manually from concentrated stock solutions. First ferulate feed is indicated by an arrow. Concentrations of substrates were monitored by simultaneous HPLC measurements. Data comprises mean values from two biological replicates for the high cell density inoculum fermentation, whereas low cell density inoculum approach was carried out in one biological replicate.

In view of increasing productivity and reducing cultivation time, another fermentation with four times higher cell density of the inoculum was put to the test. Initial concentration of glucose was set to 20 g L^{-1}, and similar to the previous fermentation, 5 mM ferulate and 30 g L^{-1} glucose pulses were added manually (**Fig. 29B**). Thereby, first ferulate pulse was injected after four hours. Consumption of ferulate started without delay, with a 68% faster rate (0.37 mM h^{-1}) than in the fermentation with low cell density inoculum. Glucose was also utilized with a quicker rate (9.28 mM h^{-1}). Consequently, second pulse of ferulate was injected almost 12 hours earlier. By the time the first ferulate feed was nearly exhausted, 276 mg L^{-1} of curcumin were formed. Notably, second glucose pulse was utilized with 64% higher rate than during the first batch (15.24 mM h^{-1}). As a results, another pulse of glucose was given to enable consumption of the second ferulate feed. Regardless, ferulate uptake rate plunged to 0.27 mM h^{-1}, and eventually the third pulse remained untouched. The highest curcumin titre of 612 mg L^{-1} was recorded after 38 hours of cultivation (**Fig. 29B**), which corroborates with the end of second feeding with ferulate. After 50 hours curcumin level slightly decreased, likely due to dilution effect of fourth glucose and third ferulate pulse. Although curcumin titre in this fermentation was nearly 200 mg L^{-1} lower than in the previous set-up, in terms of volumetric productivity high cell density inoculum strategy outperformed the low cell density inoculum approach.

Overall, in both fermentation strategies the CUR-8 strain could sustain two 5 mM ferulate pulses. Apropos curcumin titre, both approaches surpassed the so far reported

titres, indicating that *C. glutamicum* is well-suited host for heterologous production of polyphenol curcumin.

Table 7. Production performance of curcumin producing *C. glutamicum* CUR-8 during fed-batch fermentation using minimal medium with glucose as growth substrate and ferulate as biotransformation substrate. The data comprise specific (P_{spec}) and volumetric (P_{vol}) productivity during first, second, and third ferulate feeding.

Rate	Ferulate feed	Low cell density inoculum	High cell density inoculum
P_{vol} [mg L^{-1} h^{-1}]	I	12.07	15.81
	II	13.52	14.87
	III	9.16	-
P_{spec} [mg g^{-1} h^{-1}]	I	1.19	1.21
	II	0.90	1.02
	III	0.63	-

4.3. Conclusion and outlook

Due to the ever-growing body of evidence-based studies highlighting the positive correlation between plant natural products and human wellbeing, plant-derived pharmaceutical and nutraceutical market have experienced a significant expansion during the past few decades. Relying on extraction of these compounds from their native plant producers would not satisfy the needs of the market. Sourcing from plants is typically limited by plant biomass and variable environmental and growth conditions. Heterologous production of plant natural products in industrially applicable microbes is a promising alternative to traditional extraction from plants.

This work aimed to establish curcumin production in actinobacteria *C. glutamicum*. In that regard, native curcumin biosynthetic genes form turmeric, *dcs* and *curs1*, were superior among the tested cluster combinations. Next, the inbuilt catabolism of phenylpropanoids was an exceptionally big bottleneck in achieving high-level production of curcumin. Deletion of *phdBCDE* genes enabled already 4-fold increase in formed curcumin, as compared to wild type expressing the *dcs* and *curs1* genes. Subsequent deletion of *phdR* regulator enabled 13-fold increase in production, and reaching more than 100 mg L- of curcumin. Importantly, native *phdT* and *phdA* genes were not deleted, but modulating their expression through promoter engineering resulted with remarkably diminished cellular vitality. Evidently, native control of *phdTA* expression seems to be fine-tuned and optimal. The issue of precursor supply was addressed in other ways. First, optimization of growth and biotransformation substrate ratio opened considerable space for additional improvement. Increasing glucose concentration from 10 to 30 g L^{-1} enabled additional boost in production, without any genetic modification. Next, two strategies for enrichment of malonyl-CoA had opposing effects. Reducing consumption of acetyl-CoA by the TCA cycle resulted with slight increase in curcumin titre, albeit statistical significance. On the other hand, deregulation of *accBCD1* led to reduced production, when compared to the previous strain in the strain lineage without modified malonyl-CoA metabolism. Native malonyl-CoA supply seems to be sufficient to sustain high-level production of curcumin.

Heterologous production of curcumin in *C. glutamicum* highly reflected on its native metabolism. This was apparent by global changes in genes expression levels, demonstrated by differential expression of dozens of transcription factors, including global regulator GlxR, which controls expression of nearly 200 genes. Overall,

production of curcumin immensely slowed down growth of C. glutamicum, which was also reflected in decreased mRNA levels of genes associated with glycolysis, TCA cycle, PPP, and amino acid biosynthesis. Moreover, activation of oxidative and disulphide stress response genes is strong indication of curcumin-induced oxidative stress, which also reflected on each stage of central biological dogma. Genes associated with ribosome biogenesis, transcription, and translation showed diminished expression levels. Finally, production of curcumin in fed-batch mode enabled achieving, to this date, the highest known titre of curcumin (806 mg L^{-1}). Whereby sequential feeding of smaller amounts of glucose and ferulate was more suitable that batch fermentation with increased concentration of 90 g L^{-1} glucose and 15 mM ferulate. This work demonstrated suitability of *C. glutamicum* for heterologous production of curcumin.

Overall, heterologous production of curcumin had massive effect on global gene expression. These insights create many potential targets for further strain optimization, especially in the domain of resistance to oxidative stress. Next, two-phase fermentation using solvent phase to capture extracellular curcumin is another promising way for enhancing productivity. Given that ferulate, as curcumin precursor, is a common component of lingo-cellulose of monocot grains, valorisation of lignin or food waste streams would enable establishing sustainable production of curcumin.

5. Supplementary files

5.1. Supplementary figures

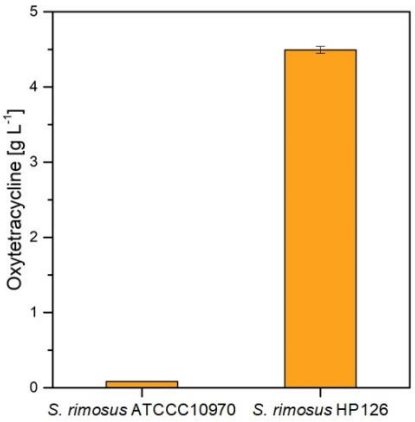

Figure S1A. Production of oxytetracycline in complex industrial medium. *S. rimosus* ATCC 10970 and *S. rimosus* HP126 were cultivated in a complex medium and samples for extraction of oxytetracycline were collected after 120 h.

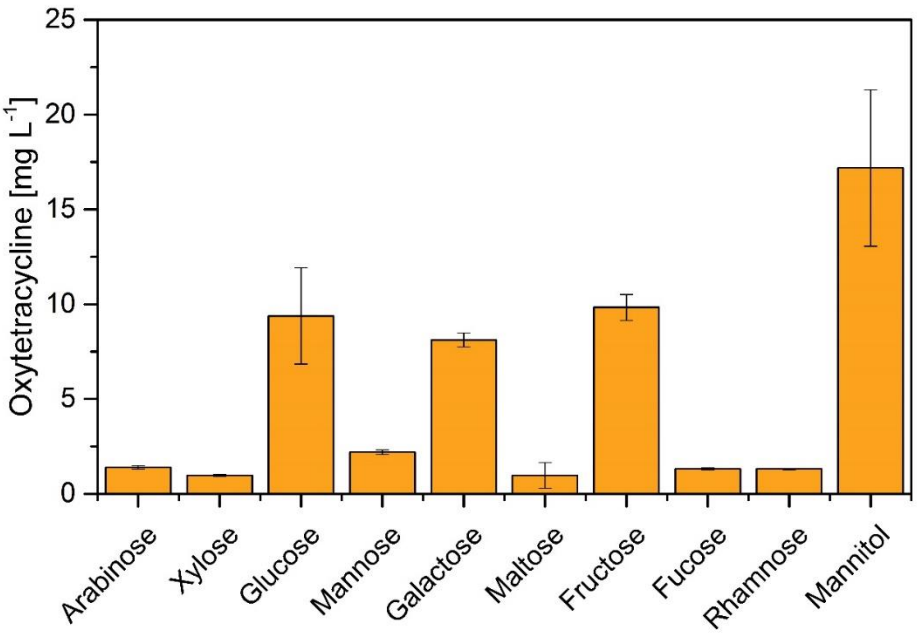

Figure S1B. Oxytetracycline production in minimal medium using different simple sugars as carbon source. *S. rimosus* ATCC 10970 was cultivated in chemically defined medium supplemented with different simple sugars. Samples for oxytetracycline quantification were collected after 120 h.

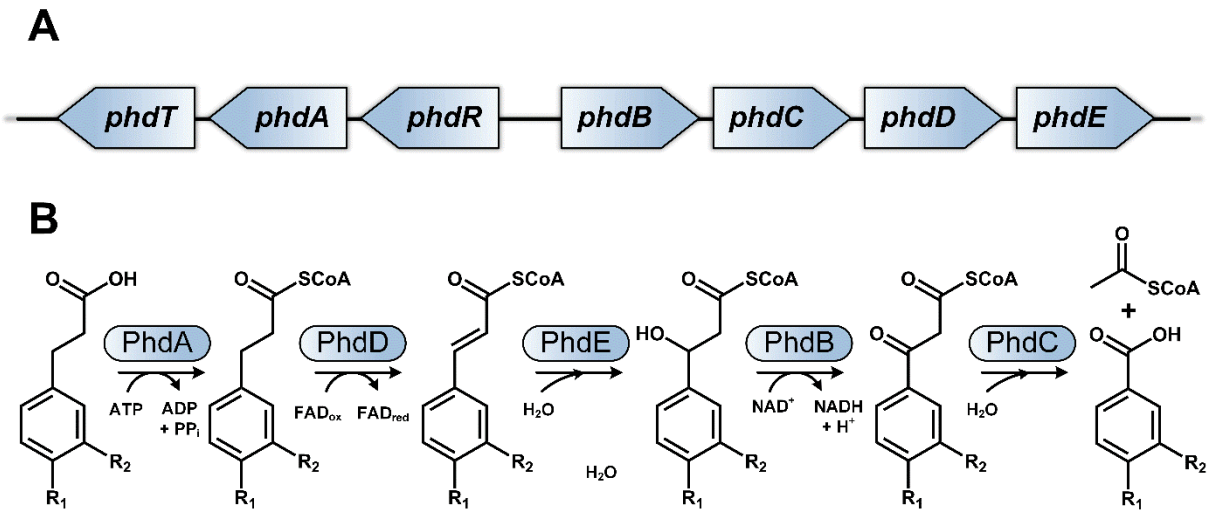

Figure S2. Phenylpropanoid degradation pathway in *C. glutamicum*. The phenylpropanoid degradation genes are organised in form of operon (**A**). CoA-dependent β-oxidation catabolic pathway results in formation of benzoate derivatives and acetyl-CoA (**B**). Benzoates are further degraded via β-ketoadipate pathway to succinyl-CoA and acetyl-CoA. R_1=OH, R_2=H, C_2-C_3 bond saturated: 3-(4-hydroxyphenyl) propionate; R_1=H, R_2=H, C_2-C_3 bond unsaturated: cinnamate; R_1=OH, R_2=H, C_2-C_3 bond unsaturated: *p*-coumarate; R_1=OH, R_2=OH, C_2-C_3 bond unsaturated: caffeate; R_1=OH, R_2=OCH_3, C_2-C_3 bond unsaturated: ferulate. *phdT*: membrane transporter; *phdA*: acyl:CoA ligase; *phdR*: MarR-type transcriptional repressor; *phdB*: 3-hydroxyacyl-CoA dehydrogenase; *phdC*: 3-oxoacyl-CoA ketohydrolase; *phdD*: acyl-CoA dehydrogenase; *phdE*: enoyl-CoA hydratase. Adapted from Kallscheuer et al. (2016).

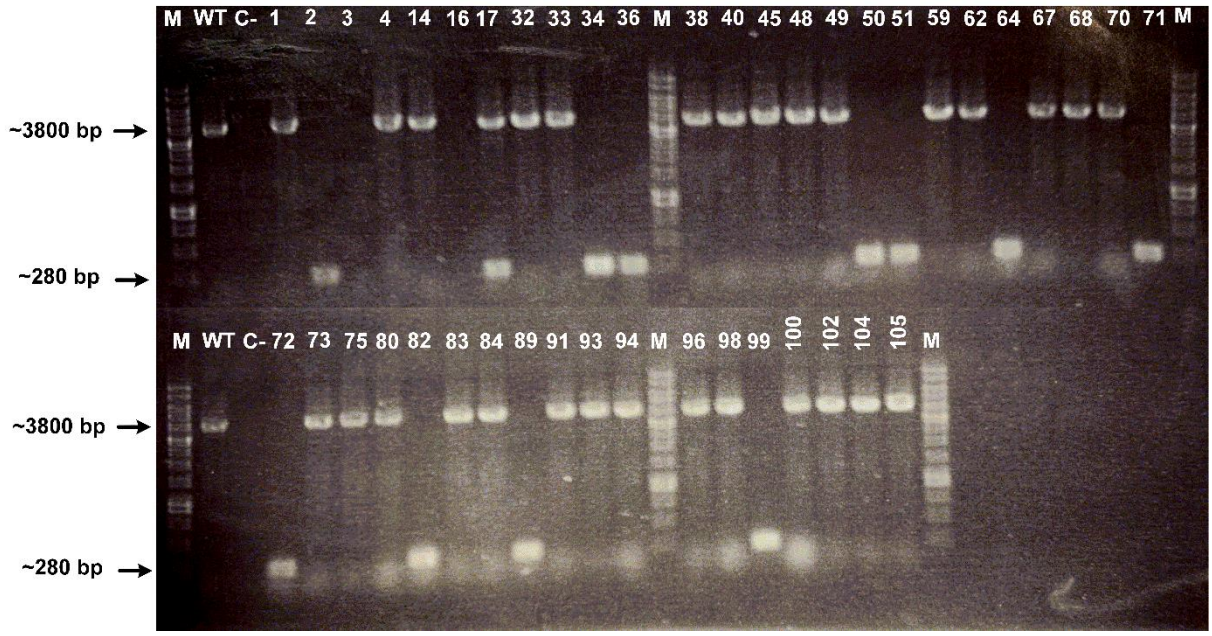

Figure S3. Agarose gel analysis of PCR fragments of *C. glutamicum* clones with putative deletion of *phdBCDE* genes obtained by two-step homologous recombination. The fragments were amplified by colony PCR using del_phdBCDE_fwd + del_phdBCDE_rev primer pair at 65°C. Fragment from the wild type control had size of 3841 bp, while shorter fragments of 289 bp indicated deletion of the target genes. M: 1kb marker; WT: *C. glutamicum* ATCC 13032.

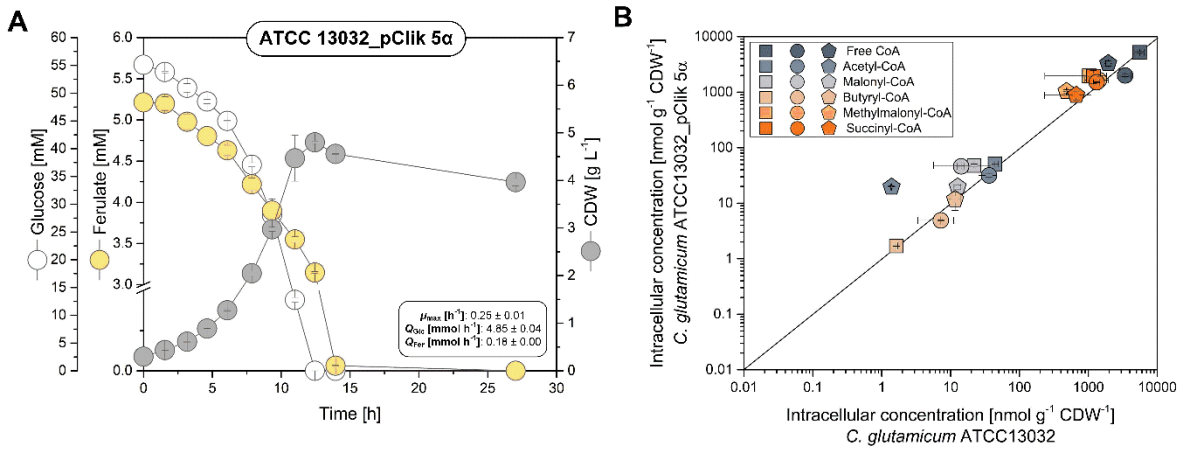

Figure S4. Ferulate utilization and CoA-thioester profile of the *C. glutamicum* wild type-derivative expressing the empty pClik5α plasmid. The data displays cultivation profile in minimal medium with 10 g L^{-1} of glucose (55 m) and 5 mM ferulate of *C. glutamicum* ATCC 13032_pClik5α during batch cultivation in shake flaks. Increase in formed biomass (g L^{-1}), depletion of glucose and ferulate (mM), as well as growth performance (μ_{max}, Q_{Glc}, Q_{Fer}), are shown (**A**); correlation of CoA-thioester dynamics (nmol g^{-1} CDW^{-1}) (**B**). Time series quantification of CoA-thioesters was carried out at the beginning (4.5 hours, square symbol), in the middle (7.8 hours, circle symbol), and towards the end of exponential growth phase (12.5 hours, pentagon symbol). The data comprise mean values and standard deviations from three biological replicates.

Description	Scientific Name	Max Score	Total Score	Query Cover	E value	Per. Ident	Acc. Len	Accession
bisdemethoxycurcumin synthase [Oryza sativa Japonica Group]	Oryza sativa Japonica Group	816	816	100%	0.0	100.00%	402	XP_015646196.1
curcuminoid synthase [synthetic construct]	synthetic construct	815	815	100%	0.0	99.75%	402	AKG06601.1
A type III polyketide synthase that produces diarylheptanoid [Oryza sativa Japonica Group]	Oryza sativa Japonica Group	814	814	100%	0.0	99.75%	416	3ALE_A
Crystal structure of curcuminoid synthase CUS from Oryza sativa [Oryza sativa Japonica Group]	Oryza sativa Japonica Group	778	778	95%	0.0	99.74%	387	3OIT_A
bisdemethoxycurcumin synthase [Aegilops tauschii subsp. strangulata]	Aegilops tauschii subsp. strang...	553	553	96%	0.0	71.72%	401	XP_020170080.1
bisdemethoxycurcumin synthase-like [Triticum dicoccoides]	Triticum dicoccoides	552	552	96%	0.0	71.47%	401	XP_037454829.1
hypothetical protein CFC21_084387 [Triticum aestivum]	Triticum aestivum	551	551	96%	0.0	71.72%	401	KAF7080284.1
bisdemethoxycurcumin synthase [Sorghum bicolor]	Sorghum bicolor	551	551	97%	0.0	72.26%	404	XP_002462898.1
bisdemethoxycurcumin synthase [Setaria italica]	Setaria italica	549	549	97%	0.0	71.36%	412	XP_004957783.1
bisdemethoxycurcumin synthase-like [Setaria viridis]	Setaria viridis	549	549	97%	0.0	71.36%	412	XP_034582575.1
predicted protein [Hordeum vulgare subsp. vulgare]	Hordeum vulgare subsp. vulgare	547	547	99%	0.0	68.97%	427	BAJ93669.1
bisdemethoxycurcumin synthase-like [Panicum miliaceum]	Panicum miliaceum	546	546	94%	0.0	71.06%	413	RLM84350.1
hypothetical protein GQ55_2G370400 [Panicum hallii var. hallii]	Panicum hallii var. hallii	545	545	94%	0.0	71.06%	409	PUZ72153.1
bisdemethoxycurcumin synthase-like [Panicum virgatum]	Panicum virgatum	544	544	97%	0.0	69.35%	413	XP_039835247.1
bisdemethoxycurcumin synthase-like [Panicum hallii]	Panicum hallii	544	544	94%	0.0	70.80%	409	XP_025802813.1
Bisdemethoxycurcumin synthase [Dichanthelium oligosanthes]	Dichanthelium oligosanthes	544	544	94%	0.0	71.47%	398	OEL30328.1
Chalcone synthase A [Hordeum vulgare]	Hordeum vulgare	543	543	96%	0.0	70.69%	403	KAE8787201.1
bisdemethoxycurcumin synthase-like [Panicum virgatum]	Panicum virgatum	542	542	97%	0.0	68.84%	413	XP_039834661.1
bisdemethoxycurcumin synthase-like [Panicum virgatum]	Panicum virgatum	540	540	97%	0.0	68.59%	412	XP_039834662.1
Bisdemethoxycurcumin synthase-like [Zea mays]	Zea mays	537	537	97%	0.0	70.41%	402	NP_001140848.1
hypothetical protein HU200_034242 [Digitaria exilis]	Digitaria exilis	531	531	98%	0.0	69.06%	478	KAF8700311.1
bisdemethoxycurcumin synthase-like [Panicum virgatum]	Panicum virgatum	530	530	97%	0.0	68.34%	412	XP_039792985.1
unnamed protein product [Miscanthus lutarioriparius]	Miscanthus lutarioriparius	530	530	94%	0.0	71.50%	452	CAD6217981.1
hypothetical protein HU200_051309 [Digitaria exilis]	Digitaria exilis	529	529	96%	0.0	68.92%	478	KAF8669508.1
unnamed protein product [Digitaria exilis]	Digitaria exilis	529	529	97%	0.0	68.75%	417	CAB3454383.1
bisdemethoxycurcumin synthase-like [Panicum virgatum]	Panicum virgatum	528	528	97%	0.0	68.09%	412	XP_039792986.1
unnamed protein product [Digitaria exilis]	Digitaria exilis	528	528	96%	0.0	69.42%	417	CAB3458022.1
bisdemethoxycurcumin synthase-like [Setaria viridis]	Setaria viridis	516	516	94%	7e-180	72.02%	412	XP_034582861.1
bisdemethoxycurcumin synthase [Setaria italica]	Setaria italica	515	515	94%	3e-179	71.76%	412	XP_004959689.1
unnamed protein product [Digitaria exilis]	Digitaria exilis	508	508	96%	9e-177	66.08%	401	CAB3454381.1
Bisdemethoxycurcumin synthase [Zea mays]	Zea mays	502	502	97%	1e-174	67.86%	384	PWZ15784.1

Figure S5. BLAST search for homologous of the curcuminoid synthase *cus* gene from rice. Based on 72.26% identity and E-value of 0.0, the gene from *S. bicolor* (accession number: XP_002462898.1) (highlighted in orange) appeared as promising candidate of one-pot-curcuminoid forming gene.

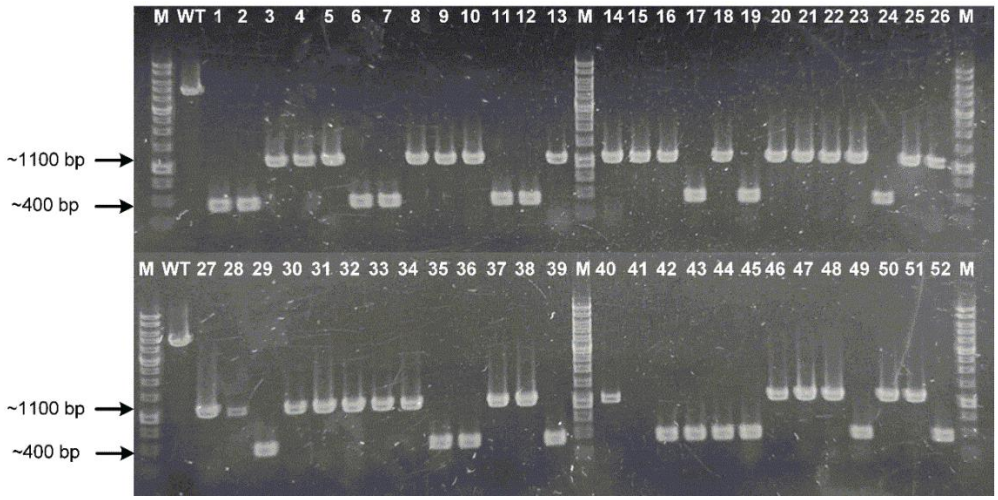

Figure S6. Agarose gel analysis of PCR fragments of *C. glutamicum* clones with putative deletion of *phdR* gene in CUR-1 as parental strain obtained by two-step homologous recombination. The fragments were amplified by colony PCR at 65°C using del_phdRBCDE_fwd + del_phdBCDE_rev primer pair. Fragments from clones that reverted to original gene architecture had size of 1129 bp, while shorter fragments of 431 bp indicated deletion of the target gene in CUR-1 strain. M: 1kb marker; WT: *C. glutamicum* ATCC 13032.

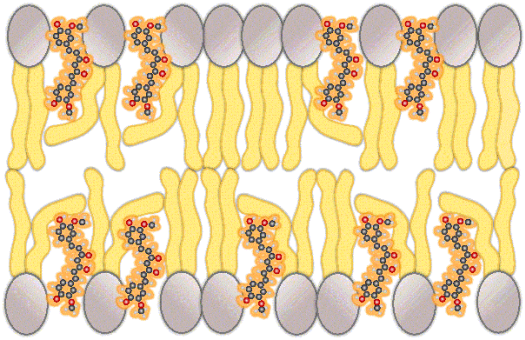

Figure S7. Schematic representation of structural changes imposed by curcumin molecule within the membrane. Similar to cholesterol molecule**,** curcumin inserts into phospholipid bilayer, bound by hydrogen bonding to the phosphate head of the lipids (Modified from Barry et al. 2009).

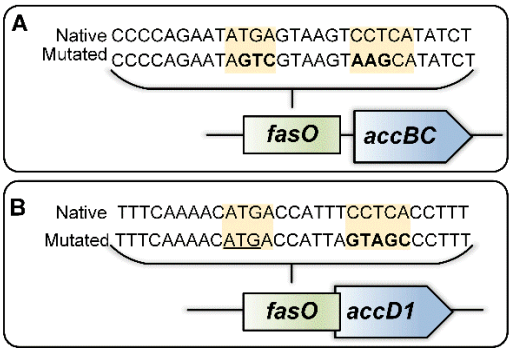

Figure S8. Mutations introduced in the *fasO* sites of the malonyl-CoA forming genes of *C. glutamicum*. The data displays native and mutated sequences of *fasO* sites in *accBC* gene (**A**); and *accD1* gene (**B**). The FasR recognition sites are highlighted in yellow, while the replaced nucleotides are depicted in bold letters. The start codon of the *accD1* gene is underlined.

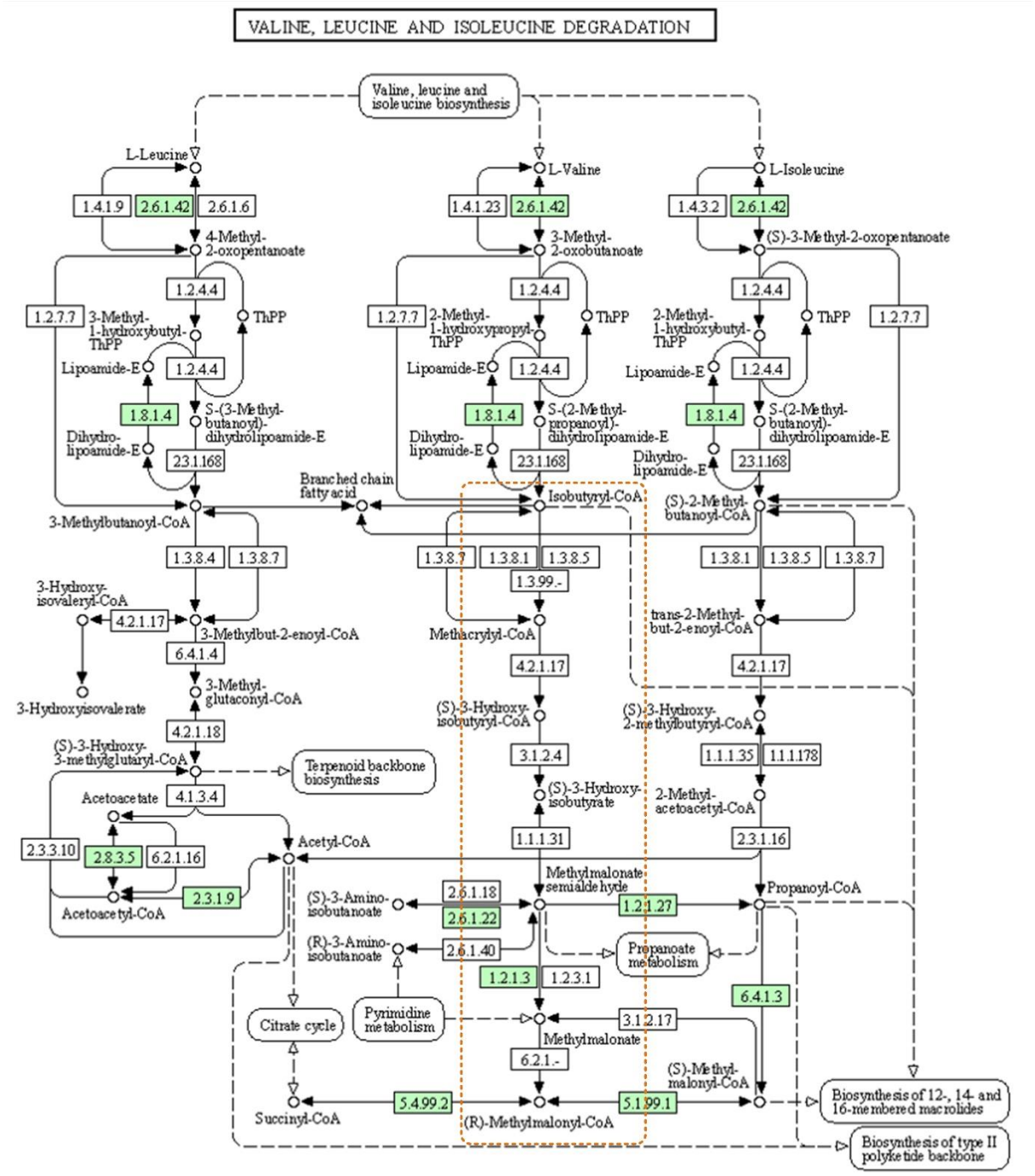

Figure S9. Metabolic pathway of butyryl-CoA (isobutyryl-CoA) to methylmalonyl-CoA in *C. glutamicum*. The metabolic route was taken from the KEGG database and is highlighted with an orange rectangular.

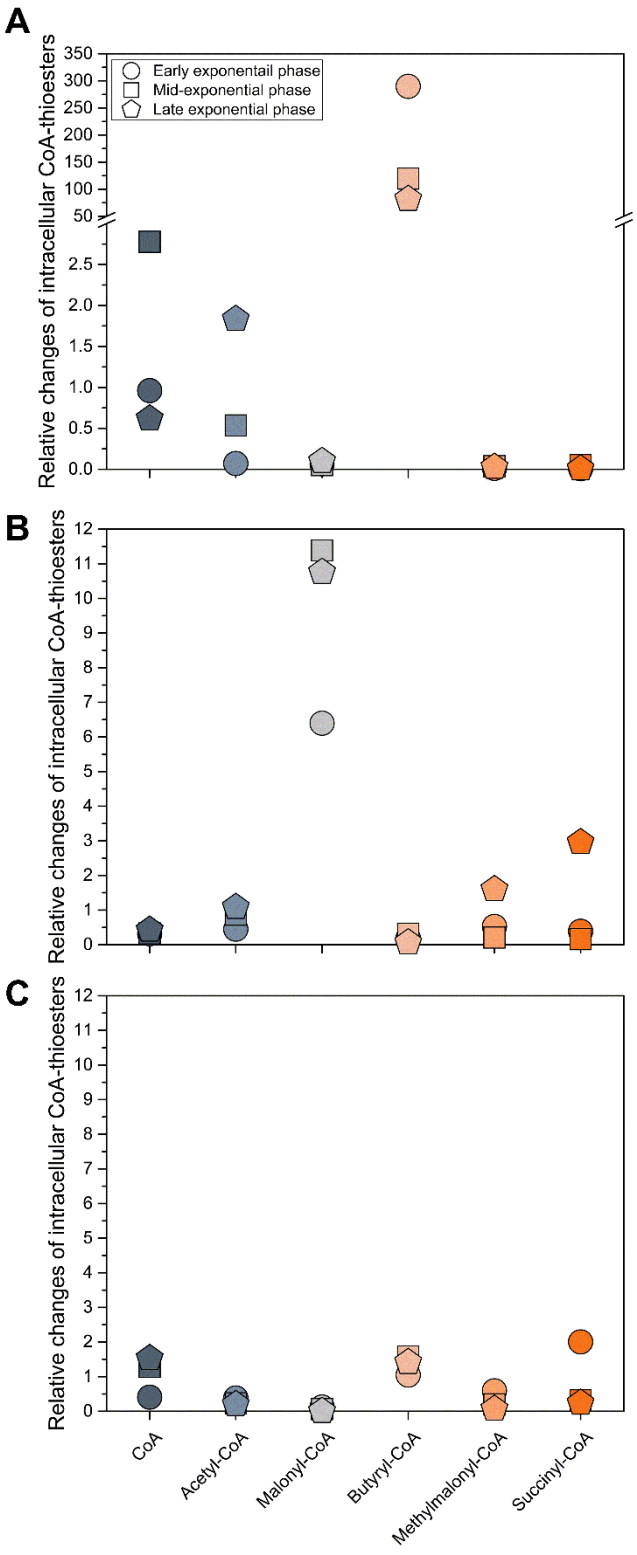

Figure S10. Relative changes of the intracellular CoA levels in curcumin producing *C. glutamicum* strains. The data displays relative changes in concentrations of the six detected CoA-thioesters during early, mid-, and late exponential phase in the CUR-8 compared to ATCC013032_pClik5α (**A**); CUR-12 compared to CUR-8 (**B**); and CUR-15 compared to CUR-8 (**C**). Early, mid-, and late exponential phases refer to the phase I, II, and III, respectively, in the cultivation profiles of CUR-8, CUR-12, and CUR-15 shown in Fig. 10.

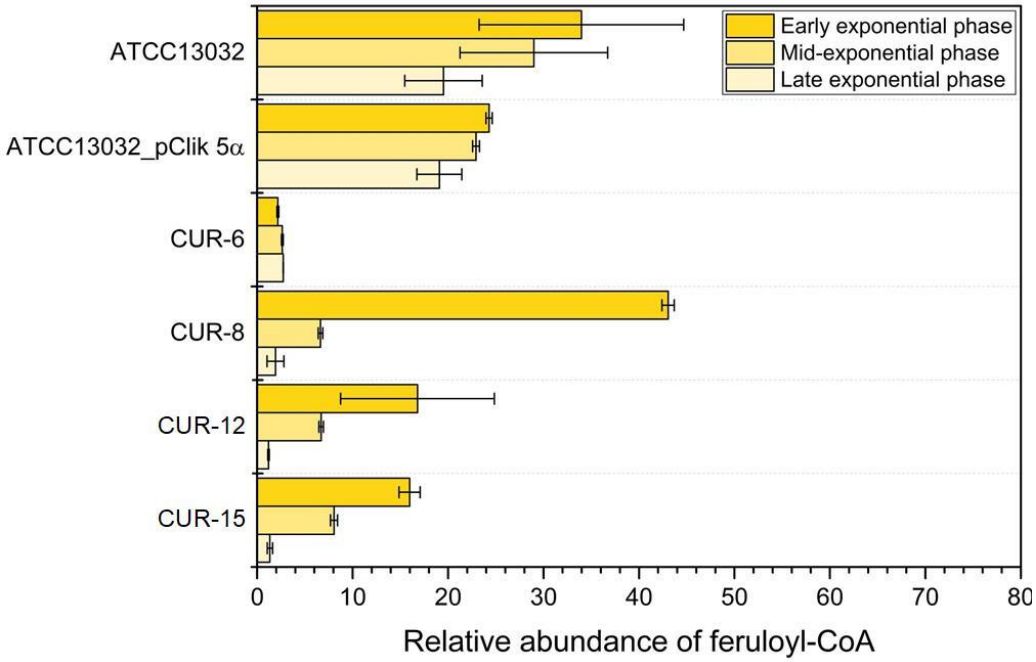

Figure S11. Relative abundance of feruloyl-CoA in curcumin producing and non-producing *C. glutamicum* strains during batch cultivation in shake flasks. The data displays relative levels of feruloyl-CoA in the samples from the curcumin non-producing wild type ATCC 13032, ATCC 13032_pClik5α, and CUR-6, CUR-8, CUR-12, and CUR-15 curcumin producers during early, mid-, and late exponential phase (indicated as phase I, II, and III in Fig. 10). Relative abundance of feruloyl-CoA was determined as compared to ^{13}C butyryl-CoA peak, as the most stable CoA-thioester during the LC-MS measurements.

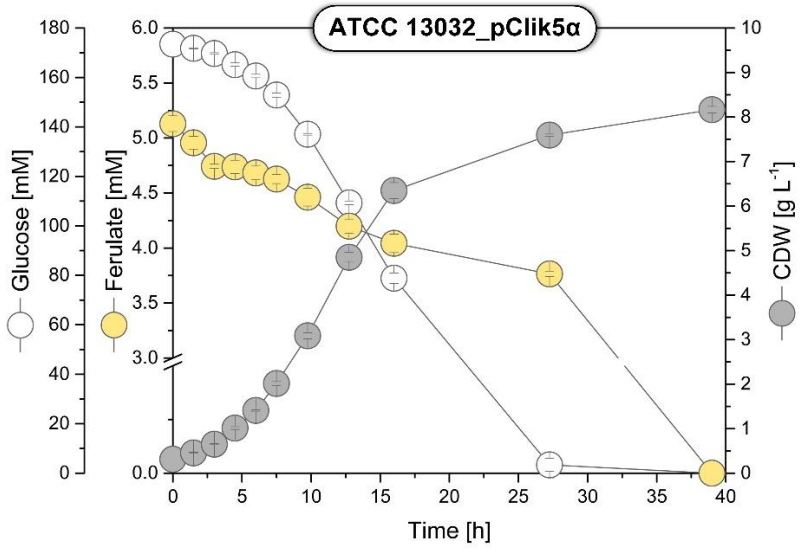

Figure S12. Ferulate utilization by *C. glutamicum* ATCC 13032_pClik5α. The data displays cultivation profile in minimal medium with 30 g L^{-1} of glucose (165 mM) and 5 mM ferulate of *C. glutamicum* ATCC 13032_pClik5α during batch cultivation in shake flaks. Increase in formed biomass (g L^{-1}), depletion of glucose and ferulate (mM) are shown. Samples for RNA extraction were taken after 3 and 6 hours, corresponding to early and mid-exponential phase. Sampling for fatty acid extraction was performed after 13 hours. The data comprise mean values and standard deviations from three biological replicates.

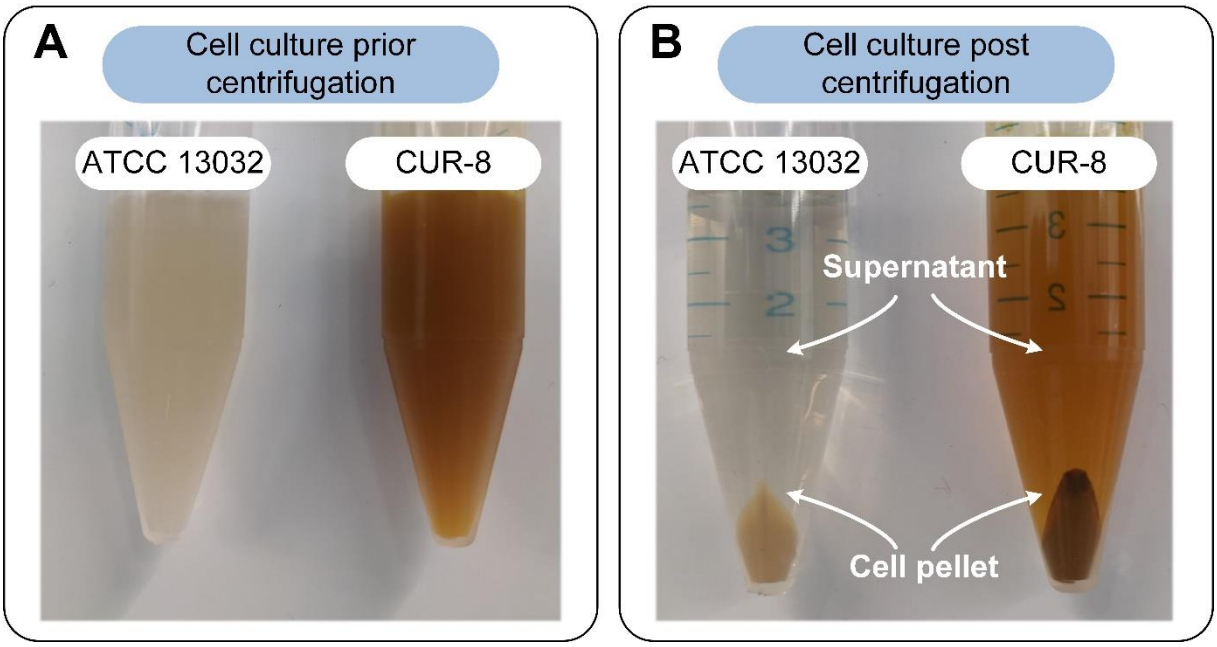

Figure S13. Cell pellet of curcumin producing and non-producing *C. glutamicum*. Difference in the colour of the wild type curcumin non-producing *C.glutamicum* and genetically engineered curcumin producer *C. glutamicum* CUR-8. The culture broth of the CUR-8 strain has deep orange colour. Upon centrifugation of the culture broth, both the pellet and the supernatant of the CUR-8 strain appear orange, indicating extracellular and intracellular presence of curcumin.

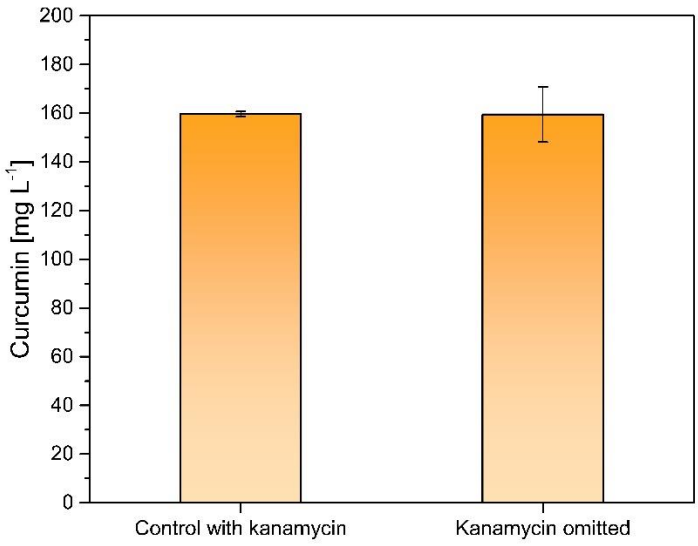

Figure S14. Effect of kanamycin supplementation on curcumin production by genetically engineered *C. glutamicum* CUR-8. The data displays curcumin titre with and without addition of kanamycin after 72 hours of cultivation. The CUR-8 strain was cultivated in test tubes in chemically defined medium (Chapter 4.1.3.) using 10 g L^{-1} glucose (55 mM) and 5 mM ferulate as growth and biotransformation substrate, respectively. The data comprise mean values and standard deviations from three biological replicates

5.2. Supplementary tables

Table S1. Impact of introduced mutations in classical oxytetracycline producing *S. rimosus* HP126 and its derivative *S. rimosus* HP126 Δv3 on expression of genes associated with CoA-thioester metabolism.

Locus tag	Annotation	*S. rimosus* HP126	*S. rimosus* HP126 Δv3
SRIMR7_19995	Branched-chain alpha-keto acid dehydrogenase E1 component subunit α	5.0	-2.9
SRIMR7_20005	Branched-chain alpha-keto acid dehydrogenase complex component E2	4.7	-2.7
SRIMR7_20000	Branched-chain alpha-keto acid dehydrogenase E1 component subunit β	4.6	-2.7
SRIMR7_19935	1,2-Phenylacetyl-CoA epoxidase, subunit E	4.1	-1.4
SRIMR7_19940	1,2-Phenylacetyl-CoA epoxidase, subunit D	3.5	-1.0
SRIMR7_19945	1,2-Phenylacetyl-CoA epoxidase, subunit C	3.3	0
SRIMR7_35410	Phenylacetate-CoA ligase	3.1	-1.3
SRIMR7_34430	Coenzyme A biosynthesis bifunctional protein CoaBC	2.9	0
SRIMR7_11535	Putative propionyl-CoA carboxylase β-chain 5	1.1	-2.6
SRIMR7_11575	Branched-chain-amino-acid aminotransferase	1.0	-1.0
SRIMR7_01685	Crotonyl-CoA carboxylase/reductase	-6.4	0
SRIMR7_07230	Methylmalonyl-CoA mutase	-2.5	2.5
SRIMR7_07225	Crotonyl-CoA carboxylase/reductase	-2.4	2.4
SRIMR7_21110	Valine dehydrogenase	-1.7	0
SRIMR7_02335	3-Hydroxybutyryl-CoA dehydrogenase	-1.9	0
SRIMR7_12355	Methylmalonyl-CoA mutase	-1.2	-1.4
SRIMR7_33660	3-Hydroxybutyryl-CoA dehydrogenase	-1.2	1.2

Note: The reference for *S. rimosus* HP126 was *S. rimosus* ATCC10970, while for *S. rimosus* HP126 Δv3 was *S. rimosus* HP126.

Table S2. Influence of introduced mutations in *S. rimosus* HP126 and *S. rimosus* HP126 Δv3 on expression of genes associated with cell wall composition.

Locus tag	Annotation	*S. rimosus* HP126	*S. rimosus* HP126 Δv3
SRIMR7_14410	Chitinase D	2.2	-2.2
SRIMR7_38545	Poly-ß-1,6-N-acetylglucosamine synthase	1.8	0
SRIMR7_12545	Chitinase 63	1.7	0
SRIMR7_24075	Murein DD-endopeptidase, MepM	1.4	0
SRIMR7_11730	Exochitinase	1.3	-2.7
SRIMR7_01200	Chitinase C	1.1	-1.1
SRIMR7_38525	Chitinase D	1.1	0
SRIMR7_01835	Chitinase	1.1	-1.1
SRIMR7_19325	Murein DD-endopeptidase, MepM	0	1.3
SRIMR7_26015	Murein DD-endopeptidase, MepH precursor	0	1.3
SRIMR7_30815	Murein DD-endopeptidase, MepM	0	-1.9
SRIMR7_25310	CDP-glycerol:poly(glycerophosphate) glycerophosphotransferase, TagF	-1.1	-1.2
SRIMR7_25990	Cellulose synthase (UDP-forming)	-1.3	0
SRIMR7_37765	Chitinase class I	-1.3	-2.6
SRIMR7_25305	Putative glycosyltransferase, EpsJ	-1.4	1.4
SRIMR7_38620	Putative poly(glycerol-phosphate) alpha-glucosyltransferas, TagE	-1.5	-1.6
SRIMR7_25250	Teichoic acid export, ATP binding protein, TagH	-5.7	0
SRIMR7_25255	Teichoic acid export, ATP binding protein, TagG	-5.8	0

Note: The reference for *S. rimosus* HP126 was *S. rimosus* ATCC10970, while for *S. rimosus* HP126 Δv3 was *S. rimosus* HP126.

Table S3: Primers used for genome-based engineering of *C. glutamicum.* Sequences and annealing temperature (AT °C) of primers for strain constructed and verification are shown.

Primer name	Sequence (5‘-3‘)	AT °C
Primers used for construction of vectors		
del_phd1_up_fwd	AATTGGGATCCTCTAGACCCGGCAACAATCTGACTTGGGT	60.6
del_phd1_up_rev	TTGCGTCGAGAAGCAAGCTTTTCAAACTCCTTTGAAGGTT	
del_phd1_down_fwd	AACCTTCAAAGGAGTTTGAAAAGCTTGCTTCTCGACGCAA	63.2
del_phd1_down_rev	TAGCGGATCATTTAAATCCCCCAAAGTGGACTCATGAGGG	
del_phd2_up_fwd	AATTGGGATCCTCTAGACCCCATCGCTGACTTCTAGGTCG	59
del_phd2_up_rev	GAAGTCCAGGAGGACATACAATGAAAGTGAACCTCGGAAT	
del_phd2_down_fwd	CATTCGCAGGGTAACGGCCAAAGCTTGCTTCTCGACGCAA	63.2
del_phd2_Peftu_fwd	TTGCGTCGAGAAGCAAGCTTTGGCCGTTACCCTGCGAATG	63.2
del_phd2_Peftu_rev	ATTCCGAGGTTCACTTTCATTGTATGTCCTCCTGGACTTC	
del_phdR_up_fwd	AATTGGGATCCTCTAGACCCAATGAGGTTCGTTGAAAAGA	71
del_phdR_up_rev	TTGCGTCGAGAAGCAAGCTTGTCTCTTAACCACGCCGGCC	
del_phdR_down_fwd	GGCCGGCGTGGTTAAGAGACAAGCTTGCTTCTCGACGCAA	71
del_phdR_down_rev	TAGCGGATCATTTAAATCCCTATGACCAGGTGTGGCCACC	
phd_prom_up_fwd	AATTGGGATCCTCTAGACCCATAACCAAGCCGACAATCAG	68
phd_prom_up_rev	GATCTAAAGCACAAAGGAGAATGACTACATCTTCCACAGC	
phd_prom_down_rev	TAGCGGATCATTTAAATCCCTTCAGGTACTCACCCAAATC	68
phd_prom_down_fwd	TCACCATCCCCGTTTCATAAAAGCTTGCTTCTCGACGCAA	
phdAT_prom_fwd	GCTGTGGAAGATGTAGTCATTCTCCTTTGTGCTTTAGATC	68
phdAT_prom_rev	CATTCGCAGGGTAACGGCCAGTCTCTTAACCACGCCGGCC	
peftu2_fwd	GGCCGGCGTGGTTAAGAGACTGGCCGTTACCCTGCGAATG	68
peftu2_rev	ATTCCGAGGTTCACTTTCATTGTATGTCCTCCTGGACTTC	
phdA_fwd	GAAGTCCAGGAGGACATACAATGAAAGTGAACCTCGGAAT	68
phdA_rev	TTGCGTCGAGAAGCAAGCTTTTATGAAACGGGGATGGTGA	
accBC_fasO_but_up_fwd	AATTGGGATCCTCTAGACCCTACCCCTCCGCCAACTACCC	65
accBC_fasO_mut_up_rev	CAGATATGCTTACTTACGACTATTCTGGGGGAATTCTTCT	
accBC_fasO_mut_down_fwd	AGAAGAATTCCCCCAGAATAGTCGTAAGTAAGCATATCTG GTTGAGTTCTTC	65
accBC_fasO_mut_down_rev	TAGCGGATCATTTAAATCCCACAACTTCTGCTGCGTCTTT	
accD1_fasO_mut_up_fwd	AATTGGGATCCTCTAGACCCGCCATTTCAGTCCGGCACCT	65
accD1_fasO_mut_up_rev	ACGTCAATCAAAGGGCTACTAATGGTCATGTTTTGAAATC	
accD1_fasO_down_fwd	AAAACATGACCATTAGTAGCCCTTTGATTGACGTCGCCAA	65
accD1_fasO_mut_down_rev	TAGCGGATCATTTAAATCCCTGCCACCTGCACATGCGCCC	
Primers used for verification of mutant strains		
del_phdBCDE_fwd	TGCATTCTGTGCGTCAAGCG	65
del_phdBCDE_rev	TGCGCTCAAGCTTAGTCACA	

del_phdRBCDE_fwd	TGCAGTGGACTCTGGTCGAA	65

Table S4: Sequences of the native (NAT) and codon-optimized (OPT) curcumin biosynthetic genes and the genes associated with biosynthesis of curcumin. The genetic constructs were synthetized by GenScript Biotech (Rijswijk, Netherlands).

Curcuma longa	
curs1^{NAT}	ATGGCCAACCTCCACGCGTTGCGCAGGGAGCAGAGGGCTCAAGGTCCCGCCA CCATCATGGCCATCGGGACGGCCACCCCTCCCAACCTCTACGAGCAGAGCACC TTCCCGGACTTCTACTTCCGCGTCACCAACTCCGACGACAAGCAGGAGCTCAAG AAAAAGTTCCGCCGCATGTGCGAGAAGACAATGGTGAAGAAGCGGTACCTGCA CTTGACCGAGGAGATCCTGAAGGAGAGGCCCAAGCTCTGCTCCTACAAGGAGG CGTCGTTCGACGACCGGCAGGACATCGTGGTGGAGGAGATACCGAGATTGGCT AAGGAAGCTGCGGAGAAGGCCATCAAGGAGTGGGGGCGGCCCAAATCGGAGA TCACCCACCTGGTCTTCTGTTCCATCAGCGGCATCGACATGCCCGGCGCCGAC TACCGCCTCGCGACGCTCCTCGGCCTCCCTCTCACCGTCAACCGCCTCATGAT CTACAGCCAGGCCTGCCACATGGGCGCCGCCATGCTCCGCATCGCCAAGGACC TCGCCGAGAACAACAGGGGCGCGCGCGTGCTGGTGGTCGCCTGCGAGATCAC CGTGCTCAGCTTCCGCGGCCCGAACGAGGGTGACTTCGAGGCGCTCGCGGGG CAGGCCGGCTTCGGCGACGGCGCGGGGGCCGTCGTCGTCGGGGCCGACCCG CTGGAAGGAATTGAAAAACCCATCTACGAGATCGCGGCGGCGATGCAGGAGAC GGTGGCGGAGAGCCAGGGGGCGGTGGGCGGCCACCTGCGGGCGTTCGGCTG GACGTTCTACTTCCTGAACCAGCTGCCGGCGATCATCGCCGACAACCTCGGGA GGAGCCTGGAGCGGGCGTTGGCGCCGCTGGGGGTGAGGGAGTGGAACGACG TCTTCTGGGTGGCGCACCCGGGCAACTGGGCCATCATGGACGCCATCGAAGCC AAGCTGCAGCTGAGCCCGGACAAGCTCAGCACCGCCCGCCACGTCTTCACAGA GTACGGCAACATGCAGAGCGCCACCGTGTACTTCGTGATGGATGAGCTGAGGA AGCGGTCGGCGGTGGAGGGGCGGAGCACCACCGGAGACGGCTTGCAGTGGG GAGTTCTCCTCGGTTTTGGGCCGGGCCTCAGCATCGAGACCGTTGTACTGCGC AGTATGCCACTGTAG
curs1^{OPT}	ATGGCCAACCTGCACGCACTGCGTCGCGAACAGCGTGCTCAGGGTCCAGCAAC CATCATGGCAATCGGCACCGCTACCCCACCAAACCTGTACGAGCAGTCCACCTT CCCAGATTTCTACTTCCGCGTCACCAACTCCGATGACAAGCAGGAACTGAAGAA GAAGTTCCGTCGCATGTGCGAGAAGACCATGGTTAAGAAGCGCTACCTGCACCT GACCGAAGAGATCCTGAAGGAACGCCCAAAGCTGTGCTCCTACAAGGAAGCAT CCTTCGATGACCGCCAGGACATCGTGGTCGAAGAGATCCCACGCCTGGCAAAG GAAGCAGCTGAGAAGGCTATCAAGGAATGGGGCCGCCCAAAGTCCGAGATCAC CCACCTGGTGTTCTGCTCCATCTCCGGTATCGATATGCCAGGTGCTGATTACCG TCTGGCAACCCTGCTGGGTCTGCCACTGACCGTCAACCGCCTGATGATCTACTC CCAGGCATGCCACATGGGTGCCGCAATGCTGCGCATCGCCAAGGATCTGGCAG AAAACAACCGCGGCGCACGTGTGCTGGTTGTGGCATGCGAGATCACCGTCCTG TCCTTCCGCGGTCCAAACGAAGGCGACTTCGAGGCTCTGGCTGGTCAGGCTGG TTTCGGTGATGGCGCAGGTGCTGTCGTTGTGGGTGCAGACCCACTGGAAGGCA TCGAGAAGCCAATCTACGAAATCGCTGCCGCAATGCAGGAAACCGTCGCAGAG TCCCAGGGTGCTGTTGGCGGTCACCTGCGCGCTTTCGGTTGGACCTTCTACTTC CTGAACCAGCTGCCAGCTATCATCGCCGATAACCTCGGTCGCTCCCTCGAACGT GCACTGGCACCACTGGGCGTTCGTGAGTGGAACGACGTGTTCTGGGTCGCTCA CCCTGGTAACTGGGCCATCATGGATGCAATCGAAGCTAAGCTGCAGCTGTCCC CAGACAAGCTGTCCACCGCTCGCCACGTGTTCACCGAGTACGGCAACATGCAG TCCGCCACCGTTTACTTCGTGATGGATGAACTGCGCAAGCGCTCCGCAGTTGAA GGTCGCTCCACCACCGGTGATGGTCTGCAGTGGGGCGTGCTGCTGGGTTTCGG TCCAGGTCTGTCCATCGAGACCGTCGTTCTGCGCTCCATGCCACTGTAA
dcs^{NAT}	ATGGAAGCGAACGGCTACCGCATAACTCACAGCGCCGACGGGCCGGCGACGA TCTTGGCCATCGGCACCGCCAACCCCACCAACGTCGTCGATCAGAACGCTTATC CCGACTTCTATTTCCGGGTCACCAACTCCGAGTATCTGCAGGAACTCAAAGCCA AGTTTAGGCGCATCTGTGAGAAAGCGGCCATCAGGAAGAGGCACTTGTACTTGA CTGAGGAGATTTTGCGGGAGAATCCTAGCTTGCTGGCTCCCATGGCGCCGTCG TTCGACGCGCGGCAGGCGATCGTGGTGGAGGCGGTGCCGAAGCTGGCGAAGG AGGCGGCGGAGAAGGCGATCAAGGAGTGGGGCCGCCCCAAATCGGACATCAC GCACCTCGTCTTCTGCTCCGCGAGCGGAATCGACATGCCCGGCTCCGACCTGC AGCTTCTCAAGCTGCTCGGGCTCCCGCCGAGCGTCAATCGCGTCATGCTCTAC AACGTCGGGTGCCACGCCGGTGGCACCGCCCTCCGCGTCGCCAAGGACCTCG

	CGGAGAACAACCGCGGCGCGCGGGTGCTCGCCGTCTGCTCCGAGGTCACCGT GCTCTCCTACCGCGGCCCCCACCCCGCCCACATCGAGAGCCTCTTCGTCCAAG CTCTGTTTGGCGACGGCGCCGCCGCGCTCGTGGTCGGGTCCGACCCCGTCGA TGGCGTCGAGCGCCCCATCTTCGAAATCGCCTCGGCATCCCAAGTGATGCTTC CGGAGAGCGCAGAGGCGGTGGGCGGCCACCTCCGCGAAATTGGGCTGACCTT CCACCTCAAGAGCCAGCTTCCGTCGATCATCGCGAGCAACATCGAGCAGAGCC TGACGACTGCGTGCTCGCCGCTGGGGCTGTCGGACTGGAACCAGCTGTTCTGG GCGGTTCACCCCGGCGGCCGAGCGATCCTGGACCAGGTGGAGGCGCGGCTCG GACTGGAGAAGGACCGGCTCGCCGCGACGCGGCACGTACTCAGCGAGTACGG CAACATGCAGAGCGCCACGGTGCTGTTCATCCTGGACGAGATGCGGAACCGCT CGGCTGCGGAGGGCCACGCCACCACCGGCGAGGGGCTCGACTGGGGCGTGC TGTTGGGCTTCGGCCCGGGACTCTCCATCGAGACCGTCGTCCTCCATAGTTGC AGACTGAACTAG
dcs^{OPT}	ATGGAAGCAAACGGCTACCGCATCACCCACTCCGCTGATGGTCCAGCCACCAT CCTGGCAATCGGCACCGCTAACCCAACCAACGTGGTCGATCAGAACGCCTACC CAGACTTCTACTTCCGCGTCACCAACTCCGAATACCTGCAGGAGCTGAAGGCTA AGTTCCGCCGCATCTGCGAAAAGGCAGCTATCCGCAAGCGCCACCTGTACCTG ACCGAAGAGATCCTGCGCGAGAACCCATCCCTGCTGGCACCAATGGCTCCATC CTTCGATGCCCGCCAGGCAATCGTTGTGGAAGCCGTGCCAAAGCTGGCAAAGG AAGCCGCAGAGAAGGCAATCAAGGAGTGGGGCCGCCCAAAGTCCGACATCACC CACCTGGTCTTCTGCTCCGCTTCCGGTATCGATATGCCAGGCTCCGACCTGCAG CTGCTGAAGCTGCTGGGTCTGCCACCATCCGTCAACCGCGTTATGCTCTACAAC GTTGGTTGCCACGCCGGCGGTACCGCACTGCGCGTCGCTAAGGATCTGGCCGA AAACAACCGCGGTGCACGTGTGCTGGCTGTCTGCTCCGAGGTTACCGTGCTGT CCTACCGTGGTCCACACCCAGCTCACATCGAATCCCTGTTCGTGCAGGCACTGT TCGGTGATGGTGCTGCAGCACTGGTCGTTGGTTCCGATCCAGTTGACGGCGTG GAACGCCCAATCTTCGAGATCGCCTCCGCATCCCAGGTCATGCTGCCAGAATCC GCTGAGGCTGTTGGCGGTCACCTGCGCGAAATCGGTCTGACCTTCCACCTGAA GTCCCAGCTGCCATCCATCATCGCATCCAACATCGAGCAGTCCCTCACCACCGC TTGCTCCCCACTGGGTCTGTCCGACTGGAACCAGCTGTTCTGGGCTGTTCACCC AGGCGGTCGTGCAATCCTGGATCAGGTGGAAGCACGCCTGGGTCTGGAGAAG GACCGTCTGGCTGCAACCCGTCACGTCCTGTCCGAATACGGCAACATGCAGTC CGCAACCGTTCTGTTCATCCTGGATGAGATGCGCAACCGCTCCGCAGCTGAAG GTCACGCTACCACCGGTGAAGGTCTGGACTGGGGCGTGCTGCTGGGTTTCGGT CCAGGTCTGTCCATCGAGACCGTGGTCCTGCACTCCTGCCGCCTGAACTAA
Arabidopsis thaliana	
4cl^{NAT}	ATGGCGCCACAAGAACAAGCAGTTTCTCAGGTGATGGAGAAACAGAGCAACAAC AACAACAGTGACGTCATTTTCCGATCAAAGTTACCGGATATTTACATCCCGAACC ACCTATCTCTCCACGACTACATCTTCCAAAACATCTCCGAATTCGCCACTAAGCC TTGCCTAATCAACGGACCAACCGGCCACGTGTACACTTACTCCGACGTCCACGT CATCTCCCGCCAAATCGCCGCCAATTTTCACAAACTCGGCGTTAACCAAAACGA CGTCGTCATGCTCCTCCTCCCAAACTGTCCCGAATTCGTCCTCTCTTTCCTCGC CGCCTCCTTCCGCGGCGCAACCGCCACCGCCGCAAACCCTTTCTTCACTCCGG CGGAGATAGCTAAACAAGCCAAAGCCTCCAACACCAAACTCATAATCACCGAAG CTCGTTACGTCGACAAAATCAAACCACTTCAAAACGACGACGGAGTAGTCATCG TCTGCATCGACGACAACGAATCCGTGCCAATCCCTGAAGGCTGCCTCCGCTTCA CCGAGTTGACTCAGTCGACAACCGAGGCATCAGAAGTCATCGACTCGGTGGAG ATTTCACCGGACGACGTGGTGGCACTACCTTACTCCTCTGGCACGACGGGATTA CCAAAAGGAGTGATGCTGACTCACAAGGGACTAGTCACGAGCGTTGCTCAGCA AGTCGACGGCGAGAACCCGAATCTTTATTTCCACAGCGATGACGTCATACTCTG TGTTTTGCCCATGTTTCATATCTACGCTTTGAACTCGATCATGTTGTGTGGTCTTA GAGTTGGTGCGGCGATTCTGATAATGCCGAAGTTTGAGATCAATCTGCTATTGG AGCTGATCCAGAGGTGTAAAGTGACGGTGGCTCCGATGGTTCCGCCGATTGTG TTGGCCATTGCGAAGTCTTCGGAGACGGAGAAGTATGATTTGAGCTCGATAAGA GTGGTGAAATCTGGTGCTGCTCCTCTTGGTAAAGAACTTGAAGATGCCGTTAAT GCCAAGTTTCCTAATGCCAAACTCGGTCAGGGATACGGAATGACGGAAGCAGG TCCAGTGCTAGCAATGTCGTTAGGTTTTGCAAAGGAACCTTTTCCGGTTAAGTCA GGAGCTTGTGGTACTGTTGTAAGAAATGCTGAGATGAAAATAGTTGATCCAGAC ACCGGAGATTCTCTTTCGAGGAATCAACCCGGTGAGATTTGTATTCGTGGTCAC CAGATCATGAAAGGTTACCTCAACAATCCGGCAGCTACAGCAGAGACCATTGAT

	AAAGACGGTTGGCTTCATACTGGAGATATTGGATTGATCGATGACGATGACGAG CTTTTCATCGTTGATCGATTGAAAGAACTTATCAAGTATAAAGGTTTTCAGGTAG CTCCGGCTGAGCTAGAGGCTTTGCTCATCGGTCATCCTGACATTACTGATGTTG CTGTTGTCGCAATGAAAGAAGAAGCAGCTGGTGAAGTTCCTGTTGCATTTGTGG TGAAATCGAAGGATTCGGAGTTATCAGAAGATGATGTGAAGCAATTCGTGTCGA AACAGGTTGTGTTTTACAAGAGAATCAACAAAGTGTTCTTCACTGAATCCATTCC TAAAGCTCCATCAGGGAAGATATTGAGGAAAGATCTGAGGGCAAAACTAGCAAA TGGATTGTGA
4cl^{OPT}	ATGGCACCACAGGAACAGGCTGTCTCCCAGGTTATGGAGAAGCAGTCCAACAA CAACAACTCCGATGTTATCTTCCGCTCCAAGCTGCCAGACATCTACATCCCAAAC CACCTGTCCCTGCACGATTACATCTTCCAGAACATCTCCGAATTCGCAACCAAG CCATGCCTGATCAACGGTCCAACCGGCCACGTGTACACCTACTCCGATGTCCAC GTTATCTCCCGCCAGATCGCAGCTAACTTCCACAAGCTGGGCGTGAACCAGAAC GACGTGGTCATGCTGCTGCTGCCAAACTGCCCAGAGTTCGTCCTGTCCTTCCTG GCTGCATCCTTCCGCGGTGCCACCGCAACCGCTGCAAACCCATTCTTCACCCCA GCTGAAATCGCCAAGCAGGCTAAGGCCTCCAACACCAAGCTGATCATCACCGA GGCTCGCTACGTTGACAAGATCAAGCCACTGCAGAACGATGACGGCGTTGTGA TCGTCTGCATCGATGACAACGAATCCGTTCCAATCCCAGAGGGTTGCCTGCGCT TCACCGAACTGACCCAGTCCACCACCGAAGCATCCGAGGTTATCGATTCCGTGG AGATCTCCCCAGATGACGTCGTTGCTCTGCCATACTCCTCCGGTACCACCGGTC TGCCAAAGGGCGTCATGCTGACCCACAAGGGTCTGGTGACCTCTGTGGCACAG CAGGTTGACGGCGAAAACCCAAACCTGTACTTCCACTCCGATGACGTCATCCTG TGCGTTCTGCCAATGTTCCACATCTACGCTCTGAACTCCATCATGCTGTGCGGT CTGCGTGTTGGTGCAGCTATCCTGATCATGCCAAAGTTCGAAATCAACCTGCTG CTGGAGCTGATCCAGCGCTGCAAGGTGACCGTCGCACCAATGGTGCCACCAAT CGTCCTGGCAATCGCTAAGTCCTCCGAAACCGAGAAGTACGATCTGTCCTCCAT CCGCGTGGTCAAGTCCGGTGCCGCACCACTGGGCAAGGAACTGGAGGACGCA GTGAACGCTAAGTTCCCAAACGCCAAGCTGGGCCAGGGTTACGGTATGACCGA AGCTGGTCCAGTGCTGGCAATGTCCCTGGGTTTCGCAAAGGAGCCATTCCCAG TCAAGTCCGGTGCTTGCGGCACCGTTGTGCGCAACGCCGAAATGAAGATCGTC GATCCAGACACCGGCGATTCCCTGTCCCGCAACCAGCCAGGCGAGATCTGCAT CCGCGGCCACCAGATCATGAAGGGTTACCTGAACAACCCAGCTGCCACCGCAG AGACCATCGATAAGGACGGCTGGCTGCACACCGGTGACATCGGCCTGATCGAT GACGATGACGAACTGTTCATCGTTGACCGCCTGAAGGAGCTGATCAAGTACAAG GGCTTCCAGGTGGCCCCAGCAGAACTGGAGGCTCTGCTGATCGGTCACCCAGA CATCACCGACGTCGCCGTCGTTGCAATGAAGGAAGAGGCAGCTGGCGAAGTTC CAGTGGCCTTCGTGGTCAAGTCCAAGGATTCCGAACTGTCCGAGGATGACGTTA AGCAGTTCGTGTCCAAGCAGGTTGTGTTCTACAAGCGCATCAACAAGGTTTTCTT CACCGAGTCCATCCCAAAGGCTCCATCCGGCAAGATCCTGCGCAAGGACCTGC GCGCTAAGCTGGCCAACGGTCTGTAA
Oryza sativa	
cus^{NAT}	ATGGCACCGACGACGACCATGGGAAGCGCCTTATACCCGCTCGGCGAAATGCG GCGGTCGCAGCGCGCCGACGGGCTCGCCGCCGTGCTCGCCATCGGCACCGCC AACCCTCCCAACTGCGTTACCCAGGAGGAGTTCCCCGACTTCTACTTCCGCGTC ACCAACAGCGACCACCTCACTGCCCTCAAGGACAAGTTCAAGCGTATCTGTCAG GAAATGGGCGTGCAGAGGCGGTACCTGCACCACACGGAGGAGATGCTGTCCG CACACCCGGAGTTCGTGGACCGCGACGCGCCGTCGCTCGACGCGCGGCTGGA CATCGCCGCGGACGCCGTGCCGGAGCTGGCGGCGGAGGCCGCCAAGAAGGC GATCGCCGAGTGGGGCCGCCCGGCCGCCGACATCACCCACCTCGTCGTCACC ACCAACTCCGGCGCCCACGTCCCGGGTGTCGACTTCCGCCTCGTCCCGCTCCT CGGCCTCCGCCCCTCCGTGCGCCGCACCATGCTCCACCTCAACGGCTGCTTCG CCGGCTGCGCCGCGCTCCGCCTCGCCAAGGACCTCGCCGAGAACAGCCGCGG CGCGCGCGTCCTCGTCGTCGCCGCCGAGCTCACCCTCATGTACTTCACCGGGC CCGACGAGGGCTGCTTCAGGACGCTCCTCGTCCAGGGCCTGTTCGGCGACGG CGCGGCCGCCGTCATTGTCGGCGCCGACGCCGACGACGTCGAGCGCCCGCTG TTCGAGATAGTGTCGGCGGCGCAGACGATCATCCCGGAGTCGGACCACGCCCT GAACATGCGGTTCACGGAGCGCCGCTTGGACGGCGTCCTCGGGCGGCAGGTC CCGGGGCTCATCGGGGACAACGTCGAGCGGTGCCTCCTGGACATGTTCGGCC CACTTCTCGGCGGCGACGGCGGCGGCGGGTGGAACGACCTGTTCTGGGCGGT GCACCCGGGCTCGTCGACGATCATGGACCAGGTCGACGCGGCGCTCGGCCTC

	GAGCCCGGCAAGCTGGCGGCGAGCCGCCGTGTGCTCAGCGACTACGGGAACA TGTCTGGCGCTACGGTGATCTTCGCGCTGGACGAGCTGCGCCGGCAGCGCAA GGAGGCGGCGGCGGCGGGTGAATGGCCGGAGTTGGGAGTGATGATGGCGTTC GGCCCGGGGATGACCGTTGATGCGATGCTGTTGCACGCCACCTCTCATGTGAA TTAA
cus^{OPT}	ATGGCCCCAACCACCACCATGGGCTCCGCACTGTACCCACTGGGTGAAATGCG CCGCTCCCAGCGTGCTGATGGTCTGGCAGCTGTGCTGGCTATCGGTACCGCCA ACCCACCAAACTGCGTCACCCAGGAAGAGTTCCCAGATTTCTACTTCCGCGTTA CCAACTCCGACCACCTGACCGCACTGAAGGATAAGTTCAAGCGCATCTGCCAG GAAATGGGCGTGCAGCGCCGCTACCTGCACCACACCGAAGAGATGCTGTCCGC TCACCCAGAGTTCGTTGATCGTGATGCACCATCCCTGGATGCACGTCTGGACAT CGCCGCAGATGCAGTGCCAGAACTGGCTGCCGAGGCAGCTAAGAAGGCAATCG CTGAATGGGGTCGTCCAGCAGCAGACATCACCCACCTGGTGGTCACCACCAAC TCCGGCGCTCACGTGCCAGGTGTCGATTTCCGTCTGGTGCCTCTGCTGGGTCT GCGTCCATCCGTCCGTCGCACCATGCTGCACCTGAACGGTTGCTTCGCTGGTT GCGCTGCACTGCGTCTGGCAAAGGACCTGGCTGAGAACTCCCGCGGCGCACG TGTCCTGGTTGTGGCAGCTGAACTGACCCTGATGTACTTCACCGGCCCAGATGA GGGTTGCTTCCGCACCCTGCTGGTGCAGGGTCTGTTCGGTGATGGTGCAGCAG CTGTCATCGTTGGTGCCGATGCAGATGACGTCGAACGCCCACTGTTCGAGATC GTTTCCGCCGCACAGACCATCATCCCAGAATCCGACCACGCTCTGAACATGCGT TTCACCGAGCGCCGCCTGGATGGTGTTCTGGGTCGTCAGGTGCCAGGTCTGAT CGGTGACAACGTGGAACGCTGCCTGCTGGATATGTTCGGTCCACTGCTGGGCG GTGACGGCGGTGGCGGTTGGAACGACCTGTTCTGGGCAGTCCACCCAGGTTCC TCCACCATCATGGATCAGGTTGATGCTGCACTGGGTCTGGAGCCAGGCAAGCT GGCAGCTTCCCGTCGCGTGCTGTCCGACTACGGCAACATGTCCGGTGCTACCG TCATCTTCGCCCTGGATGAACTGCGTCGCCAGCGTAAGGAAGCAGCAGCTGCT GGTGAATGGCCAGAGCTGGGTGTTATGATGGCATTCGGCCCTGGTATGACCGT GGACGCAATGCTGCTGCACGCTACCTCTCACGTCAACTAA
Sorghum bicolor	
cus^{NAT}	ATGGGAAGTAGTGCTGCTCCGGCCAACGTCCGCGAGATCTGCCGCGCACAGCG TGCCGACGGCCCTGCAGCCGTGCTCGCCATCGGCACGGCCAACCCGGCGAAC TGCGTGCCCCAGGACGAGTTCCCGGACTTCTACTTCCGCGCCACCAAGAGCGA CCATCTCACTGGCCTCAAGGAAAAGTTCAAGAGAGTTTGCCAGAAGCTGGGCGT GCAGAAGCGCTACCTGCACCACACCGAGGAGCTGCTGAGCGCGCACCCGGAG TTCCTCGACCACTCCTCGCCGTCCCTCGACGCGCGGCTGGACATCGTCAAGAC CGCCGTGCCGGAGCTCGCCGCGCAGGCCAGCAGGAAGGCCATCGCCGAGTGG GGCCGCCCGGCCGCCGACATCACGCACCTCGTCGTCACCACCAACTCCGGCG CGCACATCCCGGGCGTCGACTTCCGTCTGGTCCCGCTCCTGGGCCTCCGCCCG ACCGTGCGCCGCACCATGCTCTACCTCAACGGCTGCTTCGCGGGCGCCGCCG CGCTGCGCCTCGCCAGGGACCTGGCCGAGAACAACAGCGGCGCGCGCGTGCT CGTCGTCTGCGCCGAGATCACCGTCCTGCTCTTCAACGGGCCCGAGGAGGGGT GCTTCCAGACGCTCGTCAACCAGGGCCTGTTCGGCGACGGCGCTGGGGCCGT CATCGTCGGTGCCGACCCACTGGCGGCCGAGCGCCCGCTGTTCGAGATCGTGT CCGCCGCGCAGGCCATCATACCGGAGTCCGAGGACGTCATCACCATGCACCTC ACCAGGGGCGGCTACGGCGGCAACATCTCCACCAGGCAGGTCCCCGTCCTCAT CGGCGACAACATCGAGCGCTGTCTCACCGACGCTTTCGCGCCGCTCGGCGGC GTTATTGGCGCCGAATGGAACGACCTGTTCTGGGACGTGCACCCGGGCTCGTC GGCGATCCTGGACCAGGTCGACGCCGTGCTCAAGCTCAAGCCTGAGAAGCTGG CGGCGAGCAGGCGTGTCCTGAGCGAGTACGGGAACATGTTCGGCGTCACGGT GATCTTCGTGCTCGACGAGCTGCGCCGCCGGATGGAGAAGGGGGAAGAGGAG GGGGCGCCAGAGTGGGGGGTCATGGTGGCGTTCGGACCCGGGCTCACCGTTG AGACGATGGTGCTCCACCGATCAGGCACCCCAGCTGAGAAGAAACTGGCGGAG GCATGA
cus^{OPT}	ATGGGCTCCTCCGCAGCTCCAGCAAACGTGCGTGAAATCTGCCGCGCTCAGCG CGCTGATGGTCCAGCAGCAGTGCTGGCTATCGGCACCGCAAACCCAGCTAACT GCGTCCCACAGGATGAGTTCCCAGACTTCTACTTCCGCGCAACCAAGTCCGACC ACCTGACCGGTCTGAAGGAAAAGTTCAAGCGCGTTTGCCAGAAGCTGGGCGTG CAGAAGCGCTACCTGCACCACACCGAAGAGCTGCTGTCCGCTCACCCAGAATT CCTGGATCACTCCTCCCCATCCCTGGATGCCCGCCTGGACATCGTTAAGACCG CAGTTCCAGAACTCGCTGCACAGGCTTCCCGTAAGGCAATCGCAGAATGGGGT

	CGCCCAGCAGCTGACATCACCCACCTGGTGGTCACCACCAACTCCGGTGCCCA CATCCCAGGCGTGGACTTCCGTCTGGTTCCACTGCTCGGTCTGCGTCCAACCG TTCGTCGCACCATGCTGTACCTGAACGGTTGCTTCGCTGGTGCTGCAGCACTCC GTCTGGCACGTGATCTGGCAGAGAACAACTCCGGTGCTCGTGTCCTGGTTGTG TGCGCAGAAATCACCGTTCTGCTGTTCAACGGTCCAGAAGAGGGCTGCTTCCAG ACCCTGGTCAACCAGGGTCTGTTCGGCGATGGTGCTGGCGCCGTCATCGTGGG TGCTGACCCACTGGCTGCAGAGCGTCCACTGTTCGAAATCGTCTCCGCTGCCC AGGCCATCATCCCAGAGTCCGAAGACGTTATCACCATGCACCTGACCCGCGGC GGTTACGGCGGTAACATCTCCACCCGTCAGGTGCCAGTCCTGATCGGTGATAA CATCGAGCGCTGCCTGACCGACGCATTCGCTCCACTGGGCGGTGTTATCGGTG CAGAATGGAACGACCTGTTCTGGGACGTGCACCCAGGCTCCTCCGCAATCCTG GATCAGGTGGACGCTGTCCTGAAGCTGAAGCCAGAGAAGCTGGCAGCTTCCCG TCGCGTGCTGTCCGAATACGGTAACATGTTCGGCGTTACCGTGATCTTCGTCCT GGACGAGCTGCGTCGCCGCATGGAAAAGGGTGAAGAGGAAGGCGCCCCAGAG TGGGGTGTCATGGTTGCATTCGGTCCAGGCCTGACCGTCGAAACCATGGTTCT GCACCGCTCCGGCACCCCAGCTGAGAAGAAGCTGGCCGAAGCATAA

Table S5. Growth performance of the curcumin producing *C. glutamicum* CUR-8, CUR-12 and and CUR-15 during early and main curcumin production phase in shake flasks. The data comprise of maximum growth rate (μ_{max}), glucose uptake rate (Q_{Glc}), ferulate uptake rate (Q_{Fer}), specific glucose uptake rate (q_{Glc}), specific curcumin formation rate (q_{Cur}), volumetric productivity (P_{vol}), specific productivity (P_{spec}), biomass yield ($Y_{X/Glc}$), curcumin yield ($Y_{Cur/Glc}$ and $Y_{Cur/Fer}$), and curcumin titre (T_{Cur}) of the CUR-8, CUR-12, and CUR-15 strains in minimal medium with 30 g L^{-1} glucose (165 mM) and 5 mM ferulate. Early production phase refers to the phase I, while the main production phase refers to the phase II in the cultivation profiles in Fig. 10. Errors represent standard deviations from three biological replicates.

Strain	CUR-8	CUR-12	CUR-15
Rates			
μ [h^{-1}]	0.06 ± 0.00	0.06 ± 0.00	0.05 ± 0.00
	0.04 ± 0.00	0.05 ± 0.00	0.05 ± 0.00
Q_{Glc} [mmol h^{-1}]	1.12 ± 0.03	1.04 ± 0.00	0.97 ± 0.01
	4.99 ± 0.01	5.42 ± 0.08	4.92 ± 0.04
Q_{Fer} [mmol h^{-1}]	0.05 ± 0.00	0.04 ± 0.00	0.04 ± 0.00
	0.07 ± 0.00	0.09 ± 0.01	0.10 ± 0.01
q_{Glc} [g g^{-1} h^{-1}]	0.21 ± 0.00	0.17 ± 0.00	0.17 ± 0.01
	0.14 ± 0.01	0.15 ± 0.00	0.15 ± 0.00
q_{Cur} [mg g^{-1} h^{-1}]	0.90 ± 0.06	0.42 ± 0.10	0.81 ± 0.10
	0.85 ± 0.04	0.94 ± 0.10	1.10 ± 0.10
P_{vol} [mg L^{-1} h^{-1}]	0.92 ± 0.08	0.42 ± 0.13	0.79 ± 0.03
	3.25 ± 0.07	3.11 ± 0.08	3.05 ± 0.03
P_{spec} [mg g^{-1} h^{-1}]	0.42 ± 0.03	0.16 ± 0.05	0.35 ± 0.03
	0.33 ± 0.02	0.32 ± 0.01	0.34 ± 0.01
Yields			
$Y_{X/Glc}$ [g g^{-1}]	0.30 ± 0.00	0.33 ± 0.00	0.31 ± 0.02
	0.31 ± 0.02	0.34 ± 0.01	0.35 ± 0.02
$Y_{Cur/Glc}$ [mg g^{-1}]	4.30 ± 0.32	2.45 ± 0.54	4.66 ± 0.44
	6.00 ± 0.45	6.41 ± 0.64	7.45 ± 0.51
$Y_{Cur/Fer}$ [mg $mmol^{-1}$]	18.95 ± 1.56	10.53 ± 2.62	21.08 ± 2.84
	72.42 ± 2.03	66.85 ± 4.30	65.70 ± 2.14
Titres			
T_{Cur} [mg L^{-1}]	190.09 ± 7.47	203.74 ± 7.82	187.82 ± 1.37

Table S6. Gene expression data of the genes related to metabolism of amino acids during curcumin production in genetically engineered *C. glutamicum*. The data represents log_2FC of the differentially expressed genes associated with amino acid metabolism in the CUR-8 strain, as compared to the curcumin non-producing *C. glutamicum* ATCC 13032_pClik5α during the early production (T1) and the major production phase (T2).

Locus tag	Gene ID	Product	Log_2FC T1	Log_2FC T2
NCgl2098	*aroG*	3-Deoxy-7-phosphoheptulonate synthase class II	-1.07	-0.61
NCgl0950	*aroF*	3-Deoxy-D-arabino-heptulosonate 7-phosphate (DAHP) synthase	-0.69	-1.73
NCgl1567	*aroE*	Shikimate dehydrogenase	-0.49	-1.03
NCgl2927	*trpE*	Anthranilate synthase component I	-1.19	-0.85
NCgl2928	*trpG*	Anthranilate synthase component II	-1.23	-1.02
NCgl2929	*trpD*	Anthranilate phosphoribosyltransferase	-1.21	-1.18
NCgl2930	*trpCF*	Bifunctional indole-3-glycerol-phosphate synthase TrpC/phosphoribosylanthranilate isomerase TrpF	-1.06	-1.74
NCgl2931	*trpB*	Tryptophan synthase subunit beta	-0.83	-1.29
NCgl2932	*trpA*	Tryptophan synthase subunit alpha	-0.79	-1.04
NCgl2799	*pheA*	Prephenate dehydratase	-0.44	-1.05
NCgl1222	*ilvB*	Acetolactate synthase large subunit	-1.15	-2.12
NCgl1223	*ilvN*	Acetolactate synthase small subunit	-1.20	-2.21
NCgl1224	*ilvC*	Ketol-acid reductoisomerase	-0.70	-1.94
NCgl0245	*leuA*	2-Isopropylmalate synthase	-0.31	-1.38
NCgl1094	*metE*	5-Methyltetrahydropteroyltriglutamate--homocysteine S-methyltransferase	-1.46	-1.62
NCgl1137	*thrB*	Homoserine kinase	-0.56	-1.14
NCgl1548	*carA*	Glutamine-hydrolyzing carbamoyl-phosphate synthase small subunit	-0.42	-1.32
NCgl1547	*carB*	Carbamoyl-phosphate synthase large subunit	-0.24	-1.18
NCgl1235	*serA*	Phosphoglycerate dehydrogenase	-1.32	-0.22
NCgl1136	*hom*	Homoserine dehydrogenase	-0.54	-1.20
NCgl2272	*proA*	Glutamate-5-semialdehyde dehydrogenase	-0.04	-1.13
NCgl1999	*gdh*	NADP-specific glutamate dehydrogenase	-0.29	-1.28
NCgl0033	*ppiA*	Peptidylprolyl isomerase	-0.68	-1.17
NCgl1262	*lauC*	3-Isopropylmalate dehydratase large subunit	-0.87	-1.12
NCgl1875	*gluA*	Glutamate ABC transporter ATP-binding protein GluA	-1.11	-3.12
NCgl1876	*gluB*	ABC-type transporter, periplasmic component	-1.03	-2.67
NCgl1877	*gluC*	Glutamate ABC transporter permease GluC	-0.77	-1.52

Table S7. Gene expression data of the genes related to oxidative stress response during curcumin production in genetically engineered *C. glutamicum*. The data represents log_2FC of the differentially expressed genes associated with oxidative stress response in the CUR-8 strain, as compared to the curcumin non-producing *C. glutamicum* ATCC 13032_pClik5α during the early production (T1) and the major production phase (T2).

Locus tag	Gene ID	Product	Log_2FC T1	Log_2FC T2
NCgl0731	-	SOS response-associated peptidase	1.17	0.68
NCgl0942	-	Putative stress-responsive transcriptional regulator	1.17	1.20
NCgl1920	*yaaA*	Peroxide stress protein YaaA	1.16	0.40
NCgl1608	-	Dyp-type peroxidase	0.50	1.27
NCgl0023	-	Organic hydroperoxide resistance protein	1.38	1.54
NCgl1216	-	Predicted glutathione S-transferase	1.18	1.46
NCgl2739	-	3-Methyladenine DNA glycosylase	-2.37	-2.39
NCgl1880	*recA*	Recombinase RecA	-0.31	-1.04
NCgl1501	*sufC*	Fe-S cluster assembly ATPase SufC	-0.37	-1.41
NCgl1503	*sufB*	Fe-S cluster assembly protein SufB	-0.46	-1.49
NCgl1502	*sufD*	Fe-S cluster assembly protein SufD	-0.51	-1.73
NCgl0755	*pdxT*	Pyridoxal 5'-phosphate synthase lyase subunit PdxT	-1.98	-1.27
NCgl0754	*pdxS*	Pyridoxal 5'-phosphate synthase lyase subunit PdxS	-2.01	-1.37
NCgl1609	-	Copper chaperone PCu(A)C	0.43	1.15
NCgl0171	-	Cold-shock protein	-1.06	-1.01
NCgl2286	-	Carboxymuconolactone decarboxylase family protein	1.61	1.70
NCgl0615	-	Metal-dependent hydrolase	0.67	1.07
NCgl2740	-	Hemoglobin-like flavoprotein	0.28	1.08
NCgl0204	-	Type IV toxin-antitoxin system AbiEi family	1.13	0.58
NCgl2907	-	VanZ family protein	2.02	1.62
NCgl2149	-	DUF2786 domain-containing protein	1.09	1.12
NCgl1093	-	DHA2 family efflux MFS transporter permease subunit	1.09	1.32
NCgl1092	-	MFS transporter	0.92	1.14
NCgl0382	-	Hypothetical membrane protein	1.11	1.03

Table S8. Gene expression data of the genes related to ribosome biogenesis, transcription, and translation during curcumin production in genetically engineered *C. glutamicum*. The data represents log_2FC of the differentially expressed genes associated with ribosome formation, transcription, and translation in the CUR-8 strain, as compared to the curcumin non-producing *C. glutamicum* ATCC 13032_pClik5α during the early production (T1) and major production phase (T2).

Locus tag	Gene ID	Product	Log_2FC T1	Log_2FC T2
		50S ribosomal proteins		
NCgl0460	*rplA*	50S ribosomal protein L1	-0.35	-1.12
NCgl0490	*rplB*	50S ribosomal protein L2	-0.52	-1.39
NCgl0487	*rplC*	50S ribosomal protein L3	-0.43	-1.41
NCgl0488	*rplD*	50S ribosomal protein L4	-0.50	-1.38
NCgl0501	*rplE*	50S ribosomal protein L5	-0.61	-1.23
NCgl0516	*rplF*	50S ribosomal protein L6	-0.43	-1.21
NCgl2879	*rplI*	50S ribosomal protein L9	-0.60	-1.33
NCgl0459	*rplK*	50S ribosomal protein L11	-0.36	-1.21
NCgl0556	*rplM*	50S ribosomal protein L13	-0.65	-1.42
NCgl0499	*rplN*	50S ribosomal protein L14	-0.56	-1.30
NCgl0520	*rplO*	50S ribosomal protein L15	-0.69	-1.40
NCgl0494	*rplP*	50S ribosomal protein L16	-0.52	-1.30
NCgl0541	*rplQ*	50S ribosomal protein L17	-0.56	-1.17
NCgl0517	*rplR*	50S ribosomal protein L18	-0.50	-1.34
NCgl1960	*rplS*	50S ribosomal protein L19	-0.47	-1.05
NCgl1326	*rplT*	50S ribosomal protein L20	-0.48	-1.18
NCgl0492	*rplV*	50S ribosomal protein L22	-0.52	-1.38
NCgl0489	*rplW*	50S ribosomal protein L23	-0.51	-1.30
NCgl0500	*rplX*	50S ribosomal protein L24	-0.51	-1.22
NCgl0902	*rplY*	50S ribosomal protein L25	-0.44	-1.01
NCgl0834	*rpmB*	50S ribosomal protein L28	-0.48	-1.18
NCgl0495	*rpmS*	50S ribosomal protein L29	-0.59	-1.26
NCgl0519	*rpmD*	50S ribosomal protein L30	-0.62	-1.39
NCgl0837	*rpmE*	50S ribosomal protein L31	-0.48	-1.23
NCgl0838	*rpmF*	50S ribosomal protein L32	-0.44	-1.15
NCgl0833	*rpmG*	50S ribosomal protein L33	-0.52	-1.19
NCgl2993	*rpmH*	50S ribosomal protein L34	-0.35	-1.46
NCgl1325	*rpmL*	50S ribosomal protein L35	-0.43	-1.29
		30S ribosomal proteins		
NCgl0493	*rpsC*	30S ribosomal protein S3	-0.51	-1.44
NCgl0518	*rpsE*	30S ribosomal protein S5	-0.54	-1.32
NCgl0477	*rpsG*	30S ribosomal protein S7	-0.54	-1.38
NCgl0515	*rpsH*	30S ribosomal protein S8	-0.44	-1.16
NCgl0557	*rpsI*	30S ribosomal protein S9	-0.66	-1.41
NCgl0486	*rpsJ*	30S ribosomal protein S10	-0.41	-1.31
NCgl0538	*rpsK*	30S ribosomal protein S11	-0.38	-1.04
NCgl0476	*rpsL*	30S ribosomal protein S12	-0.48	-1.37
NCgl0537	*rpsM*	30S ribosomal protein S13	-0.32	-1.16
NCgl0832	*rpsN*	30S ribosomal protein S14	-0.47	-1.13
NCgl1976	*rpsP*	30S ribosomal protein S16	-0.44	-1.20

NCgl0496	*rpsQ*	30S ribosomal protein S17	-0.57	-1.26
NCgl0831	*rpsR*	30S ribosomal protein S18	-0.55	-1.27
NCgl0491	*rpsS*	30S ribosomal protein S19	-0.51	-1.38
NCgl2261	*rpsT*	30S ribosomal protein S20	-0.45	-1.08

Table S9. Gene expression data of the transcription factor-encoding genes during curcumin production in genetically engineered *C. glutamicum*. The data represents log_2FC of differentially expressed genes encoding transcription factors in the CUR-8 strain, as compared to the curcumin non-producing *C. glutamicum* ATCC 13032_pClik5α during the early production (T1) and the major production phase (T2).

Locus tag	Gene ID	Product	Log_2FC T1	Log_2FC T2
NCgl0286	*glxR*	CRP-like cAMP-activated global transcriptional regulator GlxR	-0.21	-1.16
NCgl1859	-	Transcriptional regulators of sugar metabolism	-0.55	-1.87
NCgl0358	*ramB*	Acetate metabolism transcriptional regulator RamB	0.57	-1.16
NCgl2983	*sigM*	sigma-70 family RNA polymerase sigma factor	1.14	0.98
NCgl0734	*whiB1/whcE*	WhiB family transcriptional regulator WhcE	-0.33	-1.44
NCgl0574	*whiB3*	WhiB family transcriptional regulator WhiB3	1.29	1.02
NCgl0275	*whiB4/whcA*	WhiB family transcriptional regulator WhcA	-0.29	-1.90
NCgl0942	-	Putative stress-responsive transcriptional regulator	1.17	1.20
NCgl2299	*vanR*	PadR family transcriptional regulator VanR	1.68	1.61
NCgl2877	-	PadR family transcriptional regulator	-0.92	-1.41
NCgl1248	-	TetR-like C-terminal domain-containing protein	1.80	1.96
NCgl2298	-	TetR family transcriptional regulator	1.15	0.92
NCgl2025	-	TetR/AcrR family transcriptional regulator	1.33	1.20
NCgl1578	-	TetR/AcrR family transcriptional regulator	1.15	1.00
NCgl2324	-	LuxR family transcriptional regulator	1.49	1.78
NCgl2311	-	LuxR family transcriptional regulator	1.12	1.09
NCgl2550	-	IclR family transcriptional regulator	1.16	0.21
NCgl2921	-	IclR family transcriptional regulator	1.15	0.80
NCgl2308	-	IclR family transcriptional regulator	1.37	0.94
NCgl0958	-	LysR family transcriptional regulator substrate-binding protein	1.36	0.72
NCgl0581	-	LysR substrate-binding domain-containing protein	1.02	1.05
NCgl1989	-	LysR family transcriptional regulator	1.01	0.78
NCgl2827	-	LysR family transcriptional regulator	1.01	1.05
NCgl0218	-	LysR family transcriptional regulator	0.78	1.04
NCgl1967	-	LacI family DNA-binding transcriptional regulator	1.05	0.81
NCgl0965	-	GntR family transcriptional regulator	-0.32	-1.12
NCgl2234	-	GntR family transcriptional regulator	1.03	1.23
NCgl2846	-	GntR family transcriptional regulator	0.74	1.29
NCgl2440	-	FadR/GntR family transcriptional regulator	0.03	-1.05
NCgl0035	-	AraC family transcriptional regulator	1.06	1.02
NCgl0253	*lrp*	Lrp/AsnC family transcriptional regulator	1.01	1.08
NCgl2567	-	Lrp/AsnC family transcriptional regulator	1.02	0.85
NCgl0135	-	AbrB family transcriptional regulator	0.44	1.11
NCgl1386	-	MerR family transcriptional regulator	-0.39	-1.16
NCgl1215	-	ArgP/LysG family DNA-binding transcriptional regulator	1.23	1.23
NCgl2868	-	Crp/Fnr family transcriptional regulator	1.19	1.08
NCgl0019	-	BlaI/MecI/CopY family transcriptional regulator	1.09	1.05
NCgl0836	-	Metalloregulator ArsR/SmtB family transcription factor	1.40	1.22
NCgl0869	-	Metalloregulator ArsR/SmtB family transcription factor	1.28	1.34
NCgl2441	-	Metal-dependent transcriptional regulator	1.00	1.14
NCgl2689	-	XRE family transcriptional regulator	1.13	1.00

NCgl2518	-	Response regulator transcription factor	1.03	-0.17
NCgl2330	-	Hypothetical transcriptional regulator	2.02	1.74
NCgl2333	-	Predicted transcriptional regulator	1.81	2.07
NCgl1504	-	Predicted transcriptional regulator	-0.46	-1.56
NCgl1370	-	Predicted transcriptional regulator containing the HTH domain	0.09	-1.15
NCgl2034	-	HTH-domain-containing protein	1.83	1.55
NCgl2380	-	HTH transcriptional regulator	1.27	1.16
NCgl1317	-	HTH-domain-containing protein	1.14	1.02
NCgl1301	-	HTH transcriptional regulator	1.02	0.94
NCgl1745	-	HTH transcriptional regulator	1.01	0.87
NCgl0655	-	HTH transcriptional regulator	-0.46	-1.07

Table S10. Gene expression data of the membrane protein-encoding genes during curcumin production in genetically engineered *C. glutamicum*. The data represents log_2FC of the differentially expressed genes coding for membrane-associated proteins in the CUR-8 strain, as compared to the curcumin non-producing *C. glutamicum* ATCC 13032_pClik5α during early production (T1) and major production phase (T2).

Locus tag	Gene ID	Product	Function	Log_2FC T1	Log_2FC T2
NCgl2759	-	Predicted acyltransferase	Acyltransferase	0.76	1.16
NCgl0464	-	Amino acid permease	Amino acids	1.24	1.51
NCgl2262	-	Putative threonine efflux protein	Amino acids	0.70	1.19
NCgl2566	-	Putative threonine efflux protein	Amino acids	1.19	1.09
NCgl0143	-	Putative threonine efflux protein	Amino acids	0.94	1.06
NCgl0453	-	D-serine/D-alanine/glycine transporter	Amino acids	0.62	1.04
NCgl0255	-	Branched-chain amino acid exporter BrnE	Amino acids	1.18	1.03
NCgl2514	-	Peptide MFS transporter	Amino acids	1.11	1.03
NCgl1875	*gluA*	Glutamate ABC transporter ATP-binding protein GluA	Amino acids	-1.11	-3.12
NCgl1876	*gluB*	ABC-type transporter, periplasmic component	Amino acids	-1.03	-2.67
NCgl1877	*gluC*	Glutamate ABC transporter permease GluC	Amino acids	-0.77	-1.52
NCgl0610	-	MetQ/NlpA family ABC transporter substrate-binding protein	Amino acids	-0.13	-1.08
NCgl2683	-	Sodium/glutamate symporter	Amino acids/cations	1.16	1.19
NCgl1116	*putP*	Sodium/proline symporter PutP	Amino acids/cations	-0.43	-1.19
NCgl2463	-	Dicarboxylate/amino acid:cation symporter	Amino acids/dicarboxylate	1.15	1.40
NCgl0799	-	Na+/proline, Na+/panthothenate symport	Amino acids/vitamins	-0.52	-2.46
NCgl1521	-	Ammonium transporter	Ammonium	1.58	1.70
NCgl2218	-	ATP-binding cassette domain-containing protein	Ammonium	0.60	1.07
NCgl1983	-	Ammonium transporter	Ammonium	0.50	1.07
NCgl2325	*benK*	Benzoate transporter BenK	Aromatic compound	1.87	2.28
NCgl2326	*benE*	Benzoate/H(+) symporter BenE family transporter	Aromatic compound	1.90	2.16
NCgl1883	-	Biotin transporter BioY	Biotin	0.81	1.17
NCgl2256	*dctM*	C4-Dicarboxylate transport	C4-Dicarboxylate	2.36	2.58
NCgl2257	*dtcX*	C4-Dicarboxylate transport	C4-Dicarboxylate	2.29	2.26
NCgl2258	*dctP*	TRAP transporter substrate-binding protein DctP	C4-Dicarboxylate	2.05	1.82

NCgl2506	-	C4-Dicarboxylate transporter DctA	C4-Dicarboxylate	1.35	1.39
NCgl1330	*ugpE*	Carbohydrate ABC transporter permease	Carbohydrate	1.32	1.16
NCgl1329	*ugpA*	ABC-type transporter, permease component	Carbohydrate	1.27	1.10
NCgl2953	-	Sugar porter family MFS transporter	Carbohydrate	0.87	1.07
NCgl2374	-	Sugar ABC transporter permease	Carbohydrate	-0.72	-3.72
NCgl2373	-	Carbohydrate ABC transporter permease	Carbohydrate	-0.74	-3.21
NCgl1858	*ptsI*	Phosphoenolpyruvate-protein kinase (PTS system EI component in bacteria)	Carbohydrate	-1.71	-3.19
NCgl2377	*msiK1*	ABC-type transporter, ATPase component	Carbohydrate	-0.92	-3.14
NCgl1305	*ptsG*	PTS transport of D-glucose	Carbohydrate	-1.20	-2.73
NCgl2553	*ptsS*	Phosphotransferase system IIC components, glucose/maltose/N-acetylglucosamine-specific	Carbohydrate	-2.20	-2.56
NCgl2894	-	Inositol-3-phosphate synthase	Carbohydrate	-0.74	-1.02
NCgl0595	-	Lycopene cyclase domain-containing protein	Carotenoids	0.68	1.03
NCgl1488	-	Cation-transporting P-type ATPase	Cations	0.89	1.55
NCgl1992	-	Cation diffusion facilitator family transporter	Cations	0.35	1.18
NCgl1129	-	Cation-translocating P-type ATPase	Cations	0.86	1.15
NCgl0131	-	Trimeric intracellular cation channel family protein	Cations	0.42	1.07
NCgl1968	-	DASS family sodium-coupled anion symporter	Cations/anions	1.16	1.07
NCgl2648	-	Na/Pi cotransporter family protein	Cations/phosphate	0.68	1.05
NCgl1037	-	Calcium:proton antiporter	Cations/protons	1.17	1.10
NCgl0816	-	CynX/NimT family MFS transporter	Cyanate	0.98	1.15
NCgl2370	-	Cytochrome c oxidase assembly protein	Cytochrome	0.69	1.42
NCgl1103	-	Cytochrome d ubiquinol oxidase subunit II	Cytochrome	0.55	1.32
NCgl1104	-	Cytochrome ubiquinol oxidase subunit I	Cytochrome	0.71	1.22
NCgl1102	*cydD*	ABC transporter ATP-binding protein/permease	Cytochrome	0.59	1.20
NCgl2265	-	ComEC/Rec2 family competence protein	DNA	1.98	1.83
NCgl2266	-	DNA uptake protein and related DNA-binding proteins	DNA	1.77	1.80
NCgl0887	*mmpL2*	MMPL family transporter, transporter of a drug	Drug	2.06	2.08
NCgl2647	-	Multidrug effflux MFS transporter	Drug	1.00	1.20
NCgl1468	*tetA*	ABC transporter ATP-binding protein	Drug	0.92	1.05

NCgl1907	*dinF*	MATE family efflux transporter	Drug/sodium	0.64	1.09
NCgl0413	-	ABC transporter substrate-binding protein	Extracellular solute	-1.34	-1.83
NCgl2096	-	Glycosyltransferase 87 family protein	Glycosyltransferase	0.70	1.07
NCgl1414	-	Arsenic resistance protein	Heavy metal resistance	1.16	1.19
NCgl0870	-	Cadmium resistance transporter	Heavy metal resistance	1.05	1.16
NCgl0322	-	Bifunctional UDP-sugar hydrolase/5'-nucleotidase	Hydrolase	1.27	1.25
NCgl0615	-	Metal-dependent hydrolase	Hydrolase	0.67	1.07
NCgl1221	-	Mechanosensitive ion channel family protein	Ions	1.70	1.18
NCgl1564	-	Iron chelate uptake ABC transporter family permease subunit	Iron	1.53	1.66
NCgl0484	-	Iron chelate uptake ABC transporter family permease subunit	Iron	1.28	1.59
NCgl0483	-	Iron chelate uptake ABC transporter family permease subunit	Iron	1.19	1.32
NCgl0637	-	Iron chelate uptake ABC transporter family permease subunit	Iron	1.31	1.30
NCgl1508	-	Heme A synthase	Iron	0.37	1.23
NCgl0638	-	Iron ABC transporter permease	Iron	1.00	1.12
NCgl0927	*mprF*	Bifunctional lysylphosphatidylglycerol flippase/synthetase MprF	Lipids/resistance	1.08	1.09
NCgl1378	-	ABC transporter transmembrane domain-containing protein	Multifunctional	0.97	1.15
NCgl0914	-	ABC transporter ATP-binding protein	Multifunctional	-0.13	-1.20
NCgl2503	-	SpnA family nuclease	Nuclease	1.22	1.60
NCgl2816	-	Putative L-lactate permease	Organic acids	-3.39	-2.93
NCgl0841	-	Trypsin-like peptidase domain-containing protein	Peptidase	1.87	1.22
NCgl1562	-	A24 family peptidase	Peptidase	0.88	1.19
NCgl0020	-	M56 family metallopeptidase	Peptidase	1.02	1.13
NCgl1595	-	Preprotein translocase subunit YajC	Peptide	-0.18	1.18
NCgl1915	-	ABC transporter substrate-binding protein	Peptide	-3.25	-3.97
NCgl1918	-	ABC transporter ATP-binding protein	Peptide	-3.12	-3.36
NCgl0626	*cstA*	Carbon starvation protein, predicted membrane protein	Peptide	-1.87	-2.33
NCgl1403	-	Phosphonate ABC transporter, permease protein PhnE	Phosphate	1.62	1.84
NCgl1402	-	Phosphonate ABC transporter, permease protein PhnE	Phosphate	1.71	1.83
NCgl1404	*pctB*	ABC-type transporter, ATPase component	Phosphate	1.61	1.71

NCgl1405	-	Phosphate/phosphite/phosphonate ABC transporter substrate-binding protein	Phosphate	1.49	1.43
NCgl2484	-	Phosphate ABC transporter permease PstA	Phosphate	1.05	1.41
NCgl2485	-	Phosphate ABC transporter permease subunit PstC	Phosphate	0.77	1.30
NCgl1862	-	HPr family phosphocarrier protein	Phosphate	-0.86	-1.70
NCgl2821	-	Metallophosphoesterase family protein	Phosphoesterase	1.05	1.12
NCgl2862	-	HAMP domain-containing sensor histidine kinase	Phosphorelay	1.01	1.42
NCgl0067	-	Sensor histidine kinase	Phosphorelay	0.85	1.15
NCgl1724	-	Hypothetical protein	Phosphorelay	0.92	1.06
NCgl1935	-	Sensor histidine kinase	Phosphorelay	0.62	1.06
NCgl2991	-	Membrane protein insertase YidC	Preprotein	-0.55	-1.29
NCgl0550	-	Type VII secretion-associated serine protease mycosin	Protease	1.24	1.32
NCgl2737	-	Membrane protease subunits, stomatin/prohibitin homologs	Protease	-2.53	-2.51
NCgl2962	-	Membrane protease subunits, stomatin/prohibitin homologs	Protease	-0.74	-1.50
NCgl2245	-	Bile acid:sodium symporter family protein	Sodium	1.61	1.85
NCgl2634	*mrpC*	Na^+/H^+ antiporter subunit C	Sodium	-0.53	-1.31
NCgl2633	*mrpA*	Na^+/H^+ antiporter subunit A	Sodium	-0.57	-1.31
NCgl1101	-	Thiol reductant ABC exporter subunit CydC	Sulfite	1.07	1.33
NCgl0052	-	Sulfite exporter TauE/SafE family protein	Sulfite	1.15	1.22
NCgl1258	-	Sulfite exporter TauE/SafE family protein	Sulfite	1.06	1.13
NCgl1990	-	Sulfite exporter TauE/SafE family protein	Sulfite	1.18	1.11
NCgl1936	*ssuC*	ABC transporter permease	Sulphonate	1.05	1.50
NCgl1176	*ssuA*	ABC transporter substrate-binding protein	Sulphonate	0.91	1.10
NCgl0942	-	Putative stress-responsive transcriptional regulator	Transcriptional regulator	1.17	1.20
NCgl0135	-	AbrB family transcriptional regulator	Transcriptional regulator	0.44	1.11
NCgl1568	*mltG*	Endolytic transglycosylase MltG	Transglycosylase	-0.50	-1.07
NCgl2724	*tctA*	Tripartite tricarboxylate transporter permease TctA	Tricarboxylate	1.11	1.67
NCgl2725	*tctB*	Tripartite tricarboxylate transporter TctB	Tricarboxylate	1.20	1.41
NCgl0066	*citP*	CitMHS family transporter	Tricarboxylate	1.03	1.36
NCgl1095	-	Hypothetical protein	Unknown	1.20	2.61

NCgl2338	-	DUF418 domain-containing protein	Unknown	2.19	2.27
NCgl2235	-	Hypothetical protein	Unknown	1.84	2.14
NCgl1445	-	MFS transporter	Unknown	1.49	2.05
NCgl0058	-	DUF4956 domain-containing protein	Unknown	2.39	2.01
NCgl0028	-	ABC-type transporter, ATPase component	Unknown	1.37	2.00
NCgl2244	-	PepSY domain-containing protein	Unknown	1.79	1.92
NCgl2005	-	Hypothetical protein	Unknown	1.71	1.83
NCgl2236	-	TRAP transporter permease	Unknown	1.58	1.83
NCgl2332	-	RDD family protein	Unknown	1.81	1.80
NCgl2351	-	ABC transporter permease	Unknown	1.52	1.62
NCgl2907	-	VanZ family protein	Unknown	2.02	1.62
NCgl2004	-	Hypothetical protein	Unknown	1.25	1.60
NCgl2352	-	ABC transporter permease	Unknown	1.66	1.56
NCgl2118	-	DUF3043 domain-containing protein	Unknown	0.20	1.55
NCgl2141	-	MFS transporter	Unknown	0.66	1.55
NCgl1174	-	ABC transporter permease	Unknown	1.24	1.51
NCgl2348	-	MFS transporter	Unknown	1.34	1.47
NCgl0552	-	Type VII secretion protein EccC	Unknown	1.50	1.45
NCgl1205	-	ABC transporter permease	Unknown	1.16	1.44
NCgl2231	-	Hypothetical protein	Unknown	1.25	1.43
NCgl1507	-	ABC transporter permease	Unknown	0.73	1.41
NCgl0553	-	Type VII secretion-associated protein	Unknown	1.33	1.40
NCgl0376	-	Hypothetical protein	Unknown	1.40	1.39
NCgl1636	-	Hypothetical protein	Unknown	1.22	1.39
NCgl0436	-	DoxX family protein	Unknown	1.15	1.39
NCgl0551	-	Type VII secretion integral membrane protein EccD	Unknown	1.38	1.39
NCgl1473	-	TVP38/TMEM64 family protein	Unknown	1.16	1.37
NCgl0580	-	DMT family transporter	Unknown	1.38	1.37
NCgl0546	-	Type VII secretion protein EccB	Unknown	1.30	1.37

NCgl2239	-	ABC transporter permease	Unknown	1.24	1.36
NCgl0907	-	MFS transporter	Unknown	1.22	1.33
NCgl2232	-	AEC family transporter	Unknown	1.30	1.32
NCgl1093	-	DHA2 family efflux MFS transporter permease subunit	Unknown	1.09	1.32
NCgl0074	-	MFS transporter	Unknown	1.24	1.32
NCgl2959	-	Lamin tail domain-containing protein	Unknown	1.25	1.31
NCgl0910	-	ABC transporter permease	Unknown	0.62	1.31
NCgl2757	-	DUF3367 domain-containing protein	Unknown	0.69	1.29
NCgl2282	-	Hypothetical protein	Unknown	1.18	1.28
NCgl1377	-	ABC transporter ATP-binding protein	Unknown	1.06	1.27
NCgl2729	-	MFS transporter	Unknown	0.62	1.27
NCgl1942	-	Hypothetical protein	Unknown	0.86	1.27
NCgl2936	-	ABC transporter permease	Unknown	0.83	1.26
NCgl2972	-	DUF1304 family protein	Unknown	0.66	1.26
NCgl2240	-	ABC transporter permease	Unknown	1.09	1.26
NCgl2288	-	Hypothetical protein	Unknown	1.11	1.25
NCgl1033	-	ECF transporter S component	Unknown	0.74	1.24
NCgl2969	-	MFS transporter	Unknown	1.23	1.23
NCgl1727	-	Phage tail tip lysozyme	Unknown	1.18	1.22
NCgl2522	-	MFS transporter	Unknown	1.13	1.21
NCgl2206	-	Hemolysin family protein	Unknown	0.73	1.19
NCgl0576	-	Hypothetical protein	Unknown	1.49	1.19
NCgl2462	-	DUF1648 domain-containing protein	Unknown	0.95	1.18
NCgl1737	-	ABC transporter permease	Unknown	1.14	1.17
NCgl2828	-	MFS transporter	Unknown	1.17	1.17
NCgl1714	-	Hypothetical protein	Unknown	1.19	1.16
NCgl1400	-	ABC transporter permease	Unknown	0.48	1.16
NCgl1300	-	MFS transporter	Unknown	0.82	1.15
NCgl2903	-	MFS transporter	Unknown	0.88	1.14

NCgl1092	-	MFS transporter	Unknown	0.92	1.14
NCgl1725	-	Hypothetical protein	Unknown	1.03	1.14
NCgl2563	-	ABC transporter permease	Unknown	0.83	1.14
NCgl1411	-	MFS transporter	Unknown	0.57	1.13
NCgl1707	-	Hypothetical protein	Unknown	1.09	1.11
NCgl1425	-	FxsA family protein	Unknown	0.56	1.11
NCgl0473	-	Hypothetical protein	Unknown	0.86	1.10
NCgl2770	-	YbhN family protein	Unknown	0.37	1.10
NCgl1298	-	Hypothetical protein	Unknown	1.16	1.09
NCgl0278	-	MFS transporter	Unknown	2.02	1.09
NCgl2965	-	DUF4395 domain-containing protein	Unknown	1.00	1.08
NCgl0349	-	SGNH hydrolase domain-containing protein	Unknown	0.86	1.08
NCgl2017	-	MFS transporter	Unknown	0.72	1.07
NCgl1728	-	Hypothetical protein	Unknown	1.18	1.07
NCgl1978	-	ABC transporter permease	Unknown	1.13	1.07
NCgl1729	-	Hypothetical protein	Unknown	1.18	1.06
NCgl2852	-	Hypothetical protein	Unknown	0.71	1.06
NCgl0756	-	SdpI family protein	Unknown	1.00	1.06
NCgl1718	-	Hypothetical protein	Unknown	0.91	1.05
NCgl0497	-	Hypothetical protein	Unknown	1.10	1.05
NCgl0130	-	Permease	Unknown	0.96	1.05
NCgl0382	-	Hypothetical membrane protein	Unknown	1.11	1.03
NCgl2761	-	Hypothetical protein	Unknown	0.57	1.03
NCgl0065	-	Hypothetical protein	Unknown	0.84	1.02
NCgl1768	-	Hypothetical protein	Unknown	0.76	1.02
NCgl1026	-	DMT family transporter	Unknown	0.97	1.01
NCgl1997	-	ABC transporter ATP-binding protein	Unknown	0.78	1.01
NCgl1310	-	MFS transporter	Unknown	0.54	1.01
NCgl2375	*amyE*	ABC transporter substrate-binding protein	Unknown	-0.75	-3.81

NCgl2168	-	ABC transporter ATP-binding protein	Unknown	-1.60	-3.68
NCgl2169	-	ABC-type transporter, permease components	Unknown	-1.40	-2.91
NCgl0697	-	ABC-type transporter, periplasmic component	Unknown	-1.34	-2.87
NCgl0798	-	Uncharacterized membrane protein	Unknown	-0.49	-2.74
NCgl2170	-	ABC transporter substrate-binding protein	Unknown	-1.33	-2.59
NCgl2372	-	Hypothetical membrane protein	Unknown	-0.65	-2.01
NCgl2912	-	Hypothetical membrane protein	Unknown	-1.19	-1.57
NCgl0511	-	ABC-type transporter, permease components	Unknown	-0.75	-1.07
NCgl0895	*urtC*	Urea ABC transporter permease subunit UrtC	Urea	1.67	1.68

Table S11. Gene expression data of the genes related to metabolism of CoA-thioesters during curcumin production in genetically engineered *C. glutamicum*. The data represents log_2FC of the differentially expressed genes associated with CoA-thioester metabolism in the CUR-8 strain, as compared to the curcumin non-producing *C. glutamicum* ATCC 13032_pClik5α during the early production (T1) and major production phase (T2).

Locus Tag	Gene ID	Product	Log_2FC T1	Log_2FC T2
NCgl2480	*actA*	Acetyl-CoA hydrolase/transferase family protein	-0.75	-3.10
NCgl2656	*ackA*	Acetate kinase	-1.10	-1.18
NCgl2657	*pta*	Phosphate acetyltransferase	-1.51	-2.11
NCgl2476	*sucD*	Succinate:CoA ligase subunit alpha	-1.19	-1.73
NCgl2477	*sucC*	ADP-forming succinate:CoA ligase subunit beta	-1.06	-1.38
NCgl0670	*accBC*	Acetyl/propionyl/methylcrotonyl-CoA carboxylase subunit alpha	-0.05	-1.16
NCgl0797	*accD*	Acetyl-CoA carboxylase beta subunit	-0.21	-1.00
NCgl1471	*mcmB*	Methylmalonyl-CoA mutase, N-terminal domain/subunit	-0.74	-1.60
NCgl1472	*mcmA*	Methylmalonyl-CoA mutase family protein	-0.83	-1.53
NCgl1170		Methylmalonyl-CoA epimerase	-0.28	-1.03

Table S12. Gene expression data of the genes related to cell envelope formation during curcumin production in genetically engineered *C. glutamicum*. The data represents log_2FC of genes associated the cell envelope formation in the CUR-8 strain, as compared to the curcumin non-producing *C. glutamicum* ATCC 13032_pClik5α during the early production (T1) and the major production phase (T2).

Locus Tag	Gene ID	Product	Log_2FC T1	Log_2FC T2
NCgl0906	*glmU*	Glucosamine-1-phosphate acetyltransferase [multifunctional]	-0.64	-1.14
NCgl1568	*mltG*	Endolytic transglycosylase MltG	-0.50	-1.07
NCgl2750	*udgA2*	UDP-glucose/GDP-mannose dehydrogenase family protein	-0.76	-1.08
NCgl2076	*ftsQ*	Cell division protein FtsQ	-0.73	-1.02
NCgl0769	*ftsX*	Permease-like cell division protein FtsX	1.05	1.20
NCgl0803		Septum formation family protein	-1.10	-1.09
NCgl0936		Septum formation initiator family protein	-0.62	-1.11
NCgl1333	*glpQ2*	Glycerophosphoryl diester phosphodiesterase	1.23	1.14
NCgl1426		Lipase family protein	1.35	1.48
NCgl2220		Carboxylesterase/lipase family protein	1.18	1.01
NCgl0080		Triacylglycerol lipase	1.07	0.79
NCgl2409	*fas-IA*	Fatty acid synthase	0.13	-0.73
NCgl0802	*fas-IB*	Fatty acid synthase	0.99	-0.44
NCgl1229		Acyl-CoA dehydrogenase family protein	1.00	1.00
NCgl0973		Acyl-CoA dehydrogenase family protein	1.44	1.52
NCgl0974		Acyl-CoA dehydrogenase family protein	1.30	1.40

Table S13. Gene expression data of the genes related to metabolism of aromatic compounds during curcumin production in genetically engineered *C. glutamicum*. The data represents log_2FC of genes associated with the metabolism of aromatic compounds in the CUR-8 strain, as compared to the curcumin non-producing *C. glutamicum* ATCC 13032_pClik5α during the early production (T1) and major production phase (T2).

Locus Tag	Gene ID	Product	Log_2FC T1	Log_2FC T2
NCgl0278	*phdT*	MFS transporter	2.02	1.01
NCgl0279	*phdA*	Long-chain fatty acid:CoA ligase	2.18	0.68
NCgl0280	*phdR*	MarR family transcriptional regulator	-7.81	-8.22
NCgl0281	*phdB*	3-Hydroxyacyl-CoA dehydrogenase	-8.39	-8.71
NCgl0282	*phdC*	3-Oxoacyl-CoA ketohydrolase (acetyl-CoA forming)	-9.57	-9.83
NCgl0283	*phdD*	Acyl-CoA dehydrogenase	-7.47	-7.42
NCgl0284	*phdE*	Enoyl-CoA hydratase	-5.52	-7.49
NCgl2320	*benA*	Benzoate 1,2-dioxygenase large subunit	2.02	2.20
NCgl2321	*benB*	Benzoate 1,2-dioxygenase small subunit	2.30	2.59
NCgl2322	*benC*	Benzoate 1,2-dioxygenase electron transfer component BenC	2.24	2.40
NCgl2323	*benD*	1,6-dihydroxycyclohexa-2,4-diene-1-carboxylate dehydrogenase	1.99	1.99
NCgl2326	*benE*	Benzoate/H^+ symporter BenE family transporter	1.90	2.16
NCgl2325	*benK*	Benzoate transporter BenK	1.87	2.28
NCgl2307	*pcaI*	β-ketoadipate succinyl-CoA transferase subunit A	2.25	2.45
NCgl1969	*pcaB2*	Adenylosuccinate lyase	1.22	1.23
NCgl2299	*vanR*	PadR family transcriptional regulator	1.68	1.61
NCgl2922	*genK*	Gentisate transporter	1.47	1.61
NCgl2588	*phe*	Phenol hydroxylase	1.07	1.27
NCgl2923	*nahG*	3-Hydroxybenzoate 6-hydroxylase	1.02	0.87
NCgl0234		Intradiol ring-cleavage dioxygenase	1.67	1.17
NCgl1111	*mhpA*	Bifunctional 3-(3-hydroxy-phenyl)propionate/3-hydroxycinnamic acid hydroxylase	1.24	1.24
NCgl0050		Phenol 2-monooxygenase	1.09	0.91

6. References

Abdeldaiem, M. H. 2014. Use of yellow pigment extracted from turmeric (*Curcuma longa*) rhizomes powder as natural food preservative and colorant Food Science and Quality Management. 22: 56-69.

Adahoun, M. a. A., M.-A. H. Al-Akhras, M. S. Jaafar and M. Bououdina. 2017. Enhanced anti-cancer and antimicrobial activities of curcumin nanoparticles. Artificial cells, nanomedicine, and biotechnology. 45: 98-107.

Adamczak, A., M. Ożarowski and T. M. Karpiński. 2020. Curcumin, a natural antimicrobial agent with strain-specific activity. Pharmaceuticals. 13: 153.

Adeyemi, O. S., J. I. Obeme-Imom, B. O. Akpor, D. Rotimi, G. E.-s. Batiha and A. Owolabi. 2020. Altered redox status, DNA damage and modulation of L-tryptophan metabolism contribute to antimicrobial action of curcumin. Heliyon. 6:

Akram, M. 2014. Citric acid cycle and role of its intermediates in metabolism. Cell Biochemistry and Biophysics. 68: 475-478.

Alper, H. S. and C. Wittmann. 2013. Editorial: How multiplexed tools and approaches speed up the progress of metabolic engineering. Biotechnol J. 8: 506-507.

Álvarez-Álvarez, R., A. Botas, S. M. Albillos, A. Rumbero, J. F. Martín and P. Liras. 2015. Molecular genetics of naringeninbiosynthesis, a typical plant secondary metabolite produced by *Streptomyces clavuligerus*. Microbial Cell Factories. 14: 178.

Alves, R. R. N. and I. M. L. Rosa. 2007. Biodiversity, traditional medicine and public health: where do they meet? Journal of Ethnobiology and Ethnomedicine. 3: 14.

Amer, B. and E. E. K. Baidoo. 2021. Omics-Driven Biotechnology for Industrial Applications. Front Bioeng Biotechnol. 9:

Amorim, A. G. N., J. M. T. Souza, R. C. Santos, B. Gullon, A. Oliveira, L. F. A. Santos, A. L. E. Virgino, A. C. Mafud, H. M. Petrilli and Y. P. Mascarenhas. 2018. HPLC-DAD, ESI–MS/MS, and NMR of lycopene isolated from *P. guajava* L. and its biotechnological applications. European Journal of Lipid Science and Technology. 120: 1700330.

Anand, P., A. B. Kunnumakkara, R. A. Newman and B. B. Aggarwal. 2007. Bioavailability of Curcumin: Problems and Promises. Molecular Pharmaceutics. 4: 807-818.

Anandan, R., D. Dharumadurai and G. P. Manogaran. 2016. An introduction to actinobacteria. Actinobacteria-basics and biotechnological applications. IntechOpen.

Ankri, S., I. Serebrijski, O. Reyes and G. Leblon. 1996. Mutations in the *Corynebacterium glutamicum* proline biosynthetic pathway: a natural bypass of the *proA* step. Journal of bacteriology. 178: 4412-4419.

Araújo, G. d. M. S., J. L. Rodrigues, V. C. Yurgel, C. Silva, A. M. C. Paulo, A. I. S. Loureiro and C. L. Dora. 2023. Designing and characterization of curcumin-loaded nanotechnological dressings: A promising platform for skin burn treatment. International Journal of Pharmaceutics. 635: 122712.

Arndt, A. and B. J. Eikmanns. 2007. The alcohol dehydrogenase gene *adhA* in *Corynebacterium glutamicum* is subject to carbon catabolite repression. Journal of bacteriology. 189: 7408-7416.

Atanasov, A. G., S. B. Zotchev, V. M. Dirsch, I. E. Orhan, M. Banach, J. M. Rollinger, D. Barreca, W. Weckwerth, R. Bauer, E. A. Bayer, M. Majeed, A. Bishayee, V. Bochkov, G. K. Bonn, N. Braidy, F. Bucar, A. Cifuentes, G. D'Onofrio, M. Bodkin, M. Diederich, A. T. Dinkova-Kostova, T. Efferth, K. El Bairi, N. Arkells, T.-P. Fan, B. L. Fiebich, M. Freissmuth, M. I. Georgiev, S. Gibbons, K. M. Godfrey, C. W. Gruber, J. Heer, L. A. Huber, E. Ibanez, A. Kijjoa, A. K. Kiss, A. Lu, F. A. Macias, M. J. S. Miller, A. Mocan, R. Müller, F. Nicoletti, G. Perry, V. Pittalà, L. Rastrelli, M. Ristow, G. L. Russo, A. S. Silva, D. Schuster, H. Sheridan, K. Skalicka-Woźniak, L. Skaltsounis, E. Sobarzo-

Sánchez, D. S. Bredt, H. Stuppner, A. Sureda, N. T. Tzvetkov, R. A. Vacca, B. B. Aggarwal, M. Battino, F. Giampieri, M. Wink, J.-L. Wolfender, J. Xiao, A. W. K. Yeung, G. Lizard, M. A. Popp, M. Heinrich, I. Berindan-Neagoe, M. Stadler, M. Daglia, R. Verpoorte, C. T. Supuran and T. the International Natural Product Sciences. 2021. Natural products in drug discovery: advances and opportunities. Nature Reviews Drug Discovery. 20: 200-216.

Aubel-Sadron, G. and D. Londos-Gagliardi. 1984. Daunorubicin and doxorubicin, anthracycline antibiotics, a physicochemical and biological review. Biochimie. 66: 333-352.

Auchter, M., A. Cramer, A. Hüser, C. Rückert, D. Emer, P. Schwarz, A. Arndt, C. Lange, J. Kalinowski and V. F. Wendisch. 2011. RamA and RamB are global transcriptional regulators in *Corynebacterium glutamicum* and control genes for enzymes of the central metabolism. Journal of Biotechnology. 154: 126-139.

Austin, M. B. and J. P. Noel. 2003. The chalcone synthase superfamily of type III polyketide synthases. Nat Prod Rep. 20: 79-110.

Baerson, S. R. and A. M. Rimando. 2007. A Plethora of polyketides: Structures, biological activities, and enzymes. ACS Publications.

Bagchi, D. 2014. Nutraceutical and functional food regulations in the United States and around the world. Elsevier.

Bailly, X., I. Olivieri, B. Brunel, J.-C. Cleyet-Marel and G. Béna. 2007. Horizontal gene transfer and homologous recombination drive the evolution of the nitrogen-fixing symbionts of *Medicago species*. Journal of bacteriology. 189: 5223-5236.

Bala, K., B. C. Tripathy and D. Sharma. 2006. Neuroprotective and Anti-ageing Effects of Curcumin in Aged Rat Brain Regions. Biogerontology. 7: 81-89.

Ballweg, S. and R. Ernst. 2017. Control of membrane fluidity: the OLE pathway in focus. Biological chemistry. 398: 215-228.

Ballweg, S., E. Sezgin, M. Doktorova, R. Covino, J. Reinhard, D. Wunnicke, I. Hänelt, I. Levental, G. Hummer and R. Ernst. 2020. Regulation of lipid saturation without sensing membrane fluidity. Nature Communications. 11: 756.

Banerjee, G. and P. Chattopadhyay. 2019. Vanillin biotechnology: the perspectives and future. Journal of the Science of Food and Agriculture. 99: 499-506.

Barry, J., M. Fritz, J. R. Brender, P. E. S. Smith, D.-K. Lee and A. Ramamoorthy. 2009. Determining the effects of lipophilic drugs on membrane structure by solid-state NMR spectroscopy: the case of the antioxidant curcumin. Journal of the American Chemical Society. 131: 4490-4498.

Becker, J., N. Buschke, R. Bücker and C. Wittmann. 2010. Systems level engineering of *Corynebacterium glutamicum*–Reprogramming translational efficiency for superior production. Engineering in Life Sciences. 10: 430-438.

Becker, J., G. Gießelmann, S. L. Hoffmann and C. Wittmann. 2018a. *Corynebacterium glutamicum* for Sustainable Bioproduction: From Metabolic Physiology to Systems Metabolic Engineering. Synthetic Biology – Metabolic Engineering. H. Zhao and A.-P. Zeng. Cham, Springer International Publishing. 217-263.

Becker, J., C. Klopprogge, H. Schröder and C. Wittmann. 2009. Metabolic engineering of the tricarboxylic acid cycle for improved lysine production by *Corynebacterium glutamicum*. Applied and Environmental Microbiology. 75: 7866-7869.

Becker, J., C. Klopprogge, O. Zelder, E. Heinzle and C. Wittmann. 2005. Amplified Expression of Fructose 1,6-Bisphosphatase in *Corynebacterium glutamicum* Increases In Vivo Flux through the Pentose Phosphate Pathway and Lysine Production on Different Carbon Sources. Applied and Environmental Microbiology. 71: 8587-8596.

Becker, J., C. M. Rohles and C. Wittmann. 2018b. Metabolically engineered *Corynebacterium glutamicum* for bio-based production of chemicals, fuels, materials, and healthcare products. Metab Eng. 50: 122-141.

Becker, J. and C. Wittmann. 2017. Industrial Microorganisms: *Corynebacterium glutamicum*. Industrial Biotechnology. 183-220.

Becker, J. and C. Wittmann. 2019. A field of dreams: Lignin valorization into chemicals, materials, fuels, and health-care products. Biotechnol Adv. 37: 107360.

Becker, J., O. Zelder, S. Häfner, H. Schröder and C. Wittmann. 2011. From zero to hero—Design-based systems metabolic engineering of *Corynebacterium glutamicum* for l-lysine production. Metab Eng. 13: 159-168.

Beckers, G., L. Nolden and A. Burkovski. 2001. Glutamate synthase of *Corynebacterium glutamicum* is not essential for glutamate synthesis and is regulated by the nitrogen status. Microbiology (Reading). 147: 2961-2970.

Beekwilder, J., R. Wolswinkel, H. Jonker, R. Hall, C. H. R. de Vos and A. Bovy. 2006. Production of resveratrol in recombinant microorganisms. Applied and Environmental Microbiology. 72: 5670-5672.

Berry, A., T. C. Dodge, M. Pepsin and W. Weyler. 2002. Application of metabolic engineering to improve both the production and use of biotech indigo. Journal of Industrial Microbiology and Biotechnology. 28: 127-133.

Bi, H., C. Xu, Y. Bao, C. Zhang, K. Wang, Y. Zhang, M. Wang, B. Chen, Y. Fang and T. Tan. 2023. Enhancing precursor supply and modulating metabolism to achieve high-level production of β-farnesene in *Yarrowia lipolytica*. Bioresource Technology. 382: 129171.

Bindoli, A. and M. P. Rigobello. 2013. Peroxidase Biochemistry and Redox Signaling. Encyclopedia of Biological Chemistry (Second Edition). W. J. Lennarz and M. D. Lane. Waltham, Academic Press. 407-412.

Bisht, R., A. Bhattacharyya, A. Shrivastava and P. Saxena. 2021. An Overview of the Medicinally Important Plant Type III PKS Derived Polyketides. Frontiers in Plant Science. 12:

Bodley, A., L. F. Liu, M. Israel, R. Seshadri, Y. Koseki, F. C. Giuliani, S. Kirschenbaum, R. Silber and M. Potmesil. 1989. DNA topoisomerase II-mediated interaction of doxorubicin and daunorubicin congeners with DNA. Cancer research. 49: 5969-5978.

Bott, M. 2007. Offering surprises: TCA cycle regulation in *Corynebacterium glutamicum*. Trends in microbiology. 15: 417-425.

Braga, A., P. Ferreira, J. Oliveira, I. Rocha and N. Faria. 2018. Heterologous production of resveratrol in bacterial hosts: current status and perspectives. World Journal of Microbiology and Biotechnology. 34: 122.

Brune, I., N. Jochmann, K. Brinkrolf, A. T. Hüser, R. Gerstmeir, B. J. Eikmanns, J. r. Kalinowski, A. Pühler and A. Tauch. 2007. The IclR-type transcriptional repressor LtbR regulates the expression of leucine and tryptophan biosynthesis genes in the amino acid producer *Corynebacterium glutamicum*. Journal of bacteriology. 189: 2720-2733.

Buck, D., M. E. Spencer and J. R. Guest. 1985. Primary structure of the succinyl-CoA synthetase of *Escherichia coli*. Biochemistry. 24: 6245-6252.

Buschke, N., H. Schroder and C. Wittmann. 2011. Metabolic engineering of *Corynebacterium glutamicum* for production of 1,5-diaminopentane from hemicellulose. Biotechnol J. 6: 306-317.

Cacho, R. A., J. Thuss, W. Xu, R. Sanichar, Z. Gao, A. Nguyen, J. C. Vederas and Y. Tang. 2015. Understanding programming of fungal iterative polyketide synthases: the biochemical basis for regioselectivity by the methyltransferase domain in the lovastatin megasynthase. Journal of the American Chemical Society. 137: 15688-15691.

Caffrey, P., S. Lynch, E. Flood, S. Finnan and M. Oliynyk. 2001. Amphotericin biosynthesis in *Streptomyces nodosus*: deductions from analysis of polyketide synthase and late genes. Chem Biol. 8: 713-723.

Campbell, C. D. and J. C. Vederas. 2010. Biosynthesis of lovastatin and related metabolites formed by fungal iterative PKS enzymes. Biopolymers. 93: 755-763.

Cankar, K., N. A. Henke and V. F. Wendisch. 2023. Functional food additives/ingredients production by engineered *Corynebacterium glutamicum*. Systems Microbiology and Biomanufacturing. 3: 110-121.

Cao, X., Y.-B. Lv, J. Chen, T. Imanaka, L.-J. Wei and Q. Hua. 2016. Metabolic engineering of oleaginous yeast *Yarrowia lipolytica* for limonene overproduction. Biotechnology for biofuels. 9: 1-11.

Cardenas, J. and N. A. Da Silva. 2016. Engineering cofactor and transport mechanisms in *Saccharomyces cerevisiae* for enhanced acetyl-CoA and polyketide biosynthesis. Metab Eng. 36: 80-89.

Chan, Y. A., A. M. Podevels, B. M. Kevany and M. G. Thomas. 2009. Biosynthesis of polyketide synthase extender units. Nat Prod Rep. 26: 90-114.

Chang, H.-K. and G. J. Zylstra. 2008. Examination and expansion of the substrate range of m-hydroxybenzoate hydroxylase. Biochemical and biophysical research communications. 371: 149-153.

Chaudhary, D. K., A. Khulan and J. Kim. 2019. Development of a novel cultivation technique for uncultured soil bacteria. Scientific Reports. 9: 1-11.

Chen, C., J. Pan, X. Yang, H. Xiao, Y. Zhang, M. Si, X. Shen and Y. Wang. 2017. Global transcriptomic analysis of the response of *Corynebacterium glutamicum* to ferulic acid. Archives of Microbiology. 199: 325-334.

Chen, H. and L. Du. 2016. Iterative polyketide biosynthesis by modular polyketide synthases in bacteria. Appl Microbiol Biotechnol. 100: 541-557.

Chen, J., M. Liu and L. Zhang. 2016. Avermectin, from winning the Nobel Prize to" innovation in China". Wei sheng wu xue bao= Acta microbiologica Sinica. 56: 543-558.

Cheng, C., S. Peng, Z. Li, L. Zou, W. Liu and C. Liu. 2017. Improved bioavailability of curcumin in liposomes prepared using a pH-driven, organic solvent-free, easily scalable process. RSC Advances. 7: 25978-25986.

Cheng, Y.-Q., G.-L. Tang and B. Shen. 2003. Type I polyketide synthase requiring a discrete acyltransferase for polyketide biosynthesis. Proceedings of the National Academy of Sciences. 100: 3149-3154.

Cheng, Y. Q., J. M. Coughlin, S. K. Lim and B. Shen. 2009. Chapter 8 Type I Polyketide Synthases That Require Discrete Acyltransferases. Methods in Enzymology. Academic Press. 459**:** 165-186.

Cho, J. S., G. B. Kim, H. Eun, C. W. Moon and S. Y. Lee. 2022. Designing Microbial Cell Factories for the Production of Chemicals. JACS Au. 2: 1781-1799.

Choi, K. R., W. D. Jang, D. Yang, J. S. Cho, D. Park and S. Y. Lee. 2019. Systems Metabolic Engineering Strategies: Integrating Systems and Synthetic Biology with Metabolic Engineering. Trends Biotechnol. 37: 817-837.

Choi, S.-S., Y.-A. Hur, D. H. Sherman and E.-S. Kim. 2007. Isolation of the biosynthetic gene cluster for tautomycetin, a linear polyketide T cell-specific immunomodulator from *Streptomyces sp*. CK4412. Microbiology (Reading). 153: 1095-1102.

Choi, W.-W., S.-D. Park, S.-M. Lee, H.-B. Kim, Y. Kim and H.-S. Lee. 2009. The *whcA* gene plays a negative role in oxidative stress response of *Corynebacterium glutamicum*. FEMS Microbiology Letters. 290: 32-38.

Choi, Y., E. Jung, S. Kim and S. Jung. 2003. Membrane fluidity sensoring microbial fuel cell. Bioelectrochemistry. 59: 121-127.

Chopra, I., P. M. Hawkey and M. Hinton. 1992. Tetracyclines, molecular and clinical aspects. Journal of Antimicrobial Chemotherapy. 29: 245-277.

Chopra, I. and M. Roberts. 2001. Tetracycline antibiotics: mode of action, applications, molecular biology, and epidemiology of bacterial resistance. Microbiology and molecular biology reviews. 65: 232-260.

Chouhan, S., K. Sharma, J. Zha, S. Guleria and M. A. G. Koffas. 2017. Recent Advances in the Recombinant Biosynthesis of Polyphenols. Frontiers in Microbiology. 8:

Christmann, J., P. Cao, J. Becker, C. K. Desiderato, O. Goldbeck, C. U. Riedel, M. Kohlstedt and C. Wittmann. 2023. High-efficiency production of the antimicrobial peptide pediocin PA-1 in metabolically engineered *Corynebacterium glutamicum* using a microaerobic process at acidic pH and elevated levels of bivalent calcium ions. Microbial Cell Factories. 22: 1-18.

Chu, L. L., R. P. Pandey, D. Dhakal and J. K. Sohng. 2020. Increased production of dicinnamoylmethane via improving cellular malonyl-CoA level by using a CRISPRi in *Escherichia coli*. Applied biochemistry and biotechnology. 190: 325-340.

Ciccarone, F., R. Vegliante, L. Di Leo and M. R. Ciriolo. 2017. The TCA cycle as a bridge between oncometabolism and DNA transactions in cancer. Seminars in Cancer Biology. 47: 50-56.

Coetzee, G., J. J. Smith and J. F. Görgens. 2022. Influence of codon optimization, promoter, and strain selection on the heterologous production of a β-fructofuranosidase from *Aspergillus fijiensis* ATCC 20611 in *Pichia pastoris*. Folia Microbiologica. 67: 339-350.

Contreras, G., S. Barahona, D. Sepúlveda, M. Baeza, V. Cifuentes and J. Alcaíno. 2015. Identification and analysis of metabolite production with biotechnological potential in *Xanthophyllomyces dendrorhous* isolates. World Journal of Microbiology and Biotechnology. 31: 517-526.

Court, D. L., J. A. Sawitzke and L. C. Thomason. 2002. Genetic engineering using homologous recombination. Annual review of genetics. 36: 361-388.

Couto, M. R., J. L. Rodrigues and L. R. Rodrigues. 2017. Optimization of fermentation conditions for the production of curcumin by engineered *Escherichia coli*. Journal of the Royal Society Interface. 14: 20170470.

Cragg, G. M. and D. J. Newman. 2001. Natural Product Drug Discovery in the Next Millennium. Pharmaceutical Biology. 39: 8-17.

Craney, A., S. Ahmed and J. Nodwell. 2013. Towards a new science of secondary metabolism. J Antibiot (Tokyo). 66: 387-400.

Cropp, A., S. Chen, H. Liu, W. Zhang and K. A. Reynolds. 2001. Genetic approaches for controlling ratios of related polyketide products in fermentation processes. Journal of Industrial Microbiology and Biotechnology. 27: 368-377.

Dai, C., J. Lin, H. Li, Z. Shen, Y. Wang, T. Velkov and J. Shen. 2022. The Natural Product Curcumin as an Antibacterial Agent: Current Achievements and Problems. Antioxidants (Basel). 11:

Dalle-Donne, I., R. Rossi, G. Colombo, D. Giustarini and A. Milzani. 2009. Protein S-glutathionylation: a regulatory device from bacteria to humans. Trends in biochemical sciences. 34: 85-96.

Daniel, J., T.-J. Oh, C.-M. Lee and E. Kolattukudy Pappachan. 2007. AccD6, a Member of the Fas II Locus, Is a Functional Carboxyltransferase Subunit of the Acyl-Coenzyme A Carboxylase in *Mycobacterium tuberculosis*. Journal of bacteriology. 189: 911-917.

Daube, F. W. 1870. Ueber Curcumin, den Farbstoff der Curcumawurzel. Berichte der deutschen chemischen Gesellschaft. 3: 609-613.

Davis, J. H. and J. R. Williamson. 2017. Structure and dynamics of bacterial ribosome biogenesis. Philosophical Transactions of the Royal Society B: Biological Sciences. 372: 20160181.

de Kok, A., A. F. Hengeveld, A. Martin and A. H. Westphal. 1998. The pyruvate dehydrogenase multi-enzyme complex from Gram-negative bacteria. Biochimica et Biophysica Acta (BBA)-Protein Structure and Molecular Enzymology. 1385: 353-366.

De, R., P. Kundu, S. Swarnakar, T. Ramamurthy, A. Chowdhury, G. B. Nair and A. K. Mukhopadhyay. 2009. Antimicrobial activity of curcumin against *Helicobacter pylori* isolates from India and during infections in mice. Antimicrobial agents and chemotherapy. 53: 1592-1597.

Dhakal, D., E.-S. Kim and M. Koffas. 2019. Editorial: Engineering the Microbial Platform for the Production of Biologics and Small-Molecule Medicines. Frontiers in Microbiology. 10:

Dharmaraj, S. 2010. Marine *Streptomyces* as a novel source of bioactive substances. World Journal of Microbiology and Biotechnology. 26: 2123-2139.

Dhillon, B. K., M. Smith, A. Baghela, A. H. Y. Lee and R. E. W. Hancock. 2020. Systems Biology Approaches to Understanding the Human Immune System. Frontiers in Immunology. 11:

Dias, D. A., S. Urban and U. Roessner. 2012. A historical overview of natural products in drug discovery. Metabolites. 2: 303-336.

Ding, Q. and C. Ye. 2023. Microbial cell factories based on filamentous bacteria, yeasts, and fungi. Microbial Cell Factories. 22: 20.

Dlugónska, H. 2015. The Nobel Prize 2015 in physiology or medicine for highly effective antiparasitic drugs. Annals of Parasitology. 61:

Dolan, S. K. and M. Welch. 2018. The glyoxylate shunt, 60 years on. Annual review of microbiology. 72: 309-330.

Donadio, S., M. J. Staver, J. B. McAlpine, S. J. Swanson and L. Katz. 1991. Modular Organization of Genes Required for Complex Polyketide Biosynthesis. Science. 252: 675-679.

Duarte, K., T. A. P. Rocha-Santos, A. C. Freitas and A. C. Duarte. 2012. Analytical techniques for discovery of bioactive compounds from marine fungi. TrAC Trends in Analytical Chemistry. 34: 97-110.

Duda, M., K. Cygan and A. Wisniewska-Becker. 2020. Effects of Curcumin on Lipid Membranes: an EPR Spin-label Study. Cell Biochemistry and Biophysics. 78: 139-147.

Dufossé, L., M. Fouillaud, Y. Caro, S. A. S. Mapari and N. Sutthiwong. 2014. Filamentous fungi are large-scale producers of pigments and colorants for the food industry. Curr Opin Biotechnol. 26: 56-61.

Ehlting, J., D. Büttner, Q. Wang, C. J. Douglas, I. E. Somssich and E. Kombrink. 1999. Three 4-coumarate: coenzyme A ligases in Arabidopsis thaliana represent two evolutionarily divergent classes in angiosperms. The plant journal. 19: 9-20.

Eikmanns, B. 2005. 11 Central Metabolism: Tricarboxylic Acid Cycle and Anaplerotic Reactions. *Corynebacterium glutamicum*. 241.

Eikmanns, B. J., N. Thum-Schmitz, L. Eggeling, K.-U. Lüdtke and H. Sahm. 1994. Nucleotide sequence, expression and transcriptional analysis of the *Corynebacterium glutamicum gltA* gene encoding citrate synthase. Microbiology (Reading). 140: 1817-1828.

El-Magboub, A., P. Rojsitthisak, C. Muangnoi, W. Wichitnithad, R. Romero and I. Haworth. 2014. Biological targets and pharmacology of curcumin. 103-133.

El-Naggar, N. E.-A. 2021. Chapter 11 - *Streptomyces*-based cell factories for production of biomolecules and bioactive metabolites. Microbial Cell Factories Engineering for Production of Biomolecules. V. Singh. Academic Press. 183-234.

Everse, J. 2013. Heme Proteins. Encyclopedia of Biological Chemistry (Second Edition). W. J. Lennarz and M. D. Lane. Waltham, Academic Press. 532-538.

Fadus, M. C., C. Lau, J. Bikhchandani and H. T. Lynch. 2017. Curcumin: An age-old anti-inflammatory and anti-neoplastic agent. Journal of Traditional and Complementary Medicine. 7: 339-346.

Fang, Z., J. A. Jones, J. Zhou and M. A. G. Koffas. 2018. Engineering *Escherichia coli* co-cultures for production of curcuminoids from glucose. Biotechnol J. 13: 1700576.

Farooqui, T. and A. A. Farooqui. 2019. Chapter 2 - Curcumin: Historical Background, Chemistry, Pharmacological Action, and Potential Therapeutic Value. Curcumin for Neurological and Psychiatric Disorders. T. Farooqui and A. A. Farooqui. Academic Press. 23-44.

Fasnacht, M. and N. Polacek. 2021. Oxidative Stress in Bacteria and the Central Dogma of Molecular Biology. Frontiers in Molecular Biosciences. 8:

Ferrer-Miralles, N. and A. Villaverde. 2013. Bacterial cell factories for recombinant protein production; expanding the catalogue. Microbial Cell Factories. 12: 113.

Finlay, A. C., G. L. Hobby, S. Y. P'an, P. P. Regna, J. B. Routien, D. B. Seeley, G. M. Shull, B. A. Sobin, I. A. Solomons and J. W. Vinson. 1950. Terramycin, a new antibiotic. Science. 111: 85-85.

Fischbach, M. A. and C. T. Walsh. 2006. Assembly-Line Enzymology for Polyketide and Nonribosomal Peptide Antibiotics: Logic, Machinery, and Mechanisms. Chemical Reviews. 106: 3468-3496.

Fleige, C., F. Meyer and A. Steinbüchel. 2016. Metabolic engineering of the actinomycete *Amycolatopsis sp*. strain ATCC 39116 towards enhanced production of natural vanillin. Applied and Environmental Microbiology. 82: 3410-3419.

Fowler, Z. L., W. W. Gikandi and M. A. G. Koffas. 2009. Increased malonyl coenzyme A biosynthesis by tuning the Escherichia coli metabolic network and its application to flavanone production. Applied and Environmental Microbiology. 75: 5831-5839.

Fränzel, B., C. Trötschel, C. Rückert, J. Kalinowski, A. Poetsch and D. A. Wolters. 2010. Adaptation of *Corynebacterium glutamicum* to salt-stress conditions. PROTEOMICS. 10: 445-457.

Fu, Y.-S., T.-H. Chen, L. Weng, L. Huang, D. Lai and C.-F. Weng. 2021. Pharmacological properties and underlying mechanisms of curcumin and prospects in medicinal potential. Biomedicine & Pharmacotherapy. 141: 111888.

Fumoleau, P., B. Coudert, N. Isambert and E. Ferrant. 2007. Novel tubulin-targeting agents: anticancer activity and pharmacologic profile of epothilones and related analogues. Annals of oncology. 18: v9-v15.

Gande, R., G. Dover Lynn, K. Krumbach, S. Besra Gurdyal, H. Sahm, T. Oikawa and L. Eggeling. 2007. The Two Carboxylases of *Corynebacterium glutamicum* Essential for Fatty Acid and Mycolic Acid Synthesis. Journal of bacteriology. 189: 5257-5264.

Garcea, G., D. J. Jones, R. Singh, A. R. Dennison, P. B. Farmer, R. A. Sharma, W. P. Steward, A. J. Gescher and D. P. Berry. 2004. Detection of curcumin and its metabolites in hepatic tissue and portal blood of patients following oral administration. Br J Cancer. 90: 1011-1015.

Gasovic, S. J., D. Dietrich, L. Gläser, P. Cao, M. Kohlstedt and C. Wittmann. 2023. Multi-omics view of recombinant *Yarrowia lipolytica*: Enhanced ketogenic amino acid catabolism increases polyketide-synthase-driven docosahexaenoic production to high selectivity at the gram scale. Metab Eng.

Geiman, D. E., T. R. Raghunand, N. Agarwal and W. R. Bishai. 2006. Differential gene expression in response to exposure to *antimycobacterial* agents and other stress conditions among seven *Mycobacterium tuberculosis whiB*-like genes. Antimicrobial agents and chemotherapy. 50: 2836-2841.

Gerstmeir, R., A. Cramer, P. Dangel, S. Schaffer and B. J. Eikmanns. 2004. RamB, a novel transcriptional regulator of genes involved in acetate metabolism of *Corynebacterium glutamicum*. Journal of bacteriology. 186: 2798-2809.

Ghosh, N., A. Das and C. K. Sen. 2019. Chapter 2 - Nutritional supplements and functional foods: functional significance and global regulations. Nutraceutical and Functional Food Regulations in the United States and around the World (Third Edition). D. Bagchi. Academic Press. 13-35.

Glansdorff, N. and Y. Xu. 2007. Microbial Arginine Biosynthesis: Pathway, Regulation and Industrial Production. Amino Acid Biosynthesis ~ Pathways, Regulation and Metabolic Engineering. V. F. Wendisch. Berlin, Heidelberg, Springer Berlin Heidelberg. 219-257.

Gläser, L., M. Kuhl, S. Jovanovic, M. Fritz, B. Vögeli, T. J. Erb, J. Becker and C. Wittmann. 2020. A common approach for absolute quantification of short chain CoA thioesters in prokaryotic and eukaryotic microbes. Microbial Cell Factories. 19: 160.

Goel, A., A. B. Kunnumakkara and B. B. Aggarwal. 2008. Curcumin as "Curecumin": from kitchen to clinic. Biochem Pharmacol. 75: 787-809.

Gokulan, K., S. Khare and C. Cerniglia. 2014. METABOLIC PATHWAYS | Production of Secondary Metabolites of Bacteria. Encyclopedia of Food Microbiology (Second Edition). C. A. Batt and M. L. Tortorello. Oxford, Academic Press. 561-569.

Görke, B. and J. Stülke. 2008. Carbon catabolite repression in bacteria: many ways to make the most out of nutrients. Nature Reviews Microbiology. 6: 613-624.

Goswami, S., A. S. Vidyarthi, B. Bhunia and T. Mandal. 2013. A review on lovastatin and its production. Journal of biochemical technology. 4: 581-587.

Graf, N. and J. Altenbuchner. 2014. Genetic engineering of *Pseudomonas putida* KT2440 for rapid and high-yield production of vanillin from ferulic acid. Appl Microbiol Biotechnol. 98: 137-149.

Groth, A. C. and M. P. Calos. 2004. Phage Integrases: Biology and Applications. Journal of Molecular Biology. 335: 667-678.

Guest, J. R. and P. E. Stephens. 1980. Molecular cloning of the pyruvate dehydrogenase complex genes of *Escherichia coli*. Journal of General Microbiology. 121: 277-292.

Guo, W., J. Sheng, H. Zhao and X. Feng. 2016. Metabolic engineering of *Saccharomyces cerevisiae* to produce 1-hexadecanol from xylose. Microbial Cell Factories. 15: 1-11.

Gust, B., G. L. Challis, K. Fowler, T. Kieser and K. F. Chater. 2003. PCR-targeted *Streptomyces* gene replacement identifies a protein domain needed for biosynthesis of the sesquiterpene soil odor geosmin. Proceedings of the National Academy of Sciences. 100: 1541-1546.

Gust, B., G. Chandra, D. Jakimowicz, T. Yuqing, C. J. Bruton and K. F. Chater. 2004. λ Red-Mediated Genetic Manipulation of Antibiotic-Producing *Streptomyces*. Advances in Applied Microbiology. Academic Press. 54**:** 107-128.

Ha, S., B. Shin and W. Park. 2018. Lack of glyoxylate shunt dysregulates iron homeostasis in *Pseudomonas aeruginosa*. Microbiology (Reading). 164: 587-599.

Hammer, A., A. Stolz and H. J. Knackmuss. 1996. Purification and characterization of a novel type of protocatechuate 3, 4-dioxygenase with the ability to oxidize 4-sulfocatechol. Archives of Microbiology. 166: 92-100.

Hande, K. R. 2008. Topoisomerase II inhibitors. Update on Cancer Therapeutics. 3: 13-26.

Hao, Y., Y. You, Z. Chen, J. Li, G. Liu and Y. Wen. 2022. Avermectin B1a production in *Streptomyces avermitilis* is enhanced by engineering aveC and precursor supply genes. Appl Microbiol Biotechnol. 106: 2191-2205.

Hardie, D. G. 1989. Regulation of fatty acid synthesis via phosphorylation of acetyl-CoA carboxylase. Progress in lipid research. 28: 117-146.

Hasan, H., M. H. Abd Rahim, L. Campbell, D. Carter, A. Abbas and A. Montoya. 2018. Overexpression of acetyl-CoA carboxylase in *Aspergillus terreus* to increase lovastatin production. New biotechnology. 44: 64-71.

Hatamipour, M., T. P. Johnston and A. Sahebkar. 2018. One molecule, many targets and numerous effects: the pleiotropy of curcumin lies in its chemical structure. Curr Pharm Des. 24: 2129-2136.

Haußmann, U., S. W. Qi, D. Wolters, M. Rögner, S. J. Liu and A. Poetsch. 2009. Physiological adaptation of *Corynebacterium glutamicum* to benzoate as alternative carbon source–a membrane proteome-centric view. PROTEOMICS. 9: 3635-3651.

Hazel, J. R. 1995. Thermal adaptation in biological membranes: is homeoviscous adaptation the explanation? Annual review of physiology. 57: 19-42.

Henke, N. A. and V. F. Wendisch. 2019. Improved Astaxanthin Production with *Corynebacterium glutamicum* by Application of a Membrane Fusion Protein. Marine Drugs. 17,

Henry, C. J. 2010. Functional foods. European Journal of Clinical Nutrition. 64: 657-659.

Hertweck, C., A. Luzhetskyy, Y. Rebets and A. Bechthold. 2007. Type II polyketide synthases: gaining a deeper insight into enzymatic teamwork. Nat Prod Rep. 24: 162-190.

Hewlings, S. J. and D. S. Kalman. 2017. Curcumin: A Review of Its Effects on Human Health. Foods. 6,

Hilker, R., K. B. Stadermann, O. Schwengers, E. Anisiforov, S. Jaenicke, B. Weisshaar, T. Zimmermann and A. Goesmann. 2016. ReadXplorer 2-detailed read mapping analysis and visualization from one single source. Bioinformatics. 32: 3702-3708.

Himaya, S. W. A. and S. K. Kim. 2013. Marine symbiotic microorganisms: a new dimension in natural product research. Marine Microbiology. 295-305.

Hm Leung, M., T. Harada and T. W Kee. 2013. Delivery of curcumin and medicinal effects of the copper (II)-curcumin complexes. Curr Pharm Des. 19: 2070-2083.

Holtmann, D., F. Vernen, J. M. Müller, D. Kaden, J. M. Risse, K. Friehs, L. Dähne, A. Stratmann and J. Schrader. 2017. Effects of particle addition to *Streptomyces* cultivations to optimize the production of actinorhodin and streptavidin. Sustainable Chemistry and Pharmacy. 5: 67-71.

Hopwood, D. A. and D. H. Sherman. 1990. Molecular genetics of polyketides and its comparison to fatty acid biosynthesis. Annual review of genetics. 24: 37-62.

Horinouchi, S. 2009. Combinatorial biosynthesis of plant medicinal polyketides by microorganisms. Current opinion in chemical biology. 13: 197-204.

Hu, R. W., E. J. Carey, K. D. Lindor and J. H. Tabibian. Curcumin in Hepatobiliary Disease: Pharmacotherapeutic Properties and Emerging Potential Clinical Applications. Annals of Hepatology.

Hua, D., C. Ma, L. Song, S. Lin, Z. Zhang, Z. Deng and P. Xu. 2007. Enhanced vanillin production from ferulic acid using adsorbent resin. Appl Microbiol Biotechnol. 74: 783-790.

Hurst, W. J. 2008. Methods of Analysis for Functional Foods and Nutraceuticals (2nd ed.). CRC Press.

Ikeda, H., T. Nonomiya and S. Ōmura. 2001. Organization of biosynthetic gene cluster for avermectin in *Streptomyces avermitilis*: analysis of enzymatic domains in four polyketide synthases. Journal of Industrial Microbiology and Biotechnology. 27: 170-176.

Ikeda, M. and S. Nakagawa. 2003. The *Corynebacterium glutamicum* genome: features and impacts on biotechnological processes. Appl Microbiol Biotechnol. 62: 99-109.

Injac, R., A. Mlinaric, V. Djorjevic-Milic, K. Karljikovic-Rajic and B. Strukelj. 2008. Optimal conditions for determination of zinc bacitracin, polymyxin B, oxytetracycline and

sulfacetamide in animal feed by micellar electrokinetic capillary chromatography. Food additives and contaminants. 25: 424-431.

Inui, M., S. Murakami, S. Okino, H. Kawaguchi, A. A. Vertès and H. Yukawa. 2004. Metabolic analysis of *Corynebacterium glutamicum* during lactate and succinate productions under oxygen deprivation conditions. Microbial Physiology. 7: 182-196.

Jäger, W., A. Schäfer, A. Pühler, G. Labes and W. Wohlleben. 1992. Expression of the *Bacillus subtilis sacB* gene leads to sucrose sensitivity in the gram-positive bacterium *Corynebacterium glutamicum* but not in *Streptomyces lividans*. Journal of bacteriology. 174: 5462-5465.

Jagetia, G. C. 2021. Antioxidant activity of curcumin protects against the radiation-induced micronuclei formation in cultured human peripheral blood lymphocytes exposed to various doses of γ-Radiation. International Journal of Radiation Biology. 97: 485-493.

Jaruga, E., A. Sokal, S. Chrul and G. Bartosz. 1998. Apoptosis-independent alterations in membrane dynamics induced by curcumin. Experimental cell research. 245: 303-312.

Jenner, L., A. L. Starosta, D. S. Terry, A. Mikolajka, L. Filonava, M. Yusupov, S. C. Blanchard, D. N. Wilson and G. Yusupova. 2013. Structural basis for potent inhibitory activity of the antibiotic tigecycline during protein synthesis. Proceedings of the National Academy of Sciences. 110: 3812-3816.

Jia, X. Q., Z. N. Xu, L. P. Zhou and C. K. Sung. 2010a. Elimination of the mycotoxin citrinin production in the industrial important strain *Monascus purpureus* SM001. Metab Eng. 12: 1-7.

Jia, Z., X. Zhang, Y. Zhao and X. Cao. 2010b. Enhancement of lovastatin production by supplementing polyketide antibiotics to the submerged culture of *Aspergillus terreus*. Applied biochemistry and biotechnology. 160: 2014-2025.

Jochmann, N., A.-K. Kurze, L. F. Czaja, K. Brinkrolf, I. Brune, A. T. Hüser, N. Hansmeier, A. Pühler, I. Borovok and A. Tauch. 2009. Genetic makeup of the *Corynebacterium glutamicum* LexA regulon deduced from comparative transcriptomics and in vitro DNA band shift assays. Microbiology (Reading). 155: 1459-1477.

Jones, K. L., S.-W. Kim and J. D. Keasling. 2000. Low-Copy Plasmids can Perform as Well as or Better Than High-Copy Plasmids for Metabolic Engineering of Bacteria. Metab Eng. 2: 328-338.

Joo-Young, L., N. Yoon-Ah, K. Eungsoo and L. Heung-Shick. 2016. The *Actinobacterium Corynebacterium glutamicum*, an Industrial Workhorse. J. Microbiol. Biotechnol. 26: 807-822.

Jorge, J. M. P., C. Leggewie and V. F. Wendisch. 2016. A new metabolic route for the production of gamma-aminobutyric acid by *Corynebacterium glutamicum* from glucose. Amino Acids. 48: 2519-2531.

Jovanovic, S. V., S. Steenken, C. W. Boone and M. G. Simic. 1999. H-Atom Transfer Is A Preferred Antioxidant Mechanism of Curcumin. Journal of the American Chemical Society. 121: 9677-9681.

Julien, B., S. Shah, R. Ziermann, R. Goldman, L. Katz and C. Khosla. 2000. Isolation and characterization of the epothilone biosynthetic gene cluster from *Sorangium cellulosum*. Gene. 249: 153-160.

Jung, W. S., Y. J. Yoo, J. W. Park, S. R. Park, A. R. Han, Y. H. Ban, E. J. Kim, E. Kim and Y. J. Yoon. 2011. A combined approach of classical mutagenesis and rational metabolic engineering improves rapamycin biosynthesis and provides insights into methylmalonyl-CoA precursor supply pathway in *Streptomyces hygroscopicus* ATCC 29253. Appl Microbiol Biotechnol. 91: 1389-1397.

Kaku, M., M. Ishidaira, S. Satoh, M. Ozaki, D. Kohari and S. Chohnan. 2022. Fatty acid production by enhanced malonyl-CoA supply in *Escherichia coli*. Current Microbiology. 79: 269.

Kalinowski, J., B. Bathe, D. Bartels, N. Bischoff, M. Bott, A. Burkovski, N. Dusch, L. Eggeling, B. J. Eikmanns and L. Gaigalat. 2003. The complete *Corynebacterium glutamicum* ATCC 13032 genome sequence and its impact on the production of L-aspartate-derived amino acids and vitamins. Journal of Biotechnology. 104: 5-25.

Kallscheuer, N., H. Kage, L. Milke, M. Nett and J. Marienhagen. 2019. Microbial synthesis of the type I polyketide 6-methylsalicylate with *Corynebacterium glutamicum*. Appl Microbiol Biotechnol. 103: 9619-9631.

Kallscheuer, N. and J. Marienhagen. 2018. *Corynebacterium glutamicum* as platform for the production of hydroxybenzoic acids. Microbial Cell Factories. 17: 70.

Kallscheuer, N., M. Vogt, M. Bott and J. Marienhagen. 2017. Functional expression of plant-derived O-methyltransferase, flavanone 3-hydroxylase, and flavonol synthase in *Corynebacterium glutamicum* for production of pterostilbene, kaempferol, and quercetin. Journal of Biotechnology. 258: 190-196.

Kallscheuer, N., M. Vogt, J. Kappelmann, K. Krumbach, S. Noack, M. Bott and J. Marienhagen. 2016a. Identification of the *phd* gene cluster responsible for phenylpropanoid utilization in *Corynebacterium glutamicum*. Appl Microbiol Biotechnol. 100: 1871-1881.

Kallscheuer, N., M. Vogt, A. Stenzel, J. Gätgens, M. Bott and J. Marienhagen. 2016b. Construction of a *Corynebacterium glutamicum* platform strain for the production of stilbenes and (2S)-flavanones. Metab Eng. 38: 47-55.

Kan, E., Y. Katsuyama, J.-i. Maruyama, K. Tamano, Y. Koyama and Y. Ohnishi. 2019. Production of the plant polyketide curcumin in *Aspergillus oryzae*: strengthening malonyl-CoA supply for yield improvement. Biosci Biotechnol Biochem. 83: 1372-1381.

Kang, S.-Y., K. T. Heo and Y.-S. Hong. 2018. Optimization of artificial curcumin biosynthesis in *E. coli* by randomized 5′-UTR sequences to control the multienzyme pathway. ACS Synthetic Biology. 7: 2054-2062.

Katashkina, J. I., Y. Hara, L. I. Golubeva, I. G. Andreeva, T. M. Kuvaeva and S. V. Mashko. 2009. Use of the λ Red-recombineering method for genetic engineering of *Pantoea ananatis*. BMC Molecular Biology. 10: 34.

Kates, M., E. L. Pugh and G. Ferrante. 1984. Regulation of membrane fluidity by lipid desaturases. Membrane fluidity. 379-395.

Katsuyama, Y., N. Funa, I. Miyahisa and S. Horinouchi. 2007. Synthesis of unnatural flavonoids and stilbenes by exploiting the plant biosynthetic pathway in *Escherichia coli*. Chem Biol. 14: 613-621.

Katsuyama, Y., T. Kita, N. Funa and S. Horinouchi. 2009a. Curcuminoid biosynthesis by two type III polyketide synthases in the herb *Curcuma longa*. J Biol Chem. 284: 11160-11170.

Katsuyama, Y., T. Kita and S. Horinouchi. 2009b. Identification and characterization of multiple curcumin synthases from the herb *Curcuma longa*. FEBS Lett. 583: 2799-2803.

Katsuyama, Y., M. Matsuzawa, N. Funa and S. Horinouchi. 2008. Production of curcuminoids by *Escherichia coli* carrying an artificial biosynthesis pathway. Microbiology (Reading). 154: 2620-2628.

Katsuyama, Y., K. Miyazono, M. Tanokura, Y. Ohnishi and S. Horinouchi. 2011. Structural and biochemical elucidation of mechanism for decarboxylative condensation of beta-keto acid by curcumin synthase. J Biol Chem. 286: 6659-6668.

Kaushik, V., M. Tiwari and V. Tiwari. 2022. Interaction of RecA mediated SOS response with bacterial persistence, biofilm formation, and host response. International Journal of Biological Macromolecules. 217: 931-943.

Kavšček, M., M. Stražar, T. Curk, K. Natter and U. Petrovič. 2015. Yeast as a cell factory: current state and perspectives. Microbial Cell Factories. 14: 94.

Keasling, J. D. 1999. Gene-expression tools for the metabolic engineering of bacteria. Trends Biotechnol. 17: 452-460.

Keilhauer, C., L. Eggeling and H. Sahm. 1993. Isoleucine synthesis in *Corynebacterium glutamicum*: molecular analysis of the ilvB-ilvN-ilvC operon. Journal of bacteriology. 175: 5595-5603.

Kharat, M., Z. Du, G. Zhang and D. J. McClements. 2017. Physical and Chemical Stability of Curcumin in Aqueous Solutions and Emulsions: Impact of pH, Temperature, and Molecular Environment. J Agric Food Chem. 65: 1525-1532.

Khosla, C. and J. D. Keasling. 2003. Metabolic engineering for drug discovery and development. Nature Reviews Drug Discovery. 2: 1019-1025.

Kiefer, P., E. Heinzle, O. Zelder and C. Wittmann. 2004. Comparative Metabolic Flux Analysis of Lysine-Producing Corynebacterium glutamicum Cultured on Glucose or Fructose. Applied and Environmental Microbiology. 70: 229-239.

Kieser, T., M. J. Bibb, M. J. Buttner, K. F. Chater and D. A. Hopwood. 2000. Practical streptomyces genetics. John Innes Foundation Norwich.

Kim, E. J., M. N. Cha, B.-G. Kim and J.-H. Ahn. 2017. Production of curcuminoids in engineered *Escherichia coli*. J. Microbiol. Biotechnol. 27: 975-982.

Kim, J. S., H. N. Lee, P. Kim, H. S. Lee and E. S. Kim. 2012. Negative role of wblA in response to oxidative stress in *Streptomyces coelicolor*. J. Microbiol. Biotechnol. 22: 736-741.

Kim, M., Y. J. Ko, D. W. Jeong, W.-Y. Jeong and S. O. Han. 2021. Ecofriendly Synthesis of l-Carnosine in Metabolically Engineered *Corynebacterium glutamicum* by Reinforcing Precursor Accumulation. ACS Synthetic Biology. 10: 1553-1562.

Kim, T.-H., J.-S. Park, H.-J. Kim, Y. Kim, P. Kim and H.-S. Lee. 2005. The *whcE* gene of *Corynebacterium glutamicum* is important for survival following heat and oxidative stress. Biochemical and biophysical research communications. 337: 757-764.

Kind, S., W. K. Jeong, H. Schröder and C. Wittmann. 2010. Systems-wide metabolic pathway engineering in *Corynebacterium glutamicum* for bio-based production of diaminopentane. Metab Eng. 12: 341-351.

King, R. E., J. A. Bomser and D. B. Min. 2006. Bioactivity of resveratrol. Comprehensive reviews in food science and food safety. 5: 65-70.

Kita, T., S. Imai, H. Sawada, H. Kumagai and H. Seto. 2008. The Biosynthetic Pathway of Curcuminoid in Turmeric (*Curcuma longa*) as Revealed by ^{13}C-Labeled Precursors. Biosci Biotechnol Biochem. 72: 1789-1798.

Kitade, Y., K. Hiraga and M. Inui. 2020. Aromatic Compound Catabolism in *Corynebacterium glutamicum*. Corynebacterium glutamicum: Biology and Biotechnology. M. Inui and K. Toyoda. Cham, Springer International Publishing. 323-337.

Kogure, T. and M. Inui. 2018. Recent advances in metabolic engineering of *Corynebacterium glutamicum* for bioproduction of value-added aromatic chemicals and natural products. Appl Microbiol Biotechnol. 102: 8685-8705.

Kohl, T. A. and A. Tauch. 2009. The GlxR regulon of the amino acid producer *Corynebacterium glutamicum*: Detection of the corynebacterial core regulon and integration into the transcriptional regulatory network model. Journal of Biotechnology. 143: 239-246.

Krejci, L., V. Altmannova, M. Spirek and X. Zhao. 2012. Homologous recombination and its regulation. Nucleic Acids Res. 40: 5795-5818.

Krivoruchko, A., Y. Zhang, V. Siewers, Y. Chen and J. Nielsen. 2015. Microbial acetyl-CoA metabolism and metabolic engineering. Metab Eng. 28: 28-42.

Ku, J. T., A. Y. Chen and E. I. Lan. 2020. Metabolic engineering design strategies for increasing acetyl-CoA flux. Metabolites. 10: 166.

Kuhl, M., L. Gläser, Y. Rebets, C. Rückert, N. Sarkar, T. Hartsch, J. Kalinowski, A. Luzhetskyy and C. Wittmann. 2020. Microparticles globally reprogram *Streptomyces albus* toward

accelerated morphogenesis, streamlined carbon core metabolism, and enhanced production of the antituberculosis polyketide pamamycin. Biotechnology and Bioengineering. 117: 3858-3875.

Kuhl, M., C. Rückert, L. Gläser, S. Beganovic, A. Luzhetskyy, J. Kalinowski and C. Wittmann. 2021. Microparticles enhance the formation of seven major classes of natural products in native and metabolically engineered actinobacteria through accelerated morphological development. Biotechnology and Bioengineering. 118: 3076-3093.

Kunnumakkara, A. B., B. Shabnam, S. Girisa, C. Harsha, K. Banik, T. B. Devi, R. Choudhury, H. Sahu, D. Parama, B. L. Sailo, K. K. Thakur, S. C. Gupta and B. B. Aggarwal. 2020. Inflammation, NF-kappaB, and Chronic Diseases: How are They Linked? Crit Rev Immunol. 40: 1-39.

Kwan, D. H. and F. Schulz. 2011. The Stereochemistry of Complex Polyketide Biosynthesis by Modular Polyketide Synthases. Molecules. 16, 6092-6115.

Laakel, M., A. Lebrihi, S. Khaoua, F. Schneider, G. Lefebvre and P. Germain. 1994. A link between primary and secondary metabolism: malonyl-CoA formation in *Streptomyces ambofaciens* growing on ammonium ions or valine. Microbiology (Reading). 140: 1451-1456.

Langmead, B. and S. L. Salzberg. 2012. Fast gapped-read alignment with Bowtie 2. Nat Methods. 9: 357-359.

Lanza, A. M., K. A. Curran, L. G. Rey and H. S. Alper. 2014. A condition-specific codon optimization approach for improved heterologous gene expression in *Saccharomyces cerevisiae*. BMC Systems Biology. 8: 33.

Lao, C. D., M. T. t. Ruffin, D. Normolle, D. D. Heath, S. I. Murray, J. M. Bailey, M. E. Boggs, J. Crowell, C. L. Rock and D. E. Brenner. 2006. Dose escalation of a curcuminoid formulation. BMC Complementary and Alternative Medicine. 6: 10.

Laraia, L. and H. Waldmann. 2017. Natural product inspired compound collections: evolutionary principle, chemical synthesis, phenotypic screening, and target identification. Drug Discovery Today: Technologies. 23: 75-82.

Lautie, E., O. Russo, P. Ducrot and J. A. Boutin. 2020. Unraveling Plant Natural Chemical Diversity for Drug Discovery Purposes. Frontiers in Pharmacology. 11: 397.

Lebeau, J., M. Venkatachalam, M. Fouillaud, T. Petit, F. Vinale, L. Dufossé and Y. Caro. 2017. Production and New Extraction Method of Polyketide Red Pigments Produced by *Ascomycetous* Fungi from Terrestrial and Marine Habitats. J Fungi (Basel). 3: 34.

Lee, D.-S., P. Kim, E.-S. Kim, Y. Kim and H.-S. Lee. 2018. *Corynebacterium glutamicum* WhcD interacts with WhiA to exert a regulatory effect on cell division genes. Antonie Van Leeuwenhoek. 111: 641-648.

Lee, I.-Y., T. G. Volm and J. P. N. Rosazza. 1998. Decarboxylation of ferulic acid to 4-vinylguaiacol by *Bacillus pumilus* in aqueous-organic solvent two-phase systems. Enzyme and Microbial Technology. 23: 261-266.

Lee, J.-Y., H.-J. Kim, E.-S. Kim, P. Kim, Y. Kim and H.-S. Lee. 2013a. Regulatory interaction of the *Corynebacterium glutamicum whc* genes in oxidative stress responses. Journal of Biotechnology. 168: 149-154.

Lee, J.-Y., H. J. Lee, J. Seo, E.-S. Kim, H.-S. Lee and P. Kim. 2014. Artificial oxidative stress-tolerant *Corynebacterium glutamicum*. AMB Express. 4: 15.

Lee, J.-Y., J. Seo, E.-S. Kim, H.-S. Lee and P. Kim. 2013b. Adaptive evolution of *Corynebacterium glutamicum* resistant to oxidative stress and its global gene expression profiling. Biotechnology Letters. 35: 709-717.

Lee, J. W., T. Y. Kim, Y.-S. Jang, S. Choi and S. Y. Lee. 2011. Systems metabolic engineering for chemicals and materials. Trends Biotechnol. 29: 370-378.

Lee, S. Y., H. U. Kim, T. U. Chae, J. S. Cho, J. W. Kim, J. H. Shin, D. I. Kim, Y.-S. Ko, W. D. Jang and Y.-S. Jang. 2019. A comprehensive metabolic map for production of bio-based chemicals. Nature Catalysis. 2: 18-33.

Lee, W. and D. G. Lee. 2014. Lycopene-induced hydroxyl radical causes oxidative DNA damage in Escherichia coli. J. Microbiol. Biotechnol. 24: 1232-1237.

Lee, W. H., C. Y. Loo, M. Bebawy, F. Luk, R. S. Mason and R. Rohanizadeh. 2013c. Curcumin and its derivatives: their application in neuropharmacology and neuroscience in the 21st century. Curr Neuropharmacol. 11: 338-378.

Li, L., L. Long and S. Ding. 2019. Bioproduction of high-concentration 4-vinylguaiacol using whole-cell catalysis harboring an organic solvent-tolerant phenolic acid decarboxylase from *Bacillus atrophaeus*. Frontiers in Microbiology. 10: 1798.

Li, S., Z. Li, S. Pang, W. Xiang and W. Wang. 2021a. Coordinating precursor supply for pharmaceutical polyketide production in *Streptomyces*. Curr Opin Biotechnol. 69: 26-34.

Li, S., B. Yang, G.-Y. Tan, L.-M. Ouyang, S. Qiu, W. Wang, W. Xiang and L. Zhang. 2021b. Polyketide pesticides from *Actinomycetes*. Curr Opin Biotechnol. 69: 299-307.

Li, X., X. Hu, Y. Sheng, H. Wang, M. Tao, Y. Ou, Z. Deng, L. Bai and Q. Kang. 2021c. Adaptive Optimization Boosted the Production of Moenomycin A in the Microbial Chassis *Streptomyces albus J*1074. ACS Synthetic Biology. 10: 2210-2221.

Li, Y., J. I. Kim, L. Pysh and C. Chapple. 2015. Four isoforms of *Arabidopsis* 4-coumarate: CoA ligase have overlapping yet distinct roles in phenylpropanoid metabolism. Plant physiology. 169: 2409-2421.

Liao, Y., G. K. Smyth and W. Shi. 2014. FeatureCounts: an efficient general purpose program for assigning sequence reads to genomic features. Bioinformatics. 30: 923-930.

Ligon, J., S. Hill, J. Beck, R. Zirkle, I. Molnár, J. Zawodny, S. Money and T. Schupp. 2002. Characterization of the biosynthetic gene cluster for the antifungal polyketide soraphen A from *Sorangium cellulosum* So ce26. Gene. 285: 257-267.

Lin, K., S. Han and S. Zheng. 2022. Application of *Corynebacterium glutamicum* engineering display system in three generations of biorefinery. Microbial Cell Factories. 21: 14.

Lindahl, T., B. Sedgwick, M. Sekiguchi and Y. Nakabeppu. 1988. Regulation and expression of the adaptive response to alkylating agents. Annual review of biochemistry. 57: 133-157.

Little, R. F. and C. Hertweck. 2022. Chain release mechanisms in polyketide and non-ribosomal peptide biosynthesis. Nat Prod Rep. 39: 163-205.

Liu, H. and K. A. Reynolds. 2001. Precursor supply for polyketide biosynthesis: the role of crotonyl-CoA reductase. Metab Eng. 3: 40-48.

Liu, J., W. Zhang, G. Du, J. Chen and J. Zhou. 2013. Overproduction of geraniol by enhanced precursor supply in *Saccharomyces cerevisiae*. Journal of Biotechnology. 168: 446-451.

Liu, X.-X., Y. Li and Z.-H. Bai. 2021. Chapter 12 - *Corynebacterium glutamicum* as a robust microbial factory for production of value-added proteins and small molecules: fundamentals and applications. Microbial Cell Factories Engineering for Production of Biomolecules. V. Singh. Academic Press. 235-263.

Liu, X., W. Ding and H. Jiang. 2017. Engineering microbial cell factories for the production of plant natural products: from design principles to industrial-scale production. Microbial Cell Factories. 16: 125.

Liu, Y. and G. Larrouy-Maumus. 2022. Chapter 4 - Lipids and glycolipids as biomarkers of mycobacterial infections. Biology of Mycobacterial Lipids. Z. Fatima and S. Canaan. Academic Press. 83-104.

Liu, Y., M. Ma and Y. Yuan. 2023. The potential of curcumin-based co-delivery systems for applications in the food industry: food preservation, freshness monitoring, and functional food. Food Research International. 113070.

Liu, Y. and J. Nielsen. 2019. Recent trends in metabolic engineering of microbial chemical factories. Curr Opin Biotechnol. 60: 188-197.

Liu, Z., J. D. Smart and A. S. Pannala. 2020. Recent developments in formulation design for improving oral bioavailability of curcumin: A review. Journal of Drug Delivery Science and Technology. 60: 102082.

Lobanova, J. S., N. V. Gorshkova, A. A. Krylov, N. V. Stoynova and S. V. Mashko. 2022. Genome engineering of the *Corynebacterium glutamicum* chromosome by the Extended Dual-In/Out strategy. Journal of Microbiological Methods. 200: 106555.

Loffeld, B. and H. Keweloh. 1996. cis/trans isomerization of unsaturated fatty acids as possible control mechanism of membrane fluidity in Pseudomonas putida P8. Lipids. 31: 811-815.

Lopatniuk, M., M. Myronovskyi and A. Luzhetskyy. 2017. *Streptomyces albus*: a new cell factory for non-canonical amino acids incorporation into ribosomally synthesized natural products. ACS chemical biology. 12: 2362-2370.

Love, M. I., W. Huber and S. Anders. 2014. Moderated estimation of fold change and dispersion for RNA-seq data with DESeq2. Genome Biol. 15: 550.

Lukežič, T., Š. Pikl, N. Zaburannyi, M. Remškar, H. Petković and R. Müller. 2020. Heterologous expression of the atypical tetracycline chelocardin reveals the full set of genes required for its biosynthesis. Microbial Cell Factories. 19: 1-13.

Luo, J., T. Lehtinen, E. Efimova, V. Santala and S. Santala. 2019. Synthetic metabolic pathway for the production of 1-alkenes from lignin-derived molecules. Microbial Cell Factories. 18: 48.

Ma, Y., Y. Cui, L. Du, X. Liu, X. Xie and N. Chen. 2018. Identification and application of a growth-regulated promoter for improving l-valine production in *Corynebacterium glutamicum*. Microbial Cell Factories. 17: 185.

Manteca, Á. and P. Yagüe. 2018. Streptomyces Differentiation in Liquid Cultures as a Trigger of Secondary Metabolism. Antibiotics. 7,

Mapari, S. A., U. Thrane and A. S. Meyer. 2010. Fungal polyketide azaphilone pigments as future natural food colorants? Trends Biotechnol. 28: 300-307.

Mapari, S. A. S., A. S. Meyer, U. Thrane and J. C. Frisvad. 2009. Identification of potentially safe promising fungal cell factories for the production of polyketide natural food colorants using chemotaxonomic rationale. Microbial Cell Factories. 8: 24.

Marsden, A. F. A., P. Caffrey, J. F. Aparicio, M. S. Loughran, J. Staunton and P. F. Leadlay. 1994. Stereospecific acyl transfers on the erythromycin-producing polyketide synthase. Science. 263: 378-380.

Martín, J. F., C. Barreiro, E. González-Lavado and M. Barriuso. 2003. Ribosomal RNA and ribosomal proteins in corynebacteria. Journal of Biotechnology. 104: 41-53.

Martín, J. F. and P. Liras. 2021. Molecular mechanisms of phosphate sensing, transport and signalling in streptomyces and related *Actinobacteria*. Int J Mol Sci. 22: 1129.

Martín, J. F., A. Rodríguez-García and P. Liras. 2017. The master regulator PhoP coordinates phosphate and nitrogen metabolism, respiration, cell differentiation and antibiotic biosynthesis: comparison in *Streptomyces coelicolor* and *Streptomyces avermitilis*. J Antibiot (Tokyo). 70: 534-541.

Martínez-Guerra, J., M. Palomar-Pardavé, M. Romero-Romo, S. Corona-Avendaño, A. Rojas-Hernández and M. T. Ramírez-Silva. 2019. New insights on the chemical stability of curcumin in aqueous media at different pH: Influence of the experimental conditions. International Journal of Electrochemical Science. 14: 5373-5385.

Max, B., J. Carballo, S. Cortés and J. M. Domínguez. 2012. Decarboxylation of ferulic acid to 4-vinyl guaiacol by *Streptomyces setonii*. Applied biochemistry and biotechnology. 166: 289-299.

McDowall, K. J., A. Thamchaipenet and I. S. Hunter. 1999. Phosphate control of oxytetracycline production by *Streptomyces rimosus* is at the level of transcription from promoters overlapped by tandem repeats similar to those of the DNA-binding sites of the OmpR family. Journal of bacteriology. 181: 3025-3032.

Menzella, H. G. 2011. Comparison of two codon optimization strategies to enhance recombinant protein production in *Escherichia coli*. Microbial Cell Factories. 10: 15.

Michel, A., A. Koch-Koerfges, K. Krumbach, M. Brocker and M. Bott. 2015. Anaerobic Growth of *Corynebacterium glutamicum* via Mixed-Acid Fermentation. Applied and Environmental Microbiology. 81: 7496-7508.

Miethke, M., M. Pieroni, T. Weber, M. Brönstrup, P. Hammann, L. Halby, P. B. Arimondo, P. Glaser, B. Aigle, H. B. Bode, R. Moreira, Y. Li, A. Luzhetskyy, M. H. Medema, J.-L. Pernodet, M. Stadler, J. R. Tormo, O. Genilloud, A. W. Truman, K. J. Weissman, E. Takano, S. Sabatini, E. Stegmann, H. Brötz-Oesterhelt, W. Wohlleben, M. Seemann, M. Empting, A. K. H. Hirsch, B. Loretz, C.-M. Lehr, A. Titz, J. Herrmann, T. Jaeger, S. Alt, T. Hesterkamp, M. Winterhalter, A. Schiefer, K. Pfarr, A. Hoerauf, H. Graz, M. Graz, M. Lindvall, S. Ramurthy, A. Karlén, M. van Dongen, H. Petkovic, A. Keller, F. Peyrane, S. Donadio, L. Fraisse, L. J. V. Piddock, I. H. Gilbert, H. E. Moser and R. Müller. 2021. Towards the sustainable discovery and development of new antibiotics. Nature Reviews Chemistry. 5: 726-749.

Mignon, C., R. Sodoyer and B. Werle. 2015. Antibiotic-Free Selection in Biotherapeutics: Now and Forever. Pathogens. 4, 157-181.

Milke, L., P. Ferreira, N. Kallscheuer, A. Braga, M. Vogt, J. Kappelmann, J. Oliveira, A. R. Silva, I. Rocha and M. Bott. 2019. Modulation of the central carbon metabolism of *Corynebacterium glutamicum* improves malonyl-CoA availability and increases plant polyphenol synthesis. Biotechnology and Bioengineering. 116: 1380-1391.

Milke, L. and J. Marienhagen. 2020. Engineering intracellular malonyl-CoA availability in microbial hosts and its impact on polyketide and fatty acid synthesis. Appl Microbiol Biotechnol. 104: 6057-6065.

Miłobędzka, J., S. v. Kostanecki and V. Lampe. 1910. Zur kenntnis des curcumins. Berichte der deutschen chemischen Gesellschaft. 43: 2163-2170.

Minassi, A., G. Sanchez-Duffhues, J. A. Collado, E. Munoz and G. Appendino. 2013. Dissecting the pharmacophore of curcumin. Which structural element is critical for which action? Journal of natural products. 76: 1105-1112.

Miyanaga, A. 2017. Structure and function of polyketide biosynthetic enzymes: various strategies for production of structurally diverse polyketides. Biosci Biotechnol Biochem. 81: 2227-2236.

Mohamed, S. H. and Z. Chaudrhy. 2005. Isolation of salt tolerance gene (s) from some halotolerant *Streptomyces* species using polymerase chain reaction. Pakistan Journal of Biotechnology. 2: 56-66.

Mondal, S., S. Ghosh and S. P. Moulik. 2016. Stability of curcumin in different solvent and solution media: UV–visible and steady-state fluorescence spectral study. Journal of Photochemistry and Photobiology B: Biology. 158: 212-218.

Monfil, V. O. and S. Casas-Flores. 2014. Chapter 32 - Molecular Mechanisms of Biocontrol in *Trichoderma* spp. and Their Applications in Agriculture. Biotechnology and Biology of Trichoderma. V. K. Gupta, M. Schmoll, A. Herrera-Estrellaet al. Amsterdam, Elsevier. 429-453.

Monschau, N., H. Sahm and K. P. Stahmann. 1998. Threonine aldolase overexpression plus threonine supplementation enhanced riboflavin production in *Ashbya gossypii*. Applied and Environmental Microbiology. 64: 4283-4290.

Morita, H., K. Wanibuchi, H. Nii, R. Kato, S. Sugio and I. Abe. 2010. Structural basis for the one-pot formation of the diarylheptanoid scaffold by curcuminoid synthase from *Oryza sativa*. Proceedings of the National Academy of Sciences. 107: 19778-19783.

Mortensen, A. 2006. Carotenoids and other pigments as natural colorants. Pure and Applied chemistry. 78: 1477-1491.

Mortezaee, K., E. Salehi, H. Mirtavoos-mahyari, E. Motevaseli, M. Najafi, B. Farhood, R. J. Rosengren and A. Sahebkar. 2019. Mechanisms of apoptosis modulation by curcumin: Implications for cancer therapy. Journal of Cellular Physiology. 234: 12537-12550.

Mosberg, J. A., M. J. Lajoie and G. M. Church. 2010. Lambda Red Recombineering in *Escherichia coli* Occurs Through a Fully Single-Stranded Intermediate. Genetics. 186: 791-799.

Mostofian, B., T. Zhuang, X. Cheng and J. D. Nickels. 2019. Branched-Chain Fatty Acid Content Modulates Structure, Fluidity, and Phase in Model Microbial Cell Membranes. The Journal of Physical Chemistry B. 123: 5814-5821.

Mu, D.-S., Y. Ouyang, G.-J. Chen and Z.-J. Du. 2021. Strategies for culturing active/dormant marine microbes. Marine Life Science & Technology. 3: 121-131.

Mulder, K. C. L., F. Mulinari, O. L. Franco, M. S. F. Soares, B. S. Magalhães and N. S. Parachin. 2015. Lovastatin production: From molecular basis to industrial process optimization. Biotechnol Adv. 33: 648-665.

Murphy Kenan, C. 2016. λ Recombination and Recombineering. EcoSal Plus. 7:

Nakashima, N., Y. Mitani and T. Tamura. 2005. *Actinomycetes* as host cells for production of recombinant proteins. Microbial Cell Factories. 4: 7.

Nakunst, D., C. Larisch, T. Hüser Andrea, A. Tauch, A. Pühler and J. Kalinowski. 2007. The Extracytoplasmic Function-Type Sigma Factor SigM of *Corynebacterium glutamicum* ATCC 13032 Is Involved in Transcription of Disulfide Stress-Related Genes. Journal of bacteriology. 189: 4696-4707.

Nelson, M. L. and S. B. Levy. 2011. The history of the tetracyclines. Ann N Y Acad Sci. 1241: 17-32.

Neshat, A., A. Mentz, C. Rückert and J. Kalinowski. 2014. Transcriptome sequencing revealed the transcriptional organization at ribosome-mediated attenuation sites in *Corynebacterium glutamicum* and identified a novel attenuator involved in aromatic amino acid biosynthesis. Journal of Biotechnology. 190: 55-63.

Nešvera, J. and M. Pátek. 2011. Tools for genetic manipulations in *Corynebacterium glutamicum* and their applications. Appl Microbiol Biotechnol. 90: 1641-1654.

Nett, M., H. Ikeda and B. S. Moore. 2009. Genomic basis for natural product biosynthetic diversity in the actinomycetes. Nat Prod Rep. 26: 1362-1384.

Nguyen, F., A. L. Starosta, S. Arenz, D. Sohmen, A. Dönhöfer and D. N. Wilson. 2014. Tetracycline antibiotics and resistance mechanisms. Biological chemistry. 395: 559-575.

Nickel, J., K. Irzik, J. Van Ooyen and L. Eggeling. 2010. The TetR-type transcriptional regulator FasR of *Corynebacterium glutamicum* controls genes of lipid synthesis during growth on acetate. Molecular Microbiology. 78: 253-265.

Nickels, J. D., S. Chatterjee, B. Mostofian, C. B. Stanley, M. Ohl, P. Zolnierczuk, R. Schulz, D. A. A. Myles, R. F. Standaert, J. G. Elkins, X. Cheng and J. Katsaras. 2017. *Bacillus subtilis* Lipid Extract, A Branched-Chain Fatty Acid Model Membrane. The Journal of Physical Chemistry Letters. 8: 4214-4217.

Nielsen, J. and M. C. Jewett. 2008. Impact of systems biology on metabolic engineering of *Saccharomyces cerevisiae*. FEMS Yeast Research. 8: 122-131.

Nielsen, J. and Jay D. Keasling. 2016. Engineering Cellular Metabolism. Cell. 164: 1185-1197.

Nielsen, J., C. B. Tillegreen and D. Petranovic. 2022. Innovation trends in industrial biotechnology. Trends Biotechnol.

Njenga, R., J. Boele, Y. Öztürk and H.-G. Koch. 2023. Coping with stress: How bacteria fine-tune protein synthesis and protein transport. Journal of Biological Chemistry. 299: 105163.

O'Brien, E. J., J. M. Monk and B. O. Palsson. 2015. Using genome-scale models to predict biological capabilities. Cell. 161: 971-987.

Palmer, C. M. and H. S. Alper. 2019. Expanding the Chemical Palette of Industrial Microbes: Metabolic Engineering for Type III PKS-Derived Polyketides. Biotechnol J. 14: 1700463.

Palmer, C. M., K. K. Miller, A. Nguyen and H. S. Alper. 2020. Engineering 4-coumaroyl-CoA derived polyketide production in *Yarrowia lipolytica* through a β-oxidation mediated strategy. Metab Eng. 57: 174-181.

Panzarini, E., S. Mariano, S. Tacconi, E. Carata, A. M. Tata and L. Dini. 2021. Novel Therapeutic Delivery of Nanocurcumin in Central Nervous System Related Disorders. Nanomaterials. 11,

Papich, M. G. 2016. Oxytetracycline. Saunders Handbook of Veterinary Drugs (Fourth Edition). M. G. Papich. St. Louis, W.B. Saunders. 595-598.

Park, J.-S., J.-Y. Lee, H.-J. Kim, E.-S. Kim, P. Kim, Y. Kim and H.-S. Lee. 2012. The role of *Corynebacterium glutamicum* spiA gene in whcA-mediated oxidative stress gene regulation. FEMS Microbiology Letters. 331: 63-69.

Pátek, M. 2007. Branched-Chain Amino Acids. Amino Acid Biosynthesis ~ Pathways, Regulation and Metabolic Engineering. V. F. Wendisch. Berlin, Heidelberg, Springer Berlin Heidelberg. 129-162.

Patiño-Morales, C. C., E. Soto-Reyes, E. Arechaga-Ocampo, E. Ortiz-Sánchez, V. Antonio-Véjar, J. Pedraza-Chaverri and A. García-Carrancá. 2020. Curcumin stabilizes p53 by interaction with NAD(P)H:quinone oxidoreductase 1 in tumor-derived cell lines. Redox Biology. 28: 101320.

Pelosato, R., I. Bolognino, F. Fontana and I. N. Sora. 2022. Applications of Heterogeneous Photocatalysis to the Degradation of Oxytetracycline in Water: A Review. Molecules. 27,

Peng, Y., M. Ao, B. Dong, Y. Jiang, L. Yu, Z. Chen, C. Hu and R. Xu. 2021. Anti-Inflammatory Effects of Curcumin in the Inflammatory Diseases: Status, Limitations and Countermeasures. Drug Design, Development and Therapy. 15: 4503-4525.

Pethick, F. E., A. C. MacFadyen, Z. Tang, V. Sangal, T.-T. Liu, J. Chu, G. Kosec, H. Petkovic, M. Guo and R. Kirby. 2013. Draft genome sequence of the oxytetracycline-producing bacterium *Streptomyces rimosus* ATCC 10970. Genome announcements. 1: e00063-00013.

Petkovic, H., J. Cullum, D. Hranueli, I. S. Hunter, N. a. Perić-Concha, J. Pigac, A. Thamchaipenet, D. Vujaklija and P. F. Long. 2006. Genetics of *Streptomyces rimosus*, the oxytetracycline producer. Microbiology and molecular biology reviews. 70: 704-728.

Petković, H., T. Lukežič and J. Šušković. 2017. Biosynthesis of oxytetracycline by *Streptomyces rimosus*: past, present and future directions in the development of tetracycline antibiotics. Food technology and biotechnology. 55: 3-13.

Petkovic, H., A. Thamchaipenet, L.-H. Zhou, D. Hranueli, P. Raspor, P. G. Waterman and I. S. Hunter. 1999. Disruption of an aromatase/cyclase from the oxytetracycline gene cluster of *Streptomyces rimosus* results in production of novel polyketides with shorter chain lengths. Journal of Biological Chemistry. 274: 32829-32834.

Pfeifer, B. A. and C. Khosla. 2001. Biosynthesis of polyketides in heterologous hosts. Microbiology and molecular biology reviews. 65: 106-118.

Pickens, L. B. and Y. Tang. 2010. Oxytetracycline biosynthesis. Journal of Biological Chemistry. 285: 27509-27515.

Pittard, J. and J. Yang. 2008. Biosynthesis of the Aromatic Amino Acids. EcoSal Plus. 3: 10.1128/ecosalplus.1123.1126.1121.1128.

Pogue, J. M., M. N. Dudley, A. Eranki and K. S. Kaye. 2017. 146 - Tetracyclines and Chloramphenicol. Infectious Diseases (Fourth Edition). J. Cohen, W. G. Powderly and S. M. Opal. Elsevier. 1256-1260.e1251.

Porteus, M. 2007. Using Homologous Recombination to Manipulate the Genome of Human Somatic Cells. Biotechnology and Genetic Engineering Reviews. 24: 195-212.

Poteete, A. R. 2001. What makes the bacteriophage λ Red system useful for genetic engineering: molecular mechanism and biological function. FEMS Microbiology Letters. 201: 9-14.

Poteete, A. R. 2013. Involvement of *Escherichia coli* DNA Replication Proteins in Phage Lambda Red-Mediated Homologous Recombination. PLoS One. 8: e67440.

Prapagdee, B., C. Kuekulvong and S. Mongkolsuk. 2008. Antifungal potential of extracellular metabolites produced by *Streptomyces hygroscopicus* against phytopathogenic fungi. International journal of biological sciences. 4: 330.

Priyadarsini, K. I. 2013. Chemical and structural features influencing the biological activity of curcumin. Curr Pharm Des. 19: 2093-2100.

Qian, Z. G., X. X. Xia and S. Y. Lee. 2009. Metabolic engineering of *Escherichia coli* for the production of putrescine: a four carbon diamine. Biotechnology and Bioengineering. 104: 651-662.

Qin, S., W.-J. Li, S. G. Dastager and W. N. Hozzein. 2016. *Actinobacteria* in special and extreme habitats: Diversity, function roles, and environmental adaptations. Frontiers Media SA. 7**:** 1415.

Quezada, M., G. Buitrón, I. Moreno-Andrade, G. Moreno and L. M. López-Marín. 2007. The use of fatty acid methyl esters as biomarkers to determine aerobic, facultatively aerobic and anaerobic communities in wastewater treatment systems. FEMS Microbiology Letters. 266: 75-82.

Radmacher, E., L. J. Alderwick, G. S. Besra, A. K. Brown, K. J. C. Gibson, H. Sahm and L. Eggeling. 2005. Two functional FAS-I type fatty acid synthases in *Corynebacterium glutamicum*. Microbiology (Reading). 151: 2421-2427.

Radmacher, E. and L. Eggeling. 2007. The three tricarboxylate synthase activities of *Corynebacterium glutamicum* and increase of l-lysine synthesis. Appl Microbiol Biotechnol. 76: 587-595.

Rainha, J., J. L. Rodrigues, C. Faria and L. R. Rodrigues. 2022a. Curcumin biosynthesis from ferulic acid by engineered *Saccharomyces cerevisiae*. Biotechnol J. 17: e2100400.

Rainha, J., L. R. Rodrigues and J. L. Rodrigues. 2022b. Microbial Production of Curcumin. Microbial Production of Food Bioactive Compounds. Springer. 1-35.

Rajaraman, E., A. Agarwal, J. Crigler, R. Seipelt-Thiemann, E. Altman and M. A. Eiteman. 2016. Transcriptional analysis and adaptive evolution of *Escherichia coli* strains growing on acetate. Appl Microbiol Biotechnol. 100: 7777-7785.

Ramirez-Ahumada, M. d. C., B. N. Timmermann and D. R. Gang. 2006. Biosynthesis of curcuminoids and gingerols in turmeric (*Curcuma longa*) and ginger (*Zingiber officinale*): Identification of curcuminoid synthase and hydroxycinnamoyl-CoA thioesterases. Phytochemistry. 67: 2017-2029.

Ramírez-Rendon, D., A. K. Passari, B. Ruiz-Villafán, R. Rodríguez-Sanoja, S. Sánchez and A. L. Demain. 2022. Impact of novel microbial secondary metabolites on the pharma industry. Appl Microbiol Biotechnol. 106: 1855-1878.

Rangel, A. E. T., J. M. Gómez Ramírez and A. F. González Barrios. 2020. From industrial by-products to value-added compounds: the design of efficient microbial cell factories by coupling systems metabolic engineering and bioprocesses. Biofuels, Bioproducts and Biorefining. 14: 1228-1238.

Rateb, M. E., W. E. Houssen, M. Arnold, M. H. Abdelrahman, H. Deng, W. T. A. Harrison, C. K. Okoro, J. A. Asenjo, B. A. Andrews and G. Ferguson. 2011. Chaxamycins A–D, bioactive ansamycins from a hyper-arid desert *Streptomyces* sp. Journal of natural products. 74: 1491-1499.

Rath, C. M., J. B. Scaglione, J. D. Kittendorf and D. H. Sherman. 2010. 1.11 - NRPS/PKS Hybrid Enzymes and Their Natural Products. Comprehensive Natural Products II. H.-W. Liu and L. Mander. Oxford, Elsevier. 453-492.

Ray, L. and B. S. Moore. 2016. Recent advances in the biosynthesis of unusual polyketide synthase substrates. Nat Prod Rep. 33: 150-161.

Rege, S. A., M. Arya and S. A. Momin. 2019. Structure activity relationship of tautomers of curcumin: a review. Ukrainian food journal. 45-60.

Rehbein, P., J. Berz, P. Kreisel and H. Schwalbe. 2019. “CodonWizard” – An intuitive software tool with graphical user interface for customizable codon optimization in protein expression efforts. Protein Expression and Purification. 160: 84-93.

Reuter, S., S. C. Gupta, M. M. Chaturvedi and B. B. Aggarwal. 2010. Oxidative stress, inflammation, and cancer: How are they linked? Free Radical Biology and Medicine. 49: 1603-1616.

Revill, W. P., M. J. Bibb and D. A. Hopwood. 1995. Purification of a malonyltransferase from *Streptomyces coelicolor* A3 (2) and analysis of its genetic determinant. Journal of bacteriology. 177: 3946-3952.

Reyrat, J. M., V. Pelicic, B. Gicquel and R. Rappuoli. 1998. Counterselectable markers: untapped tools for bacterial genetics and pathogenesis. Infect Immun. 66: 4011-4017.

Ribeiro da Cunha, B., L. P. Fonseca and C. R. C. Calado. 2019. Antibiotic discovery: where have we come from, where do we go? Antibiotics. 8: 45.

Risdian, C., T. Mozef and J. Wink. 2019. Biosynthesis of polyketides in *Streptomyces*. Microorganisms. 7: 124.

Robertsen, H. L. and E. M. Musiol-Kroll. 2019. Actinomycete-Derived Polyketides as a Source of Antibiotics and Lead Structures for the Development of New Antimicrobial Drugs. Antibiotics. 8,

Rodrigues, J. L., R. G. Araujo, K. L. Prather, L. D. Kluskens and L. R. Rodrigues. 2015a. Production of curcuminoids from tyrosine by a metabolically engineered *Escherichia coli* using caffeic acid as an intermediate. Biotechnol J. 10: 599-609.

Rodrigues, J. L., D. Gomes and L. R. Rodrigues. 2020. A Combinatorial Approach to Optimize the Production of Curcuminoids From Tyrosine in *Escherichia coli*. Front Bioeng Biotechnol. 8: 59.

Rodrigues, J. L., K. L. Prather, L. D. Kluskens and L. R. Rodrigues. 2015b. Heterologous production of curcuminoids. Microbiol Mol Biol Rev. 79: 39-60.

Rodríguez-García, A., C. Barreiro, F. Santos-Beneit, A. Sola-Landa and J. F. Martín. 2007. Genome-wide transcriptomic and proteomic analysis of the primary response to phosphate limitation in *Streptomyces coelicolor* M145 and in a Δ*phoP* mutant. PROTEOMICS. 7: 2410-2429.

Rodríguez-Villalón, A., J. Pérez-Gil and M. Rodríguez-Concepción. 2008. Carotenoid accumulation in bacteria with enhanced supply of isoprenoid precursors by upregulation of exogenous or endogenous pathways. Journal of Biotechnology. 135: 78-84.

Rodriguez, A., Y. Chen, S. Khoomrung, E. Özdemir, I. Borodina and J. Nielsen. 2017. Comparison of the metabolic response to over-production of p-coumaric acid in two yeast strains. Metab Eng. 44: 265-272.

Rohles, C., S. Pauli, G. Gießelmann, M. Kohlstedt, J. Becker and C. Wittmann. 2022. Systems metabolic engineering of *Corynebacterium glutamicum* eliminates all by-products for selective and high-yield production of the platform chemical 5-aminovalerate. Metab Eng. 73: 168-181.

Rohles, C. M., G. Gießelmann, M. Kohlstedt, C. Wittmann and J. Becker. 2016. Systems metabolic engineering of *Corynebacterium glutamicum* for the production of the carbon-5 platform chemicals 5-aminovalerate and glutarate. Microbial Cell Factories. 15: 154.

Rohles, C. M., L. Gläser, M. Kohlstedt, G. Gießelmann, S. Pearson, A. del Campo, J. Becker and C. Wittmann. 2018. A bio-based route to the carbon-5 chemical glutaric acid and to bionylon-6, 5 using metabolically engineered *Corynebacterium glutamicum*. Green chemistry. 20: 4662-4674.

Rozkov, A., C. A. Avignone-Rossa, P. F. Ertl, P. Jones, R. D. O'Kennedy, J. J. Smith, J. W. Dale and M. E. Bushell. 2004. Characterization of the metabolic burden on *Escherichia coli* DH1 cells imposed by the presence of a plasmid containing a gene therapy sequence. Biotechnology and Bioengineering. 88: 909-915.

Rückert, C., A. Albersmeier, T. Busche, S. Jaenicke, A. Winkler, Ó. H. Friðjónsson, G. Ó. Hreggviðsson, C. Lambert, D. Badcock and K. Bernaerts. 2015. Complete genome sequence of *Streptomyces lividans* TK24. Journal of Biotechnology. 199: 21-22.

Rückert, C., A. Pühler and J. Kalinowski. 2003. Genome-wide analysis of the L-methionine biosynthetic pathway in *Corynebacterium glutamicum* by targeted gene deletion and homologous complementation. Journal of Biotechnology. 104: 213-228.

Rugbjerg, P., K. Sarup-Lytzen, M. Nagy and M. O. A. Sommer. 2018. Synthetic addiction extends the productive life time of engineered *Escherichia coli* populations. Proceedings of the National Academy of Sciences. 115: 2347-2352.

Sabatini, M., S. Comba, S. Altabe, A. I. Recio-Balsells, G. R. Labadie, E. Takano, H. Gramajo and A. Arabolaza. 2018. Biochemical characterization of the minimal domains of an iterative eukaryotic polyketide synthase. The FEBS Journal. 285: 4494-4511.

Saha, A. K. and N. B. Ruderman. 2003. Malonyl-CoA and AMP-activated protein kinase: an expanding partnership. Molecular and Cellular Biochemistry. 253: 65-70.

Salehi, B., P. V. Fokou, M. Sharifi-Rad, P. Zucca, R. Pezzani, N. Martins and J. Sharifi-Rad. 2019. The Therapeutic Potential of Naringenin: A Review of Clinical Trials. Pharmaceuticals. 12,

Samappito, S., J. E. Page, J. Schmidt, W. De-Eknamkul and T. M. Kutchan. 2003. Aromatic and pyrone polyketides synthesized by a stilbene synthase from *Rheum tataricum*. Phytochemistry. 62: 313-323.

Sarker, S. D., L. Nahar, A. Miron and M. Guo. 2020. Chapter Two - Anticancer natural products. Annual Reports in Medicinal Chemistry. S. D. Sarker and L. Nahar. Academic Press. 55**:** 45-75.

Sawitzke, J. A., L. C. Thomason, N. Costantino, M. Bubunenko, S. Datta and D. L. Court. 2007. Recombineering: In Vivo Genetic Engineering in *E. coli*, *S. enterica*, and Beyond. Methods in Enzymology. Academic Press. 421**:** 171-199.

Scaffaro, R., F. Lopresti, A. Sutera, L. Botta, R. M. Fontana, A. M. Puglia and G. Gallo. 2016. Effect of PCL/PEG-Based Membranes on Actinorhodin Production in *Streptomyces coelicolor* Cultivations. Macromolecular bioscience. 16: 686-693.

Schlatter, D., A. Fubuh, K. Xiao, D. Hernandez, S. Hobbie and L. Kinkel. 2009. Resource amendments influence density and competitive phenotypes of *Streptomyces* in soil. Microbial ecology. 57: 413-420.

Schneider, C., O. N. Gordon, R. L. Edwards and P. B. Luis. 2015. Degradation of Curcumin: From Mechanism to Biological Implications. J Agric Food Chem. 63: 7606-7614.

Schneider, C. A., W. S. Rasband and K. W. Eliceiri. 2012. NIH Image to ImageJ: 25 years of image analysis. Nature methods. 9: 671-675.

Schröder, J. 1999. 1.27 - The Chalcone/Stilbene Synthase-type Family of Condensing Enzymes. Comprehensive Natural Products Chemistry. S. D. Barton, K. Nakanishi and O. Meth-Cohn. Oxford, Pergamon. 749-771.

Schwardmann, L. S., A. K. Dransfeld, T. Schäffer and V. F. Wendisch. 2022. Metabolic Engineering of *Corynebacterium glutamicum* for Sustainable Production of the Aromatic Dicarboxylic Acid Dipicolinic Acid. Microorganisms. 10,

Selim, M. S. M., S. A. Abdelhamid and S. S. Mohamed. 2021. Secondary metabolites and biodiversity of actinomycetes. Journal of Genetic Engineering and biotechnology. 19: 72.

Sgro, M., N. Chow, F. Olyaei, M. Arentshorst, N. Geoffrion, A. F. J. Ram, J. Powlowski and A. Tsang. 2023. Functional analysis of the protocatechuate branch of the β-ketoadipate pathway in *Aspergillus niger*. Journal of Biological Chemistry. 299:

Shaikh, A. F., M. Elfeki, S. Landolfa, U. Tanouye, S. J. Green and B. T. Murphy. 2015. Deuteromethylactin B from a Freshwater-derived *Streptomyces* sp. Natural Product Sciences. 21: 261-267.

Shang, X., X. Chai, X. Lu, Y. Li, Y. Zhang, G. Wang, C. Zhang, S. Liu, Y. Zhang, J. Ma and T. Wen. 2018. Native promoters of *Corynebacterium glutamicum* and its application in l-lysine production. Biotechnology Letters. 40: 383-391.

Sharifi-Rad, J., Y. E. Rayess, A. A. Rizk, C. Sadaka, R. Zgheib, W. Zam, S. Sestito, S. Rapposelli, K. Neffe-Skocińska, D. Zielińska, B. Salehi, W. N. Setzer, N. S. Dosoky, Y. Taheri, M. El Beyrouthy, M. Martorell, E. A. Ostrander, H. A. R. Suleria, W. C. Cho, A. Maroyi and N. Martins. 2020. Turmeric and Its Major Compound Curcumin on Health: Bioactive Effects and Safety Profiles for Food, Pharmaceutical, Biotechnological and Medicinal Applications. Frontiers in Pharmacology. 11:

Shen, B. 2003. Polyketide biosynthesis beyond the type I, II and III polyketide synthase paradigms. Current opinion in chemical biology. 7: 285-295.

Shenton, D. and C. M. Grant. 2003. Protein S-thiolation targets glycolysis and protein synthesis in response to oxidative stress in the yeast *Saccharomyces cerevisiae*. Biochemical Journal. 374: 513-519.

Shi, L. and B. P. Tu. 2015. Acetyl-CoA and the regulation of metabolism: mechanisms and consequences. Current opinion in cell biology. 33: 125-131.

Shin, S.-Y., S.-M. Jung, M.-D. Kim, N. S. Han and J.-H. Seo. 2012. Production of resveratrol from tyrosine in metabolically engineered *Saccharomyces cerevisiae*. Enzyme and Microbial Technology. 51: 211-216.

Silberbach, M., M. Schäfer, A. T. Hüser, J. r. Kalinowski, A. Pühler, R. Krämer and A. Burkovski. 2005. Adaptation of *Corynebacterium glutamicum* to ammonium limitation: a global analysis using transcriptome and proteome techniques. Applied and Environmental Microbiology. 71: 2391-2402.

Singh, N. and K. Misra. 2009. Computational screening of molecular targets in *Plasmodium* for novel non resistant anti-malarial drugs. Bioinformation. 3: 255.

Sitabja, M. and K. K. Santosh. 2021. Curcuminoids: The Novel Molecules of Nature. Herbs and Spices. A. Rabia Shabir. Rijeka, IntechOpen. Ch. 6.

Sivalingam, P., K. Hong, J. Pote and K. Prabakar. 2019. Extreme environment *Streptomyces*: potential sources for new antibacterial and anticancer drug leads? International Journal of Microbiology. 2019:

Smith, C. A., C. B. Phiefer, S. J. Macnaughton, A. Peacock, R. S. Burkhalter, R. Kirkegaard and D. C. White. 2000. Quantitative lipid biomarker detection of unculturable microbes

and chlorine exposure in water distribution system biofilms. Water Research. 34: 2683-2688.

Sohoni, S. V., P. M. Bapat and A. E. Lantz. 2012. Robust, small-scale cultivation platform for *Streptomyces coelicolor*. Microbial Cell Factories. 11: 1-10.

Soliveri, J. A., J. Gomez, W. R. Bishai and K. F. Chater. 2000. Multiple paralogous genes related to the *Streptomyces coelicolor* developmental regulatory gene whiB are present in *Streptomyces* and other actinomycetes. Microbiology (Reading). 146: 333-343.

Solymosi, K., N. Latruffe, A. Morant-Manceau and B. Schoefs. 2015. 1 - Food colour additives of natural origin. Colour Additives for Foods and Beverages. M. J. Scotter. Oxford, Woodhead Publishing. 3-34.

Song, Y., K. i. Matsumoto, M. Yamada, A. Gohda, C. J. Brigham, A. J. Sinskey and S. Taguchi. 2012. Engineered *Corynebacterium glutamicum* as an endotoxin-free platform strain for lactate-based polyester production. Appl Microbiol Biotechnol. 93: 1917-1925.

Sova, M. 2012. Antioxidant and antimicrobial activities of cinnamic acid derivatives. Mini Rev Med Chem. 12: 749-767.

Sprenger, G. A. 2007. Aromatic Amino Acids. Amino Acid Biosynthesis ~ Pathways, Regulation and Metabolic Engineering. V. F. Wendisch. Berlin, Heidelberg, Springer Berlin Heidelberg. 93-127.

Srivastava, R. M., S. Singh, S. K. Dubey, K. Misra and A. Khar. 2011. Immunomodulatory and therapeutic activity of curcumin. International Immunopharmacology. 11: 331-341.

Steyn, A. J. C., D. M. Collins, M. K. Hondalus, W. R. Jacobs Jr, R. P. Kawakami and B. R. Bloom. 2002. *Mycobacterium tuberculosis* WhiB3 interacts with RpoV to affect host survival but is dispensable for in vivo growth. Proceedings of the National Academy of Sciences. 99: 3147-3152.

Su, H.-N., K. Li, L.-S. Zhao, X.-X. Yuan, M.-Y. Zhang, S.-M. Liu, X.-L. Chen, L.-N. Liu and Y.-Z. Zhang. 2020. Structural Visualization of Septum Formation in *Staphylococcus warneri* Using Atomic Force Microscopy. Journal of bacteriology. 202: 10.1128/jb.00294-00220.

Sun, Y., X. Zhou, J. Liu, K. Bao, G. Zhang, G. Tu, T. Kieser and Z. Deng. 2002. '*Streptomyces nanchangensis*', a producer of the insecticidal polyether antibiotic nanchangmycin and the antiparasitic macrolide meilingmycin, contains multiple polyketide gene clusters. Microbiology (Reading). 148: 361-371.

Susana, M., G. Thomas, C. Martin, C. S. Christian, A. Iman, H. Johnny, H. Lucas, T. Niklas, N. Stephan, G. Michaela, T. Ralf, N. Katharina and B. Michael. 2021. Growth-rate dependency of ribosome abundance and translation elongation rate in *Corynebacterium glutamicum* differs from *Escherichia coli*. bioRxiv. 2021.2004.2001.438067.

Sutcliffe, I. C. 2010. A phylum level perspective on bacterial cell envelope architecture. Trends in microbiology. 18: 464-470.

Sversut, R. A., A. A. da Silva, T. F. M. Cardoso, N. M. Kassab, M. S. do Amaral and H. R. N. Salgado. 2017. A Critical Review of Properties and Analytical Methods for the Determination of Oxytetracyline in Biological and Pharmaceutical Matrices. Critical Reviews in Analytical Chemistry. 47: 154-171.

Szu, P.-H., S. Govindarajan, Michael J. Meehan, A. Das, Don D. Nguyen, Pieter C. Dorrestein, J. Minshull and C. Khosla. 2011. Analysis of the Ketosynthase-Chain Length Factor Heterodimer from the Fredericamycin Polyketide Synthase. Chem Biol. 18: 1021-1031.

Taguchi, A., J. E. Page, H.-C. T. Tsui, M. E. Winkler and S. Walker. 2021. Biochemical reconstitution defines new functions for membrane-bound glycosidases in assembly of

the bacterial cell wall. Proceedings of the National Academy of Sciences. 118: e2103740118.

Takeno, S., M. Takasaki, A. Urabayashi, A. Mimura, T. Muramatsu, S. Mitsuhashi and M. Ikeda. 2013. Development of fatty acid-producing *Corynebacterium glutamicum* strains. Applied and Environmental Microbiology. 79: 6776-6783.

Tan, Y., D. Xu, Y. Li and X. Wang. 2012. Construction of a novel *sacB*-based system for marker-free gene deletion in *Corynebacterium glutamicum*. Plasmid. 67: 44-52.

Tang, L., L. Chung, J. R. Carney, C. M. Starks, P. Licari and L. Katz. 2005. Generation of new epothilones by genetic engineering of a polyketide synthase in *Myxococcus xanthus*. J Antibiot (Tokyo). 58: 178-184.

Tang, Z., C. Xiao, Y. Zhuang, J. Chu, S. Zhang, P. R. Herron, I. S. Hunter and M. Guo. 2011. Improved oxytetracycline production in *Streptomyces rimosus* M4018 by metabolic engineering of the G6PDH gene in the pentose phosphate pathway. Enzyme and Microbial Technology. 49: 17-24.

Tauchen, J., L. Huml, S. Rimpelova and M. Jurášek. 2020. Flavonoids and related members of the aromatic polyketide group in human health and disease: do they really work? Molecules. 25: 3846.

Tavassoly, I., J. Goldfarb and R. Iyengar. 2018. Systems biology primer: the basic methods and approaches. Essays Biochem. 62: 487-500.

Temple, N. J. 2022. A rational definition for functional foods: A perspective. Frontiers in Nutrition. 9:

Tesch, M., A. A. De Graaf and H. Sahm. 1999. In vivo fluxes in the ammonium-assimilatory pathways in *Corynebacterium glutamicum* studied by15N nuclear magnetic resonance. Applied and Environmental Microbiology. 65: 1099-1109.

Thamchaipenet, A. 1994. Characterisation of Some Genes Involved in the Early Steps of the Biosynthetic Pathway For Oxytetracycline in Streptomyces rimosus. University of Glasgow (United Kingdom).

Thangapazham, R. L., A. Sharma and R. K. Maheshwari. 2006. Multiple molecular targets in cancer chemoprevention by curcumin. The AAPS journal. 8: E443-E449.

Thomas, R. and D. J. Williams. 1983. Oxytetracycline biosynthesis: mode of incorporation of [1-13C]- and [1,2-13C2]-acetate. Journal of the Chemical Society, Chemical Communications. 128-130.

Thompson, L. H. and D. Schild. 2001. Homologous recombinational repair of DNA ensures mammalian chromosome stability. Mutation Research/Fundamental and Molecular Mechanisms of Mutagenesis. 477: 131-153.

Till, M. and P. R. Race. 2014. Progress challenges and opportunities for the re-engineering of trans-AT polyketide synthases. Biotechnology Letters. 36: 877-888.

Tomeh, M. A., R. Hadianamrei and X. Zhao. 2019. A Review of Curcumin and Its Derivatives as Anticancer Agents. Int J Mol Sci. 20: 1033.

Tovilla-Coutiño, D. B., C. Momany and M. A. Eiteman. 2020. Engineered citrate synthase alters Acetate Accumulation in Escherichia coli. Metab Eng. 61: 171-180.

Toyoda, K., H. Teramoto, M. Inui and H. Yukawa. 2011. Genome-Wide Identification of In Vivo Binding Sites of GlxR, a Cyclic AMP Receptor Protein-Type Regulator in *Corynebacterium glutamicum*. Journal of bacteriology. 193: 4123-4133.

Traunmüller, F., M. Alexander Zeitlinger, B. Stoiser, H. Lagler, H. Abdulla Abdel Salam, E. Presterl and W. Graninger. 2003. Circulating Tuberculostearic Acid in Tuberculosis Patients. Scandinavian Journal of Infectious Diseases. 35: 790-793.

Tsutsui, A., Y. Morishita, H. Furumachi, T. Fujimoto, R. Hirai, T. Fujita and T. Machinami. 2021. Generation of cyclic glutathione via the thiolactonization of glutathione and identification of a new radical scavenging mechanism. Tetrahedron Letters. 68: 152836.

Ul-Hassan, A. and E. M. H. Wellington. 2009. *Actinobacteria*. Encyclopedia of Microbiology (Third Edition). 3: 25-44.

Ultee, E., L. T. van der Aart, L. Zhang, D. van Dissel, C. A. Diebolder, G. P. van Wezel, D. Claessen and A. Briegel. 2020. Teichoic acids anchor distinct cell wall lamellae in an apically growing bacterium. Communications biology. 3: 314.

Van Boeckel, T. P., S. Gandra, A. Ashok, Q. Caudron, B. T. Grenfell, S. A. Levin and R. Laxminarayan. 2014. Global antibiotic consumption 2000 to 2010: an analysis of national pharmaceutical sales data. The Lancet infectious diseases. 14: 742-750.

van der Heul, H. U., B. L. Bilyk, K. J. McDowall, R. F. Seipke and G. P. van Wezel. 2018. Regulation of antibiotic production in *Actinobacteria*: new perspectives from the post-genomic era. Nat Prod Rep. 35: 575-604.

van der Hoek, S. A., M. Rusnák, G. Wang, L. D. Stanchev, L. de Fátima Alves, M. M. Jessop-Fabre, K. Paramasivan, I. H. Jacobsen, N. Sonnenschein, J. L. Martínez, B. Darbani, D. B. Kell and I. Borodina. 2022. Engineering precursor supply for the high-level production of ergothioneine in *Saccharomyces cerevisiae*. Metab Eng. 70: 129-142.

van Dissel, D., D. Claessen, M. Roth and G. P. van Wezel. 2015. A novel locus for mycelial aggregation forms a gateway to improved *Streptomyces* cell factories. Microbial Cell Factories. 14: 1-10.

van Dissel, D., J. Willemse, B. Zacchetti, D. Claessen, G. B. Pier and G. P. van Wezel. 2018. Production of poly-β-1, 6-N-acetylglucosamine by MatAB is required for hyphal aggregation and hydrophilic surface adhesion by *Streptomyces*. Microbial Cell. 5: 269.

van Ooyen, J., S. Noack, M. Bott, A. Reth and L. Eggeling. 2012. Improved L-lysine production with *Corynebacterium glutamicum* and systemic insight into citrate synthase flux and activity. Biotechnology and Bioengineering. 109: 2070-2081.

Větrovský, T., K. T. Steffen and P. Baldrian. 2014. Potential of cometabolic transformation of polysaccharides and lignin in lignocellulose by soil *Actinobacteria*. PLoS One. 9: e89108.

Virklund, A., S. I. Jensen, A. T. Nielsen and J. M. Woodley. 2023. Combining genetic engineering and bioprocess concepts for improved phenylpropanoid production. Biotechnology and Bioengineering. 120: 613-628.

Vogel, A. and J. Pelletier. 1815. Examen chimique de la racine de Curcuma. Journal de Pharmacie et des Sciences Accessoires. 36: 289-300.

Wang, B. and H. Zhao. 2020. Unleashing the power of energy storage: Engineering β-oxidation pathways for polyketide production. Synthetic and Systems Biotechnology. 5: 21-22.

Wang, J., X. Xia, P. Zhao, X. He, S. Zhang, T. Wang and Z. Xu. 2022. High-level secretory production of lysostaphin in *Escherichia coli* mutant by codon optimization and atmospheric and room temperature plasma mutagenesis. LWT. 165: 113744.

Wang, J., R. Zhang, X. Chen, X. Sun, Y. Yan, X. Shen and Q. Yuan. 2020a. Biosynthesis of aromatic polyketides in microorganisms using type II polyketide synthases. Microbial Cell Factories. 19: 110.

Wang, P., G. Bashiri, X. Gao, M. R. Sawaya and Y. Tang. 2013. Uncovering the enzymes that catalyze the final steps in oxytetracycline biosynthesis. Journal of the American Chemical Society. 135: 7138-7141.

Wang, P., X. Gao, Y.-H. Chooi, Z. Deng and Y. Tang. 2011. Genetic characterization of enzymes involved in the priming steps of oxytetracycline biosynthesis in *Streptomyces rimosus*. Microbiology (Reading). 157: 2401-2409.

Wang, P., W. Zhang, J. Zhan and Y. Tang. 2009. Identification of OxyE as an ancillary oxygenase during tetracycline biosynthesis. Chembiochem. 10: 1544-1550.

Wang, S. and H. Deng. 2020. The X-factor: Enhanced β-oxidation on intracellular triacylglycerols enabling overproduction of polyketide drug-like molecules in microorganisms. Synthetic and Systems Biotechnology. 5: 19.

Wang, W., S. Li, Z. Li, J. Zhang, K. Fan, G. Tan, G. Ai, S. M. Lam, G. Shui and Z. Yang. 2020b. Harnessing the intracellular triacylglycerols for titer improvement of polyketides in *Streptomyces*. Nature Biotechnology. 38: 76-83.

Wang, X., S. Yin, J. Bai, Y. Liu, K. Fan, H. Wang, F. Yuan, B. Zhao, Z. Li and W. Wang. 2019. Heterologous production of chlortetracycline in an industrial grade *Streptomyces rimosus* host. Appl Microbiol Biotechnol. 103: 6645-6655.

Wang, Y.-b., S.-y. Guo, B.-b. Chang, R.-f. Ye and Q. Hua. 2021. Establishment of Conjugation System for the Spiramycin Producer *Streptomyces spiramyceticus*. China Biotechnology. 41: 45-52.

Watanabe, K., K. Matsuura, P. Gao, L. Hottenbacher, H. Tokunaga, K. Nishimura, Y. Imazu, H. Reissenweber and C. M. Witt. 2011. Traditional Japanese Kampo Medicine: Clinical Research between Modernity and Traditional Medicine-The State of Research and Methodological Suggestions for the Future. Evid Based Complement Alternat Med. 2011: 513842.

Watanabe, K. and H. Oikawa. 2007. Robust platform for de novo production of heterologous polyketides and nonribosomal peptides in *Escherichia coli*. Organic & Biomolecular Chemistry. 5: 593-602.

Watanabe, Y. and H. Nakajima. 2016. Chapter Twenty - Creation of a Thermally Tolerant Peroxidase. Methods in Enzymology. V. L. Pecoraro. Academic Press. 580**:** 455-470.

Wattanachaisaereekul, S., A. E. Lantz, M. L. Nielsen and J. Nielsen. 2008. Production of the polyketide 6-MSA in yeast engineered for increased malonyl-CoA supply. Metab Eng. 10: 246-254.

Weber, J. M., C. K. Wierman and C. R. Hutchinson. 1985. Genetic analysis of erythromycin production in *Streptomyces erythreus*. Journal of bacteriology. 164: 425-433.

Wegner, A., J. Meiser, D. Weindl and K. Hiller. 2015. How metabolites modulate metabolic flux. Curr Opin Biotechnol. 34: 16-22.

Wei, J., B. Chen, J. Dong, X. Wang, Y. Li, Y. Liu and W. Guan. 2022. Salinomycin biosynthesis reversely regulates the β-oxidation pathway in *Streptomyces albus* by carrying a 3-hydroxyacyl-CoA dehydrogenase gene in its biosynthetic gene cluster. Microbial Biotechnology. 15: 2890-2904.

Weiland, F., N. Barton, M. Kohlstedt, J. Becker and C. Wittmann. 2023. Systems metabolic engineering upgrades *Corynebacterium glutamicum* to high-efficiency cis, cis-muconic acid production from lignin-based aromatics. Metab Eng. 75: 153-169.

Weiland, F., M. Kohlstedt and C. Wittmann. 2022. Guiding stars to the field of dreams: Metabolically engineered pathways and microbial platforms for a sustainable lignin-based industry. Metab Eng. 71: 13-41.

Weissman, K. J. 2009. Chapter 1 Introduction to Polyketide Biosynthesis. Methods in Enzymology. Academic Press. 459**:** 3-16.

Weissman, K. J., H. Hong, M. Oliynyk, A. P. Siskos and P. F. Leadlay. 2004. Identification of a Phosphopantetheinyl Transferase for Erythromycin Biosynthesis in *Saccharopolyspora erythraea*. Chembiochem. 5: 116-125.

Weissman, K. J. and P. F. Leadlay. 2005. Combinatorial biosynthesis of reduced polyketides. Nature Reviews Microbiology. 3: 925-936.

Wen, J., L. Tian, Q. Liu, Y. Zhang and M. Cai. 2020. Engineered dynamic distribution of malonyl-CoA flux for improving polyketide biosynthesis in Komagataella phaffii. Journal of Biotechnology. 320: 80-85.

Wendisch, V. F., J. M. P. Jorge, F. Pérez-García and E. Sgobba. 2016. Updates on industrial production of amino acids using *Corynebacterium glutamicum*. World Journal of Microbiology and Biotechnology. 32: 105.

Wiesmann, K. E. H., J. Cortés, M. J. B. Brown, A. L. Cutter, J. Staunton and P. F. Leadlay. 1995. Polyketide synthesis in vitro on a modular polyketide synthase. Chem Biol. 2: 583-589.

Winkel-Shirley, B. 2001. Flavonoid biosynthesis. A colorful model for genetics, biochemistry, cell biology, and biotechnology. Plant physiology. 126: 485-493.

Wittmann, C. 2007. Fluxome analysis using GC-MS. Microbial Cell Factories. 6: 6.

Wittmann, C., P. Kiefer and O. Zelder. 2004. Metabolic Fluxes in *Corynebacterium glutamicum* during Lysine Production with Sucrose as Carbon Source. Applied and Environmental Microbiology. 70: 7277-7287.

Wolf, S., J. Becker, Y. Tsuge, H. Kawaguchi, A. Kondo, J. Marienhagen, M. Bott, Volker F. Wendisch and C. Wittmann. 2021. Advances in metabolic engineering of Corynebacterium glutamicum to produce high-value active ingredients for food, feed, human health, and well-being. Essays Biochem. 65: 197-212.

Wu, J., W. Chen, Y. Zhang, X. Zhang, J. M. Jin and S. Y. Tang. 2020. Metabolic Engineering for Improved Curcumin Biosynthesis in *Escherichia coli*. J Agric Food Chem. 68: 10772-10779.

Wu, J., O. Yu, G. Du, J. Zhou and J. Chen. 2014. Fine-tuning of the fatty acid pathway by synthetic antisense RNA for enhanced (2 S)-naringenin production from L-tyrosine in *Escherichia coli*. Applied and Environmental Microbiology. 80: 7283-7292.

Wu, X., J. Liu, D. Liu, M. Yuwen, M. A. G. Koffas and J. Zha. 2022. Biosynthesis of eriodictyol from tyrosine by *Corynebacterium glutamicum*. Microbial Cell Factories. 21: 1-11.

Xiao, Z. P., Z. Y. Peng, M. J. Peng, W. B. Yan, Y. Z. Ouyang and H. L. Zhu. 2011. Flavonoids health benefits and their molecular mechanism. Mini Rev Med Chem. 11: 169-177.

Xie, F., G. Li, Y. Wang, Y. Zhang, L. Zhou, C. Wang, S. Liu, S. Liu and C. Wang. 2017. Pyridoxal phosphate synthases PdxS/PdxT are required for *Actinobacillus pleuropneumoniae* viability, stress tolerance and virulence. PLoS One. 12: e0176374.

Xu, F., R.-C. Sun, J.-X. Sun, C.-F. Liu, B.-H. He and J.-S. Fan. 2005. Determination of cell wall ferulic and p-coumaric acids in sugarcane bagasse. Analytica Chimica Acta. 552: 207-217.

Xu, H., K. F. Chater, Z. Deng and M. Tao. 2008. A cellulose synthase-like protein involved in hyphal tip growth and morphological differentiation in *Streptomyces*. Journal of bacteriology. 190: 4971-4978.

Xu, W., L. B. Raetz, P. Wang and Y. Tang. 2016. An ATP-dependent ligase catalyzes the fourth ring cyclization in tetracycline biosynthesis. Tetrahedron. 72: 3599-3604.

Xu, X.-Y., X. Meng, S. Li, R.-Y. Gan, Y. Li and H.-B. Li. 2018. Bioactivity, Health Benefits, and Related Molecular Mechanisms of Curcumin: Current Progress, Challenges, and Perspectives. Nutrients. 10,

Yang, D., W. J. Kim, S. M. Yoo, J. H. Choi, S. H. Ha, M. H. Lee and S. Y. Lee. 2018. Repurposing type III polyketide synthase as a malonyl-CoA biosensor for metabolic engineering in bacteria. Proceedings of the National Academy of Sciences. 115: 9835-9844.

Yang, D., H. Zhou and S. Y. Lee. 2021a. Production of Diversified Polyketides by Metabolic Engineering. Biochemistry. 60: 3424-3426.

Yang, Q., S. Guo, Q. Lu, Y. Tao, D. Zheng, Q. Zhou and J. Liu. 2021b. Butyryl/Caproyl-CoA: Acetate CoA-transferase: cloning, expression and characterization of the key enzyme involved in medium-chain fatty acid biosynthesis. Bioscience reports. 41: BSR20211135.

Yang, S.-P., J. Xie, Y. Cheng, Z. Zhang, Y. Zhao and Y.-F. Qian. 2020. Response of *Shewanella putrefaciens* to low temperature regulated by membrane fluidity and fatty acid metabolism. LWT. 117: 108638.

Yang, Y., Y. Lin, L. Li, R. J. Linhardt and Y. Yan. 2015. Regulating malonyl-CoA metabolism via synthetic antisense RNAs for enhanced biosynthesis of natural products. Metab Eng. 29: 217-226.

Yao, L. H., Y. M. Jiang, J. Shi, F. A. TomÁS-BarberÁN, N. Datta, R. Singanusong and S. S. Chen. 2004. Flavonoids in Food and Their Health Benefits. Plant Foods Hum Nutr. 59: 113-122.

Yin, S., X. Wang, M. Shi, F. Yuan, H. Wang, X. Jia, J. Sun, T. Liu, K. Yang, Y. Zhang, K. Fan and Z. Li. 2017. Improvement of oxytetracycline production mediated via cooperation of resistance genes in *Streptomyces rimosus*. Science China Life Sciences. 60: 992-999.

Yixuan, L., M. A. Qaria, S. Sivasamy, S. Jianzhong and Z. Daochen. 2021. Curcumin production and bioavailability: A comprehensive review of curcumin extraction, synthesis, biotransformation and delivery systems. Industrial Crops and Products. 172: 114050.

Yoo, Y. J., H. Kim, S. R. Park and Y. J. Yoon. 2017. An overview of rapamycin: from discovery to future perspectives. Journal of Industrial Microbiology and Biotechnology. 44: 537-553.

Yu, L., N. Cao, L. Wang, C. Xiao, M. Guo, J. Chu, Y. Zhuang and S. Zhang. 2012. Oxytetracycline biosynthesis improvement in *Streptomyces rimosus* following duplication of minimal PKS genes. Enzyme and Microbial Technology. 50: 318-324.

Yuan, H., Q. Ma, L. Ye and G. Piao. 2016. The Traditional Medicine and Modern Medicine from Natural Products. Molecules. 21,

Yuan, S.-F. and H. S. Alper. 2019. Metabolic engineering of microbial cell factories for production of nutraceuticals. Microbial Cell Factories. 18: 46.

Yun, D. G. and D. G. Lee. 2016. Antibacterial activity of curcumin via apoptosis-like response in *Escherichia coli*. Appl Microbiol Biotechnol. 100: 5505-5514.

Yuzawa, S. and T. Kuzuyama. 2020. 1.05 - Engineering of Acyltransferase Domains in Polyketide Synthases. Comprehensive Natural Products III. H.-W. Liu and T. P. Begley. Oxford, Elsevier. 123-138.

Yuzawa, S., A. Zargar, B. Pang, L. Katz and J. D. Keasling. 2018. Chapter Fourteen - Commodity Chemicals From Engineered Modular Type I Polyketide Synthases. Methods in Enzymology. N. Scrutton. Academic Press. 608**:** 393-415.

Zakeri, B. and G. D. Wright. 2008. Chemical biology of tetracycline antibiotics. Biochemistry and Cell Biology. 86: 124-136.

Zduńska, K., A. Dana, A. Kolodziejczak and H. Rotsztejn. 2018. Antioxidant properties of ferulic acid and its possible application. Skin pharmacology and physiology. 31: 332-336.

Zha, J., Z. Zhao, Z. Xiao, T. Eng, A. Mukhopadhyay, M. A. G. Koffas and Y. J. Tang. 2023. Biosystem design of *Corynebacterium glutamicum* for bioproduction. Curr Opin Biotechnol. 79: 102870.

Zha, W., S. B. Rubin-Pitel, Z. Shao and H. Zhao. 2009. Improving cellular malonyl-CoA level in *Escherichia coli* via metabolic engineering. Metab Eng. 11: 192-198.

Zhang, H., Z. Li, S. Zhou, S.-M. Li, H. Ran, Z. Song, T. Yu and W.-B. Yin. 2022. A fungal NRPS-PKS enzyme catalyses the formation of the flavonoid naringenin. Nature Communications. 13: 6361.

Zhang, L., W. Liu, J. Xiao, T. Hu, J. Chen, K. Chen, H. Jiang and X. Shen. 2007a. Malonyl-CoA: acyl carrier protein transacylase from *Helicobacter pylori*: Crystal structure and its interaction with acyl carrier protein. Protein Science. 16: 1184-1192.

Zhang, L., C. Ruan, F. Peng, Z. Deng and K. Hong. 2016. *Streptomyces arcticus* sp. nov., isolated from frozen soil. International Journal of Systematic and Evolutionary Microbiology. 66: 1482-1487.

Zhang, S., J. Wu, Z. Jiang, L. Zhang, T. Song, X. Liu, C. Yin and Y. Zhang. 2023. Pigments of aminophenoxazinones and viridomycins produced by termite-associated Streptomyces tanashiensis BYF-112. Frontiers in Microbiology. 13: 1110811.

Zhang, W., D. Ames Brian, S.-C. Tsai and Y. Tang. 2006. Engineered Biosynthesis of a Novel Amidated Polyketide, Using the Malonamyl-Specific Initiation Module from the Oxytetracycline Polyketide Synthase. Applied and Environmental Microbiology. 72: 2573-2580.

Zhang, W., V. C. Jones, M. S. Scherman, S. Mahapatra, D. Crick, S. Bhamidi, Y. Xin, M. R. McNeil and Y. Ma. 2008a. Expression, essentiality, and a microtiter plate assay for mycobacterial GlmU, the bifunctional glucosamine-1-phosphate acetyltransferase and N-acetylglucosamine-1-phosphate uridyltransferase. The International Journal of Biochemistry & Cell Biology. 40: 2560-2571.

Zhang, W., K. Watanabe, X. Cai, M. E. Jung, Y. Tang and J. Zhan. 2008b. Identifying the minimal enzymes required for anhydrotetracycline biosynthesis. Journal of the American Chemical Society. 130: 6068-6069.

Zhang, W., K. Watanabe, C. C. C. Wang and Y. Tang. 2007b. Investigation of early tailoring reactions in the oxytetracycline biosynthetic pathway. Journal of Biological Chemistry. 282: 25717-25725.

Zhang, Y., Z. Lin, Q. Liu, Y. Li, Z. Wang, H. Ma, T. Chen and X. Zhao. 2014. Engineering of Serine-Deamination pathway, Entner-Doudoroff pathway and pyruvate dehydrogenase complex to improve poly (3-hydroxybutyrate) production in *Escherichia coli*. Microbial Cell Factories. 13: 1-11.

Zhang, Z., C. Du, F. de Barsy, M. Liem, A. Liakopoulos, G. P. van Wezel, Y. H. Choi, D. Claessen and D. E. Rozen. 2020. Antibiotic production in *Streptomyces* is organized by a division of labor through terminal genomic differentiation. Science advances. 6: eaay5781.

Zheng, F., Q. Long and J. Xie. 2012. The function and regulatory network of WhiB and WhiB-like protein from comparative genomics and systems biology perspectives. Cell Biochemistry and Biophysics. 63: 103-108.

Zheng, M., X. Wang, J. Templeton Lori, R. Smulski Dana, A. LaRossa Robert and G. Storz. 2001. DNA Microarray-Mediated Transcriptional Profiling of the *Escherichia coli* Response to Hydrogen Peroxide. Journal of bacteriology. 183: 4562-4570.

Zhou, S., S.-F. Yuan, P. H. Nair, H. S. Alper, Y. Deng and J. Zhou. 2021. Development of a growth coupled and multi-layered dynamic regulation network balancing malonyl-CoA node to enhance (2S)-naringenin biosynthesis in *Escherichia coli*. Metab Eng. 67: 41-52.

Zirkle, R., J. M. Ligon and I. Molnar. 2004. Heterologous production of the antifungal polyketide antibiotic soraphen A of *Sorangium cellulosum* So ce26 in *Streptomyces lividans*. Microbiology (Reading). 150: 2761-2774.

Zotchev, S., K. Haugan, O. Sekurova, H. Sletta, T. E. Ellingsen and S. Valla. 2000. Identification of a gene cluster for antibacterial polyketide-derived antibiotic biosynthesis in the nystatin producer *Streptomyces noursei* ATCC 11455. Microbiology (Reading). 146: 611-619.